Aix*Marseille université
Socialement engagée

NNT : 2023AIXM0001

THÈSE DE DOCTORAT

Soutenue à Aix-Marseille Université
le 19 novembre 2024 par

Isam BEN SOLTANE

Analytical description of linear physical response functions with the Singularity Expansion Method

Discipline
Physique et Science de la Matière

Spécialité
Optique, Photonique et Traitement d'Image

École doctorale
ED 352 Physique et Science de la Matière

Laboratoire/Partenaires de recherche
Institut Fresnel

Composition du jury

Patrick BOUCHON DR ONERA, France	Rapporteur
Matthieu DAVY Pr, Université de Rennes, France	Rapporteur
Nathalie DESTOUCHES Pr, Université de Saint-Etienne, France	Examinatrice
Anne-Laure FEHREMBACH MCF, Aix-Marseille Université, France	Examinatrice
Patrice GENEVET Full Prof, Colorado School of Mines, USA	Examinateur
Miguel ALONSO Pr, Centrale Méditerranée, France	Président du jury
Nicolas BONOD DR CNRS, Institut Fresnel, France	Directeur de thèse
Redha ABDEDDAIM MCF, Aix-Marseille Université, France	Membre invité

Affidavit

I, undersigned, Isam BEN SOLTANE, hereby declare that the work presented in this manuscript is my own work, carried out under the scientific supervision of Nicolas BONOD, in accordance with the principles of honesty, integrity and responsibility inherent to the research mission. The research work and the writing of this manuscript have been carried out in compliance with both the french national charter for Research Integrity and the Aix-Marseille University charter on the fight against plagiarism.

This work has not been submitted previously either in this country or in another country in the same or in a similar version to any other examination body.

Marseille, 18/08/2024



This work is licensed under Creative Commons Attribution-NonCommercial-NoDerivatives 4.0 International Public License

Liste de publications et participation aux conférences

Liste des publications et/ou brevets réalisées dans le cadre du projet de thèse :

1. I. Ben Soltane, R. Colom, B. Stout, N. Bonod, Derivation of the Transient and Steady Optical States from the Poles of the S-Matrix. Laser Photonics Rev 2023, 17, 2200141.
2. I. Ben Soltane, R. Colom, F. Dierick, B. Stout, N. Bonod, Multiple-Order Singularity Expansion Method. New J. Phys. 2023, 25, 103022.
3. I. Ben Soltane, F. Dierick, B. Stout, N. Bonod, Generalized Drude–Lorentz Model Complying with the Singularity Expansion Method. Adv. Optical Mater. 2024, 12, 2400093.
4. N. Bonod, I. Ben Soltane, A method for determining impedance functions (brevet, déposé le 06/09/2024)

Participation aux conférences et écoles d'été au cours de la période de thèse :

1. Juillet 2022 - 2nd Colloquim on the Physics and Applications of Metasurfaces - Florence, Italie (Poster)
2. Aout 2022 - Complex Nanophotonics Science Camp - Cumberland Lodge, Windsor Great Park, UK (Poster)
3. Septembre 2022 - C'Nano 13th Metting on Nanoscience Advances - Porquerolles, France (Poster)
4. Février 2023 - Canonical scattering problems, Isaac Newton Institute - Cambridge, UK (Poster)
5. Mars 2023 - Bremen Zoom Meeting - Remote (Presentation)
6. Avril 2024 - General assembly of the GT2 (GDR ondes), Laboratoire MPQ - Paris, France (Présentation)
7. Mai 2023 - Workshop on Optical Wave & Waveguide Theory and Numertical Modeling (OWTNM) - Marseille, France (Présentation)
8. Septembre 2023 - European Optical Society Annual Meeting (EOSAM) - Dijon, France (Présentation)

9. Octobre 2023 - Paris-Saclay Plasmonics School (PS2), Solid State Physics Laboratory (LPS) - Orsay, France (Poster)
10. Decembre 2023 - General assembly of the GDR ondes - Marseille, France (Poster)
11. Janvier 2024 - 3rd Colloquim on the Physics and Applications of Metasurfaces - Zurich, Switzerland (Poster)
12. Mai 2024 - SFO Thermics and Nanophotonics school - Les Houches, France (Poster)
13. Juillet 2024 - SFO Optique Normandie - Rouen France (Presentation + Poster)
14. Septembre 2024 - C'Nano 14th Metting on Nanoscience Advances - Porquerolles, France (Présentation)

Résumé et mots clés

Les dynamiques temporelles des systèmes physiques linéaires sont décrites par des fonctions de réponse ou de transfert dans le domaine harmonique. La caractérisation de ces fonctions de la fréquence est cruciale puisqu'elle permet de comprendre les interactions entre signaux excitateurs et systèmes, pour contrôler la réponse spectrale avec, par exemple, des résonances particulières, et concevoir des systèmes présentant des réponses bien définies.

La méthode du développement en singularités part d'observations physiques, à savoir la réponse de résonateurs à des champs électriques excitateurs sinusoïdaux, pour offrir une description analytique des fonctions de réponse dans le domaine harmonique. Ce manuscrit de thèse a pour point de départ cette méthode, et entend démontrer, généraliser et exploiter le développement en singularités.

En partant des propriétés fondamentales, et par conséquent peu restrictives, des systèmes et fonctions de réponse ou transfert rencontrés en physique, une expression exacte est obtenue avec la méthode du développement généralisé en singularités d'ordres multiples. Cette description naturelle de ces fonctions méromorphes repose sur leur ensemble discret de fréquences complexes appelées singularités, ainsi qu'un terme non résonnant rendant compte du comportement à haute fréquence. Une forme alternative, la factorisation en singularités et zéros, est également présentée, ainsi que le comportement dans le domaine temporel obtenu par transformation de Laplace inverse des expressions obtenues.

Bien que discret, l'ensemble des singularités, ou pôles, peut être infini. L'utilisation pratique du développement en singularités nécessite donc de montrer la précision des expressions tronquées, avec des nombres finis de pôles, ainsi que leur convergence. Cette étude est abordée dans un second temps dans le cas d'un système pour lequel des modèles analytiques existent : la cavité de Fabry-Perrot. D'abord dans le cas d'un slab diélectrique à indice de réfraction constant, puis dans le cas d'une fine couche d'or présentant de la dispersion et de l'absorption.

La méthode ainsi démontrée et testée avec un système maîtrisé, elle est ensuite utilisée dans le cas de la permittivité relative de différents matériaux. Cette fonction apparaissant comme une fonction de transfert dans les relations constitutives des équations de Maxwell, il est possible de lui appliquer un développement en singularités. Nous montrons que ce développement, qui résulte d'observations à l'échelle macroscopique, englobe et généralise les modèles microscopiques classiques de Lorentz, Drude et Debye utilisés pour décrire la permittivité diélectrique.

Dans un chapitre dédié, nous nous intéressons à la caractérisation des phénomènes de résonance en exploitant le développement en singularités et la factorisation en singularités et zéros. En remarquant que les termes résonnants associés aux pôles sont des transformations de Möbius transformant l'axe des fréquences réelles en cercles dans le plan complexe, nous décrivons les résonances comme des

perturbations dues à la présence des pôles et zéros. La contribution de ces derniers est quantifiée par une fonction de qualité que nous introduisons, pour toute forme de réponse spectrale, à toute fréquence. Calculée à partir de la phase des signaux, cette fonction généralise le facteur de qualité classique.

Enfin, nous présentons deux méthodes permettant de déterminer les pôles, résidus (coefficients de Laurent des pôles simples généralement rencontrés) et zéros complexes dans le domaine harmonique à partir de données simulées ou mesurées à des fréquences réelles. Les deux approches, basées sur l'auto-différentiation et la méthode de Cauchy, sont ensuite étudiées pour distinguer les pôles naturels, qui rendent compte de la physique des systèmes, des pôles effectifs, qui servent principalement à obtenir de bonnes approximations aux fréquences réelles.

Mots clés : singularités, fonctions de réponse, dispersion, modélisation, prolongement analytique, opérateurs de transfert

Abstract and keywords

The temporal dynamics of linear physical systems are described by response or transfer functions in the harmonic domain. The characterization of these functions of the frequency is highly important, as it allows to better understand the interaction of excitation signals with systems, to produce various effects such as resonances, or to design systems with well-defined and controlled responses.

The singularity expansion method starts with physical observations, namely the response of spherical resonators to sinusoidal electric fields, to analytically describe response functions in the harmonic domain. It is the starting point of this PhD manuscript, which attempts to derive, generalize and apply the singularity expansion method.

Starting from (quasi) non-restrictive fundamental properties of systems and response or transfer functions, an exact expression is obtained with the multiple-order singularity expansion. That natural description of these meromorphic functions relies on their discrete set of complex frequencies called singularities, as well as a non-resonant term accounting for the high-frequency behaviour. An alternative form, the singularity and zero factorization, is also introduced, along with the dynamics in the temporal domain by applying the inverse Laplace transform on the resulting expressions.

The discrete set of singularities can often be infinite. It is thus necessary to show that the truncated expressions are accurate in practice, and that they converge as poles are added. This task is performed in a study case for which analytical expressions are known for comparison: the Fabry-Perot cavity. We first look at a constant refractive index slab, then at the case of an absorbing and dispersive, thin layer of gold.

Once the accuracy of the method is tested and demonstrated, we use it in the case of the relative permittivity of different materials. It appears as a transfer function in the constitutive relations of the Maxwell equation, and thus possesses a singularity expansion. We show that this expansion, which results from the macroscopic behaviour of physical systems, encapsulates and generalizes the classical microscopic models of Debye, Drude and Lorentz, used to study the dielectric permittivity.

Thereafter, in the following chapter, we investigate the description of resonances by exploiting the singularity expansion and the singularity and zero factorization. By noticing that the resonant terms associated with the poles are Möbius transformations mapping the real frequency axis to circles in the complex plane, we describe resonances as perturbations induced by the presence of the poles and zeros. The contribution of the latter is quantified by a quality function that we introduce and characterize, for any form of spectral response, at any frequency. This quality function is derived from the phase of the signals and extends the classical notion of quality factor.

Finally, we present two methods to retrieve the complex poles, residues (the Laurent coefficients of simple poles, usually encountered in systems) and zeros in the harmonic domain, using experimental or simulated data acquired at real frequencies. The first approach is based on the Cauchy method, while the second one relies on auto-differentiation. We study both methods and discriminate between the natural poles, accounting for the underlying physics of the systems, and the effective poles, which mainly improve the approximations at real frequencies.

Keywords: singularities, response functions, dispersion, modeling, analytic continuation, transfer operators

Résumé étendu en français

Descriptions des fonctions de réponse dans le domaine harmonique

La notion de systèmes linéaires à invariance temporelle (LTIS = Linear Time-Invariant Systems) est apparue au cours du vingtième siècle en théorie du contrôle des systèmes et dans les domaines de l'automatique, de l'électronique, et de l'ingénierie électrique. Elle propose la description des LTIS comme des filtres agissant sur un signal excitateur pour produire une réponse. Dans le domaine harmonique, c'est-à-dire dans l'espace des fréquences plutôt que dans le temps, cette interaction est étudiée à travers une fonction dite de transfert, qui caractérise entièrement le LTIS étudié, et s'écrit comme le rapport de la réponse du système et de son excitation, peu importe le signal excitateur utilisé.

Il est courant d'approximer la fonction de transfert d'un système de deux manières différentes :

(i) Par une fonction rationnelle (le quotient de deux fonctions polynomiales) qui ne dépend que d'un nombre fini de fréquences complexes appelées zéros (les racines du numérateur) et pôles ou singularités (les racines du dénominateur). Cette modélisation est particulièrement adaptée à l'utilisation de diagrammes de Bode pour différencier les contributions individuelles des pôles et zéros à l'amplitude et la phase du signal.

(ii) Par une somme de termes résonnants ainsi qu'un terme correctif (background term), associés aux singularités des fonctions de réponse des systèmes. Bien que pouvant être déduite de l'approche précédente par décomposition en éléments simples, cette approximation apparaît intuitivement lorsqu'on considère la réponse de LTIS à des excitations sinusoïdales, comme c'est le cas dans la méthode du développement en singularités (SEM = Singularity Expansion Method).

Ces deux méthodes d'approximations sont en réalité des cas particuliers du développement généralisé en singularités d'ordres multiples (MOSEM = Multiple-Order Singularity Expansion Method), que nous démontrons dans un premier chapitre. Ce développement fournit une expression exacte d'une classe de signaux et de systèmes physiques : les LTIS causaux à conservation d'énergie. La méthode du développement en singularités permet naturellement un prolongement au plan des fréquences complexes sous forme de fonctions méromorphes.

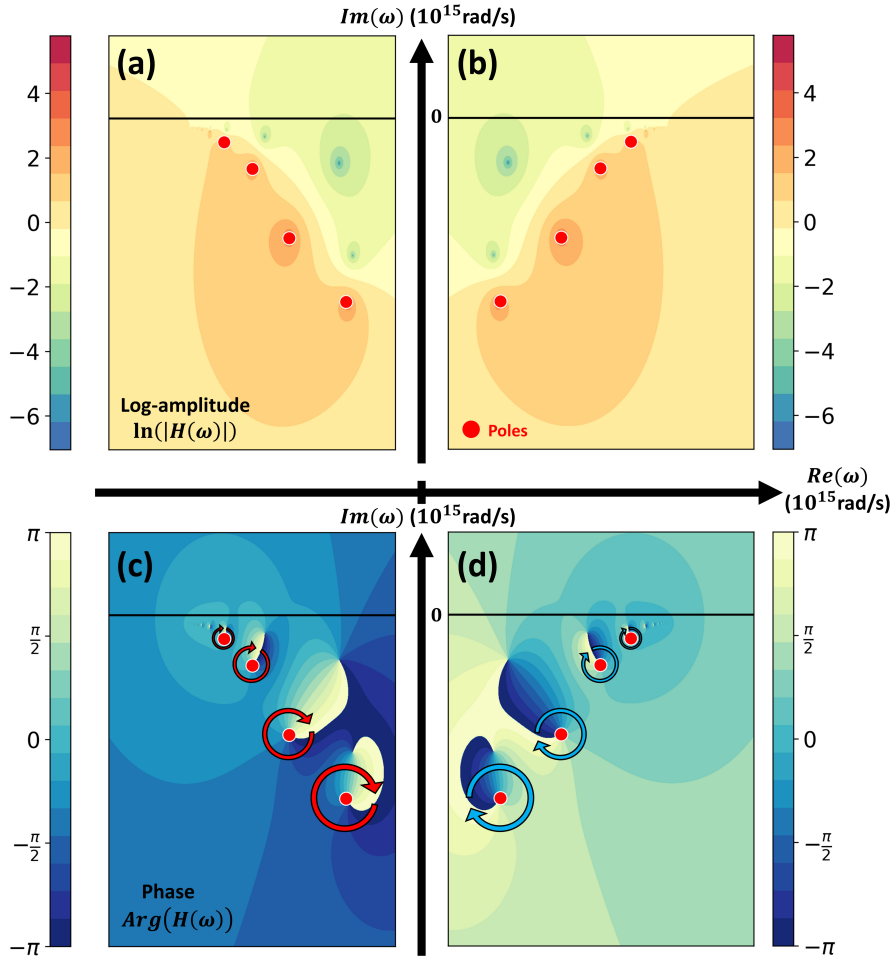

FIGURE 1. – *Diagramme de Bode complex du coefficient de réflexion $H(\omega)$ d'une fine couche d'argent. (a), (b) Log-amplitude de $H(\omega)$ dans une fenêtre spectrale complexe, symétrique par rapport à l'axe des imaginaires. (c),(d) Phase de $H(\omega)$ dans la même fenêtre spectrale, présentant cette fois-ci une antisymétrie par rapport à l'axe des fréquences imaginaires. La symétrie de la log-amplitude est associée à une distribution symétrique des pôles (points rouges) par rapport à l'axe des imaginaires. L'antisymétrie de la phase est mise en évidence par les flèches rouges et bleues, correspondant à un déphasage de 2π dans le sens trigonométrique direct autour des pôles avec des parties réelles négatives et positives respectivement.*

En résultent les deux expressions suivantes, calculées à partir des pôles p_ℓ et zéros z_ℓ ou coefficients de Laurent $\alpha(H, p_\ell, -m)$ (ou résidus à l'ordre 1) d'un signal physique $H(\omega)$:

Développement généralisé en singularités d'ordres multiples

$$H(\omega) = H_{\text{NR}} + \sum_{\ell} \sum_{m=1}^{\nu_\ell^{(p)}} \frac{\alpha(H, p_\ell, -m)}{(\omega - p_\ell)^m}$$

Factorisation en singularités et zéros

$$H(\omega) = H_0 \frac{\prod_{z_\ell}(1-\frac{\omega}{z_\ell})^{\nu_\ell^{(z)}}}{\prod_{p_\ell}(1-\frac{\omega}{p_\ell})^{\nu_\ell^{(p)}}}$$

H_{NR} est une constante qui dépend du comportement à l'infini de $H(\omega)$ dans le plan des fréquences complexes, nommée terme non-résonnant, H_0 est également une constante liée à la réponse statique $H(0)$. La symétrie Hermitienne impose des paires conjuguées de pôles, zéros, et coefficients de Laurent, ainsi que des constantes H_0 et H_{NR} réelles. Qui plus est, la causalité et la stabilité restreignent les pôles à la partie inférieure du plan complexe. Ces propriétés sont illustrées dans le cas du coefficient de réflexion d'une fine couche d'argent, Figure 1.

Connaissant le développement en singularités d'une fonction, nous montrons ensuite qu'il est possible de calculer facilement le comportement temporel par transformation de Laplace inverse, ce qui permet notamment de comprendre le rôle des pôles dans le régime transitoire, sur des temps courts, et le régime permanent.

Convergence et précision du développement en singularités

Les systèmes et signaux tels que précédemment définis sont rencontrés dans tout domaine de la physique. Le développement en singularités peut donc généralement être appliqué. Cependant, les ensembles de singularités, bien que discrets, sont potentiellement infinis. Il est alors important de vérifier que les expressions tronquées soient précises, et qu'il y a bien convergence avec le nombre de pôles.

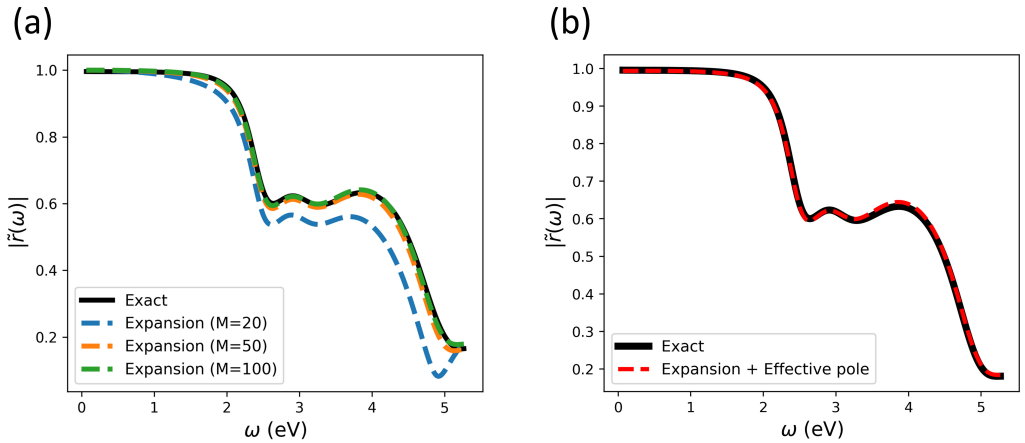

FIGURE 2. – *Module du coefficient de réflexion $|\tilde{r}(\omega)|$ pour des fréquences variant de l'IR à l'UV. (a) Convergence du développement en singularités en fonction du nombre M de paires de pôles. (b) Développement en singularités tronqué, avec $M = 15$ paires de pôles, corrigé par un pôle effectif $\omega_{\mathrm{eff}} = (10.41 - 1.38i)$ eV, son résidu associé $\rho_{\mathrm{eff}} = (1.26 + 4.62i)$ eV, et un terme non-résonnant $\hat{r}_{\mathrm{NR}} = (1.3 - 0.09i).10^{-1}$. Les trois paramètres ont été obtenus par optimisation via descente de gradient.*

Le chapitre 2 est dédié à cette tâche. L'étude des coefficients de réflexion et transmission d'une cavité de Fabry-Perrot, d'abord avec un indice de réfraction réel constant, puis avec absorption et dispersion, nous permet de tester la précision du développement en singularités dans les domaines temporels et harmoniques. Nous montrons que lorsque le nombre de pôles augmente, l'erreur entre les coefficients de réflexion et transmission calculée avec le modèle d'Airy (forme exacte) et avec le développement en singularités diminue. Nous introduisons également la notion de pôles effectifs, qui prennent en compte la contribution des singularités se trouvant en dehors de la fenêtre spectrale étudiée, et permettent ainsi d'obtenir une grande précision avec peu de pôles, comme illustré sur la Figure 2.

Application à la permittivité diélectrique

La permittivité diélectrique des matériaux linéaires apparaît naturellement comme une fonction de transfert dans les relations constitutives des équations de Maxwell. Elle est donc décrite par son développement en singularités dans le domaine harmonique.

Relative Errors of the Fitting				
Material	N	M	error_2 (%)	error_∞ (%)
Au	5	1	0.272	0.247
Ag	3	2	0.854	0.964
Co	5	1	0.145	0.070
Cr	3	1	0.542	0.834
HfO_2	2	0	0.074	0.276
SiO_2	2	0	0.287	1.192
TiO_2	3	0	0.237	0.763
Ta_2O_5	6	0	0.515	1.180
Graphene	5	1	0.331	0.843

TABLE 1. – *Erreurs relatives L_2 et L_∞ du modèle généralisé de Drude-Lorentz par rapport aux données expérimentales de 9 matériaux. Plus l'erreur relative est basse, plus la précision est élevée. Les paramètres N et M représentent respetivement le nombre de termes généralisés de Lorentz, et le nombre de termes de Debye/Drude.*

Dans un troisième chapitre, nous montrons que le développement en singularités peut être réécrit en un modèle de Drude-Lorentz généralisé (GDL = Generalized Drude-Lorentz model), qui englobe et généralise les modèles classiques de Drude, Lorentz et Debye :

Modèle de Drude-Lorentz généralisé

$$\hat{\varepsilon}(\omega) = \varepsilon_{\text{NR}} + \frac{\gamma_0}{\omega} - \sum_{\ell=1}^{M} \frac{\omega_{b,\ell}^2}{\omega^2 + \mathrm{i}\omega\gamma_\ell} - \sum_{\ell=1}^{N} \frac{\mathrm{i}s_{1,\ell}\omega\Gamma_\ell + s_{2,\ell}\omega_{0,\ell}^2}{(\omega^2 - \omega_{0,\ell}^2) + \mathrm{i}\omega\Gamma_\ell}$$

On passe ainsi d'une description à l'échelle macroscopique des matériaux comme systèmes physiques à une description à l'échelle microscopique. On montre en particulier l'importance des termes généralisés de Lorentz, qui contiennent un terme imaginaire additionnel au numérateur dépendant de la

fréquence, sans lequel la description précise de la permittivité relative de nombreux matériaux est impossible, notamment pour les diélectriques. Ce terme correspond, dans le domaine temporel, à une contribution de la dérivée du champ électrique au champ d'induction.

Nous appliquons le GDL à différents matériaux, et obtenons systématiquement des approximations très précises de la permittivité relative avec un faible nombre de paramètres. Ces résultats sont illustrés dans le Tableau 1 et la Figure 3. Les paramètres du GDL sont obtenus avec une méthode basée sur l'auto-différentiation.

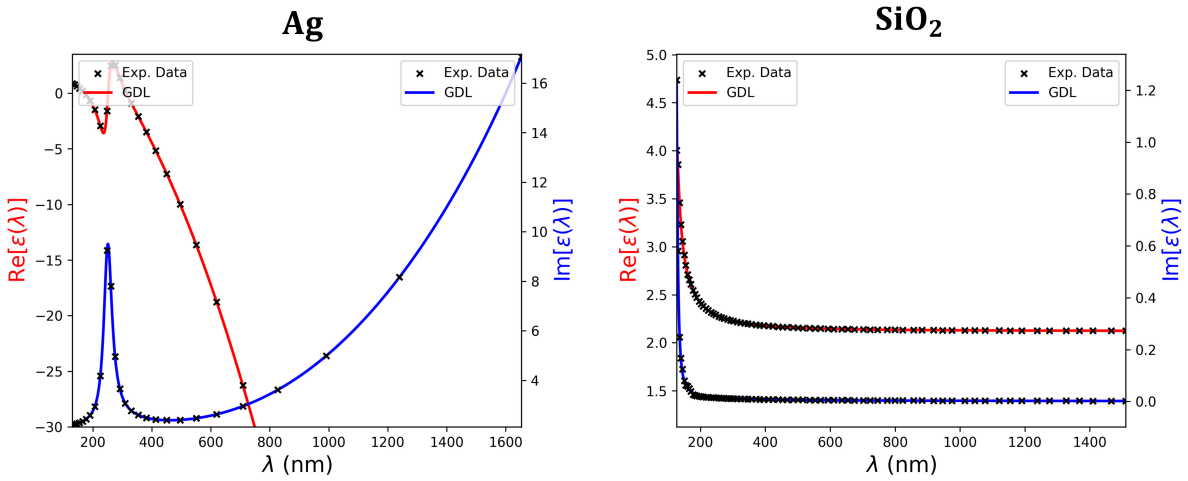

FIGURE 3. – *Partie réelle (courbe rouge, ordonnées à gauche) et partie imaginaire (courbe bleue, ordonnées à droite) des fonctions de permittivité relative de Ag et de* SiO_2*, calculées avec le modèle de Drude-Lorentz généralisé optimisé (traits pleins), et comparées aux données expérimentales (croix noirs). Les fonctions de permittivité sont exprimées ici comme des fonctions de la longueur d'onde plutôt que la fréquence, rendant ainsi mieux compte de la largeur des fenêtres spectrales, s'étendant de l'UV à l'IR. L'amplitude pour Ag croît rapidement au-delà de* $380nm$*, en accord avec son comportement métallique. Dans le cas de* SiO_2*, la permittivité relative est quasi-constante sur l'ensemble de la fenêtre, avec une partie imaginaire proche de* 0*, comme on s'y attend de la part d'un matériau diélectrique ne présentant pas d'absorption.*

Enfin, en convertissant les paramètres du GDL en pôles et résidus, nous montrons qu'il est possible de caractériser les milieux directement avec leurs distributions de pôles. Les termes de Drude sont associés à des singularités imaginaires proches de l'origine, et une à l'origine, et correspondent à des charges libres dans le milieu. Les termes de Lorentz marquent des transitions d'un régime à un autre, notamment le passage d'un comportement métallique à un comportement diélectrique.

Fonction de qualité d'une fonction de réponse

Les pôles, zéros et résidus sont des propriétés fondamentales des fonctions de réponse, et sont intrinsèquement liés à leurs résonances. Lorsqu'une résonance est isolée, il est facile de lui associer un facteur de qualité lié aux pôles, qui informe de la finesse spectrale de la résonance. Dans le cas plus général de fonctions de réponse arbitraires, la quantification de l'effet des pôles et zéros est plus complexe, et il n'est souvent pas possible de définir un facteur de qualité. Dans le chapitre 4, nous nous intéressons à

la quantification des contributions des pôles et zéros sur toute fonction de réponse.

Le développement en singularités est écrit explicitement sous la forme de transformations de Möbius, qui font correspondre des cercles dans le plan complexe à l'axe des fréquences réelles :

Transformations de Möbius dans le développement en singularités

$$H(\omega) = H_{\mathrm{NR}} + \sum_{\ell} C_\ell + |C_\ell| e^{\mathrm{i}\phi_\ell(\omega)}$$

Chacun de ces cercles, de rayon $|C_\ell|$ et de coordonnée angulaire $\phi_\ell(\omega)$ caractérise une résonance isolée particulière, et permet de décrire une résonance comme une perturbation aux alentours d'une singularité. A partir de la dérivée fréquentielle $\partial_\omega[\phi_\ell](\omega)$ de cette coordonnée angulaire, nous définissons une fonction de qualité $\eta_\ell(\omega) = \frac{\omega}{2}\partial_\omega[\phi_\ell](\omega)$ du terme résonnant associé au pôle $p^{(\ell)}$. Cette fonction de qualité est en accord avec le facteur de qualité lorsqu'on l'évalue à la fréquence spécifique correspondant à la partie réelle du pôle $\omega = \mathrm{Re}[p^{(\ell)}$. De manière plus générale, elle étend le facteur de qualité à toute fréquence en quantifiant la contribution du terme résonnant à la fonction de réponse en ω. On montre que $\eta_\ell(\omega)$ peut être obtenue directement à partir de la phase $\Psi_\ell(\omega)$ du terme résonnant :

Fonction de qualité d'un terme résonant isolé

$$\eta_\ell(\omega) = \frac{\omega}{2}\partial_\omega[\Psi_\ell](\omega)$$

Dans le cas d'interactions non négligeables entre les termes résonnants (et le terme non-résonnant), cette définition de la fonction de qualité à partir de la phase $\Psi(\omega)$ du signal est généralisée. On montre, grâce à la factorisation en singularités et zéros, que $\eta(\omega) = \frac{\omega}{2}\partial_\omega[\Psi](\omega)$ est une fonction méromorphe entièrement caractérisée par la distribution des pôles et zéros du signal $H(\omega)$, qui informe de l'influence de ces fréquences complexes sur la fonction de réponse.

Fonction de qualité $\eta(\omega)$ de la fonction de réponse $H(\omega)$

$$\eta(\omega) = +\frac{\mathrm{i}}{4}\sum_{\ell}\left[\frac{p^{(\ell)}}{\omega - p^{(\ell)}} - \frac{\overline{p^{(\ell)}}}{\omega - \overline{p^{(\ell)}}}\right] - \frac{\mathrm{i}}{4}\sum_{\ell}\left[\frac{z^{(\ell)}}{\omega - z^{(\ell)}} - \frac{\overline{z^{(\ell)}}}{\omega - \overline{z^{(\ell)}}}\right]$$

La Figure 4 illustre le calcul et l'intérêt de la fonction de qualité $\eta(\omega)$ dans le cas de la réponse en réflexion (ordre 0) d'un réseau de diffraction en or présentant des anomalies.

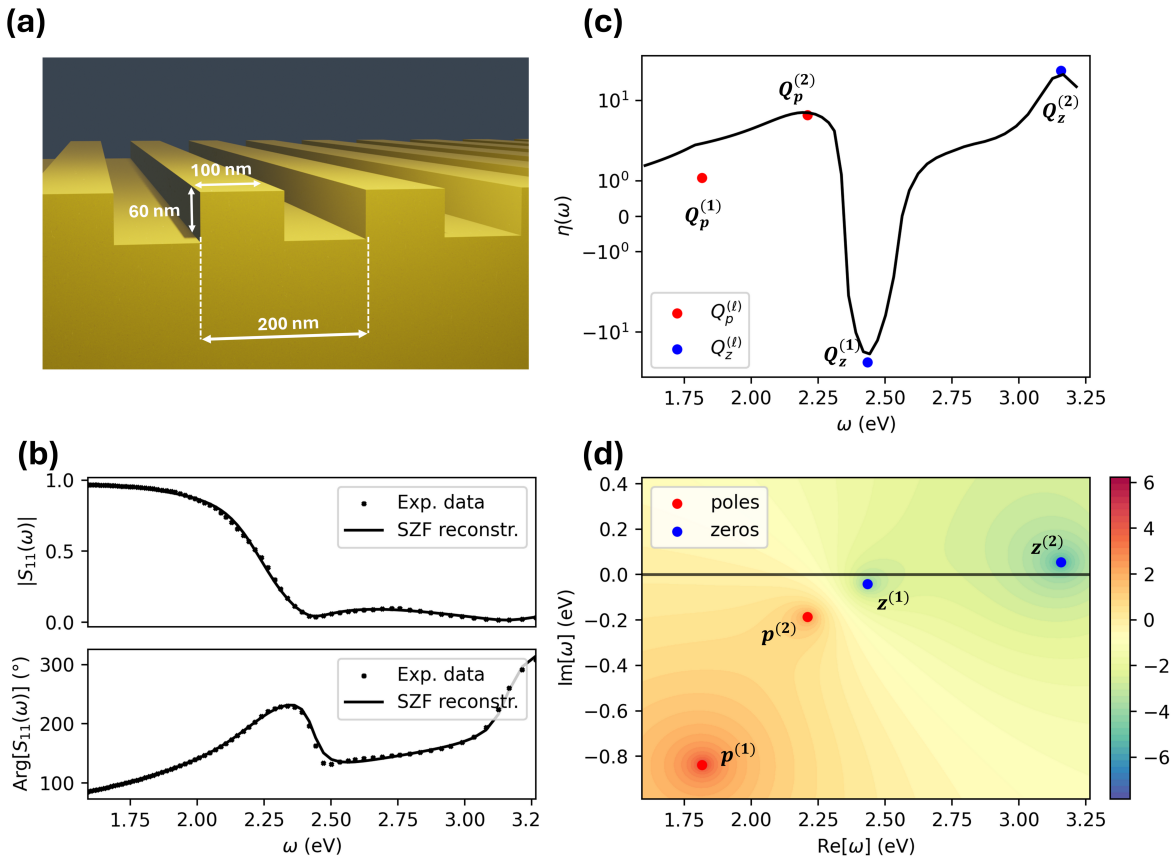

FIGURE 4. – *Fonction de qualité $\eta(\omega)$ du coefficient de réflexion $S_{11}(\omega)$ à l'ordre 0 d'un réseau de diffraction en or, illustré en (a). (b) Diagramme de Bode de $S_{11}(\omega)$ (Exp. data, pointillés), calculée avec la méthode de Cauchy (SZF reconstr., trait plein). Une résonance large est observée à faible ω, avec une amplitude lentement décroissante et un gain de phase important, qui semblent associés au pôle complexe $p^{(1)}$ en (d), loin de l'axe réel. Cependant, la fonction de qualité en (c) montre un maximum local autour de 2.20 eV, qui résulte de la présence du pôles $p^{(2)}$ plus proche de l'axe réel dans le plan des ω complexes. Le terme résonant associé à ce pôle apporte donc la plus grande contribution à la phase autour de cette fréquence. Les facteurs de qualité des pôles ($Q_p^{(\ell)}$, points rouges) et des zéros ($Q_z^{(\ell)}$, points bleus) sont représentés en (c), où un bon accord est observé avec $\eta(\omega)$, malgré de faibles écarts dus à l'influence des autres pôles et zéros.*

Calcul des pôles, zéros et résidus à partir de données expérimentales acquises aux fréquences réelles

Ayant montré l'intérêt du développement en singularités et de la factorisation en zéros et singularités comme représentations naturelles des fonctions de réponses de systèmes physiques, il reste à décrire la manière dont les paramètres de ces expressions, à savoir les pôles, résidus et zéros, peuvent être obtenus. Nous souhaitons souligner l'importance de cette tâche, sans laquelle l'ensemble des expressions ne peut être utilisé en pratique. Le calcul des paramètres est d'autant plus crucial et intéressant qu'il est réalisé à partir de données expérimentales ou de simulations aux fréquences réelles, ne demandant alors pas d'effort supplémentaire lors de la réalisation des jeux de données. Dans le dernier

chapitre, nous présentons deux approches pour approximer les fonctions de réponses avec précision en déterminant les pôles, résidus et zéros.

La première approche part de la méthode de Cauchy et l'optimise pour prendre en compte les propriétés des systèmes physiques. Cette approche fournit, par utilisation d'algèbre matricielle, une approximation rationnelle de la fonction de réponse.

La second approche est basée sur l'auto-différentiation, récemment développée dans le cadre de l'apprentissage automatique. Elle consiste à résoudre un problème d'optimisation en utilisant une fonction de coût non triviale pour laquelle il est difficile d'obtenir une expression algébrique du gradient. Cette approche est plus adaptée au calcul des paramètres du développement en singularités sous sa forme basique, comme modèle de Drude-Lorentz généralisé, ou encore comme transformations de Möbius.

Les distributions de pôles obtenues dans le plan des fréquences complexes par application des deux approches présentent deux types de singularités : les pôles naturels, qui apparaissent dans le régime transitoire de la réponse temporelle et qui sont donc physiquement pertinents, et les pôles effectifs qui permettent principalement de réduire l'erreur faite lors de l'approximation. Nous définissons de manière plus pratique les pôles naturels comme les singularités qui se trouvent à l'intersection des distributions obtenues avec les deux approches. Une méthode est proposée pour les retrouver rapidement, consistant à utiliser séquentiellement la méthode de Cauchy puis l'approche par auto-différentiation. Nous montrons que cela permet de détecter les singularités qui ne se déplacent pas ou peu dans le plan complexe et qui correspondent donc à des pôles naturels potentiels, ainsi que d'améliorer la qualité de la reconstruction, comme illustré sur la Figure 5 où la fonction de réponse est le coefficient de réflexion d'une métasurface composée de nanodisques de Si sur un substrat de verre (simulation et données fournies par Jayeeta AMBOLI).

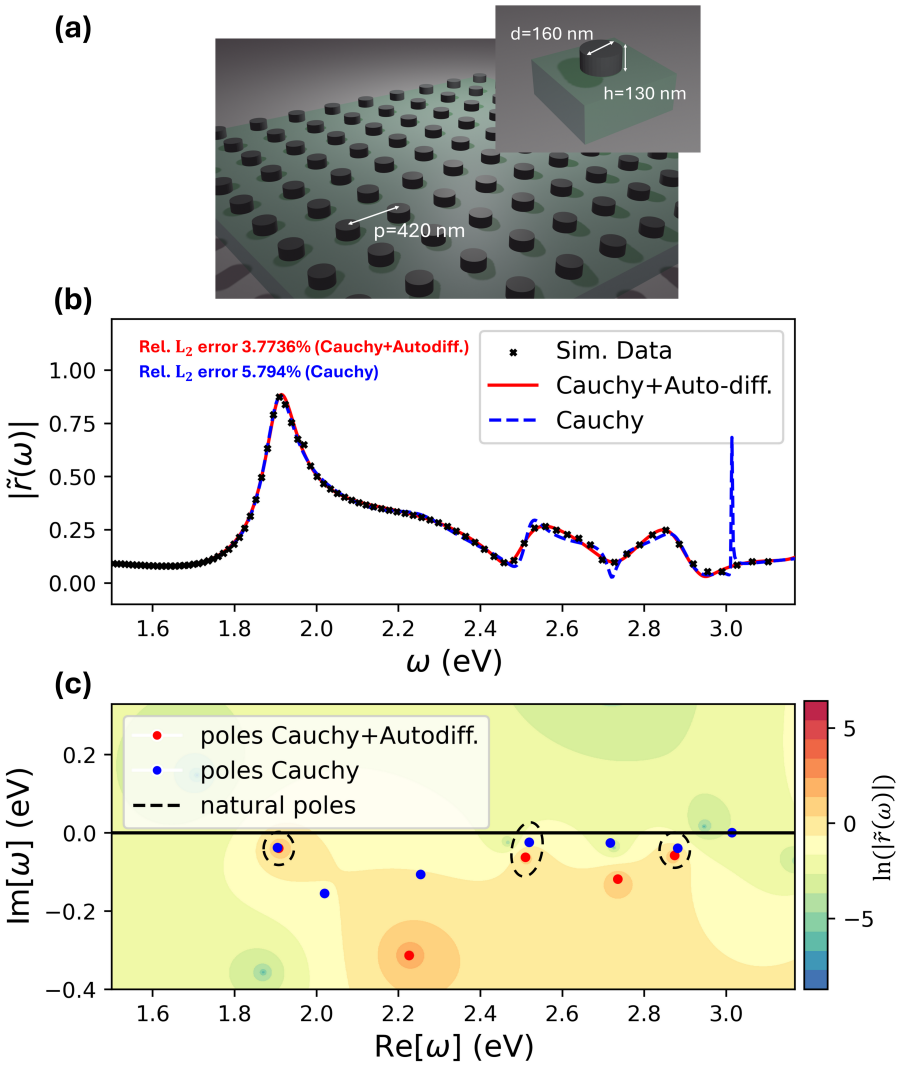

FIGURE 5. – *(a) Métasurface constituée de nanodisques de Si de diamètre $d = 160$ nm et hauteur $h = 130nm$ distribués en un réseau de période $p = 420$ nm sur un substrat de verre (simulation et données fournies par Jayeeta AMBOLI). (b) Coefficient de réflexion $\tilde{r}(\omega)$ d'une métasurface constituée de nanodisques de Si, sur substrat de verre, illuminée en incidence normale. La reconstrubtion est effectuée avec la factorization en pôles et zéros en utilisant la méthode de Cauchy seule d'abord (courbe bleue, discontinue), puis séquentiellement avec l'approche basée sur l'auto-différentiation (courbe rouge, continue). Une erreur relative L_2 de 5.794 % est obtenue pour la première approche, réduite à 3.774 % avec l'approche séquentielle. (c) Distribution des pôles associés à chaque reconstruction dans le plan des ω complexes. Des singularités supplémentaires sont situées en dehors de la fenêtre étudiées. Les singularités qui se superposent, ou sont très proches sont des pôles naturels potentiels.*

List of acronyms

DL
Drude-Lorentz model. 96, 100, 107, 183

EEE
Electric and Electronics Engineering. 29, 31, 33, 35, 37, 160

GDL
Generalized Drude-Lorentz model. 97, 104–111, 113, 147–149, 158, 161, 163, 164, 181, 183, 185

IRF
Impulse Response Function. 51, 53, 71, 76, 77, 79–82, 91, 93

LTIS
Linear Time-Invariant System. 33–35, 38, 39, 47, 48, 51–53, 65, 67, 93, 160

MOSEM
Multiple-Order Singularity Expansion Method. 42–46, 49–51, 53, 54, 61, 62, 65, 67, 68, 105, 160

MTSE
Möbius Transformations in the Singularity Expansion. 120, 148, 150, 151, 158, 162–164

ODE
Ordinary Differential Equation. 64–67

PDE
Partial Differential Equation. 64, 65

PZF
Pole and Zero Factorization. 37, 38, 47, 51

Q-factor
Quality-factor. 26, 31, 116, 124, 130–132, 162

QNM
Quasi-Normal Mode. 30, 35

SEM
Singularity Expansion Method. 26, 30, 31, 35, 71, 74, 77, 80, 85, 86, 88, 89, 91–93, 97, 98, 100, 102, 103, 114, 116, 117, 120, 126, 132, 135, 136, 142, 144, 147–150, 152, 153, 155, 157, 158, 160–162, 164

SPE

Simple Pole Expansion. 35, 37, 43, 51

SVD

Singular Value Decomposition. 141

SZF

Singularity and Zero Factorization. 47, 49–51, 53, 56, 57, 67, 68, 105, 116, 126–128, 130, 132, 135, 136, 138, 140–142, 144, 155–158, 160, 162, 163

Glossary

causal

See causality. 52–54, 59, 62–64, 66, 67, 84, 85, 87, 91, 93, 99, 117, 161

causality

Causality states that a system cannot react to an excitation before it has received it. Consequently, any physical signal must have been generated at some point in time and space.. 20, 25, 52, 53, 57, 63, 65–67, 85, 86, 119, 160

continuity

See continuous. 63

continuous

A continuous system is such that the response of the limit is the limit of the response, with respect to some (weak) topology. 20, 33

deterministic

A deterministic system always associate the same output to a set excitation. 33

energy conservation

Energy conservation states that the energy exciting a system cannot exceed what was received. By extension, it states that a physical signal must have a finite support or decay exponentially with time and space. 51, 53, 67, 93, 97, 117, 160

linear

In a linear system the response is proportional to the excitation. 20, 25, 26, 33, 37, 71, 86, 88, 117, 132, 160, 161, 164

linearity

See linear. 160

passive

Passive systems are such that the energy of their response decreases over time. 20, 21, 59, 60, 62, 64, 73, 86, 99, 117, 143, 160

passivity

See passive. 97, 143

permittivity

Permittivity tensor or function of a medium. 96, 97

physical signal

Causal signal, temporally or spatially decaying which interacts with a physical system. Physical signals are expressed as complex exponential pre-factored polynomials.. 29, 53, 57, 59–61, 63, 64, 67, 86, 97, 117, 135, 136, 143, 158, 160, 161, 163

physical system

Entity or object interacting with an input to generate an output. 25, 26, 31, 34, 53, 57, 58, 60–67, 69, 71, 73, 75–77, 93, 97, 99, 113, 114, 116, 117, 119, 126, 132, 135, 136, 140, 147, 149, 152, 158, 160, 161, 163, 164

relative permittivity

Scalar relative permittivity function of a medium. 97–111, 114, 122, 135, 142, 149, 150, 161, 181, 185, 186

stability

See passive. 25, 35, 53, 57, 60, 67, 71, 116, 119, 143, 148

system

Entity or object interacting with an input to generate an output. 25, 26, 29–31, 33–35, 37, 38, 47, 51–53, 60–62, 64, 66, 76, 86, 93, 97, 99, 114, 116, 117, 129, 132, 136, 143, 147, 158, 160, 164

time-invariant

The response of a time-invariant system does is as much time-shifted as the excitation is . 33

transfer function

Harmonic domain function linking an input signal to an output signal. 25, 31, 33–35, 37, 39, 47, 48, 51, 53, 54, 60, 62–65, 67, 69, 71, 73, 76, 93, 96, 97, 108, 113, 126, 132, 140, 156, 158

transfer operator

Harmonic domain operator linking a vector input to a vector output. 25, 29, 30, 72, 73, 135, 160

Contents

Liste de publications et participation aux conférences 3

Résumé et mots clés 5

Abstract and keywords 7

Résumé étendu en français 9

List of acronyms 18

Glossary 20

Preface 25

Introduction 27

1. Analytical Description of Physical systems 32
- 1.1. Linear time-invariant systems . . . 33
  - 1.1.1. Transfer functions and signals in the harmonic domain . . . 33
  - 1.1.2. Approximating transfer functions with poles and zeros . . . 35
- 1.2. Generalized expressions in the harmonic domain . . . 39
  - 1.2.1. Multiple-Order Singularity Expansion . . . 39
  - 1.2.2. Singularity and Zero Factorization . . . 44
- 1.3. Constraints in the harmonic domain . . . 51
  - 1.3.1. Properties of physical systems and signals . . . 51
  - 1.3.2. Hermitian symmetry . . . 53
  - 1.3.3. Stability and Causality . . . 57
- 1.4. Temporal dynamics . . . 61
  - 1.4.1. Inverse Laplace transform of harmonic signals . . . 61
  - 1.4.2. Response to a causal sinusoidal input . . . 62
  - 1.4.3. Retrieving transfer functions from the physical domain . . . 64
- 1.5. Conclusion . . . 67

2. Singularity expansion of a symmetrical Fabry-Perot cavity 70
- 2.1. Cavities and resonances . . . 71
- 2.2. S matrix and impulse response of a non-dispersive slab . . . 72
  - 2.2.1. Singularity expansion of the S matrix . . . 72
  - 2.2.2. Impulse Response Function . . . 76

2.3. Times dynamics for different excitation pulses . . . 80
2.3.1. Extremely narrow Gaussian Pulse . . . 81
2.3.2. Gaussian and rectangular envelopes . . . 81
2.3.3. Accuracy and convergence of the temporal singularity expansion . . . 82
2.3.4. From transient to permanent regime . . . 84
2.4. Case of a lossy and dispersive metallic slab . . . 88
2.4.1. Distribution of the poles . . . 88
2.4.2. Pole expansion in the harmonic and temporal domains . . . 89
2.5. Conclusion . . . 93

3. The dielectric permittivity of materials and structures 95
3.1. Derivation of the Generalized Drude-Lorentz model . . . 96
3.1.1. Different models for the permittivity . . . 96
3.1.2. The permittivity as a transfer function . . . 97
3.1.3. Generalized Drude-Lorentz expression . . . 100
3.2. Retrieving the parameters from experimental data . . . 105
3.2.1. Analytical continuation of the permittivity from experimental data . . . 105
3.2.2. Characterization of the materials with the distribution of the poles . . . 109
3.3. Conclusion . . . 113

4. Characterizing resonances in arbitrary response functions 115
4.1. Isolated resonances and resonant terms . . . 116
4.1.1. Quantifying the strength of resonances . . . 116
4.1.2. Resonant terms as Möbius transformations . . . 117
4.1.3. Describing isolated resonances with the angular coordinate . . . 120
4.2. Characterizing overlapping resonant terms . . . 126
4.2.1. From residues to zeros . . . 126
4.2.2. Quality function of the full response function . . . 129
4.3. Conclusion . . . 132

5. Retrieving the poles, residues and zeros of the response functions of an arbitrary physical system 134
5.1. Introduction . . . 135
5.2. The Cauchy method for rational approximations . . . 137
5.2.1. Overview of the original method . . . 137
5.2.2. Physics informed optimization . . . 140
5.3. Auto-differentiation approach for the singularity expansion . . . 144
5.3.1. Formulating the optimization problems . . . 144
5.3.2. Other forms of the singularity expansion . . . 147
5.4. Natural and effective poles . . . 152
5.5. Conclusion . . . 158

Conclusion 160

Bibliography 165

ANNEXES **180**

A. The dielectric permittivity of materials and structures **181**

A.1. Retrieving the generalized Drude-Lorentz model 181

A.2. Performance and parameters of the optimized models 185

Preface

Before delving into the reading of this manuscript, let me present a global overview of its content, without all the technicality and the details that might eclipse a more intuitive and physical interpretation of this work.

When studying different fields of linear wave physics, we notice similarities in the way we describe seemingly unrelated phenomena. While it can be unsettling at first, it rapidly starts to make sense: all physical systems abide by the same rules, set by the same never-changing fundamental laws of physics. That observation suffices to intuitively understand the various models which offer a unified description of the systems.

Among these models, the S-matrix formalism is among the most regularly encountered in wave physics. In electromagnetism and optics for instance, the Fresnel coefficients at an interface between two media, the reflection and transmission coefficients through a stack of thin films, the diffraction orders of a grating, or even the scattering parameters of a cavity, are all components of the S-matrix or, more generally, transfer operators.

The transfer operator (or transfer function) formalism is of great interest, for its simplicity and its ability to describe the behaviour of a system at any frequency, *i.e.* in the harmonic domain, as it interacts with an excitation field. This description frequency by frequency is useful when we perform measurements or when were are interested in a short spectral range. However, in order to obtain more information on the underlying physics of the system, we would like to connect the behaviours at these different frequencies. Is this something that can be achieved with the transfer function formalism? More generally, are there restrictions to the shape of the response of the system? Can any form be obtained?

Had the answers to these questions been negative, there would have been little use for the transfer function formalism. The transfer operators of linear systems possess complex frequencies where their values are infinite. These complex frequencies, called singularities or poles, are often used in expansions to approximate the behaviour of the systems over real frequency windows. As such, they bind the dynamics of a system over the different frequencies of that range. In addition, properties such as causality and stability constrain the positions of the singularities, and thus they shape the response curves. Some models even link the poles to specific phenomena in a system. Nonetheless, they are solely introduced and presented to us as convenient mathematical artifices. We can thus wonder how relevant these complex frequencies called poles are for physical systems. How much of the dynamics of a system can be characterized by them?

This manuscript first attempts to address all these questions. We show that the complex poles are intrinsic properties of the physical systems. They are the direct cause of the (measured) response of a system at a real frequency. The discrete set of poles appears in the unique analytical expressions of the Singularity Expansion Method (SEM), which we rigorously derive in Chapter 1. The SEM does not provide approximations, and instead it yields an exact description of the temporal dynamics and spectral response of any linear system or phenomenon encountered in physics. And it does so by expanding the response functions from the real frequency axis to the complex frequency plane. The complex plane is thus not just an efficient or convenient mathematical tool to study systems. It turns out that physical systems are naturally characterized by their behaviour in the complex frequency plane. We show these properties first in Chapter 2, where we demonstrate the accuracy of the SEM with a small, finite set of poles by studying the S-matrix of a Fabry-Perot cavity. Then, in Chapter 3, where we use experimental data acquired at real frequencies to retrieve the permittivity of various materials in the complex frequency plane and describe them with high accuracy at real frequencies.

The fundamental role of singularities allows us to go even further as we use the SEM to improve our knowledge of different important phenomena. In Chapter 4, the phenomenon we look at is that of resonances. We derive a function which extends the classical Quality-factor (Q-factor), and quantifies the effect of resonances at any frequency, for any shape of the response curve, no matter its complexity. We show that this function, even if its depends on the poles and their distribution in the complex plane, can be easily retrieved using the phase, at real frequencies, of a measured signal.

A physical system possesses a unique SEM expression, and therefore a unique distribution of singularities in theory. This further highlights the natural description of systems in the complex frequency plane, with poles as intrinsic properties. This justifies the use of data acquired at real frequencies to retrieve the poles and reconstruct the response function of a system. The final chapter, Chapter 5, focuses on the execution of that task in a way that ensures a good reconstruction, but also the identification of the singularities which are characteristic of the systems.

The first chapters introduce the SEM as a sound theoretical formalism offering a unified, natural description of physical systems. The last chapter is of the utmost importance, as it allows allows us to go beyond that. For any measured or simulated data, we are able to to find a few complex parameters which characterize the system and can be used to accurately model its behaviour at real frequencies but also in the complex frequency plane. We obtain a practical formalism with a rigorous base which can easily be applied to characterize, design and control physical systems.

Introduction

Superposition principle and modes

Let me start this manuscript with a question: what are the common features between a vibrating string, an electric circuit, a quantum well, the diffusion of heat through a metallic rod, and the light reflected by a mirror? Nowadays, we know that all these phenomena occurring in very different fields of physics, can all be described through linear partial or ordinary differential equations. The solutions to these differential equations are combinations of sinusoidal fields, functions of the time, which are obtained through a common method [1–5]. This unified description of phenomena in linear systems is extremely recent in the history of physics, and it is based on two distinct yet intertwined concepts, which are perceived as one, to this day, in many cases: the superposition principle [6–8] and the mode expansion [9, 10].

In 1690, Christiaan Huyguens published his **Treatise on Light** [11], where he developed the idea of light as waves. He described sources of light as emitters of spherical waves which would interact with the surrounding matter, from which secondary waves would then originate, interacting with matter further away, and so on and so forth. This description of light as a sum (or superposition) of all these secondary sources accurately described the propagation of visible light from a source to an observer in a particular shape or wavefront. But while many phenomena were explained by this approach, other important ones were missing. As a result, the work of Huyguens on light was eclipsed by Sir Isaac Newton's corpuscular theory of light formalized in his own treatise **Opticks** [12], published in 1704.

Newton made major contributions to a wide range of fields both in physics and mathematics. His work had a resounding impact, making him (hardly arguably) one of the most influential scientists, inspiring others to follow up on his work for the following century (although his legacy lasts to this day). Among them, the most prominent one in the second half of the eighteenth century was probably Pierre-Simon de Laplace. Laplace was considered by many (including himself) as the successor or Newton [13–16]. He rapidly obtained an outstanding position in France, thanks to Jean le Rond d'Alembert, which he used to establish an elite circle of mathematicians, chemists, and physicists (not limited to France) made of young graduates from Ecole Polytechnique, such as Claude Louis Berthollet, Jean-Baptiste Biot, François Arago, Louis Joseph Gay-Lussac, or Siméon-Denis Poisson, but also influencial figures in the likes of the Bernoulli family, Joseph-Louis Lagrange, Adrien-Marie Legendre, and later Joseph Fourier [15].
Two popular problems at the time were those of the diffusion of heat in metal plate, and of a vibrating string [9]. Daniel Bernouilli, Leonhard Euler and d'Alembert layed the foundation of the Fourier analysis as they studied these problems. Euler derived in 1748 a solution in the form $x - vt$ [17]. Concurrent to that, following a discussion started in 1727 with his father John Bernoulli, Daniel Bernoulli provided

elementary solutions in the case of the vibrating string, which could be used to expand any other solution to the problem. It resulted in the first description of the superposition principle, by him, in 1753 [7]. In such cases, where the problems can be reformulated as the studies of the temporal dynamics of systems described by ordinary differential equations, the ideas of the mode expansion and the superposition principle were thus equivalent. Euler and Lagrange rejected the idea, and it was not until 1807 that the principle was shown to be a particular case of the now called Fourier series, first introduced in Fourier's **Mémoire sur la propagation de la chaleur dans les corps solides** [8], and further developed, along with the Fourier transform, in his **Théorie analytique de la chaleur** [18] published in 1827. Laplace also took interest in the subject and would later claim that his solution was more general and rigorous than that of Fourier. In any case, these developments were the stepping stones towards wave physics, yet they had been discovered by adepts of Newtonian physics who were almost all firmly against the idea of wave phenomena. The Laplace era would also mark the beginning of mathematical physics, and a definite separation between the way models were perceived in physics: Newton believed that the sole purpose of models was to describe phenomena and that no assumptions should be made [15], while a more recent view is that a good model not only explains phenomena, but also provides accurate predictions, as stated much later by Richard Feynman during his famous lectures between 1961 and 1963 [10].

Eventually, the field of wave physics rapidly grew in the nineteenth century. First with the interference theory of Thomas Young, who continued and improved the work of Huyguens on the wave theory of light [16, 19]. He was able to go further, and could finally explain some phenomena such as interference patterns. However, the lack of mathematical rigour in his work made many scientists reluctant to accept this alternative to the light particle theory of Newton, and his work reached France quite slowly. At the same time in France, Augustin Fresnel was developing his own theory of light as waves [15]. His work was performed independently of those of Young since he did not speak english. He was however inspired by the theory of light of Huyguens, which he was made aware of by Arago. Approximately ten years after Young, starting from 1815 [16, 20], Fresnel finally published his results and theory on that novel approach. His great skills in mathematics helped him in developing integral formulae modeling the superposition of propagating waves to form different shapes, and in particular light rays. Many phenomena such as diffraction could be explained, and prediction could even be made (the Arago spot for instance). The high accuracy of the calculations that resulted from these integrals, with respect to observations and measurements, was such that it was impossible for the Académie des Sciences to reject the theory [15, 20]. Fresnel theory was different from the Newtonian approach, where solutions to ordinary differential equations describing the fundamental interactions of particles were searched for. No one knew, yet, to which differential equation, if any, Fresnel had found a solution (and it was only known much later that this was a solution to a partial differential equation). What is more, the original idea of a discrete set of modes as elementary solutions was not compatible with the continuous set of waves summed in the integrals through the superposition principle.

The superposition principle applies in most situations with no regard for the specifics of the physical problem considered and the boundary or initial conditions. As previously mentioned, the first description of that concept by Daniel Bernoulli is actually a specific case of the Fourier series. Nowadays, we can state that in a broad range of physical problems, this is tantamount to stating that the physical quantities at play possess a Fourier transform. In the particular case where we expect the solutions to

be periodic with known boundary or initial conditions, we retrieve solutions as Fourier series, which are intimately linked to the modes of the then considered system. The set of modes can thus be defined, in general, as the discrete set of elementary solutions to a homogeneous differential equation with known boundary conditions.

Singularity and mode expansions in modern physics

Following a revolution of physics initiated by Newton at the end of the 17th century, the birth of mathematical physics with the Laplace era in the 18th century, and the development of wave physics owed to Fresnel in the beginning of the 19th century, another revolution occurred in the 19th century with the work of James Clerk Maxwell, on par with the one initiated by Newton. Maxwell was a mathematician before being a physicist. Upon his discovery of the works of Fourier, he became interested in the use and description of differential forms which he later used to write the Maxwell Equations, but also in thermodynamics [15]. While many novelties were brought about by Maxwell, the main ones are his well-known contributions as pioneer in statistical physics and electromagnetism, and the lesser-known birth of control theory.

In 1868, Maxwell published his paper **On Governors** [21] where, for the first time, a means to characterize devices (windmill governors) was introduced, by relying on differential equations linking the physical properties of the device to its motion, to exterior constraints and to an excitation. From these, he was capable to study and predict the motion of governors through a rigorous approach, in order to render them autonomous. His attempt to study the stability of the systems drew in the attention of many of his peers, who would then focus on extending this new formalism by laying out its foundation through a sound mathematical formalism. Nowadays, Maxwell is considered the father of the resulting field known as control theory, which mainly studies the (automatic) control of mechanical and/or electronic systems for various applications.

The systems and signals described by this approach abode by the superposition principle, and thus possessed Fourier transforms. This allowed their study at specific frequencies, and eventually led to the notion of transfer operators describing the systems as filters acting upon the excitation signals at specific frequencies to produce an output signal. Earlier works were mainly dedicated to the establishment of stability criteria by exploiting the poles of the system or signals, *i.e.* the complex frequencies at which the response function of a system is infinite, as well as their link to the characteristic polynomial of the differential equations associated with the response of a linear system [22–24]. That representation of systems as filters was particularly appealing to the booming field of Electric and Electronics Engineering (EEE), and in particular in the design of electronic devices and antennas for telecommunication [25–30]. It allowed for the development of analytical models of the transfer operators or physical signals in the harmonic domain.

Among these models, the one introduced by Carl Baum in the 1970's is of particular interest in this manuscript. Baum studied the response of resonators to sinusoidal excitation fields [31]. He noticed that no matter which excitation frequency was used, the response always contained the same time-

decaying sinusoidal signals in the transient regime. In the harmonic-domain, these signals transform into Lorentz-like terms or resonant terms associated with complex frequencies called singularities, which generalize the concept of poles. In the particular case of electromagnetic responses, Baum derived approximations of finite-dimension operators independently of the position variables (using modal expansions for instance) in terms of these resonant terms [32–35].

Alongside the development of control theory and then of the SEM, many fields were created or gained momentum in the 20th century:

(i) Nuclear physics, from the pioneer contributions of Marie Curie to the control of nuclear processes for military or civil applications.

(ii) Quantum physics, linked to the previous one, which gave rise to numerous Nobel prizes in the 20th century, and still attracts a plethora of physicists for both the theoretical and practical prospects it offers.

(iii) Statistical physics, which also takes root in the work of Maxwell, and offered a new framework to rigorously describe macroscopic behaviours based on the knowledge of microscopic scale phenomena, in fields such as thermodynamics, quantum physics and material science.

(iv) Classical and relativistic astrophysics, which was deeply changed by the work of Albert Einstein, and then drew in a lot of attention in the second half of the century due to the international context.

Modern physics is obviously not limited to these topics, and many others were further developed or initiated, either at the same time or as consequences of the works led in these fields. Nevertheless, these four topics are all concerned (at least partially) with the description of complex phenomena involving multiple partial differential equations, or sometimes unknown ones. As a solution to that problem, an approach similar to that of transfer operators in control theory was developed: the S-Matrix model, which links the final state of a system to its initial state *via* an operator (the S-Matrix). Tremendous efforts were put into the calculation of the S-matrix or the derivation of some rules to constraint it in different fields [36–45].

The definition of modes evolved from the discrete set of solutions to a homogeneous differential equation with boundary conditions, to the eigenvectors or eigenstates of the S-matrix, for which they played the same role as the pure states of the Hermitian operators used in quantum mechanics, *i.e.* the role of a basis on which any initial or final state can be expanded. Rapidly, that definition evolved once more when the interest shifted towards the states capable of sustaining themselves over long periods of times within volumes in the absence of sources. This is tantamount to considering only homogeneous differential equations, and thus the singularities of the S-matrices associated with these operators. The inherent eventual decay of these states conferred them the name of Quasi-Normal Modes (QNMs) [6, 46–51]. While the previous definition of modes and the definition of QNMs differ, they are very related, and the completeness of the QNMs is still assumed to this day, *i.e.* any state can be expanded on the set of QNMs [52, 53]. This approach is particularly appreciated in the case of cavities and is nowadays very popular in electromagnetism and optics [52–61].

Overall, the SEM and the mode or QNM expansion are two approaches relying on distinct principles. However, the definition of modes through the singularities of the operators often blurs the limit be-

tween the two notions. In electromagnetism in particular, there are some works on the approximation of the behaviour of a physical system through the complex poles and zeros arising from the analycity of the associated scattering operators or Green functions, and the interplay between these complex quantities and the modes or physical phenomena at play [62, 63]. While the two approaches can thus be linked, this manuscript is dedicated to the study of the SEM.

The SEM as proposed by Baum has some flaws. In particular, some of the terms involved in the expression have no clear origin. It is rooted in situational observations, which makes it seem like a phenomenological law with an undefined range of applicability. In addition, it provides an approximation (a very accurate one) rather than an exact expression. However, it works very nicely in many cases (several examples can be found in reference [64]) using (relatively) simple expressions involving small sets of parameters, and it is a general formalism which requires very few hypothesis regarding the physical properties of the considered systems and quantities.

Despite these strengths of the SEM, the contributions of Baum were almost forgotten over time, and only a few works have exploited this formalism. Some in EEE [65–68], where it was directly applied to retrieve the response of systems. Others, more fundamental and of particular importance in the scope of this PhD manuscript, in electromagnetism and wave optics [69–75], which linked the resonant behaviour of cavities to their singularities and zeros in the complex frequency plane, *via* simple analytical expressions. The novelty and rigour of the discoveries arising from the latter theoretical studies have motivated our decision to work on the SEM approach and to address several changes. Throughout the manuscript, we will study the method, address its aforementioned flaws by rigorously deriving and expanding it, and we will exploit it in different situations:

1. In Chapter 1, we define a subclass of systems called physical systems with fundamental physical properties in the time domain which constrain their response functions in the harmonic domain, in the complex frequency plane. We derive an exact analytical expression of the functions in terms of their discrete but potentially infinite set of complex poles (non-essential isolated singularities), and zeros or associated Laurent series coefficients.
2. In Chapter 2, we study the accuracy and convergence of the expression resulting from the truncation of the expansion in the case of a known structure: the Fabry-Perot cavity.
3. In Chapter 3, we show that this rigorously derived SEM can offer a novel insight into the dielectric permittivity of different materials. We recast it into a form that not only encapsulates the common microscopic models but also generalizes them by relying only on the macroscopic behaviour of materials.
4. In Chapter 4, through yet another reformulation in terms of Möbius transformations mapping the real frequency axis to circles in the complex frequency plane, we also demonstrate that the unique structure of the expansion provides an analytical expression of the phase of a response or transfer function which naturally extends the Q-factor to characterize the effect of resonant terms at any frequency.
5. Finally, in Chapter 5, we describe two methods to retrieve the complex poles, residues and zeros from experimental or simulated data acquired at real frequencies. We introduce the idea of natural and effective poles and investigate the means to discriminate between their contributions.

1. Analytical Description of Physical systems

Contents

1.1. Linear time-invariant systems . . . 33
1.1.1. Transfer functions and signals in the harmonic domain . . . 33
1.1.2. Approximating transfer functions with poles and zeros . . . 35
1.2. Generalized expressions in the harmonic domain . . . 39
1.2.1. Multiple-Order Singularity Expansion . . . 39
1.2.1.1. Derivation of the expression . . . 39
1.2.1.2. Accuracy with a test function . . . 43
1.2.2. Singularity and Zero Factorization . . . 44
1.2.2.1. Derivation from MOSEM . . . 44
1.2.2.2. Accuracy testing in an exemple . . . 49
1.3. Constraints in the harmonic domain . . . 51
1.3.1. Properties of physical systems and signals . . . 51
1.3.2. Hermitian symmetry . . . 53
1.3.3. Stability and Causality . . . 57
1.4. Temporal dynamics . . . 61
1.4.1. Inverse Laplace transform of harmonic signals . . . 61
1.4.2. Response to a causal sinusoidal input . . . 62
1.4.3. Retrieving transfer functions from the physical domain . . . 64
1.5. Conclusion . . . 67

1.1. Linear time-invariant systems

1.1.1. Transfer functions and signals in the harmonic domain

Let us start by defining a system Σ as an entity or object interacting with an excitation $x(t)$ to generate an output $y(t)$:

$$x(t) \xrightarrow{\Sigma} y(t) \tag{1.1}$$

If Σ is deterministic, linear, continuous and time-invariant, it is called a Linear Time-Invariant System (LTIS). The model of LTIS is commonly used in physics to derive the response of a medium to an excitation. Such systems are usually studied in the harmonic domain where they are associated with complex-valued transfer functions that can be used to fully describe the response of the system to an arbitrary excitation [5, 76]. This formalism has been mainly developed in the research fields of automatic system control and Electric and Electronics Engineering (EEE), but it can be found in a wide variety of problems where it is called by different names. The complex impedance and admittance formalism, for instance, is used to characterize the properties of materials in electronics, acoustics and biology [77–79]. The Scattering matrix formalism, first introduced in quantum electrodynamics [40], can be used to link outgoing waves to incoming waves, or final states to initial states in scattering problems in various situations (transport phenomena, diffraction gratings, integrated circuits, chaotic systems, ...) [80–83].

While emphasis is generally placed on real and positive frequencies with clear physical interpretations, the description of an LTIS together with its input and response signals often requires an analytical continuation into the complex frequency plane [84, 85]. Instead of considering individual responses at specific real frequencies, complex frequencies provide us with some intuition as to how a system behaves or how a signal is shaped over a large spectral width. The analysis of the electromagnetic response in terms of complex zeros and singularities has turned out to be highly efficient for several applications such as quantum waveguides [86], highly selective filters [87], plasmonic metasurfaces [71], anapoles [75], coherent perfect optical absorbers [73, 88–91] or analog computing [92]. In addition, studying the order of the zeros and singularities can help in providing better interpretations of the associated phenomena [30].

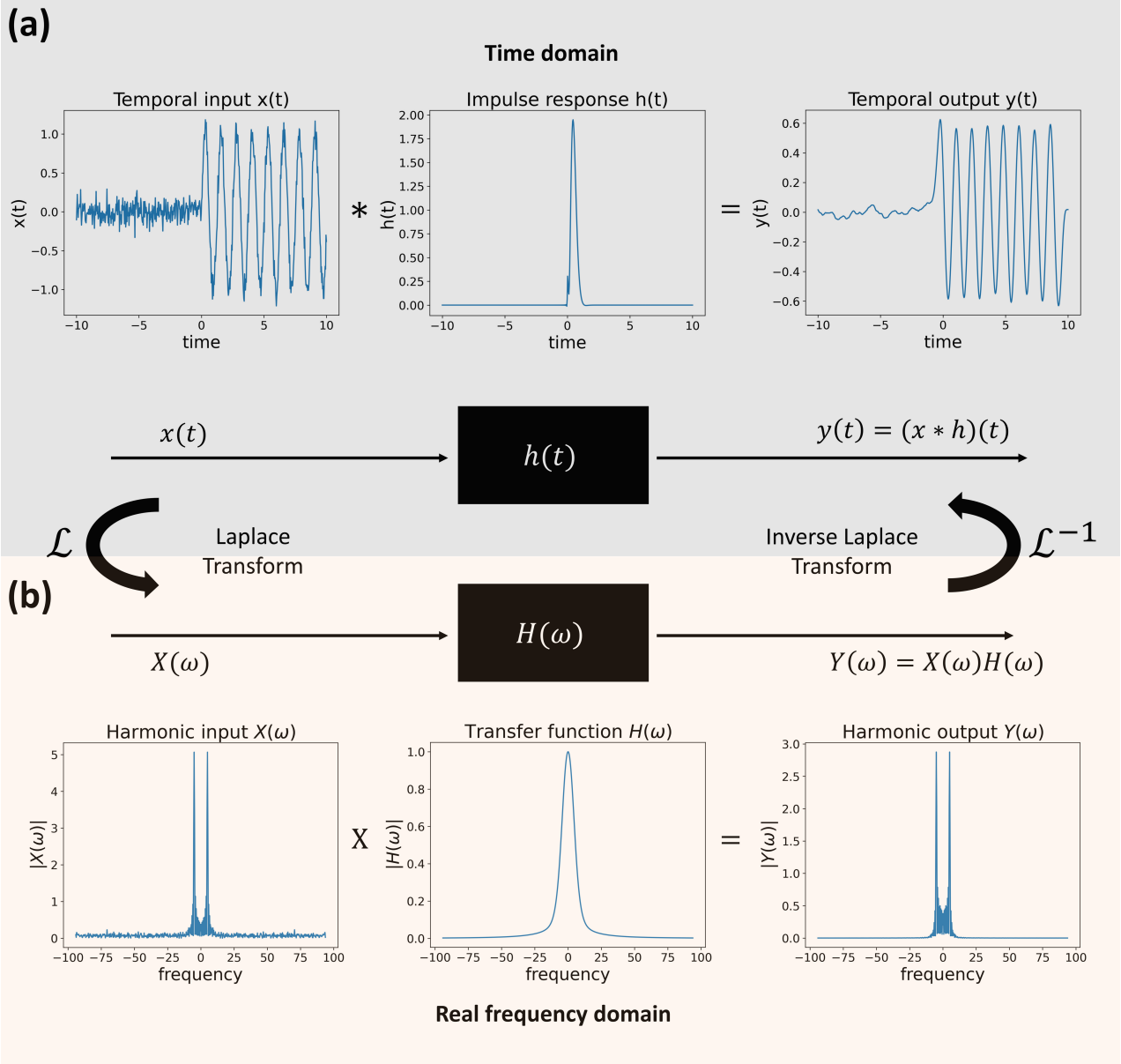

Figure 1.1. – *General representation of a physical system. (a) In the temporal domain, the system is characterized by its impulse response $h(t)$ which can be used to obtain the output $y(t)$ after a convolution with the input $x(t)$. (b) In the harmonic domain, the physical system is described by its transfer function $H(\omega)$. It is a filter acting in the frequency domain on the input $X(\omega)$ to generate an output $Y(\omega)$. In this case, $H(\omega)$ is a low-pass filter which partially removes the noise present at higher frequencies, as it can be seen by comparing the temporal input $x(t)$ to the temporal output $y(t)$. The output $Y(\omega)$ is the product of $H(\omega)$ and $X(\omega)$. The harmonic domain functions $X(\omega)$, $H(\omega)$ and $Y(\omega)$ are obtained by bilateral Laplace transform of the temporal signals $x(t)$, $h(t)$ and $y(t)$. The temporal signals can then be recovered using an inverse Laplace transform.*

In the LTIS formalism, the Laplace transform of the impulse response $h(t)$, which is characteristic of the system in the physical domain, is the transfer function $H(\omega)$, which describes the system in

the harmonic domain, and links the input to the output. The LTIS is thus regarded as a filter acting upon the input in the harmonic domain (see Figure 1.1). Different methods have been developed to express $H(\omega)$ with respect to its zeros and poles in the complex frequency plane. The most relevant methods, in our case, can be traced back to the Weierstrass and Hadamard factorization theorems for holomorphic and meromorphic functions respectively, which provide general expressions of $H(\omega)$ as opposed to local expressions such as the Laurent series expansion.

(i) With the rapid development of electronics and automated machines, the control of the LTIS stability often favoured the factorization of the transfer function $H(\omega)$, in the simple form of the ratio of complex polynomials [93], in order to monitor the evolution of the phase and amplitude with respect to the frequency in Bode diagrams [94]. In EEE and control theory, singularities and zeros of multiple-order are not uncommon (n^{th} order Butterworth filters [27] for instance).

(ii) Alongside this progress, pioneer works led to the development of the Singularity Expansion Method (SEM) [31, 34]. It was first developed to approximate the time dynamics of systems associated with arbitrary-order singularities in the harmonic-domain and helped in describing many problems in electromagnetism [32, 35, 95, 96] (an exhaustive set of references dating back to the early developments of the SEM can be found in ref. [64]). The SEM has received a renewed interest in the recent years in the case of simple poles, *i.e.* singularities of order 1, where accurate expressions have been derived and applied to various problems [70, 74, 97–100]. In addition, pole or singularity expansions have been increasingly used in the framework of Quasi-Normal Modes (QNMs) or resonant state expansions [61, 101–104]. However, exact expansions have not been obtained in the case of poles of arbitrary order, despite the prospects they offer in describing more complex systems and/or their input and output signals [105–107].

These two methods, *i.e.* the SEM for simple poles and the multiple-order pole and zero factorization used in EEE, are generally used to obtain an approximation of the transfer function of an LTIS.

1.1.2. Approximating transfer functions with poles and zeros

The first singularity expansions were developed in the aforementioned SEM [31, 34] based on the observation of a system's response to a sinusoidal input in the transient regime. It was shown to be a combination of damped sinusoidal functions associated with complex frequencies which were the singularities of the transfer function of the system. While Baum first derived the singularity expansion by taking into account the order of these singularities, most applications made use of (and later demonstrated) this expansion in the case of simple poles, *i.e.* isolated singularities of order 1 [70, 74, 97]. The resulting expansion is here referred to as the Simple Pole Expansion (SPE), and it has the following expression:

$$H(\omega) = H_{\text{bgrd}}(\omega) + \sum_p \frac{\text{Res}(H,\omega_p)}{\omega - \omega_p} \tag{1.2}$$

where ω_p denotes the simple poles of $H(\omega)$, *i.e.* the isolated complex frequencies such that $H(\omega_p) = \infty$. The SPE is composed of a background term $H_{\text{bgrd}}(\omega)$ which does not possess poles [102], and a sum of resonant terms $\text{Res}(H,\omega_p)/(\omega - \omega_p)$. This translates the idea that the shape of $H(\omega)$ in a specific

frequency range is chiefly affected by the nearby singularities, with the background term compensating for the offset introduced by the singularities with respect to the average (or background) value of $H(\omega)$ in that range. The background term is often used as a means to accurately fit a target curve once the singularities have been determined.

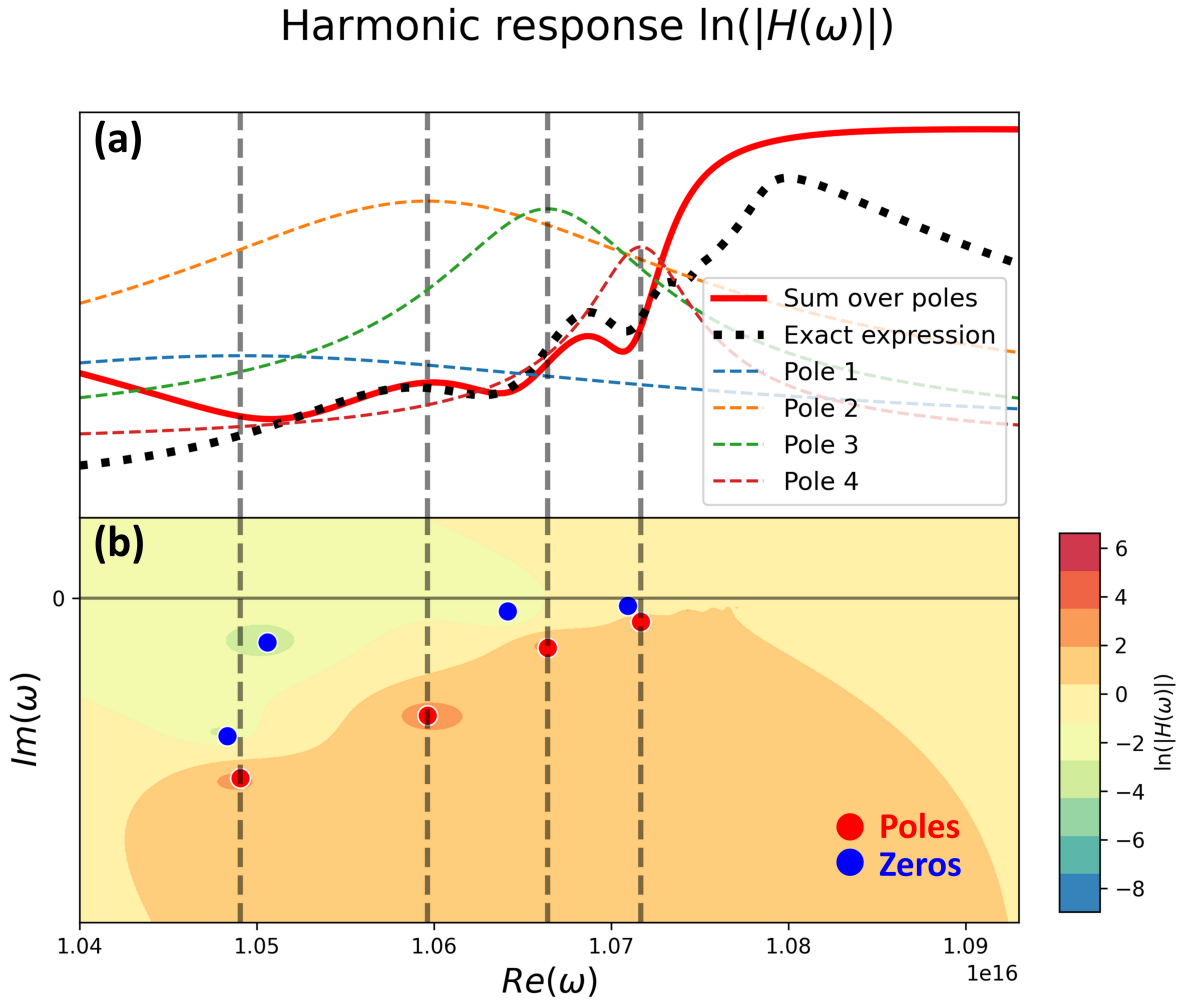

Figure 1.2. – *(a) Modulus of the reflection coefficient $H(\omega)$ of a thin layer of silver, defined in Eq. (1.3), as well as its resonant terms $\mathrm{Res}(H,\omega_p)/(\omega-\omega_p)$ associated with the poles p_l and the modulus of the sum of these resonant terms. The frequencies range from 1.040×10^{16} Hz to 1.093×10^{16} Hz, which is equivalent to ultraviolet wavelengths between 172.9 nm and 181.3 nm. (b) Log-amplitude of $H(\omega)$ in the complex frequency plane, in a limited complex frequency window. The poles in (a) are highlighted in (b) as red points. The sum over the poles gives an approximation of the shape of $H(\omega)$ on the real axis (the minimum and maximum frequencies), but with the background term of Eq. (1.2) omitted, the reconstructed red curve poorly matches the exact expression. The background term is often defined as the difference between the target and the reconstructed curve.*

The contribution of the poles to the shape of $H(\omega)$ is illustrated in Fig. 1.2 for $H(\omega)$ defined as the

reflection coefficient of a thin layer of silver illuminated from one side at normal incidence:

$$H(\omega) := r(\omega) - \frac{t(\omega)\,t'(\omega)\,r(\omega)\,e^{2i\omega\frac{n(\omega)d}{c}}}{1 - r(\omega)^2 e^{2i\omega\frac{n(\omega)d}{c}}} \tag{1.3}$$

where $d = 70$ nm is the thickness of the silver layer, c is the speed of light in the air, $n(\omega)$ is the refractive index of silver [108], $r(\omega) = (n(\omega)-1)/(n(\omega)+1)$ is the Fresnel reflection coefficient at the air/silver interface, and $t(\omega) = 2/(n(\omega)+1)$ and $t'(\omega) = 2n(\omega)/(n(\omega)+1)$ are the Fresnel transmission coefficients at the air/silver and silver/air interfaces respectively. The zeros, the poles and the residues of $H(\omega)$ were determined numerically. Each pole ω_p in the complex frequency plane, in Fig. 1.2 (b) is associated with a resonant term $\mathrm{Res}(H,\omega_p)/(\omega-\omega_p)$, the moduli of which are plotted in Fig. 1.2 (a). The sum of the resonant terms associated with the poles in the plotted complex frequency window gives the red curve in Fig. 1.2 (a), which matches the local shape of the exact response (dashed line which corresponds to Eq. (1.3), *i.e.* the approximate position of the local minimum and maximum frequencies. The poor match between this sum of resonant terms and the exact expression is due to the missing background term $H_{\mathrm{bgrd}}(\omega)$ which is often defined as the difference between the target curve (experimental data or simulation) and the model.

Since most linear systems are described by poles of order 1, the SPE is well suited for the description of the transfer functions of such systems, or their response to a temporal or spatial sinusoidal input [69, 70, 74, 99, 109]. Other expressions must be used when the order of the poles is increased. One commonly used alternative in EEE is what we refer to as the Pole and Zero Factorization (PZF). The PZF is obtained by making the assumption that the harmonic-domain function $H(\omega)$ is the ratio of two polynomials of the complex frequency variable ω, and that any system responds instantaneously to an input signal [5, 76, 93], resulting in:

$$H(\omega) = \frac{N(\omega)}{D(\omega)} = \frac{N_0 \prod_{\ell=1}^{deg(N)}(\omega - z_\ell)}{D_0 \prod_{\ell=1}^{deg(D)}(\omega - p_\ell)} \tag{1.4}$$

where z_ℓ and p_ℓ are the zeros of N and D respectively, with potentially identical zeros and poles (in which case their order is higher). Using a partial fraction expansion [110], it is possible to write an expression similar to the SPE:

$$\begin{aligned} H(\omega) =& \alpha_{1,0} + \frac{\alpha_{1,1}}{\omega - p_1} + \ldots + \frac{\alpha_{1,2}}{(\omega - p_1)^{\nu_1}} \\ &+ \alpha_{2,0} + \frac{\alpha_{2,1}}{\omega - p_2} + \ldots + \frac{\alpha_{2,2}}{(\omega - p_2)^{\nu_2}}. \\ &+ \ldots \\ =& H_{\mathrm{bgrd}} + \sum_\ell \sum_{m=1}^{\nu_\ell} \frac{\alpha_{\ell,m}}{(\omega - p_\ell)^m} \end{aligned} \tag{1.5}$$

where $H_{\mathrm{bgrd}} = \sum_\ell \alpha_{\ell,0}$ and the poles p_ℓ are considered with their order or multiplicity ν_ℓ. The constants $\alpha_{\ell,1}$ can be identified as the residues, and they can be calculated with the zeros and poles using

Equation (1.5) [31, 70]:

$$\begin{aligned}\alpha_{k,1} &= \mathrm{Res}(H, p_k) \\ &= \frac{1}{(\nu_k-1)!}\lim_{\omega\to p_k}\partial_\omega^{(\nu_k-1)}\left[\omega\mapsto\left((\omega-p_k)^{\nu_k}H(\omega)\right)\right](\omega) \\ &= \frac{N_0}{D_0(\nu_k-1)!}\partial_\omega^{(\nu_k-1)}\left[\omega\mapsto\frac{\prod_{\ell=1}^{deg(N)}(\omega-z_\ell)}{\prod_{\ell\neq k}^{deg(D)}(\omega-p_\ell)}\right](p_k)\end{aligned} \tag{1.6}$$

In the case of simple poles, this expression becomes:

$$\begin{aligned}\alpha_{k,1} &= \mathrm{Res}(H, p_k) \\ &= \lim_{\omega\to p_k}(\omega-p_k)H(\omega) \\ &= \frac{N_0\prod_{\ell=1}^{deg(N)}(p_k-z_\ell)}{D_0\prod_{\ell\neq k}^{deg(D)}(p_k-p_\ell)}\end{aligned} \tag{1.7}$$

[Intermediary observations]

— The PZF and the resulting pole expansion are widely used in electronics and control engineering where they provide highly accurate results when studying systems at time scales larger than the transient regime duration.

— However, this is no longer true for other fields such as wave physics, in which case the PZF is missing, in particular, a complex exponential factor depending on the frequency ω which can be interpreted as the result of a time delay required by a system to respond to different frequencies (*i.e.* a dispersive system) [70, 74].

— This term, which is particularly important for systems which interact with signals with respect to both time and space cannot be obtained from the restrictive hypothesis that $H(\omega)$ is a ratio of two polynomials.

The derivation of more general expressions taking into account the potentially infinite order of the singularities is thus of high interest. In the next section, we rigorously derive these generalized expansions and factorization forms, which are exact, analytical expressions for most LTIS.

1.2. Generalized expressions in the harmonic domain

1.2.1. Multiple-Order Singularity Expansion

1.2.1.1. Derivation of the expression

We start with a more general setting than transfer functions of LTIS. Let us study a meromorphic function $H(z)$. It is holomorphic everywhere on $\mathbb{C}$ except for a discrete set of complex points $\mathscr{P} = \{p_1, p_2, ..., p_i, ...\}$, which is the set of its isolated singularities: we implicitly assume that the singularities of $H(\omega)$ are poles (of potentially infinite order).

We consider a domain $\mathscr{B}$ bounded by a closed curve γ containing a subset $\mathscr{P}_\gamma$ of the singularities. We write ω a complex number within $\mathscr{B}$, as depicted in Figure 1.3.

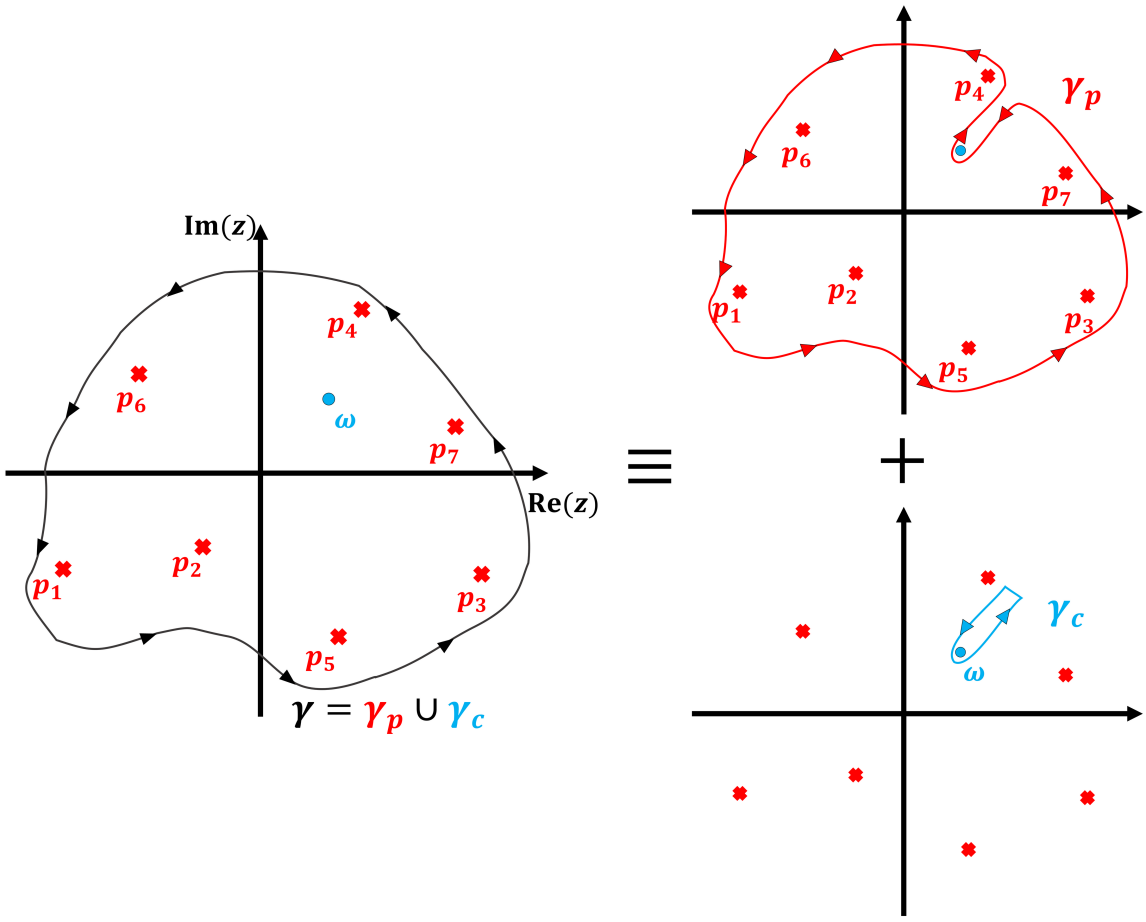

Figure 1.3. – *Separation of the integration curve γ (black curve) into γ_C containing only ω (blue curve) and γ_P (green curve) around the singularities.*

Let us set $R(z)$ a function defined within $\mathscr{B}$ as:

$$R(z) := \frac{H(z)}{z-\omega} \tag{1.8}$$

[Key properties]

By definition, $R(z)$ is meromorphic within $\mathscr{B}$, with its poles being $\mathscr{P}_\gamma \cup \{\omega\}$. We separate the closed curve γ into γ_p around the singularities and excluding ω, and γ_C around only ω. We integrate $R(z)$ over γ_p and γ_C using the residue theorem [111, 112]:

$$\frac{1}{2i\pi}\oint_\gamma R(z)dz = \mathrm{Res}(R,\omega) + \sum_{p_i\in\mathscr{P}_\gamma} \mathrm{Res}(R,p_i) \tag{1.9}$$

The first term $\mathrm{Res}(R,\omega)$ in Equation (1.9) is obtained *via* the Cauchy integration theorem:

$$\mathrm{Res}(R,\omega) = H(\omega) \tag{1.10}$$

Let us derive an expression of the other residues $\mathrm{Res}(R,p_i)$.

[Derivation]

By definition, they are the coefficients of order -1 in the Laurent series expansions of $R(z)$ around the poles p_i, which read as

$$R(z) := \sum_{n=-\nu_i}^{+\infty} \alpha(R,p_i,n).(z-p_i)^n \tag{1.11}$$

where $\alpha(R,p_i,n)$ is the coefficient of order n associated with the pole p_i for the function R, and ν_i is the order of the pole p_i. We want to obtain an expression of $\alpha(R,p_i,n)$ which depends on the Laurent series coefficients $\alpha(H,p_i,\ell)$ of $H(z)$ and the fixed value ω. To do so, let us first consider $D(z)$ defined by:

$$\begin{aligned} R(z) &= H(z)D(z) \\ D(z) &= \frac{1}{z-\omega} \end{aligned} \tag{1.12}$$

Since $D(z)$ is holomorphic at the poles p_i, it has a Taylor expansion:

$$D(z) = \sum_{k=0}^{+\infty} \beta(D,p_i,k).(\omega-p_i)^k \tag{1.13}$$

The Taylor series coefficients $\beta(D,p_i,k)$ can be explicitly calculated:

$$\beta(D,p_i,k) = \frac{\partial_z^{(k)}(D)(p_i)}{k!} = -\frac{1}{(\omega-p_i)^{k+1}} \tag{1.14}$$

Similarly, $H(z)$ is meromorphic and thus has the following Laurent series expansion around the poles p_i:

$$H(z) = \sum_{\ell=-\nu_i}^{+\infty} \alpha(H,p_i,\ell).(z-p_i)^\ell \tag{1.15}$$

[Derivation]

By combining Equations (1.13) and (1.15), we can write:

$$R(z) = \sum_{\ell=-\nu_i}^{+\infty} \sum_{k=0}^{+\infty} \alpha(H, p_i, \ell)\beta(D, p_i, k).(z-p_i)^{(\ell+k)} \tag{1.16}$$

Using:

$$\forall \ell \in \mathbb{Z}, \quad (z-p_i)^n = (z-p_i)^{\ell}(z-p_i)^{n-\ell} \tag{1.17}$$

as well as the unicity of the Laurent series expansion, the terms associated with exponent $n = \ell + m$ in Equation (1.11) must be linked to the Laurent series coefficient of order n in Equation (1.16):

$$\alpha(R, p_i, n) = \sum_{\ell=-\infty}^{+\infty} \alpha(H, p_i, \ell).\beta(D, p_i, k = n-\ell) \tag{1.18}$$

Since D is holomorphic $m \geq 0 \Rightarrow \ell \leq n$. Similarly, the order of p_i for $H(\omega)$ imposes that $\ell \geq -\nu_i$:

$$\alpha(R, p_i, n) = \sum_{\ell=-\nu_i}^{+n} \alpha(H, p_i, \ell).\beta(D, p_i, n-\ell) \tag{1.19}$$

The Taylor series coefficient $\beta(D, p_i, m)$ was provided in Equation (1.14):

$$\beta(D, p, k) = \frac{\partial_z^k(D)(p_i)}{k!} = -\frac{1}{(\omega - p_i)^{k+1}} \tag{1.20}$$

which leads to:

$$\alpha(R, p, n) = -\sum_{\ell=-\nu_i}^{n} \frac{\alpha(H, p_i, \ell)}{(\omega - p_i)^{n-\ell+1}} \tag{1.21}$$

In particular, since $\mathrm{Res}(R, p_i) = \alpha(R, p_i, -1)$,

$$\mathrm{Res}(R, p_i) = -\sum_{\ell=-\nu_i}^{-1} \frac{\alpha(H, p_i, \ell)}{(\omega - p_i)^{-\ell}} \tag{1.22}$$

For convenience, the residue is written with $m = -\ell$:

$$\mathrm{Res}(R, p_i) = -\sum_{m=1}^{\nu_i} \frac{\alpha(H, p_i, -k)}{(\omega - p_i)^{k}} \tag{1.23}$$

[Key properties]

Finally, the following expression of $H(z)$ is obtained from Equation (1.9):

$$H(\omega) = \frac{1}{2i\pi} \int_{\gamma} \frac{H(z)}{z-\omega} dz + \sum_i \sum_{m=1}^{\nu_i} \frac{\alpha(H, p_i, -m)}{(\omega - p_i)^m} \tag{1.24}$$

Equation (1.24) shows two contributions to $H(\omega)$ evaluated at the frequency ω:

(i) The nearby singularities p_i, within the closed curve γ.

(ii) The set of values of $H(\omega)$ on the closed curve γ, represented by the integral term, which accounts for the contribution of the singularities outside of γ.

The bigger the closed curve gets, the less the integral affects the value of $H(\omega)$ since the singularities outside the curve become too far from ω, provided that $H(\omega)$ does not grow faster than $|\omega|$ in the complex plane.

If $H(\omega)$ is asymptotically well-behaved, *i.e.* it does not diverge faster than $|\omega|$ when ω tends towards ∞ in the complex plane, then the integral term can be calculated using an arbitrary frequency a different from ω. We show that by considering the following integral:

$$\begin{aligned}\left|\int_{\mathscr{C}(\rho)}\frac{H(z)}{z-\omega}dz-\int_{\mathscr{C}(\rho)}\frac{H(z)}{z-a}dz\right| &\leq \int_{\mathscr{C}(\rho)}\left|H(z)\left[\frac{1}{z-\omega}-\frac{1}{z-a}\right]\right|dz \\ &\leq 2\pi\frac{\max_{\theta\in[0,2\pi]}\left|H(\rho e^{i\theta})\right||\omega|\rho}{(\rho-|a|)(\rho-|\omega|)}\end{aligned} \tag{1.25}$$

where $\mathscr{C}(\rho)$ is the circle of radius ρ centered at 0, and a is within that circle. We want to replace $H(z)/(z-\omega)$ by the frequency-independent term $H(z)/(z-a)$. If the asymptotic behaviour is not verified, then Equation (1.25) gives an upper-bound on the error introduced by considering that the two terms are equivalent. Otherwise, as the radius ρ becomes infinite, the upper-bound tends towards 0, which leads to:

$$\int_{\mathscr{C}(\rho)}\frac{H(z)}{z-\omega}dz\to\int_{\mathscr{C}(\rho)}\frac{H(z)}{z-a}dz \tag{1.26}$$

In addition, setting $\omega=a$ in Equation (1.24) yields:

$$\frac{1}{2i\pi}\int_{\mathscr{C}(\rho)}\frac{H(z)}{z-a}dz=H(a)-\sum_p\sum_{m=1}^{\nu_p}\frac{\alpha(H,p,-m)}{(a-p)^m} \tag{1.27}$$

Therefore, when ρ is large enough, *i.e.* when the closed curve $C(\rho)$ around the singularities tends towards $+\infty$, and provided that the convergence of $|\frac{H(z)}{z}|$ holds:

Multiple-Order Singularity Expansion Method (MOSEM)

$$\begin{aligned}H(\omega)&=H_{\text{NR}}+H_{\text{R}}(\omega)\\ H_{\text{NR}}&=H(a)-\sum_p\sum_{m=1}^{\nu_p}\frac{\alpha(H,p,-m)}{(a-p)^m}\\ H_{\text{R}}(\omega)&=\sum_p\sum_{m=1}^{\nu_p}\frac{\alpha(H,p,-m)}{(\omega-p)^m}\end{aligned} \tag{1.28}$$

Equation (1.28) corresponds to the Multiple-Order Singularity Expansion Method (MOSEM).

Let us stress that the choice of a has no influence over the value of the constant term H_{NR}. The residue of $H(\omega)$ associated with the pole p_i is defined as $\text{Res}(H, p_i) = \alpha(H, p_i, -1)$. Therefore by identifying H_{NR} as a constant background term H_{bgrd} when all the singularities are taken into account in the resonant terms, we obtain the SPE expression defined in Equation (1.2) in the case of simple poles.:

$$H(\omega) = H_{\text{bgrd}} + \sum_p \frac{\text{Res}(H, p)}{\omega - p} \tag{1.29}$$

1.2.1.2. Accuracy with a test function

We show the accuracy of MOSEM in the case of poles of order 2 in a purely theoretical example by considering the following function:

$$H(\omega) = e^{\text{i}\omega} \frac{\omega - 1}{1 - \sin(\omega)} \tag{1.30}$$

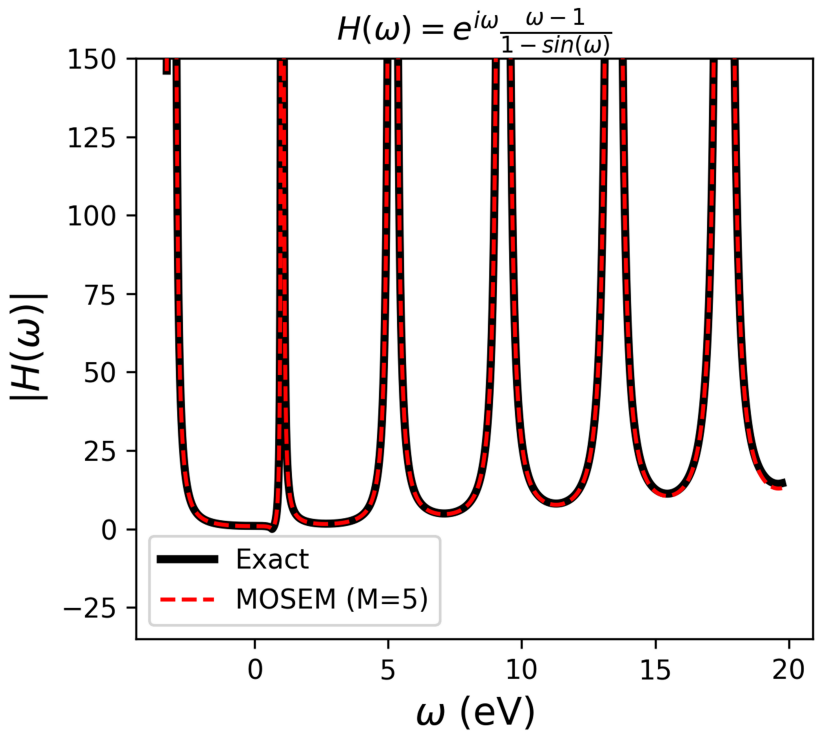

Figure 1.4. – *Modulus of the function $H(\omega)$ defined in Equation (1.30). The poles of $H(\omega)$ are the complex frequencies $\omega_p^{(n)} = 4n\pi + \pi/2$. The exact expression in black is compared to the truncated MOSEM expression in red: $-M \leq n \leq M$, with $M = 5$.*

The poles $p_n = \frac{(2n+1)\pi}{2}$ and their associated Laurent series coefficients $\alpha(p_n, -1)$ and $\alpha(p_n, -2)$ can be

explicitly calculated:

$$\begin{aligned}\alpha(p_n,-2) &= 2e^{ip_n}(p_n-1)\\ \alpha(p_n,-1) &= 2e^{ip_n}\end{aligned} \tag{1.31}$$

We apply the MOSEM expression from Equation (1.28) to $H(\omega)$ with $a=0$, and truncate at the Mth poles around a window centered on 0:

$$\begin{aligned}H(\omega) \approx H(0) &+ \sum_{n=-M}^{M} 2e^{ip_n}\left[\frac{1}{p_n} - \frac{p_n-1}{(p_n)^2}\right]\\ &+ \sum_{n=-M}^{M} 2e^{ip_n}\left[\frac{1}{\omega-p_n} + \frac{p_n-1}{(\omega-p_n)^2}\right]\end{aligned} \tag{1.32}$$

In Figure (1.4), we compare this expression for $M=5$ to that of Equation (1.30), and show that a small set of poles is sufficient to accurately reconstruct a function.

For more complex functions with a less regular distribution of poles, an accurate approximation can still be obtained. The influence of the poles outside of the region of interest can be accounted for by considering effective singularities [99], as we show in Chapter 2, Section 2.4, where we study the accuracy and convergence of MOSEM in the case of a dispersive optical Fabry-Perot cavity.

1.2.2. Singularity and Zero Factorization

1.2.2.1. Derivation from MOSEM

The Weierstrass and Hadamard factorization theorems state that any meromorphic function can be written as the ratio of two complex polynomials multiplied by a complex exponential. Starting from this consideration, expressions such as the PZF (in which the complex exponential is usually removed) can be obtained (although not straightforwardly) to study the phase and amplitude variations at real frequencies. The poles and zeros can be defined in the resulting rational fractions as the zeros of the denominator and numerator respectively. Alternatively, a factorization involving the singularities and zeros can be obtained from MOSEM, providing a clearer link between the expanded and factorized forms as was done in References [70, 71] in the case of poles of order 1.

[Key properties]

We derive a factorized form of the MOSEM expression from Equation (1.28). $H(\omega)$ can always be written as:

$$H(\omega) := \omega^m G(\omega) \tag{1.33}$$

with $m \geq 0$ the order of the zero at the origin (0) of $H(\omega)$, and $G(\omega)$ a meromorphic function which does not possess 0 as a zero. If $m=0$, we have $G(\omega)=H(\omega)$.

Let us consider $F(\omega)$ the log-derivative of $G(\omega)$, with $G'(\omega)$ the complex derivative of G:

$$\begin{aligned} F(\omega) &= \frac{G'(\omega)}{G(\omega)} \\ G'(\omega) &= \partial_\omega[G](\omega) \end{aligned} \tag{1.34}$$

$G'(\omega)$ is calculated by taking the derivative of the MOSEM expression applied to $G(\omega)$. With the Laurent and Taylor series expansions of $G(\omega)$ and $G'(\omega)$, we show that the singularities of $F(\omega)$ are the zeros and poles of $H(\omega)$, that they are simple poles (their order is 1), and that their residue are their order in $H(\omega)$.

[Derivation]

Let us consider a pole p of order ν_p of $G(\omega)$ (and thus of $H(\omega)$). In the vicinity of p, $G(\omega)$ and $G'(\omega)$ can be approximated as:

$$\begin{aligned} G(\omega) &\approx \frac{\alpha(H,p,-\nu)}{(\omega-p)^{\nu_p}} \\ G'(\omega) &\approx \frac{-\nu_p\ \alpha(H,p,-\nu)}{(\omega-p)^{\nu_p+1}} \end{aligned} \tag{1.35}$$

It follows that $F(\omega)$ is approximated as:

$$F(\omega) \approx \frac{-\nu_p}{\omega-p} \tag{1.36}$$

Similarly, for ω in the vicinity of a zero $z \neq 0$ of $G(\omega)$, of order ν_z:

$$\begin{aligned} G(\omega) &\approx \alpha(G,z,-\nu_z)(\omega-z)^{\nu_z} \\ G'(\omega) &\approx \nu_z\ \alpha(G,z,-\nu_z)(\omega-z)^{\nu_z-1} \\ F(\omega) &= \frac{G'(\omega)}{G(\omega)} \approx \frac{\nu_z}{\omega-z} \end{aligned} \tag{1.37}$$

Therefore:

$$\begin{aligned} \forall (p,\nu_p) \in \mathscr{P}_G,\ \mathrm{Res}(F,p) &= -\nu_p \\ \forall (z,\nu_z) \in \mathscr{Z}_G,\ \mathrm{Res}(F,z) &= +\nu_z \end{aligned} \tag{1.38}$$

where $\mathscr{P}_G$ and $\mathscr{Z}_G$ are respectively the sets of poles and zeros of G.

[Derivation]

Since $F(\omega)$ is a meromorphic function, it is possible to apply MOSEM:

$$\begin{aligned} F(\omega) &:= F_{\mathrm{NR}} + F_{\mathrm{R}}(\omega) \\ F_{\mathrm{NR}} &:= F(a) - \sum_{p} \sum_{m=1}^{\nu_p} \frac{\alpha(F,p,-m)}{(a-p)^m} \\ F_{\mathrm{R}}(\omega) &:= \sum_{p} \sum_{m=1}^{\nu_p} \frac{\alpha(F,p,-m)}{(\omega-p)^m} \end{aligned} \tag{1.39}$$

with $p \in \{z_\ell, p_\ell\}$, $\nu_p = 1$, and $\alpha(F,p,-1) = 1$ if $p = z_\ell$ is a zero of $H(\omega)$ or $\alpha(F,p,-1) = -1$ if $p = p_\ell$ is a pole of $H(\omega)$.

With the residues and poles from Equation (1.37), we obtain:

$$\begin{aligned} F(\omega) &= F_{\mathrm{NR}} + F_{\mathrm{R}}(\omega) \\ F_{\mathrm{NR}} &= F(a) + \sum_{p_\ell} \frac{\nu_\ell^{(p)}}{a-p_\ell} - \sum_{z_\ell} \frac{\nu_\ell^{(z)}}{a-z_\ell} \\ F_{\mathrm{R}}(\omega) &= -\sum_{p_\ell} \frac{\nu_\ell^{(p)}}{\omega-p_\ell} + \sum_{z_\ell} \frac{\nu_\ell^{(z)}}{\omega-z_\ell} \end{aligned} \tag{1.40}$$

We integrate the log-derivative of $F(\omega)$, on a path from an arbitrary frequency a to ω, which yields:

$$\begin{aligned} Log(\frac{G(\omega)}{G(a)}) = &\left(\frac{G'(a)}{G(a)} - \sum_{z_\ell} \frac{\nu_\ell^{(z)}}{a-z_\ell} + \sum_{p_\ell} \frac{\nu_\ell^{(p)}}{a-p_\ell} \right)(\omega - a) \\ &+ \sum_{z_\ell} \nu_\ell^{(z)} Log(\frac{\omega - z_\ell}{a-z_\ell}) \\ &- \sum_{p_\ell} \nu_\ell^{(p)} Log(\frac{\omega - p_\ell}{a-p_\ell}) \end{aligned} \tag{1.41}$$

The values of $G(a)$ and $G'(a)$ are calculated using $H(\omega)$ and its derivative. The former reads as:

$$\begin{aligned} G(a) &= \frac{H(a)}{a^m} && \text{if } a \neq 0, \\ G(a) &= \frac{\partial_\omega^m [H](0)}{m!} && \text{otherwise.} \end{aligned}$$

while the latter is:

$$\begin{aligned} G'(a) &= \frac{\partial_\omega [H](a)}{a^m} - m\frac{H(a)}{a^{m+1}} && \text{if } a \neq 0, \\ G'(a) &= \frac{\partial_\omega^{(m+1)} [H](0)}{(m+1)!} && \text{otherwise.} \end{aligned}$$

Finally, applying the exponential function to Equation (1.41) yields:

Singularity and Zero Factorization (SZF)

$$H(\omega) = \omega^m \, G(a) \, \frac{\prod_{z_\ell} (1 - \frac{\omega - a}{z_\ell - a})^{\nu_\ell^{(z)}}}{\prod_{p_\ell} (1 - \frac{\omega - a}{p_\ell - a})^{\nu_\ell^{(p)}}} \, e^{\mathrm{i}\tau(\omega - a)}$$
$$\tau = -i \left(\frac{G'(a)}{G(a)} - \sum_{z_\ell} \frac{\nu_\ell^{(z)}}{a - z_\ell} + \sum_{p_\ell} \frac{\nu_\ell^{(p)}}{a - p_\ell} \right) \tag{1.42}$$

We refer to Equation (1.42) as the Singularity and Zero Factorization (SZF).

[Key properties]

Let us point out the presence of the aforementioned complex exponential $e^{-\mathrm{i}\tau\omega}$ missing from the PZF, but also of the known response $G(a)$ (the static response in the case of $a = 0$). Let us also stress that in the case of an LTIS, the phase introduced by the complex exponential can be set to an arbitrary position by changing the time origin or the space-origin (for a system with coupled space and time variables). Shifting the time origin by τ_0 in the temporal domain results in a multiplication by $e^{\mathrm{i}\omega\tau_0}$ of the input $X(\omega)$ in the harmonic domain.

This is tantamount to considering the transfer function $H(\omega)e^{\mathrm{i}\omega\tau_0}$ with the same input $X(\omega)$ as depicted in Figure 1.5 for $H(\omega)$ defined as:

$$H(\omega) = 5 + \frac{2 + 0.1\mathrm{i}}{\omega - (2 + 0.3\mathrm{i})} + \frac{4 + 0.1\mathrm{i}}{\omega - (5 + 1.4\mathrm{i})} + \frac{6 + 0.1\mathrm{i}}{\omega - (6.5 + 0.7\mathrm{i})} \tag{1.43}$$

In Figure 1.5 (a), the phase of the transfer function $H(\omega)$ is shown in the complex plane. In Figure 1.5 (b), it is plotted for $H(\omega)$ multiplied by $e^{\mathrm{i}\omega\tau_0}$ with τ_0 arbitrarily set to $\pi/6$. We show that the position of the zeros and singularities remains the same after switching from $H(\omega)$ to $H(\omega)e^{\mathrm{i}\omega\tau_0}$, but a non-constant phase-shift is introduced in the complex frequency plane by the phasor $e^{\mathrm{i}\omega\tau_0}$. It is thus possible to set τ_0 in such a way that $\tau + \tau_0 = 0$, where τ is the time constant naturally appearing in the SZF in Equation (1.42).

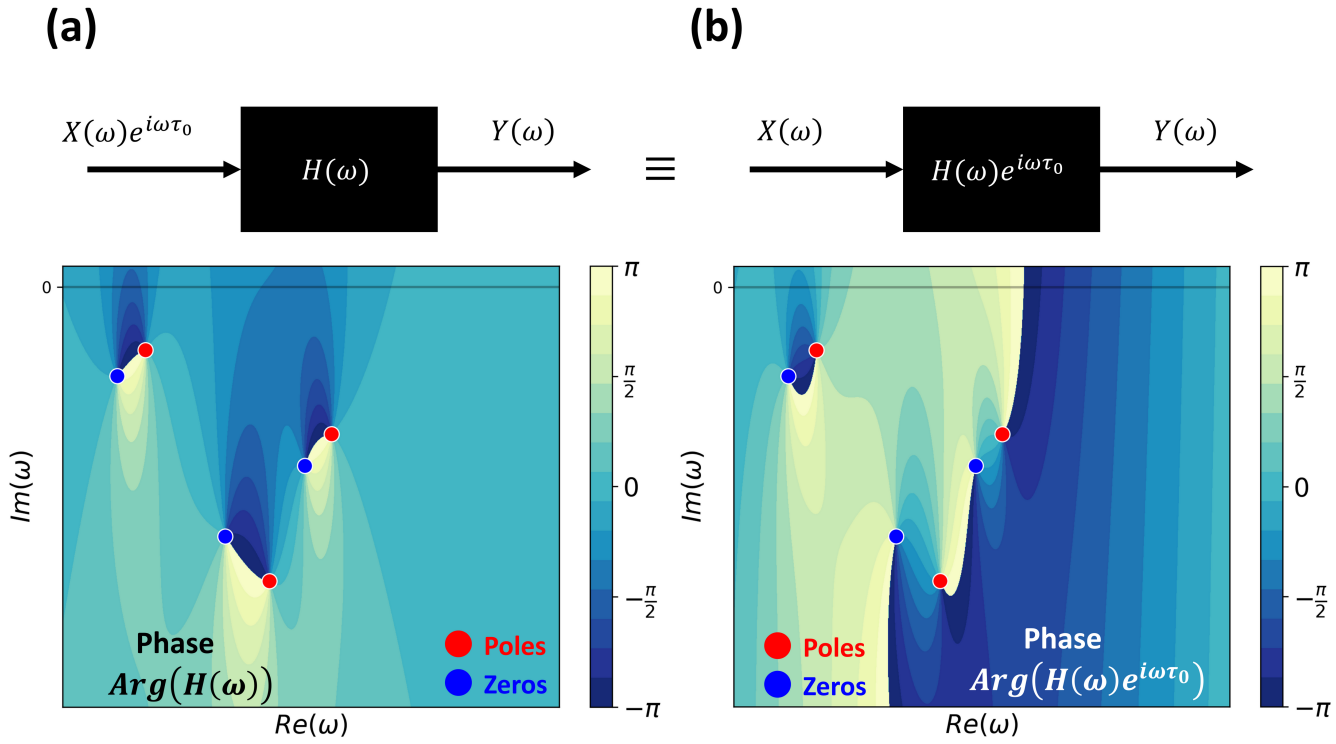

Figure 1.5. – *(a) Phase diagram in the complex frequency plane of the transfer function $H(\omega)$ of an LTIS defined in Equation (1.43) as $H(\omega) = 5 + \frac{2+0.1\mathrm{i}}{\omega-(2+0.3\mathrm{i})} + \frac{4+0.1\mathrm{i}}{\omega-(5+1.4i)} + \frac{6+0.1\mathrm{i}}{\omega-(6.5+0.7\mathrm{i})}$. (b) Phase diagram of the transfer function $H(\omega)e^{\mathrm{i}\omega\tau_0}$, with $\tau_0 = \pi/6$, of the same LTIS with a distinct time origin. Shifting the time-origin of the input $X(\omega)$ in (a) is tantamount to considering $H(\omega)e^{\mathrm{i}\omega\tau_0}$ for the transfer function in (b). The distribution of the poles (red points) and zeros (blue points) remains the same, only the phase is affected.*

By setting $\tau = 0$, $a = 0$, and appropriately defining two constants N_0 and D_0, we recover the PZF described in the previous section by considering only N_s poles and N_z zeros:

$$
\begin{aligned}
H(\omega) &= \frac{N_0 \prod_{\ell=1}^{N_z} (i\omega - i z_\ell)}{D_0 \prod_{\ell=1}^{N_s} (i\omega - i p_\ell)} \\
N_0 &= \left[\prod_{\ell=1}^{N_z} \frac{\mathrm{i}}{z_\ell} \right] \omega^m \, G(0) \\
D_0 &= \prod_{\ell=1}^{N_s} \frac{\mathrm{i}}{p_\ell}
\end{aligned}
\tag{1.44}
$$

[Intermediary observations]

The MOSEM and SZF expressions are two equivalent means to characterize a function:

(i) The MOSEM expression, which relies on the behaviour in the vicinity of the singularities only and thus depends on the poles and Laurent series coefficients associated with them, is useful to get a fast and accurate approximation of a function in the harmonic-domain.

(ii) The SZF is more convenient to look at the phase and better understand the behaviour on the real frequency axis.

The calculation of the Laurent series coefficients, and thus the MOSEM expression, from the SZF using the definition of the Laurent series coefficients is straightforward:

$$\begin{aligned} \alpha(H, p_0, -m) &= \lim_{\omega \to p_0} \frac{1}{m!} \partial_\omega^{m-1} [\eta](\omega) \\ \eta(\omega) &= (\omega - p_0)^{\nu_{p_0}} H(\omega) \end{aligned} \tag{1.45}$$

where p_0 is a pole of order ν_{p_0} of $H(\omega)$, and $H(\omega)$ is given by the SZF in Equation (1.42). It is however more difficult to obtain the zeros from the MOSEM expression, although they can be approximated in a specific frequency range by writing MOSEM as a rational function involving only the singularities in the selected complex frequency window and solving for the zeros of the numerator.

1.2.2.2. Accuracy testing in an exemple

Similarly to the MOSEM expression, we test the accuracy of the SZF on the function $H(\omega)$ defined in Equation (1.30). The poles were already calculated:

$$\omega_p^{(n)} = \frac{(2n+1)\pi}{2}, \; n \in \mathbb{N} \tag{1.46}$$

The only zero is 1, and the derivation of $H(0) = -1$ and $H'(0) = -1\mathrm{i}$ is straightforward. If we consider M poles, we obtain the following approximation of τ:

$$\tau_M = -\mathrm{i}\left(\mathrm{i} + 1 - \sum_{n=-M}^{M} \frac{2}{\omega_p^{(n)}}\right) \tag{1.47}$$

Hence the following M^{th} order truncated SZF of $H(\omega)$:

$$H(\omega) \approx -e^{\mathrm{i}\tau_M \omega} \frac{1-\omega}{\prod_{n=-M}^{M} \left(1 - \frac{\omega}{\omega_p^{(n)}}\right)^2} \tag{1.48}$$

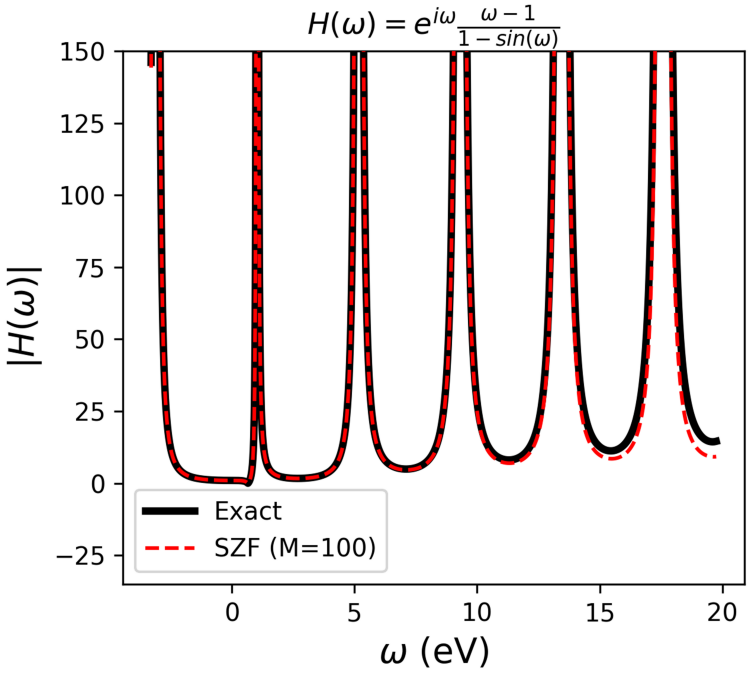

Figure 1.6. – *Modulus of the function $H(\omega)$ defined in Equation (1.30). The poles of $H(\omega)$ are the complex frequencies $\omega_p^{(n)} = 2n\pi + \pi/2$. The exact expression in black is compared to the truncated SZF in red: $-M \leq n \leq M$, with $M = 100$, given in Equation (1.48).*

In Figure 1.6, we set $M = 100$ poles to compare the truncated SZF to the exact expression of $H(\omega)$. Let us point out that many more poles M are usually necessary for the SZF than for MOSEM to accurately fit the test function.

1.3. Constraints in the harmonic domain

1.3.1. Properties of physical systems and signals

MOSEM and the SZF provide two expressions of meromorphic functions in the harmonic domain using either the poles and zeros or the poles and Laurent series coefficients, provided that the studied function $H(\omega)$ is asymptotically well-behaved. These expressions encapsulate the classical SPE or PZF and are thus particularly well-suited to study transfer functions. However, the derivation of MOSEM does not account for the constraints of physics, and thus appears, so far, as a useful mathematical tool to study transfer functions in particular situations. We show in this section that, starting from the physical domain, *i.e.* the domain in which real-valued signals abiding by fundamental properties of physics are considered, we can justify the hypothesis which led to the derivation of MOSEM, add constraints on the different parameters of the expressions, and extend the use of the expressions to the excitation and response functions of systems.

Let us consider an LTIS Σ in the temporal domain, which interacts with an excitation $x(t)$ to produce a response $y(t)$:

$$x(t) \xrightarrow{\Sigma} y(t) \tag{1.49}$$

The properties of Σ lead to the definition of a function $h(t)$ which is its response to an impulse, hence the name Impulse Response Function (IRF):

$$\delta(t) \xrightarrow{\Sigma} h(t) \tag{1.50}$$

with $\delta(t)$ the Dirac delta function.

[Key properties]

The IRF $h(t)$ completely characterizes the system in the physical domain, and any response $y(t)$ can be written as a convolution of the IRF with the excitation $x(t)$:

$$x(t) \xrightarrow{\Sigma} y(t) = (h * x)(t) \tag{1.51}$$

In the physical domain, the signals $x(t)$ and $y(t)$ must be real-valued. In addition, energy conservation imposes that both signals must decay in time (or space) and thus have Fourier transforms $X(\omega)$ and $Y(\omega)$:

$$\begin{aligned} \mathscr{F}[x](\omega) &= \int_{-\infty}^{+\infty} x(t) e^{\mathrm{i}\omega t} dt \\ \mathscr{F}[y](\omega) &= \int_{-\infty}^{+\infty} y(t) e^{\mathrm{i}\omega t} dt \end{aligned} \tag{1.52}$$

where $\mathscr{F}$ is the Fourier transform operator. This also means that the signals are bounded in the temporal domain by exponential functions $e^{-\mathrm{i}\omega t}$, with $\omega \in \mathbb{C}$.

[Key properties]

Such functions are eigenvectors or eigenstates of *LTIS*:

$$e^{-i\omega t} \xrightarrow{\Sigma} \sigma_\omega e^{-i\omega t} \tag{1.53}$$

where σ_ω is the eigenvalue associated with $e^{-i\omega t}$.

Causality states that the signals $x(t)$ and $y(t)$ must be generated after a certain time (or position) t_0, and can thus be written using the Heaviside step function $u(t)$ defined as:

$$\begin{aligned} u(t) &= 0 \quad \text{If } t < t_0 \\ u(t) &= \frac{1}{2} \quad \text{If } t = t_0 \\ u(t) &= 1 \quad \text{If } t > t_0 \end{aligned} \tag{1.54}$$

We can set $t_0 = 0$ in $1D$-systems without losing in generality (the same logic also applies in higher dimension systems with some subtleties):

$$\begin{aligned} x(t) &= x_0(t)u(t) \\ y(t) &= y_0(t)u(t) \end{aligned} \tag{1.55}$$

where $x_0(t)$ and $y_0(t)$ are non-causal signals.
The Fourier transforms thus become the Laplace transforms $X(\omega)$ and $Y(\omega)$:

$$\begin{aligned} \mathscr{F}[x](\omega) &= \int_{-\infty}^{+\infty} x(t)u(t)e^{i\omega t}\,dt \\ &= \int_0^{\infty} x_0(t)e^{i\omega t}\,dt \\ &= \mathscr{L}[x](\omega) \\ &= X(\omega) \end{aligned} \tag{1.56}$$

with $\mathscr{L}$ the Laplace transform operator. We write the Laplace transforms of functions with capital letters as a convention.

The Stone-Weierstrass theorem [113] states that the bounded-support signals can be written as polynomials. We extend that property to causal signals which are exponentially decaying with time by considering only those which can be written as the product of a polynomial $P_k(t)$ of degree k, a complex exponential function $e^{-i\omega t}$, and the Heaviside step function $u(t)$.

[Key properties]

It turns out that such functions are stable *via* the LTIS:

$$P_k(t)e^{-i\omega t}u(t) \xrightarrow{\Sigma} Q_k(t)e^{-i\omega t}u(t) \tag{1.57}$$

where $Q_k(t)$ is another polynomial of degree k. If the imaginary part of ω is positive, the function exponentially grows, but it is still possible to define its Laplace and inverse Laplace transform. Therefore, we do not constrain ω to the lower part of the complex ω-plane. The upper part will be used to study the stability of the systems.

[Intermediary observations]

By adding causality and energy conservation to LTIS, we obtain what we refer to as physical systems. Similarly, we call physical signals the associated causal signals drawn from the space of complex exponential pre-factored polynomials $P_k(t)e^{i\omega t}u(t)$.

Let us stress that, due to the symmetric role played by the excitation $x(t)$ and the IRF $h(t)$, if $y(t)$ and $x(t)$ are physical signals, so is $h(t)$. We also add $\delta(t)$ to the space of physical signals to include the case of the identity physical system:

$$x(t) \xrightarrow{\Sigma} y(t) = x(t) \tag{1.58}$$

The Laplace transform $H(\omega)$ of the IRF $h(t)$ is the transfer function, which fully characterizes the physical system in the harmonic domain as previously stated in this chapter. The harmonic output $Y(\omega)$ can be calculated from the knowledge of $H(\omega)$ and the harmonic excitation $X(\omega)$:

$$Y(\omega) = H(\omega)X(\omega) \tag{1.59}$$

[Key properties]

MOSEM is thus not limited to the transfer function $H(\omega)$, but can also be applied to the harmonic excitation $X(\omega)$ and response $Y(\omega)$, which is in agreement with the idea that an excitation was generated by another physical system and thus has a similar form.

The interaction between the excitation, the response and the IRF in both the physical domain (temporal domain) and the harmonic domain is described in Figure 1.1.

By using the properties of physical signals, we can further constraint the poles, zeros and Laurent coefficients in MOSEM and the SZF.

1.3.2. Hermitian symmetry

Let us consider $H(\omega)$ which is the Laplace transform of a physical signal $h(t)$.

[Key properties]

Since $h(t)$ is real, $H(\omega)$ is Hermitian-symmetric in the complex ω-plane [70, 114]:

$$\overline{H(-\overline{\omega})} = H(\omega) \tag{1.60}$$

with $\overline{A}$ the complex conjugate of A.

This property leads to constraints on the distribution of the poles and singularities in the complex frequency plane. By evaluating the complex conjugate of the singularity expansion in Equation (1.28) evaluated at $-\overline{\omega}$, it can be shown that for any pole p_i of order $\nu_i^{(p)}$, $-\overline{p_i}$ is also a pole of order $\nu_i^{(p)}$.

[Key properties]

We can also obtain the Laurent coefficients associated with $-\overline{p_i}$ from those of p_i *via*:

$$\begin{gathered}(p_i, \nu_i^{(p)}) \in \mathscr{P}_G \implies (-\overline{p_i}, \nu_i^{(p)}) \in \mathscr{P}_G \\ \forall m \in \mathbb{Z},\ \alpha(H, -\overline{p_i}, -m) = (-1)^m \overline{\alpha(H, p_i, -m)}\end{gathered} \tag{1.61}$$

The Laurent series coefficients of $H(\omega)$ at $-\overline{p_i}$ are thus related to those at p_i, and we show similarly that the non-resonant term H_{NR} must be real-valued.

Let us point out that Equation (1.61) imposes that the coefficients $\alpha(H, p_i, -m)$ associated with an imaginary pole $p_i \in i\mathbb{R}$ must be imaginary if m is odd, and real if m is even.

Hermitian-symmetric MOSEM

This leads to the following Hermitian-symmetric MOSEM expression:

$$\begin{aligned}H(\omega) = H_{\text{NR}} &+ \sum_{p_i \in i\mathbb{R}} \sum_{m=1}^{\nu_i^{(p)}} \frac{\alpha(H, p_i, -m)}{(\omega - p_i)^m} \\ &+ \sum_{Re[p_i]>0} \sum_{m=1}^{\nu_i^{(p)}} \left[\frac{\alpha(H, p_i, -m)}{(\omega - p_i)^m} + (-1)^m \frac{\overline{\alpha(H, p_i, -m)}}{(\omega + \overline{p_i})^m} \right]\end{aligned} \tag{1.62}$$

The poles and Laurent series coefficients thus always come in pairs, as shown in Figure 1.7 where the transfer function $H(\omega)$ is the reflection coefficient of a dispersive slab of silver, defined in Equation (1.3). In (a) and (b), the log-amplitude in a complex frequency window as well as its symmetric window is plotted, highlighting the symmetry of the amplitude and thus of the singularities. In (c) and (d), the same frequency windows were chosen for the phase plots. They show the antisymmetry of the phase with respect to the imaginary axis in the complex frequency plane, which is tantamount to an antisymmetry of the Laurent series coefficients. Let us stress that the Hermitian symmetry only arises from the fact that we have real-valued signals in the temporal domain. Considering a causal plane

wave $e^{-i\omega_0 t}u(t)$, with $u(t)$ the Heaviside step function and $\omega_0 < 0$ is not equivalent to considering that time flows backward. It only means that the variations of the phase are opposed to those of $e^{i\omega_0 t}u(t)$.

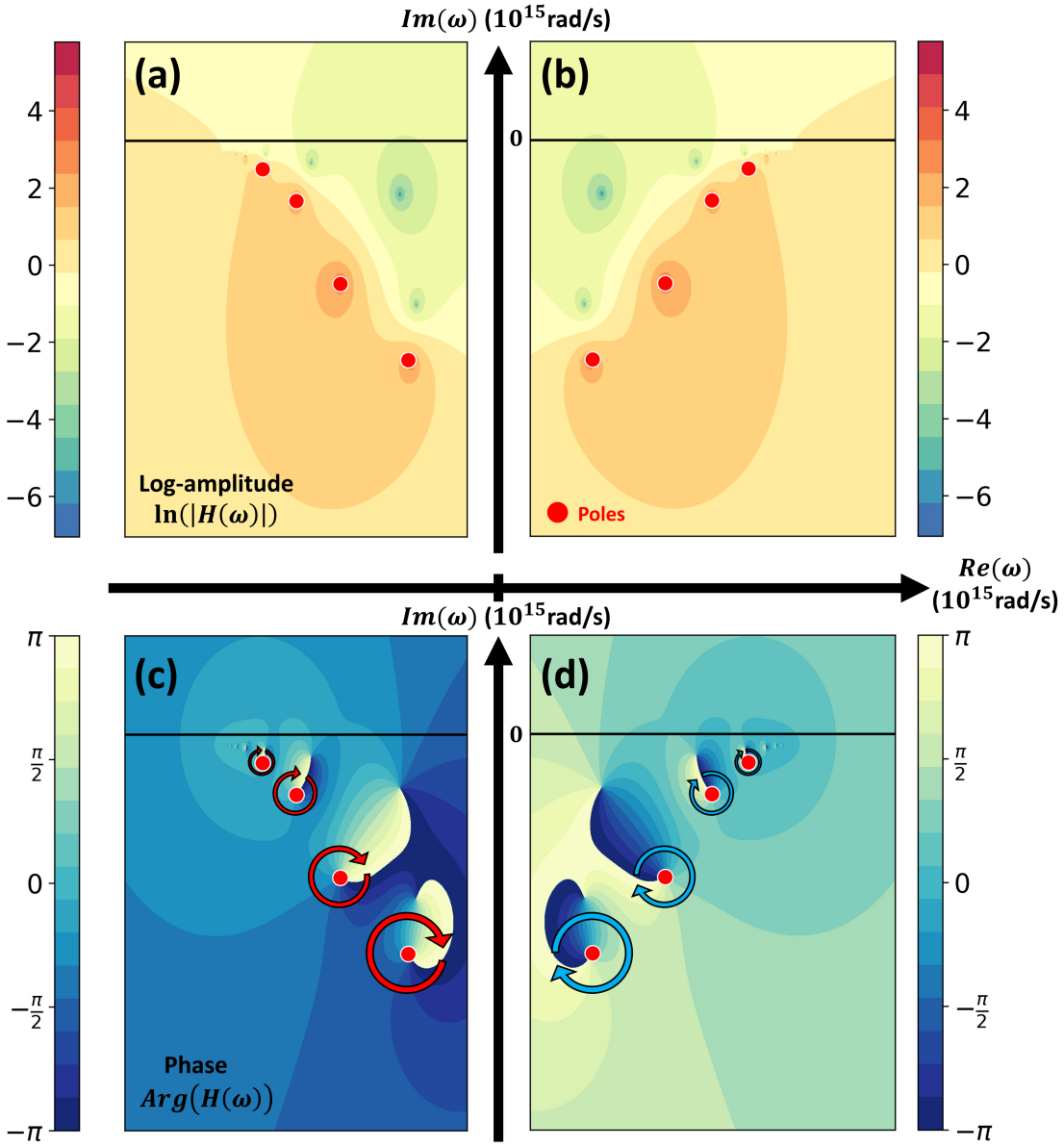

Figure 1.7. – *Complex Bode diagram of the function $H(\omega)$ defined inin Equation (1.3). (a),(b) Log-amplitude of $H(\omega)$ for a complex frequency window in (a) and its symmetric window with respect to the imaginary axis in (b). (c),(d) The phase of $H(\omega)$ in the same frequency window (c) and its symmetric window (d). The amplitude is symmetric with respect to the imaginary axis and results in a symmetric distribution of the poles (red points). The phase is antisymmetric, as shown with the red and blue arrows indicating a clockwise 2π phase-shift around the poles with a negative and positive real part respectively.*

Similarly, we can constraint the parameters of the SZF in Equation (1.42), the expression of which is:

$$\begin{aligned} H(\omega) &= \omega^m \, G(a) \, \frac{\prod_{z_\ell}(1-\frac{\omega-a}{z_\ell-a})^{\nu_\ell^{(z)}}}{\prod_{p_\ell}(1-\frac{\omega-a}{p_\ell-a})^{\nu_\ell^{(p)}}} \, e^{\mathrm{i}\tau(\omega-a)} \\ \tau &= -i\left(\frac{G'(a)}{G(a)} - \sum_{z_\ell}\frac{\nu_\ell^{(z)}}{a-z_\ell} + \sum_{p_\ell}\frac{\nu_\ell^{(p)}}{a-p_\ell}\right) \end{aligned} \tag{1.63}$$

[Key properties]

If we evalaute the SZF (Equation (1.42)) at a frequency $-\overline{\omega}$, we can show that if z_i is a zero of order $\nu_i^{(z)}$ of $H(\omega)$, then $-\overline{z_i}$ is also a zero of the same order $\nu_i^{(z)}$, *i.e.* :

$$(z,\nu_z) \in \mathcal{Z}_G \implies (-\overline{z},\nu_z) \in \mathcal{Z}_G \tag{1.64}$$

In addition, we demonstrate that the Hermitian symmetry forces the time constant τ to be real-valued.

[Derivation]

Let us write the complex quantities a, ω and τ:

$$\begin{aligned} a &= a' + \mathrm{i}a" \\ \omega &= \omega' + \mathrm{i}\omega" \\ \tau &= \tau_R + \mathrm{i}\tau_I \end{aligned} \tag{1.65}$$

with τ_R and τ_I the real and imaginary parts of τ respectively. The symmetry of the poles and zeros in Equations (1.61) and (1.64), along with the Hermitian symmetry of the SZF in Equation (1.63) lead to:

$$\begin{aligned} &\omega^m \, e^{\mathrm{i}[\tau_R(\omega'-a')-\tau_I(\omega"-a")]} \, e^{-[\tau_R(\omega"-a")+\tau_I(\omega'-a')]} G(a) \\ &= \\ &(-1)^m \, \omega^m \, e^{-\mathrm{i}[\tau_R(-\omega'-a')-\tau_I(\omega"-a")]} \, e^{-[\tau_R(\omega"-a")+\tau_I(-\omega'-a')]} \overline{G(a)} \end{aligned} \tag{1.66}$$

Equation (1.66) can only by satisfied if $\tau_I = 0$. In addition, $G(a)e^{-\mathrm{i}\tau_R a'}$ must be real-valued or purely imaginary depending on the parity of m, *i.e.* the order of the zero at the origin (0):

$$\begin{aligned} \mathrm{Im}[G(a)e^{-\mathrm{i}\tau_R a'}] = 0 \text{ if m even} \\ \mathrm{Re}[G(a)e^{-\mathrm{i}\tau_R a'}] = 0 \text{ if m odd} \end{aligned} \tag{1.67}$$

[Key properties]

Using Equation (1.63), we retrieve the expression of $\tau = \tau_R$:

$$\tau = \text{Im}\left[\frac{G'(a)}{G(a)} - \sum_{z_\ell}\left[\frac{\nu_\ell^{(z)}}{a-z_\ell} + \frac{\nu_\ell^{(z)}}{a+\overline{z_\ell}}\right] + \sum_{p_\ell}\left[\frac{\nu_\ell^{(p)}}{a-p_\ell} + \frac{\nu_\ell^{(p)}}{a+\overline{p_\ell}}\right]\right] \tag{1.68}$$

In physical system for which the space and time variables are coupled, the phase shift introduced by τ can be modified by moving the spatial or temporal origin. In this case, the zeros and poles are identical, and only the constant term linked to the static response is changed. In particular, in 1D-physical systems, τ can be cancelled, *i.e.* set to 0, by appropriately choosing the origin.

Hermitian-symmetric SZF

The combination of these properties on the poles, the zeros, and the time constant lead to the Hermitian-symmetric SZF:

$$H(\omega) = \omega^m\, G(a)\, \frac{\prod_{z_\ell}\left[\left(1-\frac{\omega-a}{z_\ell-a}\right)\left(1+\frac{\omega-a}{\overline{z_\ell}+a}\right)\right]^{\nu_\ell^{(z)}}}{\prod_{p_\ell}\left[\left(1-\frac{\omega-a}{p_\ell-a}\right)\left(1+\frac{\omega-a}{\overline{p_\ell}+a}\right)\right]^{\nu_\ell^{(p)}}}\, e^{\mathrm{i}\tau(\omega-a)} \tag{1.69}$$

$$\tau = \text{Im}\left[\frac{G'(a)}{G(a)} - \sum_{z_\ell}\left[\frac{\nu_\ell^{(z)}}{a-z_\ell} + \frac{\nu_\ell^{(z)}}{a+\overline{z_\ell}}\right] + \sum_{p_\ell}\left[\frac{\nu_\ell^{(p)}}{a-p_\ell} + \frac{\nu_\ell^{(p)}}{a+\overline{p_\ell}}\right]\right]$$

1.3.3. Stability and Causality

Stability and causality are linked but distinct principles which can both be expressed in terms of the position of the poles in the complex plane depending on the convention used to perform a Fourier transform [115]. As previously mentioned, causality states that any physical signal $h(t)$ must be generated at a certain time t_h (usually set to 0), and that it cannot depend on its future values. It is thus written using the Heaviside step function $u(t)$, as:

$$h(t) = h_0(t)\,u(t) \tag{1.70}$$

with h_0 a non-causal signal. By definition of physical signals, $h(t)$ is a combination of complex-exponential pre-factored polynomials:

$$h(t) = \sum_\ell P_\ell(t)\, e^{-\mathrm{i}\omega_\ell t}\, u(t) \tag{1.71}$$

If one of the frequencies ω_ℓ has a positive imaginary part, then $h(t)$ diverges at large times. In such a case, let us consider ω_0 the complex frequency with the highest strictly positive imaginary part. We can regularize $h(t)$ using a function h_γ, $\gamma > \mathrm{Im}[\omega_0] = p_I$, which does not diverge:

$$\begin{aligned} h(t) &= e^{\gamma t} h(t) e^{-\gamma t} u(t) \\ h(t) &= e^{\gamma t} h_\gamma(t) \end{aligned} \tag{1.72}$$

[Key properties]

By construction, $h_\gamma(t)$ possesses a Fourier transform $H_\gamma(\omega)$ from which the harmonic domain physical system $H(\omega)$ associated with $h(t)$ can be determined:

$$H(\omega) = H_\gamma(\omega - \mathrm{i}\gamma) \tag{1.73}$$

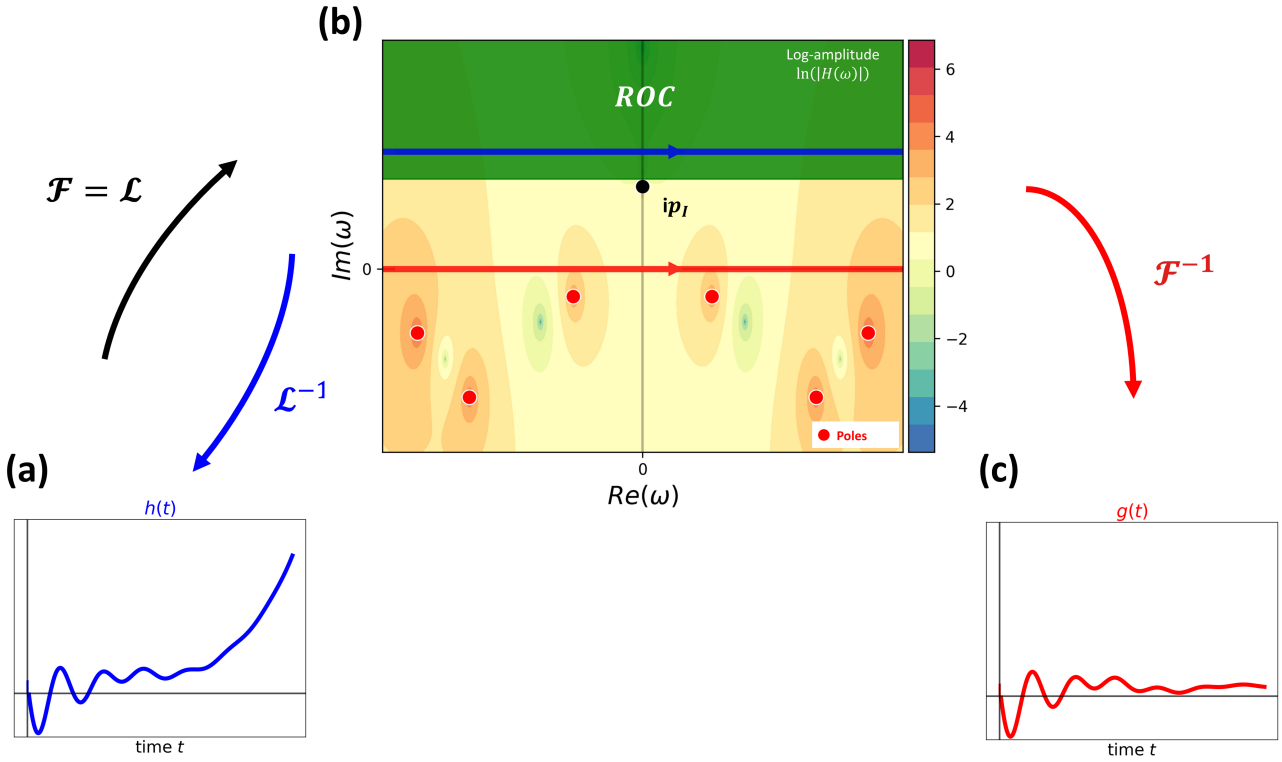

Figure 1.8. – *(a) An unstable temporal signal $h(t)$ equivalent to $e^{p_I t}$ for long times, with $p_I = 0.9$. It is obtained via inverse Laplace transform of the function $H(\omega)$ from Eq. (1.43) to which a pole $\mathrm{i}p_I$ with residue $8 + 0.1\mathrm{i}$ was added. (b) The harmonic-domain function $H(\omega)$, which can be obtained by Fourier or Laplace transform of $h(t)$. (c) A passive temporal function $g(t)$ obtained via inverse Fourier transform of $H(\omega)$. The Laplace and Fourier transformation are equivalent since the signal is causal, i.e. $h(t) = h(t)u(t)$. The Region Of Convergence (ROC) corresponds to the part of the complex frequency plane where the usual Laplace transform is defined, and within which the inverse Laplace transform should be performed to retrieve the signal $h(t)$ in (a). Below the ROC, another function would be obtained. In particular, the inverse Fourier transform is performed on the real axis, and leads to the passive function $g(t)$ in (c).*

The physical signal $h(t)$ is recovered by inverse Laplace transform, which corresponds to the integration of $H(\omega)e^{-\mathrm{i}\omega t}$ over a horizontal line within the region of convergence of $H(\omega)$, lower-bounded by $\mathrm{i}p_I$ (see Figure 1.8). Using the residue theorem, it can thus be shown that any pole possessing a positive imaginary part in the complex frequency plane is associated with a causal diverging exponential function in the temporal domain, *i.e.* an unstable signal. Therefore, any pole of the harmonic-domain function associated with a stable signal must have a negative imaginary part.

[Intermediary observations]

The stability of the signals can be interpreted with energy considerations.

— As an input or excitation signal interacts with a system, it exchanges energy with it. This leads to a modification of the input signal and results in the output signal. For a passive system, the energy is transferred from the excitation to the system.

— The output thus has a lower energy and cannot diverge if the system is passive. For the output to diverge or become unstable, it must result from a sufficient energy transfer from the system to the input, or the interaction of an already diverging input with the system.

— Therefore, the only way to obtain an unstable output is through a high-energy, unstable input, or an active system. In terms of singularities, this means that the poles of the transfer function of a passive physical system or non-diverging physical signal always possess a negative imaginary part (using our Fourier transform convention).

— If we inject energy into the physical system, *i.e.* it is active, we move the singularities closer and closer to the real axis until they cross it and the system becomes unstable.

1.4. Temporal dynamics

1.4.1. Inverse Laplace transform of harmonic signals

The singularity expansion obtained with MOSEM can be used to derive an analytical expression in the temporal domain [74, 99]. For physical systems, unstable behaviours might appear, which prevent the use of the inverse Fourier transform [116]. It is therefore preferable to use the more general inverse Laplace transform to retrieve the temporal dynamics of a system or its response (and/or input) [115].

In this section, we derive a generalized expression of the temporal domain signal $h(t)$ knowing the singularity expansion of $H(\omega)$.

[Derivation]

Since $h(t)$ is a physical signal, it reads as:

$$\begin{aligned} h(t) = \mathscr{L}^{-1}[H](t) &= H_{\text{NR}}\delta(t) + \int_{-\infty}^{+\infty} \left(\sum_{\ell} \sum_{m=1}^{\nu_\ell^{(p)}} \frac{\alpha(H, p_\ell, -m)}{(\omega - p_\ell)^{(n)}} \right) e^{-\mathrm{i}\omega t} \\ &= H_{\text{NR}}\delta(t) + \left(\sum_{\ell} \sum_{m=1}^{\nu_\ell^{(p)}} \alpha(H, p_\ell, -m) f_{m,\ell}(t) \right) \end{aligned} \tag{1.74}$$

where $\mathscr{L}^{-1}$ is the inverse Laplace transform operator, and $f_{m,\ell}(t)$ are the base functions defined as:

$$\begin{aligned} F_{m,\ell}(\omega) &= \frac{1}{(\omega - p_\ell)^m} \\ f_{m,\ell}(t) &= \mathscr{L}^{-1}[F_{m,\ell}](t) \end{aligned} \tag{1.75}$$

By recurrence, the inverse Laplace transform $f_{m,\ell}(t)$ of $F_{m,\ell}(\omega)$ can be expressed from $f_{1,\ell}(t)$:

$$f_{m,\ell}(t) = \frac{(-\mathrm{i}t)^{(m-1)}}{(m-1)!} f_{1,\ell}(t) \tag{1.76}$$

In addition:

$$f_{1,\ell}(t) = -\mathrm{i}e^{-\mathrm{i}p_\ell t} u(t) \tag{1.77}$$

This leads to the following expression of $f_{m,\ell}$:

$$f_{m,p}(t) = \frac{(-\mathrm{i})^m}{(m-1)!} t^{m-1} e^{-\mathrm{i}p_\ell t} u(t) \tag{1.78}$$

Time-Domain Singularity Expansion

The inverse Laplace transform $h(t)$ of $H(\omega)$ can therefore be derived from the singularity expansion obtained with MOSEM (Equation (1.28)):

$$h(t) = H_{\mathrm{NR}}\delta(t) + \left(\sum_{\ell} \sum_{m=1}^{\nu_\ell^{(p)}} \frac{(-\mathrm{i})^m \alpha(H,\ell,-m)}{(m-1)!} t^{m-1} e^{-\mathrm{i}p_\ell t} \right) u(t) \tag{1.79}$$

1.4.2. Response to a causal sinusoidal input

In many problems, the main focus is the global temporal response of the physical system at a specific frequency. In these situations, the characterization of the system in the harmonic domain is sufficient since it is almost equivalent to a study of the temporal permanent-regime. We expect the response of a passive system to an excitation to be composed of that same input, scaled and phase-shifted in the permanent-regime, as well as exponentially decaying functions in the transient-regime [74, 99]. It is worth demonstrating this known result by deriving the response $y(t)$ to a sinusoidal input $x(t) = Re[e^{-\mathrm{i}\omega_0 t}u(t)]$ of a physical system of impulse response $h(t)$.

[Derivation]

Since $y(t)$ and $x(t)$ are real-valued, so must be $h(t)$, which leads to:

$$\begin{aligned} y(t) = &\quad (h * \mathrm{Re}\,[x])(t) \quad = \mathrm{Re}\,[(h*x)(t)] \\ &= \mathrm{Re}\left[\mathscr{L}^{-1}[H.X](t)\right] = \mathrm{Re}\left[\mathscr{L}^{-1}[Y](t)\right] \end{aligned} \tag{1.80}$$

Let us stress that, for physical systems, unstable behaviours might be observed, which prevent the use of the inverse Fourier transform [116]. It is therefore preferable to use the more general inverse Laplace transform to retrieve the temporal dynamics [115]. The response to a sinusoidal input is the real part of the response to a causal plane wave $t \mapsto e^{-\mathrm{i}\omega_0 t}u(t)$.

In the harmonic domain, $Y(\omega)$ and $X(\omega)$ can be written as:

$$\begin{aligned} Y(\omega) &:= X(\omega)H(\omega) \\ X(\omega) &:= \mathscr{L}^{-1}[e^{-\mathrm{i}\omega_0 t}u(t)] = \frac{\mathrm{i}}{\omega - \omega_0} \end{aligned} \tag{1.81}$$

Therefore, the set of isolated singularities of the harmonic response includes the singularities of the transfer function with the same order, as well as ω_0 of order 1 introduced by the harmonic input signal $X(\omega)$. Applying MOSEM to $Y(\omega)$ gives:

$$Y(\omega) = Y_{\mathrm{NR}} + \sum_{\ell} \sum_{m=1}^{\nu_\ell^{(p)}} \frac{\alpha(Y,p_\ell,-m)}{(\omega-p_\ell)^m} + \frac{\alpha(Y,\omega_0,-1)}{\omega-\omega_0} \tag{1.82}$$

[Derivation]

The calculation of the residue of $Y(\omega)$ at ω_0 yields a result proportional to the transfer function evaluated at the plane wave frequency ω_0:

$$\begin{aligned}\alpha(Y,\omega_0,-1) &= \lim_{\omega\to\omega_0}(\omega-\omega_0)X(\omega)H(\omega),\\ \alpha(Y,\omega_0,-1) &= \mathrm{i}H(\omega_0)\end{aligned} \tag{1.83}$$

By replacing the corresponding term in Equation (1.82), we obtain:

$$Y(\omega) = Y_{\mathrm{NR}} + \mathrm{i}\frac{H(\omega_0)}{\omega-\omega_0} + \sum_{\ell}\sum_{m=1}^{\nu_\ell^{(p)}}\frac{\alpha(Y,p_\ell,-m)}{(\omega-p_\ell)^m} \tag{1.84}$$

It follows that the inverse Laplace transform of $Y(\omega)$ can be written as the sum of a Dirac delta function multiplied by Y_{NR}, an expansion on the resonant states similarly to the resonant terms in Equation (1.79) after replacing $\alpha(H,p_\ell,-m)$ by $\alpha(Y,p_\ell,-m)$, and the scaled and phase-shifted sinusoidal function $t\mapsto e^{-\mathrm{i}\omega_0 t}$:

$$\begin{aligned}\mathscr{L}^{-1}[Y](t) = Y_{\mathrm{NR}}\delta(t) + H(\omega_0)e^{-\mathrm{i}\omega_0 t}u(t)\\ +\sum_{\ell}\sum_{m=1}^{\nu_\ell^{(p)}}\alpha(Y,p_\ell,-m)f_{m,\ell}(t)\end{aligned} \tag{1.85}$$

where:

$$f_{m,\ell}(t) = \frac{(-\mathrm{i})^m}{(m-1)!}t^{m-1}e^{-\mathrm{i}p_\ell t}\ u(t) \tag{1.86}$$

Let us stress that $y(t)$ has the form of a physical signal in Equation (1.85), *i.e.* it is written as the sum of a Dirac delta function and complex exponential pre-factored causal polynomials.

The continuity and causality of the physical system impose that $\lim_{t\to 0^+} y(t) = 0$. The initial value theorem applied to $y(t)$ leads to:

$$0 = \lim_{t\to 0^+} y(t) = \lim_{\omega\to+\infty} i\omega Y(\omega) \tag{1.87}$$

It follows that the constant, non-resonant term must be equal to 0:

$$\lim_{\omega\to+\infty} i\omega Y_{NR} = 0 \Rightarrow Y_{NR} = 0 \tag{1.88}$$

Temporal response to a causal sinusoidal excitation

We obtain the aforementioned expected result: the response $y(t)$ of a passive system to a causal sinusoidal input is only composed of the scaled and phase-shifted input in the permanent regime. In the transient regime, $y(t)$ must be expanded on the set of resonant states $f_{p,n}$ of the system:

$$y(t) = H(\omega_0)e^{-i\omega_0 t}u(t) + \sum_{\ell}\sum_{m=1}^{\nu_\ell^{(p)}} \alpha(Y, p_\ell, -m) f_{m,\ell}(t) \tag{1.89}$$

This expansion remains valid in the case of an unstable system, although the concepts of transient and permanent regime no longer hold. In this case, the resonant states contain information regarding the diverging speed of $y(t)$.

1.4.3. Retrieving transfer functions from the physical domain

Complex physical systems are usually described directly in the harmonic domain through their transfer functions. There are however some situations which are better described using the known behaviour of certain quantities in the temporal or physical domain. These quantities are associated with differential equations. We will show in particular how physical systems and physical signals are retrieved from Ordinary Differential Equations (ODEs) (the common case of Partial Differential Equations (PDEs) which presents some similarities is not addressed in this manuscript).

[Derivation]

We want to solve for an ODE with a physical signal $f(t)$ and a source $s(t)$:

$$\sum_{\ell} c_\ell \partial_t^{(\ell)}[f](t) = s(t) \tag{1.90}$$

Equation (1.90) can be regarded as an operator $d = \sum_{\ell} c_\ell \partial_t^{(\ell)}$ acting upon the signal $f(t)$:

$$d[f](t) = s(t) \tag{1.91}$$

The Laplace transform of $\partial_t^{(n)}[f]$ reads as:

$$\mathscr{L}\left[\partial_t^{(n)}[f]\right](\omega) = (-i\omega)^n F(\omega) - F_{0,n}(\omega) \tag{1.92}$$

where $F(\omega)$ is the Laplace transform of $f(t)$, and $F_{0,n}$ is a harmonic source term related to the initial condition of $f(t)$.

[Derivation]

It follows that the Laplace transform of Equation (1.91) is:

$$\begin{aligned} D(\omega)F(\omega) &= S(\omega) + F_0(\omega) \\ F(\omega) &= \frac{1}{D(\omega)}\left(S(\omega) + F_0(\omega)\right) \end{aligned} \tag{1.93}$$

where:

$$\begin{aligned} S(\omega) &= \mathscr{L}[s](\omega) \\ D(\omega) &= \sum_{\ell} c_\ell (-\mathrm{i}\omega)^\ell \\ F_0(\omega) &= \sum_{\ell} c_\ell F_{0,\ell}(\omega) \end{aligned} \tag{1.94}$$

Setting $Y(\omega) = F(\omega)$, $H(\omega) = 1/D(\omega)$ and $X(\omega) = S(\omega) + F_0(\omega)$, we recover the transfer function of a physical system described by the ODE, interacting with an excitation set by both the source and the initial conditions to generate the response:

$$Y(\omega) = H(\omega)X(\omega) \tag{1.95}$$

Unique solution to an ODE in the set of physical signals

We can apply MOSEM to the transfer function $H(\omega)$ to obtain an expression in terms of its poles and analytically recover $f(t)$ which reads as:

$$\begin{aligned} f(t) &= \mathscr{L}^{-1}[Y](t) \\ &= \mathscr{L}^{-1}[H](t) * \mathscr{L}^{-1}[S + F_0](t) \end{aligned} \tag{1.96}$$

[Key properties]

Let us stress that $f(t)$ is uniquely defined in a physical system, but not in an LTIS. In time-dependent ODEs, this is due to causality which implicitly requires to take into account initial conditions. More generally, in PDEs, the use of boundary conditions are also accounted for by domain membership function which result in specific input terms in the harmonic-domain, and thus ensure once again the unicity of the solution.

[Derivation]

To demonstrate this property in ODEs, let us consider a solution $f(t)$ of Equation (1.91):

$$\begin{aligned} f(t) &= (h * x)(t) \\ d[f](t) &= s(t) \end{aligned} \tag{1.97}$$

Let us add non-causal exponential functions to $y(t)$, at the pole frequencies $\omega_p^{(m)}$:

$$f(t) = (h * x)(t) + \sum_m c_m e^{-i\omega_p^{(m)} t} \tag{1.98}$$

The poles $\omega_p^{(m)}$ of $H(\omega)$ are zeros of $D(\omega)$. Their associated eigenstates $t \mapsto e^{-i\omega_p^{(m)}}$ are thus also zeros of the system in the temporal domain:

$$\begin{aligned} d\left[e^{-i\omega_p^{(m)} t}\right](t) &= D\left(\omega_p^{(m)}\right) e^{-i\omega_p^{(m)} t} \\ &= 0 \times e^{-i\omega_p^{(m)} t} \end{aligned} \tag{1.99}$$

Therefore, the operator $d[.]$, and thus the system, are transparent to the additional non-causal terms in $f(t)$:

$$\begin{aligned} d[f](t) &= s(t) + \sum_m c_m D(\omega_p^{(m)}) e^{-i\omega_p^{(m)} t} \\ &= s(t) \end{aligned} \tag{1.100}$$

[Intermediary observations]

We recover the general solutions of any ODE as the sum of a particular solution $(h * x)(t)$ and the solutions to the homogeneous problem $\sum_m c_m e^{-i\omega_p^{(m)} t}$.

— Causality ensures the unicity of the response of a physical system. As a consequence, knowing exactly the response of a physical system in the temporal domain as well as its impulse response is enough to perform an inverse problem and retrieve the excitation or input signal.

— By virtue of the aforementioned symmetric role of the excitation and impulse response function, it is possible to retrieve the impulse response from the exact knowledge of the input and output signals in the temporal domain.

1.5. Conclusion

Summary and conclusion

This first post-introduction chapter served as an introduction to the physical systems and physical signals which are used throughout the manuscript.

— The idea of Linear Time-Invariant System (LTIS) has been long known and exploited for the models that result from this formalism, with an excitation and a response functions linked together by an impulse response in the temporal domain, and a transfer function which can easily be approximated in terms of complex frequencies called poles and zeros.

— We have demonstrated that these accurate approximations, which can be intuited, are in fact special cases of the more general Multiple-Order Singularity Expansion Method (MOSEM) and Singularity and Zero Factorization (SZF) which we have rigorously derived under simple, non-restrictive hypothesis.

— We have shown that in the case of physical systems, a sub-class of LTIS abiding by the rules of causality and energy conservation, the parameters of the SZF and MOSEM could be constrained and linked to the stability of the system and its response.

— In addition, the class of physical signals was introduced, which extends and justifies the use of these harmonic domain expressions to describe both the excitation and response functions.

— Finally, by focusing on MOSEM, we have derived the exact analytical expressions of the physical signals from the knowledge of their associated harmonic domain functions.

— We demonstrated the classical result stating that the response to a causal sinusoidal excitation, although time-shifted, was proportional to that excitation in the steady regime, while the transient regime held information regarding the poles and Laurent coefficients of the physical system.

— Starting from the temporal-domain where Ordinary Differential Equations (ODEs) describe a field or function generated by a source or initial-condition, we have also shown that transfer functions are related to the ODE operator. There is a one-to-one relation between the impulse response function and the excitation or response function and the impulse response for physical systems. This leads to the unicity of the solutions to inverse problems in case of absolute knowledge of the *a priori* information in the temporal domain.

Summary and conclusion

This chapter is associated with the publication in reference [117], where MOSEM and the SZF, as well as their inverse Laplace transforms in the temporal domain, are derived.

The next chapter is dedicated to the study of MOSEM in the practical case of a simple Fabry-Perot cavity, where the singularities and residues can only be retrieved in a finite-size spectral window. We shall show that in such a setting, highly accurate analytical expressions in agreement with the expected physical behaviour of the system can still be obtained in both the time and harmonic domains.

Summary of the results

Hermitian-symmetric SZF

$$H(\omega) = \omega^m \, G(a) \, \frac{\prod_{z_\ell} \left[\left(1 - \frac{\omega - a}{z_\ell - a}\right)\left(1 + \frac{\omega - a}{\overline{z_\ell} + a}\right) \right]^{\nu_\ell^{(z)}}}{\prod_{p_\ell} \left[\left(1 - \frac{\omega - a}{p_\ell - a}\right)\left(1 + \frac{\omega - a}{\overline{p_\ell} + a}\right) \right]^{\nu_\ell^{(p)}}} \, e^{\mathrm{i}\tau(\omega - a)}$$

$$\tau = \mathrm{Im}\left[\frac{G'(a)}{G(a)} - \sum_{z_\ell} \left[\frac{\nu_\ell^{(z)}}{a - z_\ell} + \frac{\nu_\ell^{(z)}}{a + \overline{z_\ell}} \right] + \sum_{p_\ell} \left[\frac{\nu_\ell^{(p)}}{a - p_\ell} + \frac{\nu_\ell^{(p)}}{a + \overline{p_\ell}} \right] \right]$$

Hermitian-symmetric MOSEM

$$H(\omega) = H_{\mathrm{NR}} + \sum_{p_i \in i\mathbb{R}} \sum_{m=1}^{\nu_i^{(p)}} \frac{\alpha(H, p_i, -m)}{(\omega - p_i)^m}$$
$$+ \sum_{Re[p_i] > 0} \sum_{m=1}^{\nu_i^{(p)}} \left[\frac{\alpha(H, p_i, -m)}{(\omega - p_i)^m} + (-1)^m \frac{\overline{\alpha(H, p_i, -m)}}{(\omega + \overline{p_i})^m} \right]$$

Time-Domain Singularity Expansion

$$h(t) = H_{\mathrm{NR}} \delta(t) + \left(\sum_{\ell} \sum_{m=1}^{\nu_\ell^{(p)}} \frac{(-\mathrm{i})^m \alpha(H, \ell, -m)}{(m-1)!} \, t^{m-1} e^{-\mathrm{i} p_\ell t} \right) u(t)$$

Temporal response to a causal sinusoidal excitation

$$y(t) = H(\omega_0)e^{-i\omega_0 t}u(t) + \sum_{\ell}\sum_{m=1}^{\nu_\ell^{(p)}} \alpha(Y, p_\ell, -m) f_{m,\ell}(t)$$

Unique solution to an ODE in the set of physical signals

$$f(t) = \mathscr{L}^{-1}[](t) * \mathscr{L}^{-1}[S + F_0](t)$$

with $H(\omega)$ the transfer function of the physical systems, $S(\omega)$ the source term, and $F_0(\omega)$ the initial conditions.

2. Singularity expansion of a symmetrical Fabry-Perot cavity

Contents

2.1. Cavities and resonances . . . 71
2.2. S matrix and impulse response of a non-dispersive slab . . . 72
2.2.1. Singularity expansion of the S matrix . . . 72
2.2.2. Impulse Response Function . . . 76
2.3. Times dynamics for different excitation pulses . . . 80
2.3.1. Extremely narrow Gaussian Pulse . . . 81
2.3.2. Gaussian and rectangular envelopes . . . 81
2.3.3. Accuracy and convergence of the temporal singularity expansion . . . 82
2.3.4. From transient to permanent regime . . . 84
2.4. Case of a lossy and dispersive metallic slab . . . 88
2.4.1. Distribution of the poles . . . 88
2.4.2. Pole expansion in the harmonic and temporal domains . . . 89
2.5. Conclusion . . . 93

2.1. Cavities and resonances

Resonances play a fundamental role in various fields of wave physics, such as acoustics, electronics, mechanics and electromagnetism. In optics and photonics, resonant light interaction with optical resonators is a key concept occurring in a variety of applications such as laser cavities [118], non-linear optics [119] and enhanced Purcell factors [120]. Resonances originate from the excitation of resonant states of the photonic cavities [55, 70, 71, 101, 121, 122]. In the framework of linear light-matter interaction, optical cavities are physical systems coupled with their surroundings, and are thus lossy, which ensures their stability. With the convention introduced in Chapter 1 for the inverse Laplace transform, the poles thus have a negative imaginary part [58, 123].

The study of the optical response in terms of the resonant states has been the topic of a growing interest over the last years [54, 56, 70, 103, 124, 125], and this theory is now widely used to describe and design advanced photonic components with significant advances in non-linear optics [59], dispersive materials [125], chiral and bi-anisotropic materials [56], Purcell factors and complex effective mode volumes [88, 124, 126–129], diffraction gratings [57], shape optimization [130] or also quantum electrodynamics [131]. The S matrix formalism is commonly used to describe the response of a system to a given excitation in the harmonic domain [43, 132–135]. It provides the outgoing field with respect to the incident field [136–140]. The S matrix formalism is very general [90, 122, 137, 141–143] and can be applied to all types of geometries of photonic cavities, such as 2D [32] and 3D scatterers [74, 75], or periodic structures like diffraction gratings or metasurfaces [71, 100]. Important efforts have been put to produce expressions of scattering operators in terms of poles and zeros [70, 71, 101, 122], which were used to provide novel insights on the resonant light scattering, physical bounds and anomalies in the spectral response of metasurfaces [71, 121, 137, 138, 144].

The role of poles in the time dynamics of scattered fields in cavities was investigated in the 1970's in the context of radars and electromagnetic scattering by targets and hidden objects [31, 35, 145]. These pioneering groups paid particular attention to the response of the scatterers in the time domain [33, 146]. Resonant state theory has also recently been used to provide a better understanding of the response of optical systems in the time domain by directly expanding the incident and scattered fields on the set of resonant states [74, 104, 147–152].

In this chapter, we look at the simplest and most widespread type of cavity: the symmetrical slab geometry, also known as the Fabry-Perot cavity [153, 154]. The components of the S matrix of this structure have known expressions. By considering them as the transfer functions of physical systems, we will expand them on their sets of poles and test the accuracy of the Singularity Expansion Method (SEM). We will also look at the dynamics of the reflection and transmission coefficients in the temporal domain *via* inverse Laplace transforms. The resulting Impulse Response Functions (IRFs) will be compared to simulations and we will highlight the role of the poles in the different types of regime introduced in the previous chapter.

2.2. S matrix and impulse response of a non-dispersive slab

2.2.1. Singularity expansion of the S matrix

Let us consider a symmetrical Fabry-Perot cavity of permittivity $\varepsilon(\omega)$ and thickness d, illuminated at normal incidence, as depicted in Figure 2.1 (a). The S matrix links the incoming fields from the left $E_L^{(-)}(\omega)$ and the right $E_R^{(-)}(\omega)$ to the ougoing fields $E_L^{(+)}(\omega)$ and $E_R^{(+)}(\omega)$:

$$\begin{pmatrix} E_L^{(+)}(\omega) \\ E_R^{(+)}(\omega) \end{pmatrix} = S(\omega) \begin{pmatrix} E_L^{(-)}(\omega) \\ E_R^{(-)}(\omega) \end{pmatrix} \tag{2.1}$$

The S matrix is written in terms of the reflection coefficient $\tilde{r}(\omega)$ and the transmission coefficient $\tilde{t}(\omega)$ of the cavity:

$$S(\omega) = \begin{pmatrix} \tilde{r}(\omega) & \tilde{t}(\omega) \\ \tilde{t}(\omega) & \tilde{r}(\omega) \end{pmatrix} \tag{2.2}$$

Since $S(\omega)$ is a transfer operator of the cavity, it characterizes it. The latter can thus be entirely described by the components of the S matrix, as illustrated in Figure 2.1 (b).

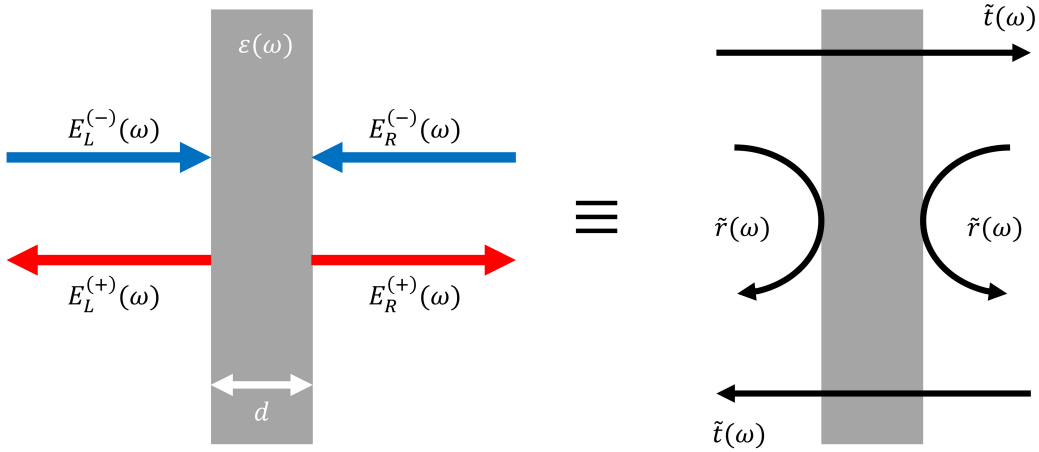

Figure 2.1. – *(a) Representation of the incoming (in blue) and outgoing (in red) waves on the symmetrical Fabry-Perot cavity. The refractive index of the slab is $n(\omega) = \sqrt{\varepsilon(\omega)}$ its thickness is d. Outgoing and incoming waves propagate along the z-axis, and $z = 0$ is taken at the left interface. (b) Equivalent representation of the slab via the components of its S matrix, name $\tilde{r}(\omega)$ and $\tilde{t}(\omega)$.*

Using the Airy model or the S matrix formalism, the reflection and transmission coefficients can be derived with respect to the Fresnel coefficients at the two air-dielectric interfaces that are respectively equal to $r = \frac{1-n}{1+n}$, $t = \frac{2}{1+n}$ (air/medium interface) and $r' = \frac{n-1}{n+1}$, $t' = \frac{2n}{n+1}$ (medium/air interface), with $n(\omega) = \sqrt{\varepsilon(\omega)}$ the refractive index

$$\tilde{r}(\omega) = r + \frac{tt'r'e^{2ink d}}{1-\left(r'e^{ink d}\right)^2}; \quad \tilde{t}(\omega) = \frac{tt'e^{ink d}}{1-\left(r'e^{ink d}\right)^2} \tag{2.3}$$

The symmetry of the slab translates into a symmetry of the S matrix itself. As a consequence, $\begin{pmatrix}1\\1\end{pmatrix}$, and $\begin{pmatrix}1\\-1\end{pmatrix}$ are two eigenvectors associated with two different eigenvalues $S_e(\omega)$ and $S_o(\omega)$:

$$S\begin{pmatrix}1\\1\end{pmatrix} = S_e(\omega)\begin{pmatrix}1\\1\end{pmatrix}; \quad S\begin{pmatrix}1\\-1\end{pmatrix} = -S_o(\omega)\begin{pmatrix}1\\-1\end{pmatrix} \tag{2.4}$$

The eigenvalues $S_e(\omega)$ and $S_o(\omega)$ are respectively the even and odd eigenvalues. From Equation (2.4), we see that the S matrix can be diagonalized into $S = PS_DP^{-1}$, in the basis of the two previous eigenvectors [71]:

$$S = PS_DP^{-1} \tag{2.5}$$

$$S_D = \begin{pmatrix}S_e(\omega) & 0\\0 & -S_o(\omega)\end{pmatrix}; \quad P = \frac{1}{\sqrt{2}}\begin{pmatrix}1 & 1\\1 & -1\end{pmatrix} \tag{2.6}$$

Hence $\tilde{r}(\omega)$ and $\tilde{t}(\omega)$ can be expressed in terms of the eigenvalues $S_e(\omega)$ and $S_o(\omega)$:

$$\tilde{r}(\omega) = \frac{S_e(\omega) - S_o(\omega)}{2} \tag{2.7}$$

$$\tilde{t}(\omega) = \frac{S_e(\omega) + S_o(\omega)}{2} \tag{2.8}$$

[Key properties]

— Equations (2.7) and (2.8) highlight an important property of transfer operators: **if the change-of-basis matrix P is frequency-independent, *i.e.* the eigenvectors are static, then the coefficients of the transfer operator all share the same poles.**

— In this case, the poles of $\tilde{r}(\omega)$ and $\tilde{t}(\omega)$ are exactly those of $S_e(\omega)$ and $S_o(\omega)$.

— What characterizes the transmission and reflection coefficients of the Fabry-Perrot cavity is therefore the set of zeros or residues associated with the poles.

A resonant states analysis of light-scattering involves a pole expansion of the S matrix coefficients [70, 71, 74, 75, 155]. To do so, we must first retrieve the poles of the eigenvalues $S_e(\omega)$ and $S_o(\omega)$. Let us first consider a non-dispersive slab with a constant dielectric permittivity $n = 3$. Since $\tilde{r}(\omega)$ and $\tilde{t}(\omega)$ are transfer functions of physical systems, any linear combination of the two also is. Therefore $S_e(\omega)$ and $S_o(\omega)$ must share the properties of transfer functions of physical systems. With the conventional time dependence $e^{-i\omega t}$, and for a passive slab, *i.e.* it does not receive energy, the poles must have a negative imaginary part and are therefore all located in the lower part of the complex frequency plane. Their expressions, as well as the ones of their associated residues can be derived analytically. We first consider even modes:

$$S_e(\omega) = \tilde{r}(\omega) + \tilde{t}(\omega) = \frac{e^{inkd} - r'}{1 - r'e^{inkd}}. \tag{2.9}$$

[Derivation]

$S_e(\omega)$ is composed of the functions $f(z) = \frac{z-r'}{1-r'z}$ and $g(\omega) = e^{i\omega\tau_0}$ with $\tau_0 = \frac{nd}{c}$ a constant time corresponding to a propagation of the field through the slab. $\frac{1}{r'}$ is the unique pole of $f(z)$. Therefore, all the poles of $S_e(\omega)$ are solutions of $\frac{1}{r'} = g(\omega)$. Let us call $\omega_0^{(e)}$ one such solution. We have:

$$\omega_0^{(e)} = i\frac{\ln(|r'|)}{\tau_0} \tag{2.10}$$

$$\omega_\alpha^{(e)} = \frac{2\pi\alpha}{\tau_0} + \omega_0^{(e)} \tag{2.11}$$

with α an integer. $S_e(\omega)$ thus has an infinite amount of poles $\omega_\alpha^{(e)}$ of order 1. We can derive the explicit expressions of the residues $r_\alpha^{(e)}$ of $S_e(\omega)$ from the residue $\mathrm{Res}\left(f, \frac{1}{r'}\right)$ of $f(z)$ at $\frac{1}{r'}$:

$$r_\alpha^{(e)} = \frac{-i}{\tau_0}\,\mathrm{Res}\left(f, \frac{1}{r'}\right) g(-\omega_\alpha^{(e)}) = \frac{-ir'}{\tau_0}\,\mathscr{R}, \tag{2.12}$$

with $\mathscr{R} = \mathrm{Res}\left(f, \frac{1}{r'}\right) = (r'^2 - 1)/(r'^2)$.

The odd eigenvalue reads as:

$$S_o(\omega) = \tilde{t}(\omega) - \tilde{r}(\omega) = \frac{e^{inkd} + r'}{1 + r'e^{inkd}}. \tag{2.13}$$

Similar calculations for its poles and residues lead to:

$$\omega_\alpha^{(o)} = \frac{(2\alpha - 1)\pi}{\tau_0} + i\frac{\ln\left(|r'|\right)}{\tau_0} \tag{2.14}$$

$$r_\alpha^{(o)} = \frac{ir'}{\tau_0}\,\mathscr{R} = -r_\alpha^{(e)} \tag{2.15}$$

SEM of the reflection and transmission coefficients

The SEM expressions of the reflection and transmission coefficients are retrieved by applying the SEM to $S_e(\omega)$ and $S_o(\omega)$ in Equations (2.7) and (2.8):

$$\tilde{r}(\omega) = \tilde{r}_{\mathrm{NR}} - \frac{i\mathscr{R}r'}{2\tau_0} \sum_{\alpha=-\infty}^{+\infty} \left(\frac{1}{\omega - \omega_\alpha^{(e)}} + \frac{1}{\omega - \omega_\alpha^{(o)}} \right) \tag{2.16}$$

$$\tilde{t}(\omega) = \frac{-i\mathscr{R}r'}{2\tau_0} \sum_{\alpha=-\infty}^{+\infty} \left(\frac{1}{\omega - \omega_\alpha^{(e)}} - \frac{1}{\omega - \omega_\alpha^{(o)}} \right) \tag{2.17}$$

The non-resonant term $\tilde{r}_{\mathrm{NR}}$ reads as:

$$\tilde{r}_{\mathrm{NR}} = -\frac{\mathrm{i}\mathscr{R}r'}{2\tau_0}\sum_{\alpha=-\infty}^{+\infty}\left(\frac{1}{\omega_\alpha^{(e)}}+\frac{1}{\omega_\alpha^{(o)}}\right) \tag{2.18}$$

Let us stress that the transmission coefficient cannot have a non-resonant term. The inverse Laplace transform of the non-resonant term is that term multiplied by the Dirac delta function, associated with an instantaneous response of the physical system, as described in the previous chapter. Since the field must travel through the slab before being transmitted, this instantaneous response is not possible for $\tilde{t}(\omega)$:

$$\tilde{t}_{\mathrm{NR}} = 0 = 1 - \frac{\mathrm{i}\mathscr{R}r'}{2\tau_0}\sum_{\alpha=-\infty}^{+\infty}\left(\frac{1}{\omega_\alpha^{(e)}}-\frac{1}{\omega_\alpha^{(o)}}\right) \tag{2.19}$$

Let us also point out that the instantaneous response in reflection is due to the constant refractive index of the medium, which imposes a constant Fresnel reflection coefficient at the interface, and thus a first reflection without dispersion.

The accuracy of the pole expansions of the reflection and transmission coefficients can only be tested after truncation:

$$\tilde{r}(\omega) = \tilde{r}_{\mathrm{NR}} - \frac{\mathrm{i}\mathscr{R}r'}{2\tau_0}\sum_{\alpha=-M}^{+M}\left(\frac{1}{\omega-\omega_\alpha^{(e)}}+\frac{1}{\omega-\omega_\alpha^{(o)}}\right) \tag{2.20}$$

$$\tilde{t}(\omega) = \frac{-\mathrm{i}\mathscr{R}r'}{2\tau_0}\sum_{\alpha=-M}^{+M}\left(\frac{1}{\omega-\omega_\alpha^{(e)}}-\frac{1}{\omega-\omega_\alpha^{(o)}}\right) \tag{2.21}$$

where M is the truncation order, corresponding to the number of poles accounted for. We plot the results for $M = 30$ in Figure 2.2.

The transmission coefficients is better approximated than the reflection one, hinting at the aforementioned fact that poles far from the spectral window of interest are contributing to the response within that window through the non-resonant term.

Let us stress that although the truncation number M is set to 30 in Figure 2.2, it was tested for different values, and a good convergence was observed for $\tilde{r}(\omega)$ for $M > 50$. A more thorough study of the convergence in the harmonic domain is performed in the last section, in the case of a dispersive slab of gold, where we deemed it more relevant.

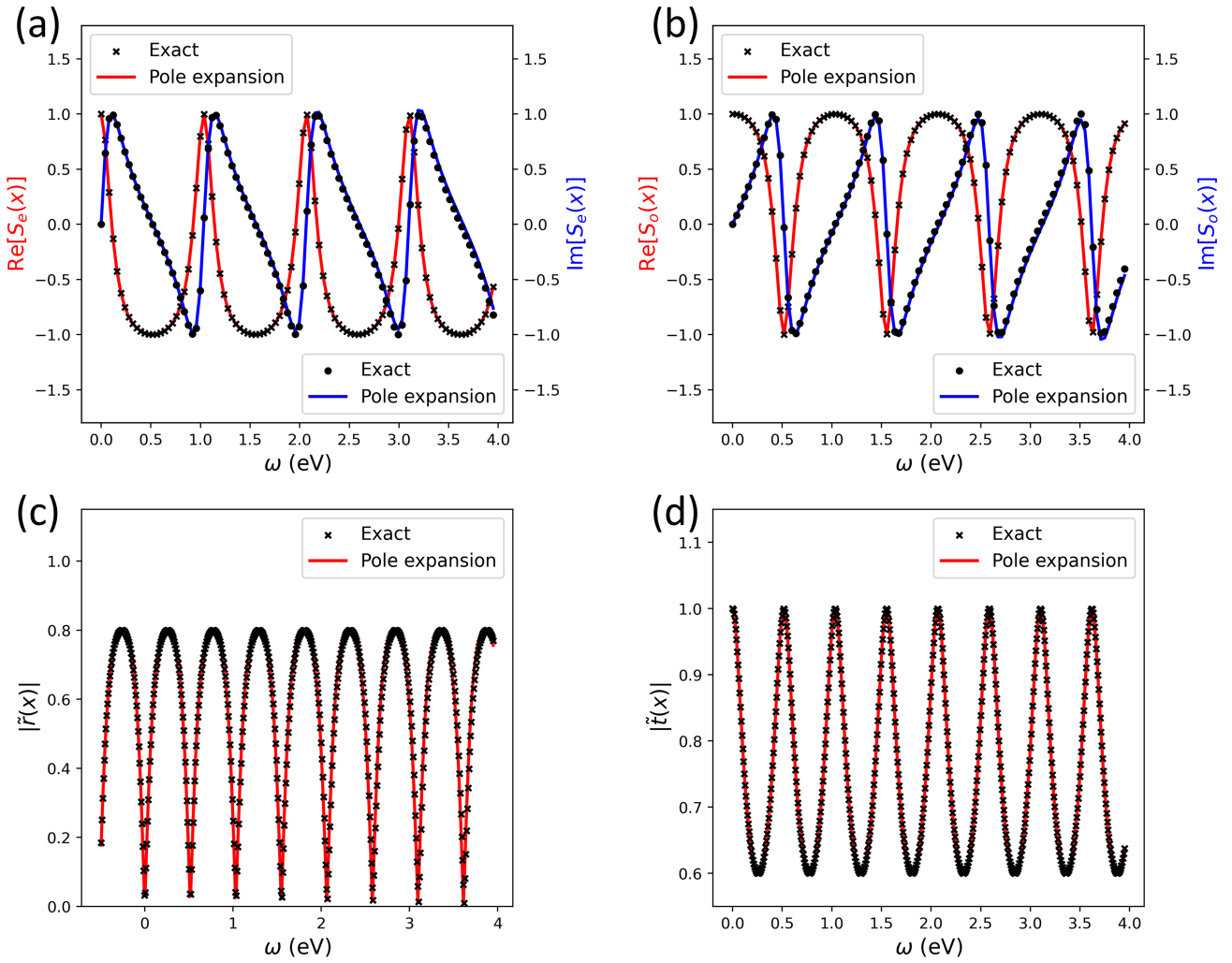

Figure 2.2. – *Comparison between modal expansions and exact calculations. (a,b) Real and imaginary parts of the even and odd eigenvalues $S_e(x)$ (a) and $S_o(x)$ (b); Modulus of the reflection (c) and transmission (d) coefficients. The pole expansions are calculated with a truncation number $M = 30$ ($-M \leq \alpha \leq M$) in Equations (2.20) and (2.21).*

2.2.2. Impulse Response Function

The IRF of a physical system, introduced in Chapter 1 as the inverse Laplace transform of the transfer function, is related to the time-dependent Green function. It is an intrinsic characteristic function of the system since it provides the response of the system to an excitation $E_{\text{exc}}(z = 0, t)$ with an arbitrary temporal shape:

$$E_{\tilde{r}}(z, t) = \text{Re}\left[(E_{\text{exc}}(z = 0, t) * \text{IRF}_{\tilde{r}}(z, t)\right] \tag{2.22}$$

$$E_{\tilde{t}}(z, t) = \text{Re}\left[(E_{\text{exc}}(z = 0, t) * \text{IRF}_{\tilde{t}}(z, t)\right] \tag{2.23}$$

with $*$ the convolution product. This is usually referred to as the Fourier method. The computation of the IRF is often complicated even when the Fourier or Laplace transforms of the reflection or transmission coefficients are known. However, the SEM offers the significant advantage of providing an exact expression of the IRF from the singularities of the reflection and transmission coefficients.

[Derivation]

The expressions of the reflected and transmitted IRFs are obtained by calculating the inverse Fourier transform of the frequency-dependent pole expansion of the fields obtained in the previous section. Let us detail here the case of the reflected field:

$$E_{\tilde{r}}(z,t) = \int_{-\infty}^{\infty} \tilde{r}(\omega)\tilde{E}_{\text{exc}}(z=0,\omega)e^{-\mathrm{i}kz}e^{-\mathrm{i}\omega t}d\omega = E_{\text{exc}}(z=0,t) * \text{IRF}_{\tilde{r}}(z,t) \tag{2.24}$$

The IRF corresponds to the case where $E_{\text{exc}}(z=0,t)=\delta(t)$. In order to take into account the propagation through space, the IRF is not directly the inverse Laplace transform of $\tilde{r}(\omega)$, and must instead be defined as $\text{IRF}_{\tilde{r}}(z,t) = \mathscr{L}^{-1}[\tilde{r}(\omega)e^{\mathrm{i}kz}](t)$. Using the expression of the reflection coefficient in Equation (2.12), as well as the formula for the impulse response in Chapter 1, Equation (1.79), and by taking into account the Hermitian symmetry, we obtain:

$$\begin{aligned}\text{IRF}_{\tilde{r}}(z,t) =& \tilde{r}_{\text{NR}}\delta\left(t+\frac{z}{c}\right)\\ &-\frac{\mathscr{R}r'}{\tau_0}\cos\left(\frac{\pi(t+\frac{z}{c})}{2\tau_0}\right)e^{-\mathrm{i}\frac{\pi(t+\frac{z}{c})}{2\tau_0}}u\left(t+\frac{z}{c}\right)\sum_{\alpha=-\infty}^{+\infty}e^{-\mathrm{i}\omega_\alpha^{(e)}(t+\frac{z}{c})}.\end{aligned} \tag{2.25}$$

A similar expression is obtained for $\text{IRF}_{\tilde{t}}(z,t)$:

$$IRF_{\tilde{t}}(z,t) = -\frac{\mathscr{R}r'}{2\tau_0}u\left(t-\frac{z-d}{c}\right)\sum_{\alpha=-\infty}^{+\infty}\left(e^{-\mathrm{i}\omega_\alpha^{(e)}\left(t-\frac{z-d}{c}\right)}-e^{-\mathrm{i}\omega_\alpha^{(o)}\left(t-\frac{z-d}{c}\right)}\right) \tag{2.26}$$

[Intermediary observations]

— As expected from the expression of the IRFs of a physical system derived in the previous chapter, the response of a Fabry-Perot cavity to a Dirac excitation is a superposition of a Dirac delta function and a set of oscillating sinusoidal functions with an exponentially decreasing envelope.

— At first glance, this seems in contradiction with the classical description of the response of a Fabry-Perot cavity to a Dirac excitation, as a series of Dirac distributions with a decreasing envelope depending on the number of times light has been reflected back and forth inside the slab. By further manipulating Equation (2.25), we will show that the two descriptions are equivalent.

[Derivation]

Let us consider the expression of the Dirac comb Ш_T :

$$\text{Ш}_T(t) = \sum_{\alpha=-\infty}^{\infty} \delta(t-\alpha T) = \frac{1}{T}\sum_{\alpha=-\infty}^{\infty} e^{-\mathrm{i}\frac{2\pi\alpha}{T}t} \tag{2.27}$$

Since all the complex frequencies $\omega_\alpha^{(e)} = \frac{2\pi\alpha}{\tau_0} + \mathrm{i}\frac{\ln(|r'|)}{\tau_0}$ have the same imaginary part, we can substitute the sum of resonant states in Equation (2.25) with a Dirac comb:

$$\begin{aligned}\frac{1}{\tau_0}\sum_{\alpha=-\infty}^{+\infty} e^{-i(2\pi\alpha+i\ln(|r'|))\frac{\left(t+\frac{z}{c}\right)}{\tau_0}} &= \frac{e^{\ln(|r'|)\frac{t+\frac{z}{c}}{\tau_0}}}{\tau_0}\sum_{\alpha=-\infty}^{+\infty} e^{-\mathrm{i}2\pi\alpha\frac{\left(t+\frac{z}{c}\right)}{\tau_0}} \\ &= e^{\ln(|r'|)\frac{t+\frac{z}{c}}{\tau_0}}\sum_{\alpha=-\infty}^{+\infty}\delta(t+\frac{z}{c}-\alpha\tau_0).\end{aligned} \tag{2.28}$$

where $\tau_0 = \frac{nd}{c}$ is the period. Thus the expression in Equation (2.25) is a superposition of Dirac's delta functions with exponentially decreasing amplitudes. What is more, let us point out that the cosinus term in Equation (2.25) takes on only two values: 1 when α is even, and 0 otherwise:

$$\begin{aligned}\cos\left(\frac{\pi}{2\tau_0}(\alpha\tau_0)\right)e^{-\mathrm{i}\frac{\alpha\pi}{2}} &= 1 \quad \text{if } \alpha \text{ even,} \\ &= 0 \quad \text{otherwise.}\end{aligned} \tag{2.29}$$

Finally, using the Heaviside step function and the fact that τ_0 is positive, we have:

$$\begin{aligned}u\left(t+\frac{z}{c}\right)\delta\left(t+\frac{z}{c}-\alpha\tau_0\right) &= \delta\left(t+\frac{z}{c}-\alpha\tau_0\right) \quad \text{if } \alpha>0, \\ &= \frac{1}{2}\delta\left(t+\frac{z}{c}\right) \quad \text{if } \alpha=0, \\ &= 0 \quad \text{otherwise.}\end{aligned} \tag{2.30}$$

Exact expression of the IRF of a non-dispersive slab in reflection

Combining these elements, we recast the exact expression of $\text{IRF}_{\tilde{r}}(z,t)$ as:

$$\text{IRF}_{\tilde{r}}(z,t) = \left(\tilde{r}_{\text{NR}} - \frac{\mathscr{R}r'}{2}\right)\delta(t+\frac{z}{c}) - \mathscr{R}r'\sum_{\alpha=1}^{\infty}\delta\left(t+\frac{z}{c}-2\alpha\tau_0\right)e^{2\alpha\ln(|r'|)} \tag{2.31}$$

This result is in complete agreement with the intuitive picture of the interaction of a Dirac excitation with a Fabry-Perot cavity.

Exact expression of the IRF of a non-dispersive slab in transmission

Similarly, in transmission, we have:

$$\mathrm{IRF}_{\tilde{t}}(z,t) = -\mathscr{R}r' \sum_{\alpha=1}^{\infty} \delta\left(t - \frac{z-d}{c} - 2(\alpha-1)\tau_0\right) e^{2(\alpha-1)\ln(|r'|)} \tag{2.32}$$

Using Equations (2.22) and (2.23) along with the calculated IRFs involving Dirac delta functions, we derive the following expressions of the reflected and transmitted fields, for any excitation E_{exc}:

$$E_{\tilde{r}}(z,t) = \left(\tilde{r}_{\mathrm{NR}} - \frac{\mathscr{R}r'}{2}\right) E_{\mathrm{exc}}\left(z=0,\ t+\frac{z}{c}\right) - \mathscr{R}r' \sum_{\alpha=1}^{\infty} E_{\mathrm{exc}}\left(z=0,\ t+\frac{z}{c}-2\alpha\tau_0\right) e^{2\alpha\ln(|r'|)} \tag{2.33}$$

$$E_{\tilde{t}}(z,t) = -\mathscr{R}r' \sum_{\alpha=1}^{\infty} E_{\mathrm{exc}}\left(z=0,\ t+\frac{z-d}{c}-2(\alpha-1)\tau_0\right) e^{2(\alpha-1)\ln(|r'|)} \tag{2.34}$$

2.3. Times dynamics for different excitation pulses

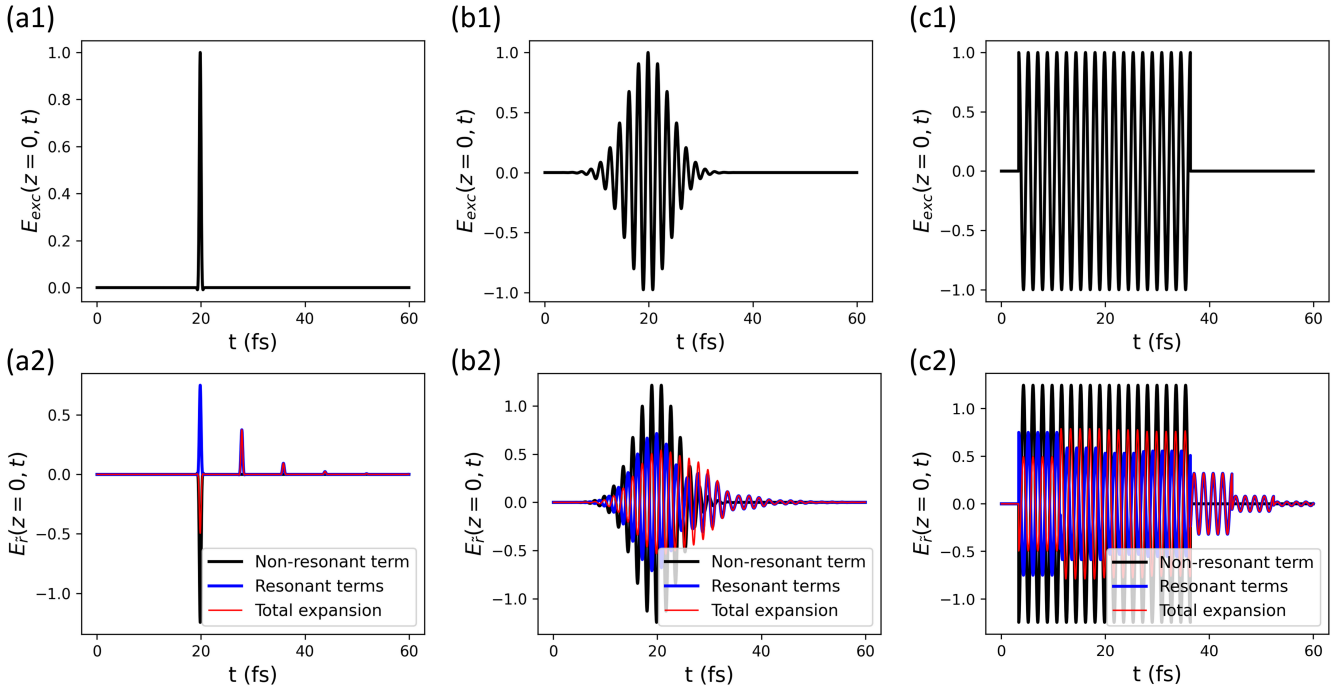

Figure 2.3. – *Three different excitation fields: a very narrow Gaussian excitation (a1), a Gaussian envelope (b1), a rectangular function (c1), and the associated reflected electric fields (a2, b2 and c2) predicted by Equations* (2.22) *and* (2.31) *where the sum was approximated with truncation number* $M = 100$. *The reflected fields are calculated at* $z = 0$ *on the left interface of a slab in air composed of a material of refractive index of* $n = 3$ *with a thickness of* 400 *nm.*

The versatility of the IRF approach combined with the SEM is now illustrated by the study of the electric field reflected by the cavity at $z = 0$ (Figure 2.3 (a1), (b1) and (c2)) excited by different pulses: a sinusoidal electric field with an extremely narrow Gaussian envelope (Figure 2.3 (a1)), a conventional Gaussian envelope (Figure 2.3 (b1)) and a rectangular envelope (Figure 2.3 (c1)). The field distributions are such that their centers are emitted at $t = 0$ from position $-(z_s + \frac{ac}{2})$ towards the left size of the slab ($z = 0$), with $z_s = 1000$nm. It thus takes roughly 20 fs for the centers to reach the slab. Each distribution is bounded by a window function of temporal width a. The refractive index of the slab is $n = 3$ and its thickness 400 nm while the surrounding medium is air. The reflected electric field is calculated by plugging in Equation (2.24) the expression of the incident electric field in the time domain at $z = 0$ and that of the IRF expanded in Equation (2.31).

2.3.1. Extremely narrow Gaussian Pulse

The main features of the IRF function can be retrieved by considering a pulse in the time domain with an extremely narrow Gaussian envelope described by the function:

$$E_{\text{exc}}(z,t) = \Pi\left(\frac{t-\frac{z}{c}-\frac{z_s}{c}-\frac{a}{2}}{a}\right) e^{-\left(\frac{t-\frac{z}{c}-\frac{z_s}{c}-\frac{a}{2}}{\tau}\right)^2} \cos\left(\omega\left(t-\frac{z}{c}-\frac{z_s}{c}-\frac{a}{2}\right)\right) \tag{2.35}$$

with $\tau := \frac{1}{2\pi f}$, $z_s = 1000$ nm, $\omega := 2\pi f$, $f = 545$ THz and $a := \frac{36\pi}{\omega}$.

The results displayed in Figure 2.3(a2) show that the reflected field is a series of peaks with a decreasing amplitude. It additionally clarifies the role of each term in Equation (2.31). It is in particular noticeable that there is an important difference in the first peak when the non-resonant term is taken into account.

[Intermediary observations]

This first peak corresponds to the direct reflection of light at the first interface of the dielectric slab. Its amplitude is therefore equal to the Fresnel coefficient $r = \frac{1-n}{1+n}$ when considering an excitation field with an amplitude of 1. In the considered case, $n = 3$ and the Fresnel coefficient is equal to $r = \frac{1-3}{3+1} = -0.5$. This is indeed what is observed when all the terms are taken into account while the amplitude of the first peak is far from this value when only the contribution of resonant terms is considered.

2.3.2. Gaussian and rectangular envelopes

This method allows to compute the response of the optical cavity to any type of excitation. It is worth mentioning that the IRF is calculated only once for a given cavity and that it permits to retrieve the time dynamics of the optical response by a single convolution with the excitation field. We illustrate this property by plotting in Figures 2.3 (b2, c2) the real part of the reflected electric field when considering an excitation electric field with (i) a Gaussian envelope in Figure 2.3 (b1, b2) and (ii) a rectangular function in Figure 2.3 (c1, c2). The excitation electric field with a Gaussian envelope, in Figure 2.3 (b1), is described by the function:

$$E_{\text{exc}}(z,t) = \Pi\left(\frac{t-\frac{z}{c}-\frac{z_s}{c}-\frac{a}{2}}{a}\right) e^{-\left(\frac{t-\frac{z}{c}-\frac{z_s}{c}-\frac{a}{2}}{\tau}\right)^2} \sin\left(\omega\left(t-\frac{z}{c}-\frac{z_s}{c}-\frac{a}{2}\right)\right) \tag{2.36}$$

where $\tau = \frac{20}{2\pi f}$, $z_s = 1000$ nm, $\omega = 2\pi f$, $f = 545$ THz and $a = \frac{36\pi}{\omega}$. In Figure 2.3(c1), the excitation reads as:

$$E_{\text{exc}}(z,t) = \Pi\left(\frac{t-\frac{z}{c}-\frac{z_s}{c}-\frac{a}{2}}{a}\right) \sin\left(\omega\left(t-\frac{z}{c}-\frac{z_s}{c}-\frac{a}{2}\right)\right) \tag{2.37}$$

with $z_s = 1000$ nm, $\omega = 2\pi f$, $f = 545$ THz and $a = \frac{18\pi}{\omega}$. M refers to the truncation number in the infinite sum of Equation (2.33). In all three cases in Figure 2.3, $M = 10$.

[Intermediary observations]

— We can again notice the role of the non-resonant part: at short times, the non-resonant contribution interferes with the resonant contribution.

— In a second step, the non-resonant part has propagated away from the $z = 0$ sampling position, leaving the reflected field amplitude to be fully described by the resonant response.

2.3.3. Accuracy and convergence of the temporal singularity expansion

We now study the convergence and accuracy of the expression of the IRF in Equation (2.31). For that purpose, we consider the same Fabry-Perot cavity as in the previous section (refractive index $n = 3$ and width $d = 400$ nm). This cavity is excited by a sinusoidal electric field with the Gaussian envelope considered in the numerical experiment in Figure 2.5(b1).

Let us start by studying the influence of the truncation number M on the accuracy of the pole expansion provided in Equation (2.31). In Figure 2.4, we display the comparison for the total field at $z = 0$: $E_{tot}(z = 0, t) = E_{exc}(z = 0, t) + E_{\tilde{r}}(z = 0, t)$ between the analytical results of Equations (2.33) and (2.34) for different values of M (3, 10, 100) and numerical results computed with the time-domain solver of the software CST (CST Studio Suite®). To better visualize the convergence of the pole expansion with respect to the truncation number, the difference between the fields calculated with the two different methods is also plotted.

We can see the fast convergence of the singularity expansion, indicated in Figure 2.4 (d) by the the mean squared error between the singularity expansion of the total field for a given number of poles M in Equation (2.31), and the limit expansion obtained by setting $M = 200$, for different values of $\tau\omega$ corresponding to the Gaussian width. A very good agreement is observed for M=3, despite the small number of poles taken into account in the expansion. The agreement further improves when increasing M as seen in Figure 2.4 (b) and (c) with M=10 and M=100. In Figure 2.4

[Intermediary observations]

Fewer poles are needed for obtaining a good approximation in the time domain than in the harmonic domain (see Figure 2.2). There are two main causes to this observation.

(i) The non-resonant term is explicitly calculated in the temporal domain, and it thus does not require the use of several poles unlike in the case of the harmonic domain.

(ii) The number of relevant poles differ in the time and harmonic domain. In the temporal domain, the frequency distribution is centered around a specific frequency ω, and only the nearby poles $\omega_\alpha(e)$ and $\omega_\alpha(o)$ are relevant. However, in the harmonic domain, a small set of poles is required for every frequency, resulting in an overall larger set of poles.

The excellent agreement between analytical and numerical results when $M = 10$ can be observed in

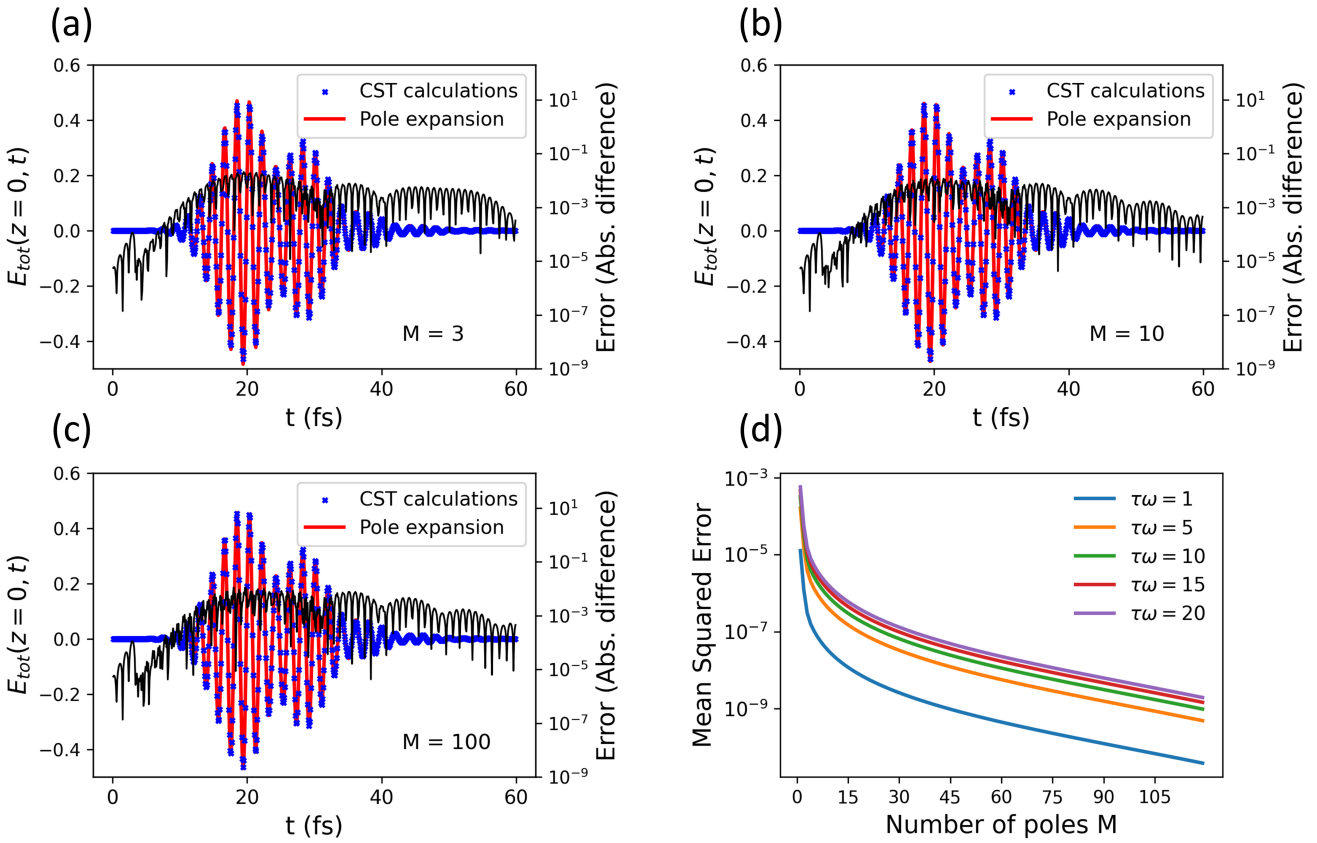

Figure 2.4. – *Convergence of the pole expansion of the reflected field (Equations (2.24) and (2.31)). Calculations are carried out for a dielectric slab with a refractive index $n = 3$ and a width $d = 400$ nm. Comparison between numerical results (black full line) and the analytical results (red dotted line) for $E_{tot}(z = 0, t)$. The analytical results are provided by Equations (2.33) and (2.34) by replacing the infinite sum with a truncated sum containing M poles. We chose $M = 3$ (a), $M = 10$ (b) and $M = 100$ (c). The blue line indicates the absolute difference between the pole expansion and the CST calculations. The convergence of the pole expansion towards its limit as a function of the number of poles M is represented in (d), with different values of the Gaussian width, represented by the parameter $\tau\omega$. The mean squared error is calculated between the pole expansion of the total field for different values of M, and the pole expansion for $M = 200$.*

Figure 2.5 for both the reflected and transmitted fields. Let us point out that the calculations performed with the pole expressions in Equations (2.33) and (2.34) match very finely those obtained with the time solver of the software CST (CST Studio Suite®) in the time domain.

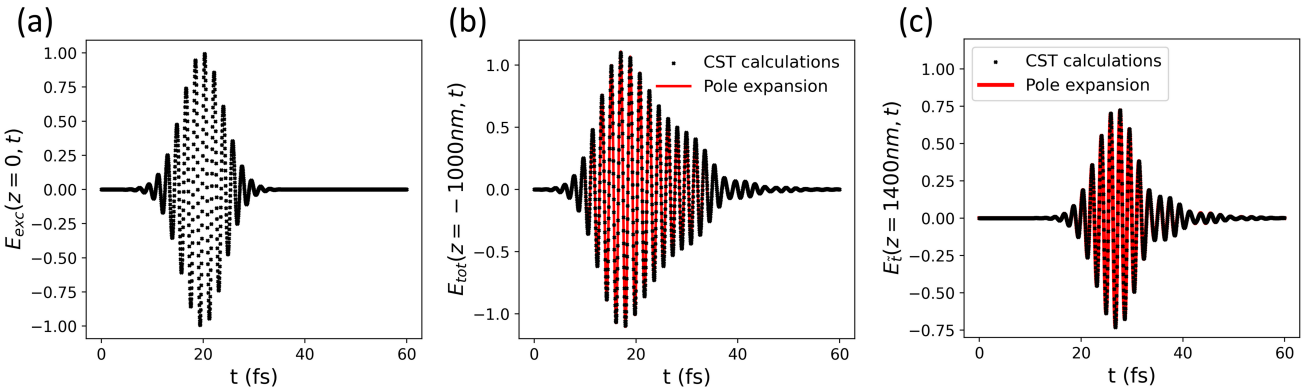

Figure 2.5. – *Optical response of a slab in the time domain. An excitation field propagating along the z-axis with a Gaussian envelope impinges at normal incidence on a slab of thickness d = 400 nm, composed of a material of refractive index n = 3. The ordinate z = 0 nm is taken at the left interface. (a) Amplitude of the incident electric field at z = 0 nm with respect to time (in fs). (b) Total (incident+reflected) electric field amplitude calculated on the incident medium (z = −1000 nm). (c) Transmitted electric field calculated at 1000 nm after the slab (z = 1400 nm). The electric field amplitude is plotted with respect to time and calculated with analytical expressions in Equations (2.33) and (2.34) (red lines) and with CST (black lines). The truncation number M for the pole expansions was set to* 10

2.3.4. From transient to permanent regime

Let us now establish the role of resonant states in the transition from transient to permanent regimes. For that purpose, we calculate the optical response of a Fabry-Perot resonator to a causal sinusoidal excitation field characterized by:

$$E_{\text{exc}}(0,t) = \sin(\omega t) \tag{2.38}$$

By using this excitation in Equation (2.24), we obtain:

$$\begin{aligned} E_{\tilde{r}}(z,t) =& \text{Re}\left[\mathrm{i}\tilde{r}(\omega_0)e^{-\mathrm{i}\omega_0\left(t+\frac{z}{c}\right)}\right] u\left(t+\frac{z}{c}\right) \\ &- \frac{\mathscr{R}r'}{2\tau_0}\sum_{\alpha=-\infty}^{+\infty}\left(\frac{e^{-\mathrm{i}\omega_\alpha^{(e)}\left(t+\frac{z}{c}\right)}}{\omega_0-\omega_\alpha^{(e)}}+\frac{e^{-\mathrm{i}\omega_\alpha^{(o)}\left(t+\frac{z}{c}\right)}}{\omega_0-\omega_\alpha^{(o)}}\right) u\left(t+\frac{z}{c}\right) \end{aligned} \tag{2.39}$$

Similarly, the transmitted field is:

$$\begin{aligned} E_{\tilde{t}}(z,t) =& \text{Re}\left[\mathrm{i}\tilde{t}(\omega_0)e^{-\mathrm{i}\omega_0\left(t-\frac{z-d}{c}\right)}\right] u\left(t-\frac{z-d}{c}\right) \\ &- \frac{\mathscr{R}r'}{2\tau_0}\sum_{\alpha=-\infty}^{+\infty}\left(\frac{e^{-\mathrm{i}\omega_\alpha^{(e)}\left(t-\frac{z-d}{c}\right)}}{\omega_0-\omega_\alpha^{(e)}}-\frac{e^{-\mathrm{i}\omega_\alpha^{(o)}\left(t-\frac{z-d}{c}\right)}}{\omega_0-\omega_\alpha^{(o)}}\right) u\left(t-\frac{z-d}{c}\right) \end{aligned} \tag{2.40}$$

When comparing the results obtained with these formulas to numerical results computed with CST, a very good agreement is observed, as shown in Figure 2.6.

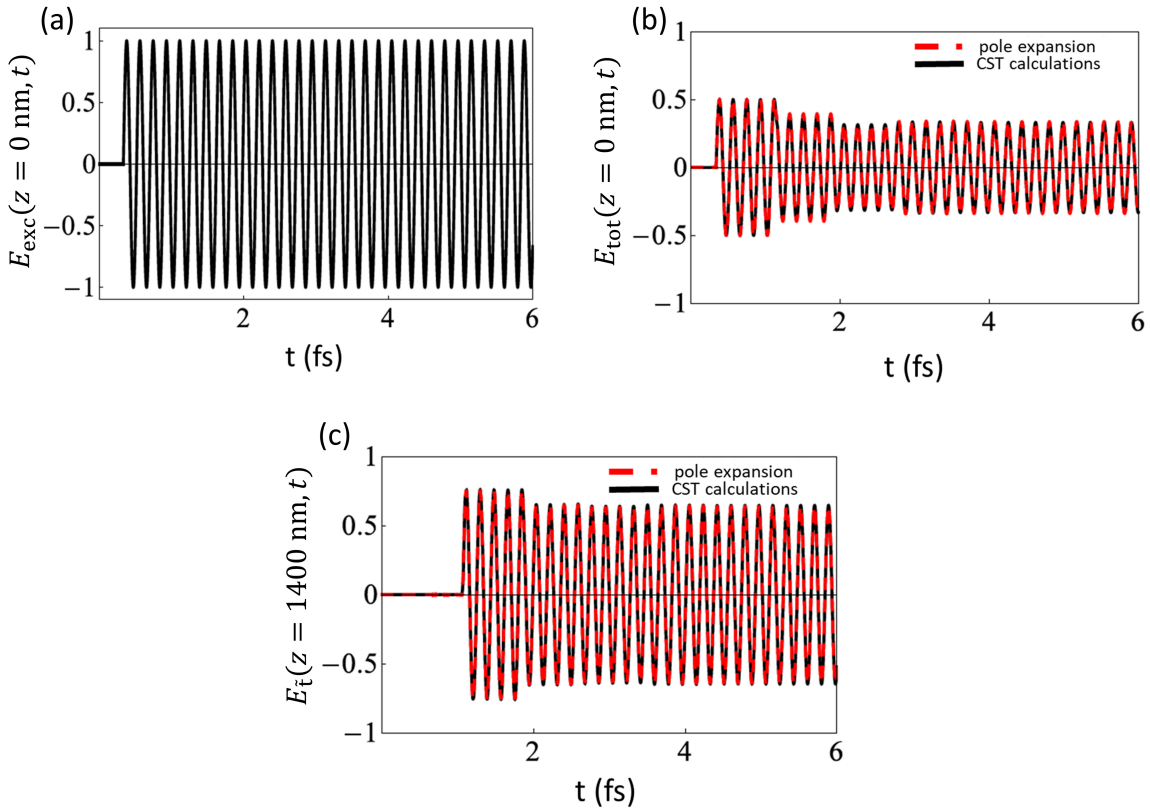

Figure 2.6. – *Response of the slab when excited by a causal excitation field. (a) Causal excitation field defined in Equation (2.38) calculated at $z = 0$ nm. (b) Total electric field calculated at $z = 0$ nm with the temporal SEM expression in Equation (2.39) (dashed red curve), compared to a CST simulation (black curve). (c) Transmitted field calculated at $z = 200$ nm using Equation (2.40).*

[Key properties]

Let us stress that the Heaviside step function $u(t)$ puts constraints on the time variable t and space variable z.

- Without it, we would observe an exponential increase of the response as we move away from the Fabry-Perot cavity at a given time.
- This coupling of space and time is naturally obtained with the Heaviside function when we perform the inverse Laplace transform of the harmonic domain expressions.
- **It translates the idea that the optical response cannot be observed at a given position before it had time to propagate to that position.**
- This is another consequence of causality.

In the temporal expressions of the fields, we recover the two contributions described in Chapter 1 Section 1.4.2, namely the modified excitation $e^{-i\omega_0 t}$, and a combination of the resonant states $e^{-i\omega_\alpha^{(e)}\left(t+\frac{z}{c}\right)}$ and $e^{-i\omega_\alpha^{(o)}\left(t+\frac{z}{c}\right)}$ associated with the poles. These resonant states, which only appear in the transient

regime, correspond to complex poles associated with both time and space, $t+\frac{z}{c}$, an important property resulting from causality.

[Intermediary observations]

— At a given point of space z, the resonant states decrease exponentially with respect to time and consequently vanish when $t \to \infty$ since the poles are passive, *i.e.* $\mathrm{Im}\left(\omega_\alpha^{(e)}\right) = \mathrm{Im}\left(\omega_\alpha^{(o)}\right) < 0$.

— The term $\mathrm{i}\tilde{r}(\omega_0)\,u\left(t+\frac{z}{c}\right)$, has a constant amplitude in time and describes the response of the resonator in the permanent regime (see Figure 2.7).

— While the poles $\omega_\alpha^{(e)}$ and $\omega_\alpha^{(o)}$ do not explicitly appear in the permanent regime, they are contained within the expression of $\tilde{r}(\omega_0)$ and thus influence the response of the system in that regime.

This result is consistent with the fact that linear systems illuminated with a monochromatic wave at frequency ω_0 feature a monochromatic optical response at the same frequency ω_0 and cannot include resonant states in the permanent regime.

Let us point out that the opposite result is observed when a sinusoidal excitation is shut-off: the signal transitions from purely monochromatic before the cut-off to a fading interference with the resonant states after the cut-off [156]. It is important to note that, in the SEM, the spatial dependence associated with complex singularity frequencies cannot be separated from their time dependence. As a result, any passive physical signal featuring a spatial dependence has to exponentially decay with time and to vanish in the permanent regime. In the harmonic domain, the information about resonances is thus fully contained in the poles and residues of the reflection and transmission coefficients, which are also the frequencies associated with the resonant states.

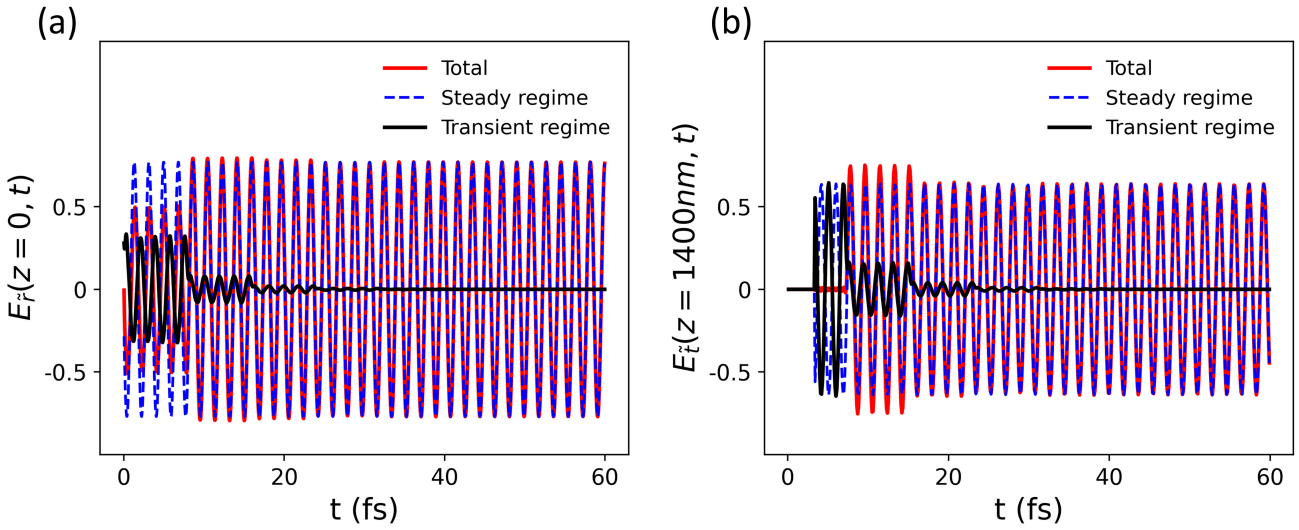

Figure 2.7. – *Total electric field amplitude when the slab is excited by the causal sinusoidal electric field* $E_{\text{inc}}(z=0,t) = u(t)\sin(\omega_0 t)$. *Total (incident+reflected) electric field calculated on the incident medium* ($z = 0$ *nm (a)), and transmitted field calculated 1000 nm after the slab* ($z = 1400$ *nm (b)). The electric field amplitude is calculated with the full expression in Equations* (2.39) *and* (2.40) *(total; red curve), with the first term depending on* ω_0 *(permanent regime term; dashed blue curve) and the second term depending on* $\omega_\alpha^{(i)}$ *(transient regime term; black curve).*

2.4. Case of a lossy and dispersive metallic slab

We now consider the important case of dispersive media where one no longer has explicit expressions for the poles. The case of a frequency-dependent permittivity (and thereby the refractive index) generally involves numerical pole-finding methods and consideration of their limitations. In this section, we show that the SEM still offers an accurate description of the reflected electric field in both the harmonic and temporal domain.

2.4.1. Distribution of the poles

We consider a slab surrounded by air, with a thickness d of 150nm and a refractive index defined as $n(\omega) = \sqrt{\varepsilon(\omega)/\varepsilon_0}$ where $\varepsilon(\omega)$ is the complex relative permittivity of gold. Although Chapter 3 is dedicated to the derivation and retrieval of a generalized Drude-Lorentz model based on the SEM to describe the permittivity of various linear materials, we use in this section an extended Drude model defined in reference [60] as:

$$\varepsilon(\omega) = \varepsilon_\infty - \frac{\omega_{pD}^2}{\omega^2 + \mathrm{i}\omega\Gamma_D} - s_1 \frac{\omega_{p1,L}^2}{\omega^2 - \omega_{p1,L}^2 + \mathrm{i}\Gamma_{1,L}\omega} - s_2 \frac{\omega_{p2,L}^2}{\omega^2 - \omega_{p2,L}^2 + \mathrm{i}\Gamma_{2,L}\omega} \tag{2.41}$$

with all the parameters detailed in the referenced article.

From the knowledge of the complex poles ω_p, it is possible to analytically determine their residues $\rho_p = \mathrm{Res}\left(\tilde{r}, \omega_p\right)$ using the definition of the reflection coefficient in Equation (2.3):

$$\rho_p = -\frac{\frac{1}{r'(\omega_p)}^2 - 1}{\frac{2}{r'(\omega_p)}} \times \frac{1}{\frac{2.\partial_\omega[n](\omega_p)}{(n(\omega_p)+1)^2}\frac{1}{r'((\omega_p))} + \frac{\mathrm{i}d}{c}\left(n(\omega_p) + \omega_p.\partial_\omega[n](\omega_p)\right)} \tag{2.42}$$

with $r'(\omega)$ the frequency-dependant reflection coefficient at the slab/air interface:

$$r'(\omega) = \frac{n(\omega) - 1}{n(\omega) + 1} \tag{2.43}$$

Let us stress once more that the Hermitian symmetry implies that the poles and their associated residues come in pairs: $(\omega_p, -\overline{\omega_p})$, $(\rho_p, -\overline{\rho_p})$.

In Figure 2.8, we show the log-amplitude of the reflection coefficient $\mathrm{Log}(|\tilde{r}(\omega)|$ in the complex frequency plane to visualize the position of the singularities, which are found using an algorithm based on the Newton method. The first 17 poles are indicated by the red dots.

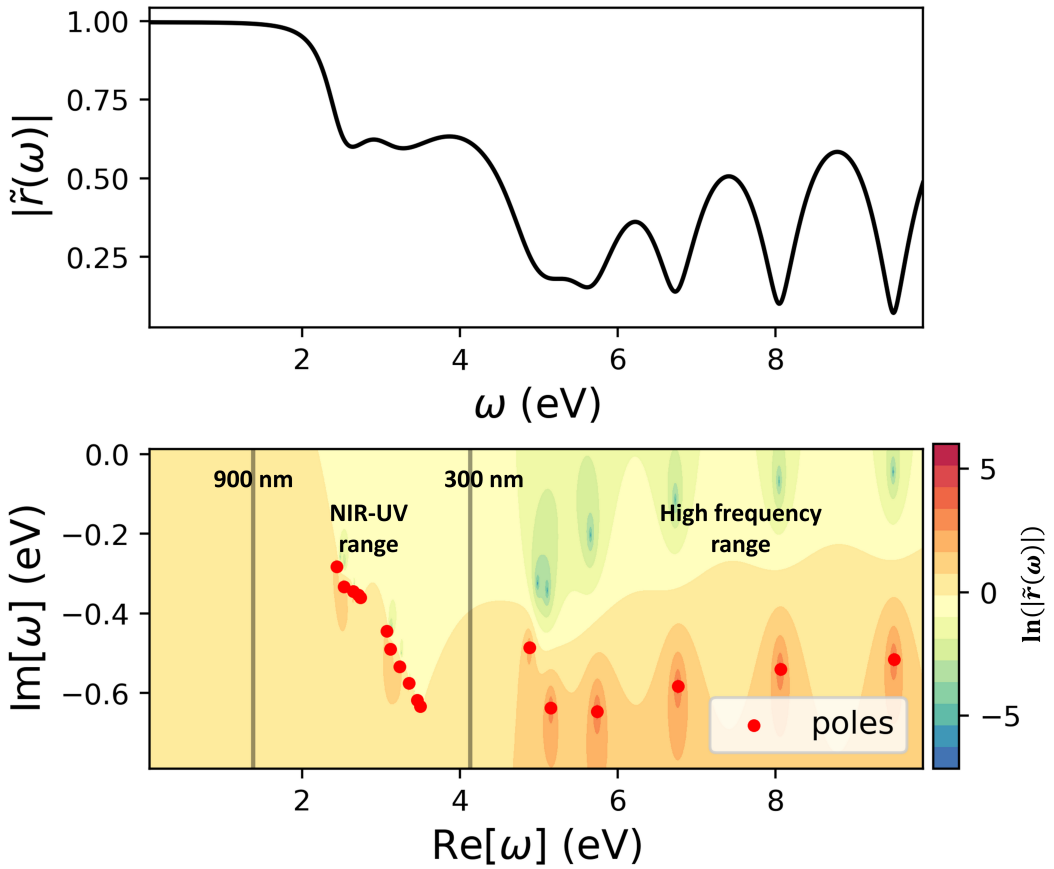

Figure 2.8. – *Log-amplitude* $\mathrm{Log}(|\tilde{r}(\omega)|$ *of the reflection coefficient* $\tilde{r}(\omega)$ *in the complex frequency plane, i.e.* $\omega \in \mathbb{C}$. *The vertical black lines are the bounds of the* 300 *nm to* 800 *nm wavelength range. The red dots correspond to the numerically estimated poles.*

2.4.2. Pole expansion in the harmonic and temporal domains

The SEM is applied with a truncated summation at the Mth pair of poles to approximate the reflection coefficient $\tilde{r}(\omega)$. It turns out that there is an infinite number of poles, and only a small set is contained within the spectral window of interest, delimited by the vertical black lines in Figure 2.8. One would expect the poles outside this range to have only small influence over the approximation of the reflection coefficient in the visible range. However, it can be seen in Figure 2.9 that the convergence of the expansion is achieved but at a price of high number of poles ($M > 50$).

[Key properties]

The resonant term of the pole expansion is only slightly affected by the poles away from the studied frequency range, but it is not the case for the non-resonant term which provides an offset between the response shaped by the poles and the actual reflection coefficient $\tilde{r}(\omega)$.

To obtain an accurate expression within the visible range using only the nearby poles, it is thus neces-

sary to approximate the non-resonant term. This can be achieved following two different methods.

(i) For the first approach, let us point out that the model considered for the permittivity describes the slab as a lossless dielectric medium with a constant refractive index $n = \sqrt{\varepsilon_\infty}$ at frequencies higher than ω_{pD}. Using the study carried out in the previous section on a lossless system, we can analytically determine the poles with a real part greater than ω_{pD} and their associated residues and use them to correct the truncated pole expansion at $M = 20$.

(ii) The second approach relies on the separation of the contributions of the poles outside the range of interest to the resonant term that shapes the response curve, and to the non-resonant term. The truncated pole expansion is completed by an effective pair of poles and their associated residues for the resonant term, and a constant for the non-resonant term. These three additional parameters are obtained thanks to a gradient-descent algorithm applied with an error function corresponding to the absolute difference between the approximation and the model for wavelengths ranging from 200nm to 900nm.

We compare the results of both methods to the model of the reflection coefficient in Figure 2.9 (b).

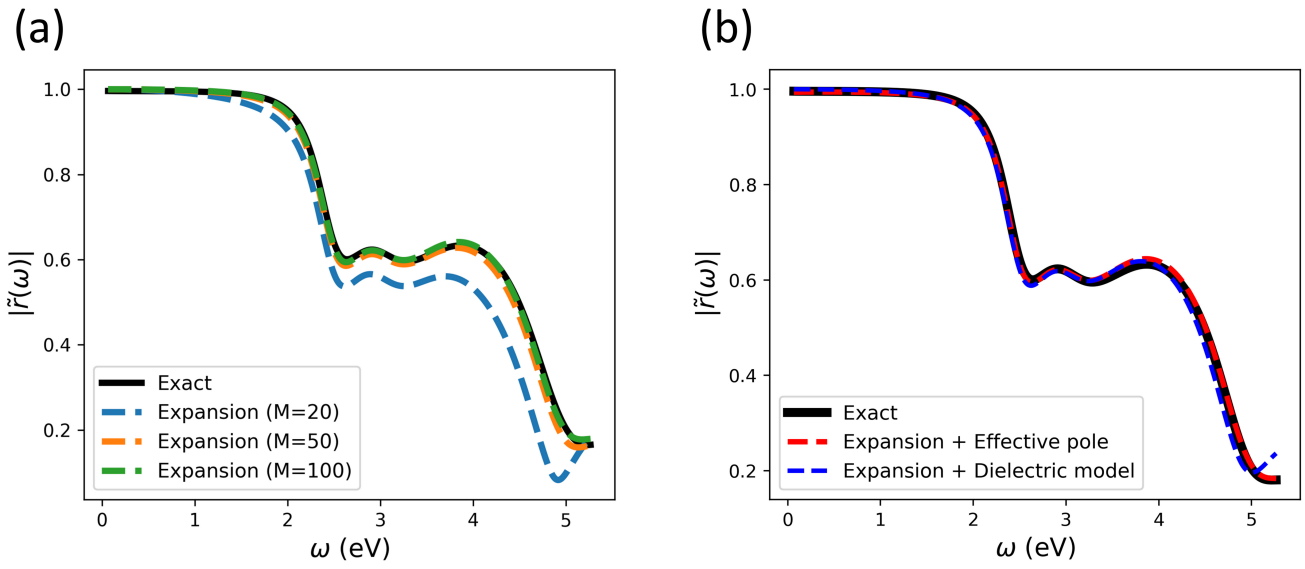

Figure 2.9. – *Modulus of the reflection coefficient* $|\tilde{r}(\omega)|$ *on the real axis for wavelengths ranging from the UV to the IR. In (a), convergence of the pole expansion with respect to the number M of pairs of poles. In (b), comparison of two methods designed to complete the pole expansion: the red curve corresponds to the truncated pole expansion with M*=15 *poles corrected by an effective pole* $\omega_{\text{eff}} = (10.41 - 1.38i)$ *eV, its associated residue* $\rho_{\text{eff}} = (1.26 + 4.62i)$ *eV, and a non resonant term* $\hat{r}_{\text{NR}} = (1.3 - 0.9i).10^{-2}$. *All three parameters were obtained by gradient descent. The blue curve is obtained with the* 15 *numerically determined poles in the frequency range of interest, plus* 100 *poles analytically obtained in the dielectric approximation of the metallic slab for high frequencies* ($\omega > \omega_{pD}$).

[Intermediary observations]

— We observe that the two methods provide an accurate approximation of the reflection coefficient $\tilde{r}(\omega)$.

— The second method is particularly efficient since only 3 parameters are needed. In practice, only the poles in the frequency range of interest and these three fitted parameters are thus required to obtain a valid expression of the optical response.

Effective IRF of a lossy dispersive slab in reflection

In the temporal domain, the derivation of the response function $\mathrm{IRF}_{\tilde{r}}(\omega)$ is straightforward once we know the approximated SEM of $\tilde{r}(\omega)$. It yields:

$$\begin{aligned}\mathrm{IRF}_{\tilde{r}}(z,t) =&(-1+\hat{r}_{\mathrm{NR}})\delta(t+\frac{z}{c})\\ &-\left[\mathrm{i}\sum_{m=-M}^{M}\rho_{p,m}e^{-\mathrm{i}\omega_{p,m}(t+\frac{z}{c})}-\mathrm{i}\rho_{\mathrm{eff}}e^{-\mathrm{i}\omega_{\mathrm{eff}}(t+\frac{z}{c})}+\mathrm{i}\overline{\rho_{\mathrm{eff}}}e^{\mathrm{i}\overline{\omega_{\mathrm{eff}}}(t+\frac{z}{c})}\right]u(t+\frac{z}{c})\end{aligned} \tag{2.44}$$

where $\rho_{p,m}$ is the residue of the mth pole $\omega_{p,m}$, $\hat{r}_{\mathrm{NR}}$ is the fitted non-resonant term, and ω_{eff} is the fitted effective pole with residue ρ_{eff}.

The values obtained for the three fitted parameters are $\omega_{\mathrm{eff}} = (10.41-1.38\mathrm{i})$ eV, $\rho_{\mathrm{eff}} = (1.26+4.62i)$ eV and $\hat{r}_{\mathrm{NR}} = (1.3-0.09i).10^{-1}$. Let us point out that the residues have the same units as the poles for the coefficients of a scattering operator. The IRF therefore has the unit of a frequency, which is cancelled out by the time variable in the convolution with the excitation field, thus ensuring that the response and excitation functions have the same unit.

Finally, we consider, once again, the response $E_{\tilde{r}}(z,t)$ of the slab to a causal sinusoidal input $E_{inc}(z,t) = \mathrm{Re}\left[\mathrm{i}e^{-\mathrm{i}\omega_0(t-\frac{z}{c}+t_0)}u(t)\right]$, with $t_0 = \frac{z_0}{c}$ a time constant corresponding to the generation of the field at the position $z_0 = -1\mu$m:

$$\begin{aligned}E_{\tilde{r}}(z,t) =&\mathrm{Re}\left[\mathrm{i}\tilde{r}(\omega_0)e^{-\mathrm{i}\omega_0(t+\frac{z}{c}+t_0)}-\mathrm{i}\sum_{m=-20}^{20}\frac{\rho_{p,m}e^{-\mathrm{i}\omega_{p,m}(t+\frac{z}{c}+t_0)}}{\omega_0-\omega_{p,m}}-\right.\\ &\left.\mathrm{i}\frac{\rho_{\mathrm{eff}}e^{-\mathrm{i}\omega_{\mathrm{eff}}(t+\frac{z}{c}+t_0)}}{\omega_0-\omega_{\mathrm{eff}}}+\mathrm{i}\frac{\overline{\rho_{\mathrm{eff}}}e^{\mathrm{i}\overline{\omega_{\mathrm{eff}}}(t+\frac{z}{c}+t_0)}}{\omega_0+\overline{\omega_{\mathrm{eff}}}}\right]u\left(t+\frac{z}{c}+t_0\right)\end{aligned} \tag{2.45}$$

[Intermediary observations]

The reflected field in Equation (2.45) is similar to the previous case of a non-dipsersive slab in Equation (2.39), showcasing the versatility of the SEM.

— The permanent regime term $i\tilde{r}(\omega_0)e^{-i\omega_0(t+\frac{z}{c}+t_0)}$ depends only on the harmonic response at the excitation frequency ω_0.

— The temporally decaying resonant states $\frac{\rho_{p,m}}{\omega_0-\omega_{p,m}}e^{-i\omega_{p,m}(t+\frac{z}{c}+t_0)}$ correspond to the transient regime.

This is highlighted in Figure 2.10 (a), which shows the contribution of the permanent and transient-regime terms to the reflected field. Let us point out that the transient-regime term decays much faster (in just 4fs) than in the case of a non-absorbing dielectric medium. This result was expected since the field now interacts with a metallic slab, *i.e.* an absorbing medium. This temporal expression, obtained *via* the corrected pole expansion, is compared to a CST simulation in Figure 2.10 (b) where a good agreement is observed despite small discrepancies which are assumed to result from the numerical calculations on a dispersive media.

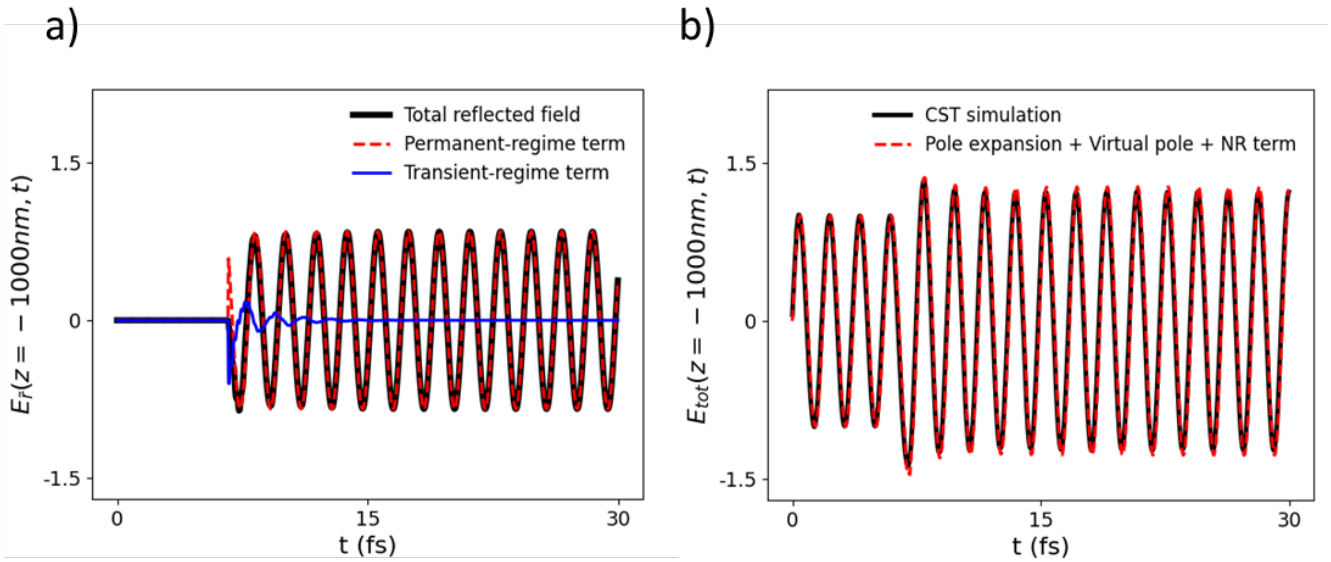

Figure 2.10. – *(a) Reflected field defined in Equation (2.45), as well as the permanent-regime and transient-regime terms constituting it. (b) Total electric field $E_{tot} = E_{inc} + E_{\tilde{r}}$ in the case of a sinusoidal incident field $E_{inc}(z,t) = u(t)sin(\omega_0(t-\frac{z}{c}+t_0) = \mathrm{Re}(iu(t)e^{-i\omega_0(t-\frac{z}{c}+t_0)})$ on a dispersive slab. The time constant $t_0 = -\frac{z_0}{c}$, with $z_0 = -1\mu m$ is the delay required by the field generated at the position z_0 reaches the left interface of the slab.*

2.5. Conclusion

Summary and conclusion

Physical systems as defined in the previous chapter, *i.e.* causal LTIS abiding by the rule of energy conservation, are encountered in every field of physics. In that respect, the expressions we derived are of high interest since they allow us to study these systems under a common framework based on the distribution of the singularities of their response functions.

- We have shown in this chapter that the formalism we have introduced provides accurate and practical expressions.
- We derived the exact and analytic expression of the IRFs of an optical slab by applying the SEM on the coefficients of the S matrix.
- We studied the convergence with the number of poles for different pulse excitations, in both the harmonic and temporal domains.
- What is more, by considering the case of a dispersive slab, we have shown that accurate expressions could be obtained from numerically approximated singularities.
- The contributions of the poles far from the spectral window of interest can be accounted for by effective poles, which drastically reduce the total number poles.

This chapter is also associated with a publication, in reference [99], dealing with the derivation of the temporal dynamics of a Fabry-Perot cavity.

In the next chapter, we will apply the SEM to the fundamental case of the constitutive relation in the Maxwell equations, linking the displacement field to the electric field *via* the dielectric permittivity function which we will consider as a transfer function for various materials.

Summary of the results

SEM of the reflection and transmission coefficients

$$\tilde{r}(\omega) = \tilde{r}_{\mathrm{NR}} - \frac{\mathrm{iRe}}{2\tau_0 p}\sum_{\alpha=-\infty}^{+\infty}\left(\frac{1}{\omega-\omega_\alpha^{(e)}}+\frac{1}{\omega-\omega_\alpha^{(o)}}\right)$$

$$\tilde{t}(\omega) = \frac{-\mathrm{iRe}}{2\tau_0 p}\sum_{\alpha=-\infty}^{+\infty}\left(\frac{1}{\omega-\omega_\alpha^{(e)}}-\frac{1}{\omega-\omega_\alpha^{(o)}}\right)$$

Exact expression of the IRF of a non-dispersive slab in reflection

$$\mathrm{IRF}_{\tilde{r}}(z,t) = \left(\tilde{r}_{\mathrm{NR}} - \frac{\mathscr{R}r'}{2}\right)\delta(t+\frac{z}{c}) - \mathscr{R}r'\sum_{\alpha=1}^{\infty}\delta\left(t+\frac{z}{c}-2\alpha\tau_0\right)e^{2\alpha\ln(|r'|)}$$

Exact expression of the IRF of a non-dispersive slab in transmission

$$\mathrm{IRF}_{\tilde{t}}(z,t) = -\mathscr{R} r' \sum_{\alpha=1}^{\infty} \delta\left(t - \frac{z-d}{c} - 2(\alpha-1)\tau_0\right) e^{2(\alpha-1)\ln(|r'|)}$$

Effective IRF of a lossy dispersive slab in reflection

$$\begin{aligned}\mathrm{IRF}_{\tilde{r}}(z,t) =& (-1+\hat{r}_{\mathrm{NR}})\delta(t+\frac{z}{c}) - \mathrm{i}\sum_{m=-M}^{M} \rho_{p,m} e^{-\mathrm{i}\omega_{p,m}(t+\frac{z}{c})} \\ & - \mathrm{i}\rho_{\mathrm{eff}} e^{-\mathrm{i}\omega_{\mathrm{eff}}(t+\frac{z}{c})} + \mathrm{i}\overline{\rho_{\mathrm{eff}}} e^{\mathrm{i}\overline{\omega_{\mathrm{eff}}}(t+\frac{z}{c})},\end{aligned}$$

3. The dielectric permittivity of materials and structures

Contents

3.1. Derivation of the Generalized Drude-Lorentz model 96
3.1.1. Different models for the permittivity 96
3.1.2. The permittivity as a transfer function 97
3.1.3. Generalized Drude-Lorentz expression 100
3.2. Retrieving the parameters from experimental data 105
3.2.1. Analytical continuation of the permittivity from experimental data 105
3.2.2. Characterization of the materials with the distribution of the poles 109
3.3. Conclusion 113

3.1. Derivation of the Generalized Drude-Lorentz model

3.1.1. Different models for the permittivity

The description of the permittivity and permeability (or electric and magnetic susceptibilities) of materials *via* analytical expressions is of fundamental interest in the fields of optics and electromagnetism. Analytical models are relevant to provide simple and relevant descriptions of the interaction between materials and excitation fields [157, 158]. They are also of strong interest for computational modeling and numerical methods such as time-domain numerical methods [159, 160]. Besides the need of analytical description of the dielectric permittivity at real frequencies, modal analysis of open systems and non-Hermitian photonics requires the description of the dielectric permittivities in the complex frequency plane [100, 143, 144, 161, 162].

Common tools or models describe the behaviour of charged particles in materials with combinations of the Drude, Lorentz and sometimes Debye models to obtain the permittivity on spectral windows extending over a few dozens of wavelengths [163–166]. The Lorentz model is often used to model the behaviour of the electric charges of a medium excited by an electromagnetic-field. It leads to an expression of the permittivity as a sum of N_e Lorentz functions, each associated with a group of electric charges possessing a different behaviour. The Drude model describes free charges in a metal or a gaz of charged particules. By simply putting them together, we obtain the classical Drude-Lorentz model (DL):

$$\varepsilon(\omega) = \varepsilon_\infty - \frac{\omega_b^2}{\omega^2 + \mathrm{i}\omega\gamma} - \sum_{m=1}^{N_e} \frac{\omega_{p,m}^2}{(\omega^2 - \omega_{0,m}^2) + \mathrm{i}\omega\Gamma_m} f_m \tag{3.1}$$

The Drude term is characterized by its plasma frequency ω_b and γ which corresponds to a friction-like term acting on the free charged particles within the medium. The N_e Lorentz terms have a similar expression, but are associated with forces acting upon bound charged particles. They mainly differ by the presence of the frequency $\omega_{0,m}$ which is associated with a spring-like force restoring the particles to their equilibrium position. N_e usually ranges from 1 and 5, with the usual convention that $\sum_{m=1}^{N_e} f_m = 1$, which corresponds to N_e groups of charged particles with different behaviours [167].

Alternatively, the permittivity (or the susceptibility) can be modeled with the complex-conjugate pole-residue pairs model (ccprp) [72, 109, 168–171], which approximates the permittivity using a finite set of complex conjugated pairs of poles contained within or close to a spectral window of interest, with the aim of providing simple analytical expressions to numerical methods [168, 172, 173].

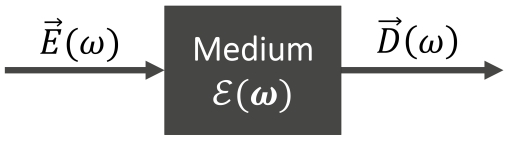

Figure 3.1. – *The linear dielectric permittivity of a material is defined in the constitutive relations by a transfer function linking the output displacement field $\vec{D}$ to the input electric field $\vec{E}$. It shares the properties of a linear transfer and can be analytically expressed using the singularity expansion method.*

By expressing the permittivity as the transfer function of a physical system (see Figure (3.1)), we generalize these approaches and show that the SEM is the natural way to obtain an exact expression of the permittivity.

We show that the SEM can be recast into a form including the Drude, Lorentz and Debye models which we refer to as the Generalized Drude-Lorentz model (GDL). We discuss in particular what the additional terms appearing in the generalized Lorentz model translates into when we revert back to the temporal domain. We propose an approach to retrieve the parameters of the GDL. It is an optimization method relying on the auto-differentiation tools from current machine-learning libraries, and more specifically PyTorch [174]. We test this approach and show its accuracy with experimental data corresponding to the dielectric permittivity of 9 materials including metals, dielectrics and 2D materials. Finally, we show how the distribution of the poles associated with Debye, Drude or Lorentz terms can characterize the behaviour of the materials at different frequencies. While we focus on non-magnetic, isotropic media for simplicity but also and mainly because these account for most of the regularly encountered media, the study presented in this work can also be applied to non-isotropic media with tensors for both the permittivity and the permeability.

3.1.2. The permittivity as a transfer function

Let us look at the constitutive relation between the displacement field $\vec{D}(\omega)$ and the electric field $\vec{E}(\omega)$ in the harmonic domain, in a linear non-magnetic medium:

$$\frac{1}{\varepsilon_0}\vec{D}(\omega) = \vec{E}(\omega) + \bar{\bar{\chi}}(\omega)\vec{E}(\omega) \tag{3.2}$$

where $\bar{\bar{\chi}}$ is the electric susceptiblity tensor. We consider isotropic media. The constitutive relation thus simplifies into:

$$\begin{aligned} D(\omega) &= \varepsilon_0(1+\chi(\omega))E(\omega) \\ &= \varepsilon_0\varepsilon(\omega)E(\omega) \end{aligned} \tag{3.3}$$

with $\chi(\omega)$ and $\varepsilon(\omega)$ the scalar electric susceptibility and relative permittivity respectively. Let us point out that the isotropy allows us to consider the scalar functions $D(\omega)$ and $E(\omega)$ instead of the vectors $\vec{D}(\omega)$ and $\vec{E}(\omega)$. We chose, for this chapter, to focus on the relative permittivity $\varepsilon(\omega)$ rather than the susceptibility $\chi(\omega)$. However, the following derivations would essentially remain the same with the susceptibility, provided that the polarization vector field $\vec{P}(\omega)$ is studied instead of the displacement field $\vec{D}(\omega)$. Similarly, in magnetic linear media, each component of the magnetic susceptibility tensor or relative permeability could be studied exactly as in the case of the permittivity.

We see from Equation (3.3) that the displacement field $D(\omega)$ can be described as the response of the medium to the electric field $E(\omega)$. Because of passivity (we do not inject energy into the systems), and with energy conservation, the media are physical systems. As a result, $D(\omega)$ and $E(\omega)$ are physical signals, while the relative permittivity $\varepsilon(\omega)$ is a transfer function. The SEM can thus be applied [31, 117]. Although poles of order more than 1 could theoretically be observed, they are not easily encountered in nature and are generally found in engineered systems. It is thus safe to assume that all the poles are

simple, *i.e.* of order 1, yielding the following classical SEM expression:

$$\varepsilon(\omega) = \varepsilon(a) - \sum_p \frac{r_p}{a-\omega_p} + \sum_p \frac{r_p}{\omega-\omega_p} \tag{3.4}$$

with r_p the residue of $\varepsilon(\omega)$ at the simple pole ω_p and a an arbitrary complex frequency. Similarly to the case of the Fresnel coefficients of a Fabry-Perot cavity in Chapter 2, the set of poles of $\varepsilon(\omega)$ is potentially infinite. In practice, however, the SEM expression must be truncated. In addition, two types of poles result from the Hermitian symmetry: the purely imaginary ones on the imaginary frequency axis, and the pairs of poles $(\omega_p^{(\ell)}, -\overline{\omega_p}^{(\ell)})$ in the complex ω-plane, as highlighted in Figure 3.2 where the relative permittivity of Cr is plotted at real frequencies and in the complex plane.

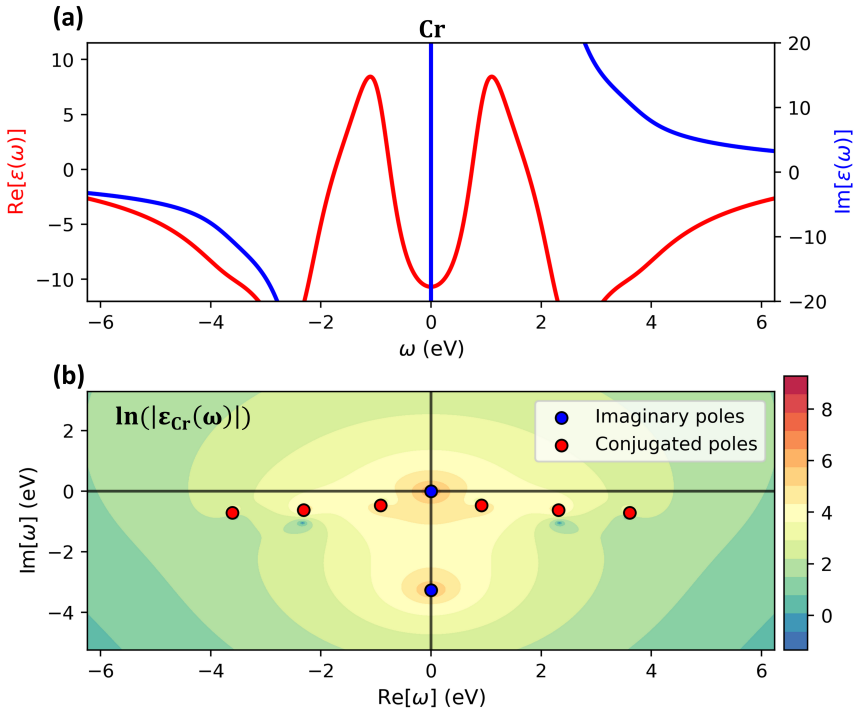

Figure 3.2. – *Real (red line, left axis) and imaginary (blue line, right axis) parts of the relative permittivity function of Cr at real frequencies (a) and in the complex ω-plane (b). The purely imaginary poles (blue dots) and conjugated pairs (red dots) are highlighted.*

We separate the M purely imaginary poles $\omega_I^{(\ell)}$ from the other N complex ones $\omega_p^{(\ell)}$ in the truncation, leading to:

$$\begin{aligned}\varepsilon(\omega) = \varepsilon(a) &- \sum_{\ell=1}^{M} \frac{r_I^{(\ell)}}{a-\omega_I^{(\ell)}} - \sum_{\ell=1}^{N}\left[\frac{r_p^{(\ell)}}{a-\omega_p^{(\ell)}} - \frac{\overline{r_p}^{(\ell)}}{a+\overline{\omega_p}^{(\ell)}}\right] \\ &+ \sum_{\ell=1}^{M} \frac{r_I^{(\ell)}}{\omega-\omega_I^{(\ell)}} + \sum_{\ell=1}^{N}\left[\frac{r_p^{(\ell)}}{\omega-\omega_p^{(\ell)}} - \frac{\overline{r_p}^{(\ell)}}{\omega+\overline{\omega_p}^{(\ell)}}\right]\end{aligned} \tag{3.5}$$

It is generally assumed that the Kramers-Kronig relations must hold for the susceptibility. This is

equivalent to considering that it is analytic in the upper half of the complex-frequency plane, which in turns implies that the media are passive and causal systems which only possess passive poles, *i.e.* poles with a negative imaginary part. By definition of the relative permittivity as $\varepsilon(\omega) = 1 + \chi(\omega)$, these properties also hold for $\varepsilon(\omega)$, which is in agreement with the definition of the media as physical systems.

[Key properties]

As a consequence, the displacement field and electric field must decay in the temporal domain. In the case of the displacement field, this is only possible if the relative permittivity itself decays. It follows that the final value theorem yields:

$$\lim_{t\to+\infty} \mathscr{L}^{-1}[\varepsilon](t) = \lim_{\omega\to 0+} i\omega\varepsilon(\omega) = cst \tag{3.6}$$

where $\mathscr{L}^{-1}$ is the inverse Laplace transform operator. In case the displacement field does not completely disappear, the theorem only holds if 0 is a pole of $\varepsilon(\omega)$ of order 1 at most. **In other words: if there is a pole at the origin, it must be a simple pole.**

We make the assumption that 0 is always a singularity of $\varepsilon(\omega)$. Should that hypothesis prove wrong, the residue r_0 associated with that simple pole will be null, turning the pole into a removable singularity. This is generally the case for non-metallic media. This property is evidenced in Figure 3.3, where we compare the relative permittivity functions of $Ta_2O_5$and Cr, showing that the pole at the origin is missing from the singularities of Ta_2O_5.

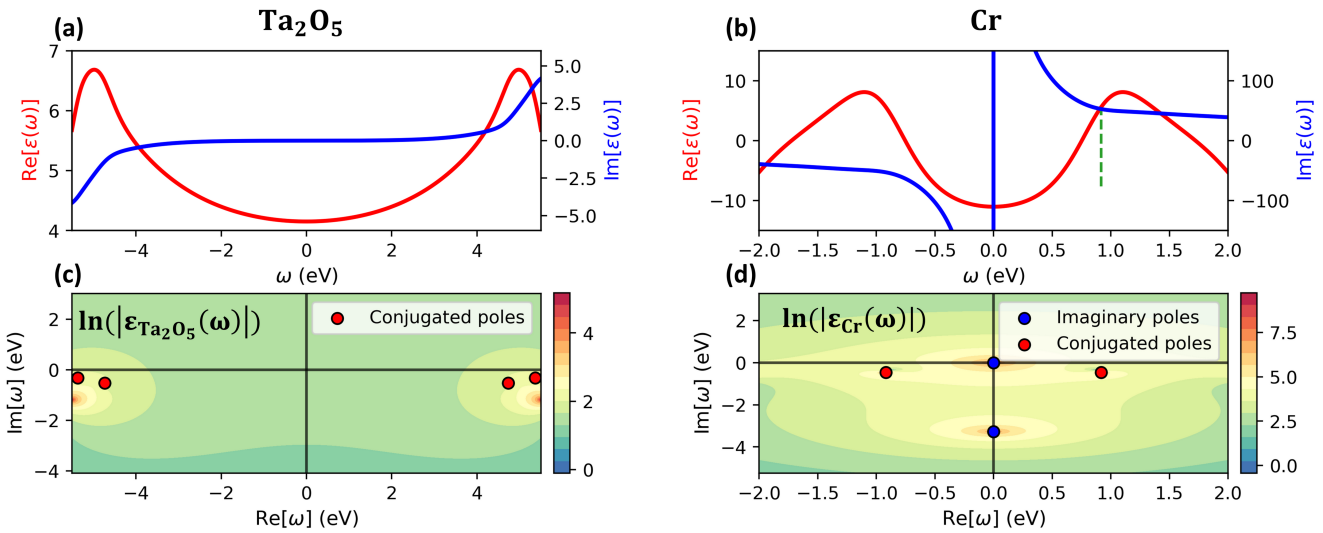

Figure 3.3. – *Real (red line, left axis) and imaginary (blue line, right axis) parts of the relative permittivity functions of* Ta_2O_5 *and Cr at real frequencies (a), (b) and in the complex* ω*-plane (c), (d). Purely imaginary poles (blue dots) are observed for Cr, while only conjugated pairs (red dots) are present for* Ta_2O_5.

SEM applied to the relative permittivity function

In the end, the truncated SEM applied to the relative permittivity reads as:

$$\varepsilon(\omega) = \varepsilon_{NR} + \frac{r_0}{\omega} + \sum_{\ell=1}^{M} \frac{r_I^{(\ell)}}{\omega - \omega_I^{(\ell)}} + \sum_{\ell=1}^{N} \left[\frac{r_p^{(\ell)}}{\omega - \omega_p^{(\ell)}} - \frac{\overline{r_p}^{(\ell)}}{\omega + \overline{\omega_p}^{(\ell)}} \right] \tag{3.7}$$

where ε_{NR} is the constant, non-resonant term.

[Intermediary observations]

The second sum over l ranging from 1 to N in Equation (3.7) is exactly the classical ccprp method. We have thus shown that it is a special case of the truncated SEM.

3.1.3. Generalized Drude-Lorentz expression

We will now detail how to use this macroscopic description of the behaviour of a medium to retrieve the microscopic models of the dynamics of charged particles, namely the Drude and Lorentz models. We want to recast Equation (3.7) into a form that encompasses the DL in Equation (3.1).

The imaginary poles in the truncated singularity expansion, including 0, can be written as Drude terms. Let us consider an imaginary pole $\omega_I^{(\ell)}$ and its associated imaginary residue $r_I^{(\ell)}$. Setting $\gamma_\ell = -\mathrm{Im}(\omega_I^{(\ell)})$ and $\omega_{b,\ell} \in \mathbb{C}$ such that $-\mathrm{i}\omega_{b,\ell}^2/\gamma_\ell = r_I^{(\ell)}$ leads to:

$$\frac{r_I^{(\ell)}}{\omega - \omega_I^{(\ell)}} = -\frac{\omega_{b,\ell}^2}{\mathrm{i}\gamma_\ell} \left[\frac{1}{\omega} - \frac{1}{\omega + \mathrm{i}\gamma_\ell} \right] + \frac{\omega_{b,\ell}^2}{\mathrm{i}\gamma_\ell} \frac{1}{\omega} \tag{3.8}$$

In addition, we define γ_0 as the difference between the residue r_0 of the pole at the origin, and the residues of the other imaginary poles:

$$\gamma_0 = r_0 + \sum_{\ell=1}^{M} \frac{\omega_{b,\ell}^2}{\mathrm{i}\gamma_\ell} \tag{3.9}$$

The terms associated with the imaginary poles can thus be written as:

$$\frac{r_0}{\omega} + \sum_{\ell=1}^{M} \frac{r_I^{(\ell)}}{\omega - \omega_I^{(\ell)}} = \frac{\gamma_0}{\omega} - \sum_{\ell=1}^{M} \frac{\omega_{b,\ell}^2}{\omega^2 + \mathrm{i}\omega\gamma_\ell} \tag{3.10}$$

[Key properties]

The sum over ℓ is equivalent to considering M groups of freely moving charges, each associated with different parameters γ_ℓ and $\omega_{b,\ell}$. In practice, $\omega_{b,\ell}^2$ is positive. Equation (3.10) thus spans the set of functions described by the regular Drude model written in Equation (3.1).

Similarly, the terms involving the complex poles $\omega_p^{(\ell)}$ can be written as Lorentz-like terms. For any pole $\omega_p^{(\ell)}$, we have:

$$\frac{r_p^{(\ell)}}{\omega-\omega_p^{(\ell)}}-\frac{\overline{r_p}^{(\ell)}}{\omega+\overline{\omega_p}^{(\ell)}}=2\frac{\mathrm{i}\omega\mathrm{Im}(r_p^{(\ell)})+\mathrm{Re}(r_p^{(\ell)}\,\overline{\omega_p}^{(\ell)})}{\omega^2-|\omega_p^{(\ell)}|^2-2i\omega\mathrm{Im}\,(\omega_p^{(\ell)})} \tag{3.11}$$

Let us set $\omega_{0,\ell}=|\omega_p^{(\ell)}|$ and $\Gamma_\ell=-2\mathrm{Im}(\omega_p^{(\ell)})$, and two constants $s_{1,\ell}$ and $s_{2,\ell}$ such that $s_{1,\ell}\Gamma_l=-2\mathrm{Im}(r_p^{(\ell)})$ and $s_{2,\ell}\omega_{0,\ell}^2=-2\mathrm{Re}(r_p^{(\ell)}\,\overline{\omega_p}^{(\ell)})$. The previous expression becomes:

$$\frac{r_p^{(\ell)}}{\omega-\omega_p^{(\ell)}}-\frac{\overline{r_p}^{(\ell)}}{\omega+\overline{\omega_p}^{(\ell)}}=-\frac{\mathrm{i}s_{1,\ell}\omega\Gamma_\ell+s_{2,\ell}\omega_{0,\ell}^2}{(\omega^2-\omega_{0,\ell}^2)+\mathrm{i}\omega\Gamma_\ell}=\frac{P_{(\ell)}(\omega)}{Q_{(\ell)}(\omega)} \tag{3.12}$$

[Intermediary observations]

— The main difference between the generalized Lorentz terms in Equation (3.12) and the classical ones in Equation (3.1) is the presence of the frequency-dependent imaginary terms $\mathrm{i}s_{1,\ell}\omega\Gamma_\ell$ in the numerators $P_{(\ell)}(\omega)$.

— By imposing that the residues $r_p^{(\ell)}$ must be real-valued, we get rid of these additional terms and retrieve the classical Lorentz terms.

— There is, however, no justification for such an assumption in general.

We now consider the contribution of only one generalized Lorentz function $\frac{P_{(\ell)}(\omega)}{Q_{(\ell)}(\omega)}$ to the relative permittivity. The constitutive relation linking the displacement field $\vec{D}(\omega)$ and the electric field $\vec{E}(\omega)$ now becomes:

$$Q_{(\ell)}(\omega)\vec{D}(\omega)=\varepsilon_0\,P_{(\ell)}(\omega)\vec{E}(\omega) \tag{3.13}$$

Or, by replacing $P_{(\ell)}(\omega)$ and $Q_{(\ell)}(\omega)$ by their expressions:

$$-\left((\omega^2-\omega_{0,\ell}^2)+\mathrm{i}\omega\Gamma_\ell\right)\vec{D}(\omega)=\varepsilon_0\left(\mathrm{i}s_{1,\ell}\omega\Gamma_\ell+s_{2,\ell}\omega_{0,\ell}^2\right)\vec{E}(\omega) \tag{3.14}$$

It follows that the additional imaginary term $\mathrm{i}\omega\Gamma_\ell$ accounts for a new contribution of the electric field to the displacement field when we compare it to the classical Lorentz function numerator $s_{2,\ell}\omega_{0,\ell}^2$. We can perform an inverse Laplace transform of Equation (3.14):

$$\left((\partial_t^2+\omega_{0,\ell}^2)+\Gamma_\ell\partial_t\right)[\vec{d}](t)=\varepsilon_0\left(s_{1,\ell}\Gamma_\ell\partial_t-s_{2,\ell}\omega_{0,\ell}^2\right)[\vec{e}](t) \tag{3.15}$$

[Key properties]

In the temporal domain, the imaginary term translates into a contribution of the scaled derivative of the electric field $s_{1,\ell}\Gamma_\ell\partial_t[\vec{e}](t)$ to the displacement field $\vec{d}(t)$.

This new dependency can be explained *via* the relation linking the displacement field, the electric field, and the polarization density field $\vec{p}$: $\vec{d} = \varepsilon_0\vec{e} + \vec{p}$. The polarization density vector is connected to the electric field *via* the electric susceptibility. As stated in reference [109], this is equivalent to considering two linear operators $\mathscr{L}_1$ and $\mathscr{L}_2$ such that:

$$\mathscr{L}_1\left[\vec{p}\right](t) = \varepsilon_0\mathscr{L}_2\left[\vec{e}\right](t) \tag{3.16}$$

which results in

$$\mathscr{L}_1[\vec{d}](t) = \varepsilon_0\left(\mathscr{L}_1 + \mathscr{L}_2\right)[\vec{e}](t) \tag{3.17}$$

$\mathscr{L}_1$ and $\mathscr{L}_2$ can be retrieved *via* identification in Equation (3.15):

$$\mathscr{L}_1 = \left(\partial_t^2 + \omega_{0,\ell}^2\right) + \Gamma_\ell\partial_t \tag{3.18}$$

$$\left(\mathscr{L}_1 + \mathscr{L}_2\right) = s_{1,\ell}\Gamma_\ell\partial_t - s_{2,\ell}\omega_{0,\ell}^2 \tag{3.19}$$

In the classical Lorentz approach, the last term reduces to $\left(\mathscr{L}_1 + \mathscr{L}_2\right) = -s_{2,\ell}\omega_{0,\ell}^2$, and Equation (3.17) describes electrons as damped harmonic oscillators driven by the electric field. In the generalized model, the time derivative term $s_{1,\ell}\Gamma_\ell\partial_t$ accounts for the contribution of the derivative of the electric field to the motion of the charged particles.

[Key properties]

The additional term appears as a correction at the macroscopic scale to the errors introduced by the classical description of the dynamics of electrons in the vicinity of atoms.

Therefore, the classical Lorentz model is an accurate model only when free electrons are present, *i.e.* in some metals at a clear transition (given by one resonance) between the metallic and dielectric regimes. We will show in the last section that transitions between regimes are indicated by Lorentz poles (singularities associated with generalized Lorentz terms). In the case of a clear metal-dielectric transition in metals such as Ag or Co, the resonance corresponds to a pole close to the real axis, with a real-valued residue. This is evidenced in Figure 3.4 where we look at the Lorentz poles and residues responsible for the transitions in the relative permittivity functions of these metals. For this specific figure, and for the sake of simplicity, the poles and residues in the SEM expression were retrieved using the Cauchy method described in Chapter 5.

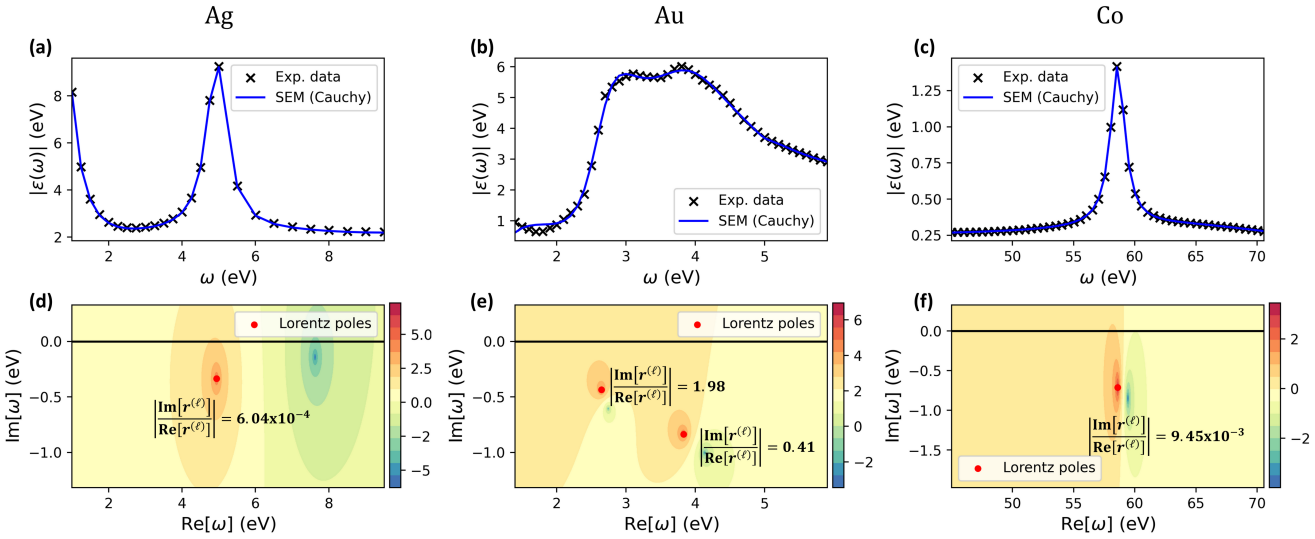

Figure 3.4. – *Amplitude of the relative permittivity functions of silver (Ag), gold (Au), and cobalt (Co) at real frequencies (a), (b), (c), and in the complex frequency plane (d), (e), (f). The spectral window was selected as to highlight the Lorentz poles associated with a transition from the metallic regime to the dielectric regime. The log-amplitude in the complex ω-plane is obtained by retrieving the SEM expression using the Cauchy method. The absolute ratio of the imaginary and real parts of the Lorentz poles are indicated next to the singularities. In the case of a clear transition corresponding to one resonance (Ag and Co), the residue is almost real-valued. Otherwise, it must be complex (Au). This highlights the fact that the classical Lorentz model fails to accurately describe materials in the general case, and must be substituted with the generalized one in Equation (3.12).*

[Intermediary observations]

— It turns out that in dielectric materials, the motion of electrons happens in the vicinity of the atom nuclei.

— Even with a classical description of this motion, the rotational orbits of the charged particles around the nuclei is incompatible with a simple $1D$ description involving a spring-like force.

— Counter-intuitively, the classical Lorentz model thus fails to accurately describe the behaviour of these materials.

We can now combine Equation (3.8) and Equation (3.10) to recast the truncated SEM expression:

Generalized Drude-Lorentz model (GDL)

$$\hat{\varepsilon}(\omega) = \varepsilon_{\mathrm{NR}} + \frac{\gamma_0}{\omega} - \sum_{\ell=1}^{M} \frac{\omega_{b,\ell}^2}{\omega^2 + \mathrm{i}\omega\gamma_\ell} - \sum_{\ell=1}^{N} \frac{\mathrm{i}s_{1,\ell}\omega\Gamma_\ell + s_{2,\ell}\omega_{0,\ell}^2}{(\omega^2 - \omega_{0,\ell}^2) + \mathrm{i}\omega\Gamma_\ell} \tag{3.20}$$

We obtain what we refer to as the GDL, as it encompasses both models (and also the Debye model) and generalizes the Lorentz terms *via* the additional imaginary terms.

It follows that the relative permittivity can be equivalently approximated as a pole expansion with Equation (3.5), and as a GDL expression with Equation (3.20).

3.2. Retrieving the parameters from experimental data

While we possess a model with an analytical description for the relative permittivity, we now have to demonstrate that it is the natural description of the response of linear media. To do so, we must retrieve the parameters of the GDL using experimental data at real frequencies, and show that these experimental data can be fitted with a small set of poles. Although Chapter 5 is dedicated to the study of methods to retrieve the parameters of the MOSEM expression or SZF using experimental data, there is no redundancy with this section, which tackles the specific case of the parameters which appear in the GDL expression. We describe our approach and test it on the 9 materials listed in Table 3.1, including oxides, metals and 2D materials, and obtained *via* the Refractive Index Database [175].

Experimental Refractive Indices			
Material	Range (μm)	Samples	Ref.
Gold (Au)	0.207 - 12.40	57	[176]
Silver (Ag)	0.018 – 2.480	23	[108]
Cobalt (Co)	0.018 – 2.480	23	[108]
Chromium (Cr)	0.262 – 2.500	65	[177]
Hafnium dioxide (HfO_2)	0.385 – 500	65	[178]
Silicon dioxide (SiO_2)	0.030 - 1.500	65	[179]
Titanium dioxide (TiO_2)	0.300 - 1.690	65	[66]
Tantalum pentoxide (Ta_2O_5)	0.030 - 1.500	65	[179]
Graphene	0.193 – 1.690	65	[180]

Table 3.1. – *Summary of the experimental data used in the article. All of them are available on the Refractive Index Database [175]*

3.2.1. Analytical continuation of the permittivity from experimental data

Each material is associated with a set of experimental data points $(\omega_i, \varepsilon_i)$ with $\varepsilon_i = \varepsilon(\omega_i)$ the relative permittivity measured at the real frequency ω_i.

[Key properties]

Starting from the expression of the GDL in Equation (3.20), we wish to find the set of parameters $\mathscr{P} = \{\varepsilon_{NR}, \gamma_0, \omega_{b,\ell}, \gamma_\ell, s_{1,\ell}, \Gamma_\ell, s_{2,\ell}, \omega_{0,\ell}\}$, which **analytically expands the relative permittivity into the complex frequency plane** while minimizing the loss function L associated with the problem.

[Derivation]

Let us write the relative L_q error functions error_q quantifying the distance between the experimental points ε_i and the estimated GDL value $\tilde{\varepsilon}_{i,\mathscr{P}} = \tilde{\varepsilon}(\omega_i, \mathscr{P})$:

$$\text{error}_q\left[\hat{\varepsilon}_i, \varepsilon_i\right] = \frac{||\hat{\varepsilon}_i - \varepsilon_i||_q}{||\varepsilon_i||_q} \tag{3.21}$$

with $q \in \{2, \infty\}$, and the norms reading as:

$$||A_i||_2 = \sqrt{\sum_i |A(\omega_i)|^2} \tag{3.22}$$

$$||A_i||_\infty = \max_i |A(\omega_i)| \tag{3.23}$$

We define the loss function L as a combination of the relative error functions and the ∞ norm applied to the relative permittivity, as well as relative error terms quantifying the error on the real part, the imaginary part and the modulus:

$$\begin{aligned} L(\varepsilon_i, \hat{\varepsilon}_i, \mathscr{P}) = 0.5 \times \text{error}_2\left[\hat{\varepsilon}_i, \varepsilon_i\right] + 2 \times \text{error}_\infty\left[\hat{\varepsilon}_i, \varepsilon_i\right] + 10 \left\| \frac{\hat{\varepsilon}_i - \varepsilon_i}{\varepsilon_i} \right\|_\infty \\ + 5 \left\langle \frac{A(\omega_i)}{\delta A(\omega_i)} \right\rangle + 5 \left\langle \frac{B(\omega_i)}{\delta B(\omega_i)} \right\rangle + 5 \left\langle \frac{C(\omega_i)}{\delta C(\omega_i)} \right\rangle \end{aligned} \tag{3.24}$$

where the notation $< . >$ corresponds to the averaging operation over all the sampled frequencies. $A(\omega_i)$ is the error between the real part of the model $\hat{\varepsilon}_i$ and experimental data ε_i, and $\delta A(\omega_i)$ accounts for the value of the real part of experimental data at the frequency ω_i. It is used to change the weight of $A(\omega_i)$. $B(\omega_i)$ and $\delta B(\omega_i)$ do the same for the imaginary part, and $C(\omega_i)$ and $\delta C(\omega_i)$ directly for the modulus:

$$A(\omega_i) = |\text{Re}[\hat{\varepsilon}_i - \varepsilon_i]|, \qquad \delta A(\omega_i) = |\text{Re}[\varepsilon_i]| + .1 \tag{3.25}$$

$$B(\omega_i) = |\text{Im}[\hat{\varepsilon}_i - \varepsilon_i]|, \qquad \delta B(\omega_i) = |\text{Im}[\varepsilon_i]| + .1 \tag{3.26}$$

$$C(\omega_i) = |\hat{\varepsilon}_i - \varepsilon_i|, \qquad \delta C(\omega_i) = |\varepsilon_i| + .01 \tag{3.27}$$

[Key properties]

The optimized set of parameters is thus obtained by minimizing L:

$$\mathscr{P}^* = \underset{\mathscr{P}}{\arg\min}\, L(\varepsilon_i, \tilde{\varepsilon}_{i,\mathscr{P}}) \tag{3.28}$$

This operation is performed through auto-differentiation, a method that has been increasingly used in optimization problems in electromagnetism thanks to the versatility and efficiency that this tool offers [181–184].

In this study, we use the open-source tools provided by the machine-learning library PyTorch.
The analytical continuation of the relative permittivity using experimental data is illustrated in Fig-

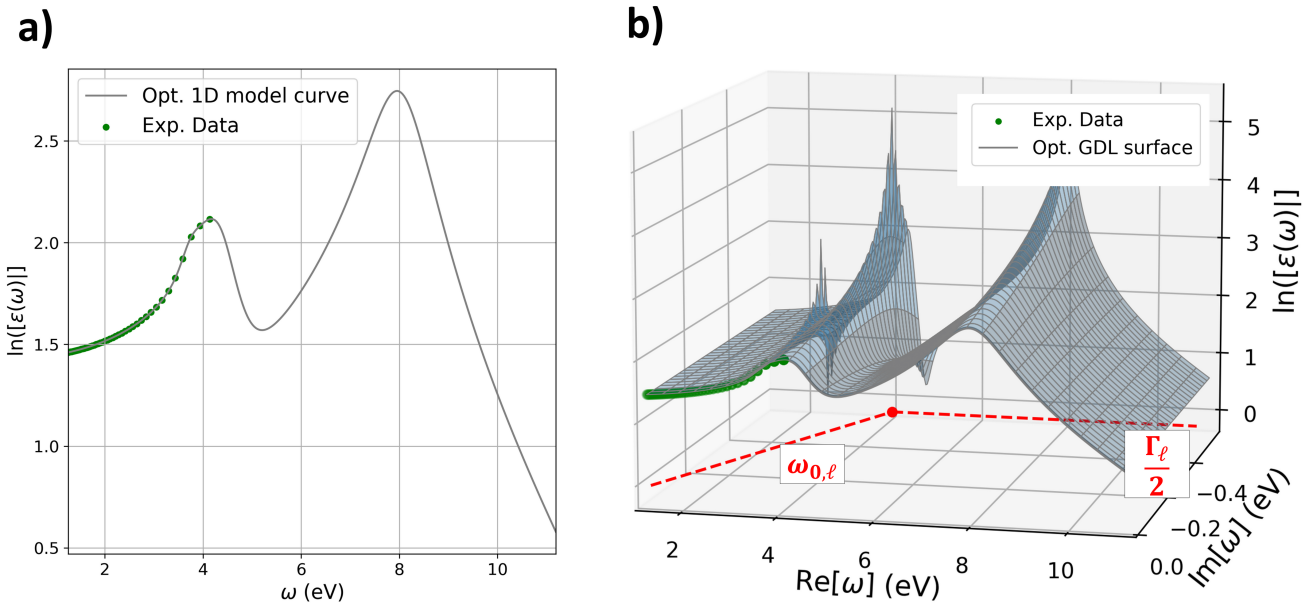

Figure 3.5. – *Optimization of a model for the relative permittivity of* TiO_2 *using experimental data. (a) Classical* 1*D optimization by a curve that fits experimental data available at low frequencies (below* 5 *eV). The* 1*D model provides a value of the relative permittivity at any real frequency. (b) Retrieval of the GDL parameters by auto-differentiation based on gradient-descent-like optimization. The parameters are chosen to minimize a loss function L as described in Equation (3.28). The process is equivalent to the optimization of a surface in the complex* ω *plane by moving the poles* $\omega_p^{(\ell)}$ *to fit the experimental data at real frequencies.*

ure 3.5 in the case of TiO_2, where the calculated function is represented by a $1D$ curve at real frequencies in Figure 3.5 (a), and as a surface in the complex frequency plane in Figure 3.5 (b). Let us stress that by setting the coefficients $s_{1,\ell}$ to 0 in Equation (3.20), we end up reducing the generalized Lorentz terms to the classical Lorentz terms.

To justify the use of the GDL rather than the classical DL model, the two of them are compared in Figures (A1) and (A2) of Annexe 1, where we observe that the GDL provides more accurate expressions than the DL model when a small number of singularities are involved. The GDL outperforms the DL model due to the presence of the imaginary terms contained within the generalized Lorentz terms in Equation (3.12), which are required for the GDL to comply with the SEM. This is especially true in non-metallic media. As we add more and more singularities, the models both start to account for the noise rather than the relative permittivity data itself, which leaves no room for comparison.

Relative Errors of the Fitting				
Material	N	M	$error_2$ (%)	$error_\infty$ (%)
Au	5	1	0.272	0.247
Ag	3	2	0.854	0.964
Co	5	1	0.145	0.070
Cr	3	1	0.542	0.834
HfO_2	2	0	0.074	0.276
SiO_2	2	0	0.287	1.192
TiO_2	3	0	0.237	0.763
Ta_2O_5	6	0	0.515	1.180
Graphene	5	1	0.331	0.843

Table 3.2. – *Relative L_2 error ($error_2$) and L_∞ error ($error_\infty$) of the optimized GDL expressions of the relative permittivity for the 9 materials listed in Table 3.1. The lower the errors, the higher the accuracy. The parameters N and M represent respectively the number of generalized Lorentz terms and the number of Drude/Debye terms in Equation (3.20).*

We quantify the accuracy of the approach *via* the calculation of the relative L_2 and L_∞ errors between the experimental data and the optimized models, introduced in Equations (3.21), (3.22) and (3.23). The errors are summarized in Table 3.2, and show the excellent accuracy reached with the GDL in a broad spectral range and for a large set of materials, using a small set of poles.

[Intermediary observations]

— We observe an excellent agreement of the GDL with the experimental data for all 9 materials in a large spectral window, using a very small set of poles.

— The applicability of this expansion for a wide range of materials comes from its compliance with complex analysis required by the fact that the relative permittivity is a linear transfer function.

We graphically highlight these results for SiO_2 and *Ag* in Figure 3.6 where their associated GDL are compared to the experimental data.

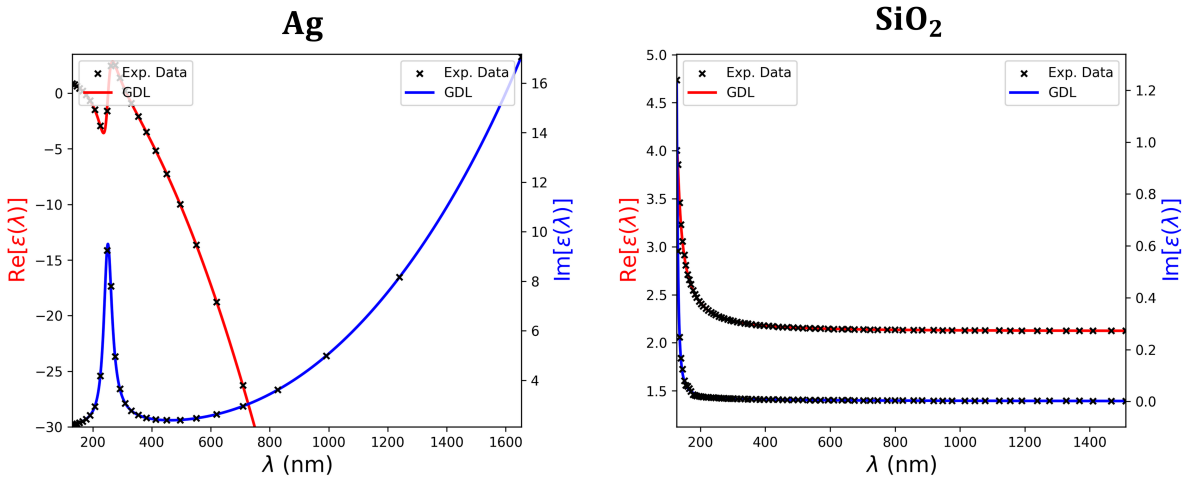

Figure 3.6. – *Real (red line, left axis) and imaginary (blue line, right axis) parts of the relative permittivitys of* Ag *and* SiO_2 *calculated with the optimized GDL (full line) and compared to the experimental data (dotted line). The relative permittivitys are expressed as functions of the wavelength instead of the frequency, to better highlight the spectral windows of the experimental data ranging from the UV to the NIR. The amplitude of the relative permittivity of* Ag *quickly increases for wavelength above* 380 *nm, in agreement with its metallic behaviour. In the case of* SiO_2, $\varepsilon(\omega)$ *is quasi-constant in the whole spectral window, with an imaginary part close to* 0 *as one would expect in an absorbtion-free dieletric material.*

3.2.2. Characterization of the materials with the distribution of the poles

By inverting the relations introduced in Equations (3.10) and (3.12), we convert the Debye, Drude and generalized Lorentz terms back into complex poles and residues which are then highlighted in the complex frequency plane.

[Key properties]

The poles and residues which do not contribute to significantly improving the matching between the model and the experimental data mostly help in fitting experimental are considered as numerical noise and are therefore removed. The numbers of imaginary poles M and pairs of poles N obtained after this step are those indicated in Table 3.2.

We plot in Figure 3.7 the log-amplitude of the relative permittivity of Au and TiO_2 in the complex frequency-plane and show qualitatively the correlation between the distribution of the poles and the amplitude of the relative permittivity at real frequencies.

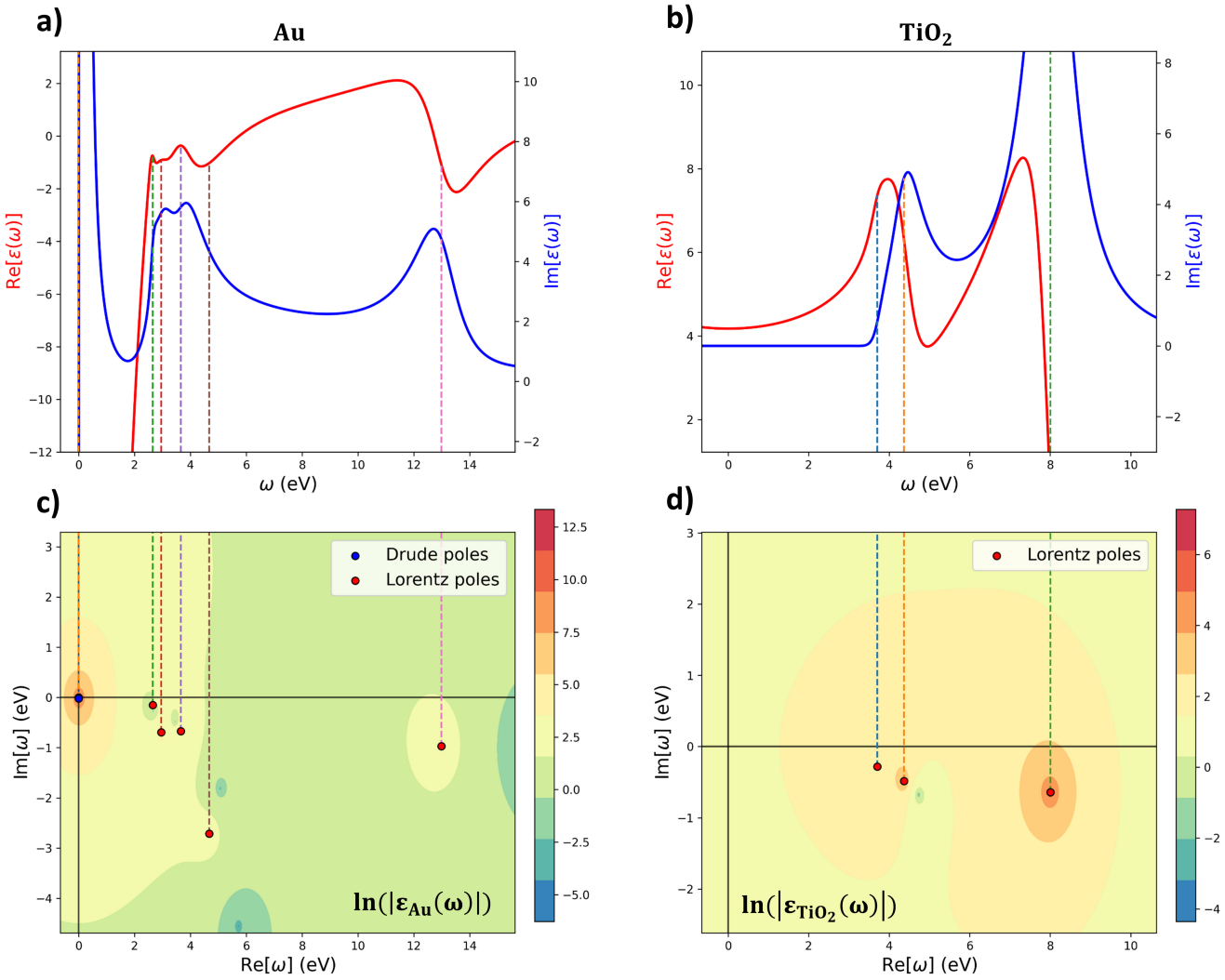

Figure 3.7. – *(a, b) Real and imaginary parts of the relative permittivity of* Au *(a) and* TiO_2 *(b) at real frequencies, calculated using the optimized GDL. (c,d) Log-amplitudes of the relative permittivity function in the complex frequency plane obtained with the GDL. The poles associated with Lorentz or Drude terms are indicated by red dots in the complex ω-plane. Vertical dashed lines highlight the link between the real parts of the poles and the spectral features of the real and imaginary parts of the relative permittivity at real frequencies.*

[Intermediary observations]

At first glance, the real part of the poles is a good indicator of resonances and anti-resonances phenomena at real-frequencies. The distribution of the poles can be used to directly assess the behaviour of the material, *i.e.* dielectric or metal, as one would expect.

Au				
Drude/Debye terms				
M	$\omega_{b,\ell}$ (eV)		γ_ℓ (eV)	
1	6.0e+00+0.0e+00j		1.8e-02	
Lorentz terms				
N	$s_{1,\ell}$	Γ_ℓ (eV)	$\omega_{0,\ell}$ (eV)	$s_{2,\ell}$
1	-9.0e-01	3.0e-01	2.7e+00	1.4e-01
2	-2.1e+00	1.4e+00	3.0e+00	2.7e+00
3	-3.6e+00	1.3e+00	3.7e+00	6.9e-01
4	-7.9e-01	5.4e+00	5.4e+00	9.5e-02
5	2.3e+00	1.9e+00	1.3e+01	5.3e-01
Non-resonant term				
ε_{NR}	4.7e-01			

Table 3.3. – *Parameters of the optimized GDL expression from Equation 3.20 obtained via auto-differentiation for the permittivity of* Au. *The frequencies $\omega_{0,\ell}$ are the moduli of the Lorentz poles, and are thus systematically larger than the imaginary parts Γ_ℓ of the poles. Since* Au *is a metal, the coefficient γ_0 is null, and only the Drude terms remain instead of the Drude/Debye terms. $-\mathrm{i}\gamma_\ell$ are purely imaginary Drude poles, while the frequencies $\omega_{b,\ell}$ appear in the residues associated with the poles and are related to the frequency range within which the material still behaves as a metal.*

[Intermediary observations]

— Let us first consider the case of gold (Au). At low frequencies, the free electrons of the metal allow for a great reflectivity, and thus a high amplitude of the permittivity, and in particular a real part far below -1. This observation is associated with the presence of Drude poles on the imaginary axis along with a singularity at the origin.

— After 2.7 eV, which corresponds to approximately 430nm, the material starts behaving like a dielectric with a rapidly varying and sign-changing real part. This phenomenon occurs at the real frequency of the first Lorentz pole.

— In low-absorption dielectrics such as TiO_2, the imaginary part of the permittivity is close to 0, and the permittivity is quasi-constant on a wide spectral window. In this case, the Lorentz poles are located far from that window, and thus weakly affect them.

Overall, **the Lorentz poles mostly mark the transitions between the different regimes**, *i.e.* the metallic regime, the dispersive dielectric regime, and the near-constant regime, while **the Drude poles are associated with extremely high values of the relative permittivity due to the free charged particles within a metal**. Therefore, it is possible to characterize the nature of the materials based on the position the poles.

[Key properties]

The values of the poles put forth in Figure 3.7 for Au and their associated residues are presented in Table 3.3. The moduli of the Lorentz poles $\omega_{0,\ell}$ located in the studied frequency window (approximately 1 to 10 eV) are in concordance with the tabulated band gaps found in the literature [185], which goes to show that the retrieved poles hold information regarding the behaviour of the materials at the microscopic scale and below.

3.3. Conclusion

Summary and conclusion

The dielectric permittivity is a transfer function that is naturally described by its singularity expansion in the harmonic domain.

- This expression can be recast into the GDL, which fully complies with the requirements and constraints of physical system.
- The generalized Lorentz model, in particular, contains an additional frequency-dependent imaginary term which corresponds to a contribution of the first derivative of the electric field to the displacement field in the temporal domain.
- This additional imaginary term is associated with a complex residue if the harmonic domain, which sets the generalized Lorentz terms apart from the classical Lorentz terms.

Using a method relying on auto-differentiation, described in Chapter 5, we have retrieved the parameters of the GDL.

- This approach has been applied to the retrieval of the permittivity of 9 different materials including oxides, metals and 2D materials.
- It systematically provides very low errors using a small set of Drude and generalized Lorentz terms in a wide spectral window extending from the UV to the NIR.
- This showcases not only the efficiency of the method, but also the high-accuracy of the generalized model.

In addition, by converting the parameters of the GDL back into poles and residues, it is possible to characterize a medium *via* the distribution of singularities of the permittivity.

- Drude singularities are associated with a singularity at the origin and purely imaginary poles and residues very close to the origin.
- In transparent medium, a near-constant permittivity over a frequency range translates into a lack of singularities into and close to the associated complex frequency window.
- The transition from one regime to another (for instance metallic to dieletric behaviour) comes along with a Lorentz pole with a relatively small imaginary part corresponding to a resonance phenomenon, hence a rapidly varying permittivity.
- Far from only adding degrees of freedom in the generalized Drude-Lorentz model, the imaginary parts of the residues associated with Lorentz poles are what allows the expression of the permittivity to be so accurate with so few of singularities.

Summary and conclusion

Overall, we have demonstrated in this chapter that the natural description of physical systems at the macroscopic scale through the SEM, using only fundamental properties of such systems, allows us to obtain information at the microscopic level.

— In the studied case of the relative permittivity, we have retrieved the classical Drude-Lorentz model and corrected one of its flaws.

— With the exemple of gold, we have also highlighted the agreement of the distribution of poles with tabulated band gaps values found in the literature.

In the next chapter, we will show that the SEM can further be used to understand and characterize the effect of resonances on arbitrary response functions at any frequency, hinting once again at the fact that the singularities are an intrinsic property of physical systems.

Summary of the results

Generalized Drude-Lorentz model (GDL)

$$\hat{\varepsilon}(\omega) = \varepsilon_{\text{NR}} + \frac{\gamma_0}{\omega} - \sum_{\ell=1}^{M} \frac{\omega_{b,\ell}^2}{\omega^2 + \mathrm{i}\omega\gamma_\ell} - \sum_{\ell=1}^{N} \frac{\mathrm{i}s_{1,\ell}\omega\Gamma_\ell + s_{2,\ell}\omega_{0,\ell}^2}{(\omega^2 - \omega_{0,\ell}^2) + \mathrm{i}\omega\Gamma_\ell}$$

4. Characterizing resonances in arbitrary response functions

Contents

4.1. Isolated resonances and resonant terms . . . 116
4.1.1. Quantifying the strength of resonances . . . 116
4.1.2. Resonant terms as Möbius transformations . . . 117
4.1.3. Describing isolated resonances with the angular coordinate . . . 120
4.2. Characterizing overlapping resonant terms . . . 126
4.2.1. From residues to zeros . . . 126
4.2.2. Quality function of the full response function . . . 129
4.3. Conclusion . . . 132

4.1. Isolated resonances and resonant terms

4.1.1. Quantifying the strength of resonances

The key role of resonances in different phenomena was discussed in the first section of Chapter 1, where we were interested in their use in the study of cavities. More generally, resonances play an important part in wave physics as they result from an efficient coupling between the excitation and the resonances of a physical system. The response function of a physical system can be entirely retrieved from the complex singularities and zeros associated with the resonances of the systems [117], as we have shown in Chapter 1. Resonances are of particular interest for studying the stability of the response of systems [5, 99, 186–188], for enhancing light matter interactions by confining light at subwavelength scales [189–195], of for tuning the wavefront [100, 196–198].

The strength of the resonance is quantified by the Quality-factor (Q-factor) while the strength of the interaction is characterized by the Purcell factor defined as the ratio between the quality factor and the effective volume [124, 127, 128, 199]. The Q-factor is determined from the spectral response as the ratio between the maximum frequency of the response (in amplitude) and the width at mid-height [200, 201], or from the complex frequency singularity p associated with the resonances, as $\frac{\mathrm{Re}[p]}{2\mathrm{Im}[p]}$ [63, 201].

These methods assume a complex pole isolated from other singularities in the complex plane, a situation yielding an almost Lorentzian shape of the spectral response. However, the majority of non-Hermitian physical systems features a dense distribution of singularities in the complex ω space, deforming the Lorentzian shape and yielding spectral anomalies for which the aforementioned methods cannot be applied for determining the quality factor. Also, the Q-factor fails to provide any information regarding the behaviour of the physical system at any frequency other than the given resonance frequency.

In this chapter, we rigorously make use of the Singularity Expansion Method (SEM) and the Singularity and Zero Factorization (SZF) to derive a function that quantifies the effect of resonances on response functions of arbitrary physical system. We show that the resonances can be characterized in the whole spectrum by a meromorphic function of the frequency. This real-valued function can be cast as a product between the frequency and the frequency-derivative of the phase of the response function, or equivalently as a sum of functions depending on poles and their conjugates. It is derived by expressing a single resonant term as a Möbius transformation mapping the real frequency axis to a circle. The radius of the circle provides the strength of the resonance while the angular coordinate is related to the width of the resonance. This transformation allows us to derive a relative phase variation function. This function identifies with the conventional definition of the Q-factor at the position of the real part of the pole. It characterizes the resonances at any frequency and for arbitrary continuous spectral response functions.

4.1.2. Resonant terms as Möbius transformations

Let us consider an arbitrary response function $H(\omega)$ associated with a physical system, which we thus assume to be linear, causal, to abide by the rules of energy conservation, and to interact with real-valued physical signals. It follows that $H(\omega)$ must be a Hermitian-symmetric meromorphic function, *i.e.* $H(\overline{\omega}) = \overline{H(\omega)}$ with $H(\omega)$ analytical everywhere except at some complex frequencies which are its poles $p^{(\ell)}$, and it diverges slower than $|\omega|$ in the complex frequency plane. If, in addition, the system is passive, then $H(\omega)$ is fully analytical in the upper part of the complex ω-plane, and the poles all have a negative imaginary part. The response function $H(\omega)$ can be written through the SEM [71, 117]:

$$H(\omega) = H_{\text{NR}} + \sum_{\ell} \frac{r^{(\ell)}}{\omega - p^{(\ell)}} \tag{4.1}$$

with H_{NR} the non-resonant term, $p^{(\ell)}$ the complex poles, and $r^{(\ell)}$ their associated residues (for poles of order 1). We first consider the case of an isolated resonance which is associated with only one pole $p^{(\ell)}$ to which corresponds the resonant term $H_\ell(\omega)$ from Equation(4.1):

$$H_\ell(\omega) := \frac{r^{(\ell)}}{\omega - p^{(\ell)}} = \frac{|r^{(\ell)}|e^{i\theta_{r^{(\ell)}}}}{\omega - p^{(\ell)}} \tag{4.2}$$

[Key properties]

$H_\ell(\omega)$ is a Möbius transformation of ω [111], which maps the real frequency axis to a circle in the complex frequency plane, as illustrated in Figure 4.1.

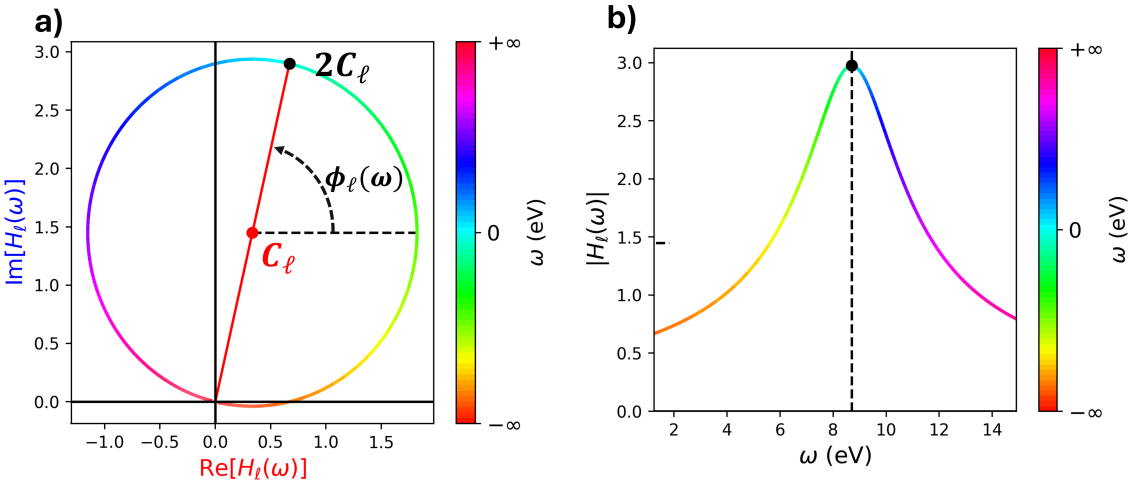

Figure 4.1. – *Resonant term $H_\ell(\omega) = r^{(\ell)}/(\omega - p^{(\ell)})$ of the response function of a physical system, associated with an isolated resonance. (a) $H_\ell(\omega)$ is a Möbius transformation mapping the real ω axis to a circle in the complex frequency plane, characterized by its center C_ℓ, its radius $|C_\ell|$ and its angular coordinate $\phi_\ell(\omega)$ giving the position on the circle depending on the frequency. At $\omega = p_R^{(\ell)} = \mathrm{Re}[p^{(\ell)}]$, the furthest point $2C_\ell$ from the origin 0 is reached, corresponding to the resonance peak in (b).*

The equation of a circle in the complex plane classically reads as:

$$C + Re^{\mathrm{i}f(s)} \tag{4.3}$$

where C is the center of the circle, R is the radius, and $f(s)$ is the angle, varying from 0 to 2π as a function of some parameter s. In the case of a Möbius circle associated with a resonant term $H_\ell(\omega)$, it yields:

$$H_\ell(\omega) = C_\ell + R_\ell e^{\mathrm{i}\phi_\ell(\omega)} \tag{4.4}$$

with C_ℓ the center of the circle, R_ℓ the radius, and $\phi_\ell(\omega)$ the angular coordinate playing the role of $f(s)$ in Equation (4.3), which indicates where we are on the circle at a given frequency, *i.e.* which value is taken by the resonant term $H_\ell(\omega)$ at the frequency ω.

The parameters of the Möbius circle can be calculated in terms of the pole $p^{(\ell)}$ and residue $r^{(\ell)}$.

[Derivation]

We start by deriving the circle center C_ℓ and the radius R_ℓ. By subtracting C_ℓ and considering the modulus for any real frequency ω in Equation (4.4), we have:

$$|H_\ell(\omega) - C_\ell| = R_\ell \tag{4.5}$$

We inject the resonant term $H_\ell(\omega)$ as defined in Equation (4.2):

$$\left|\frac{r^{(\ell)}}{\omega - p^{(\ell)}} - C_\ell\right| = \left|\frac{r^{(\ell)} + C_\ell p^{(\ell)} - C_\ell \omega}{\omega - p^{(\ell)}}\right| = R_\ell \tag{4.6}$$

leading to:

$$|C_\ell|\left|\frac{\omega - \left(\frac{r^{(\ell)}}{C_\ell} + p^{(\ell)}\right)}{\omega - p^{(\ell)}}\right| = R_\ell \tag{4.7}$$

Since Equation (4.7) must be true for any frequency ω, it can only hold if the radius is equal to the modulus of the circle center:

$$R_\ell = |C_\ell| \tag{4.8}$$

and if the numerator and denominator have the same modulus:

$$\left|\omega - \left(\frac{r^{(\ell)}}{C_\ell} + p^{(\ell)}\right)\right| = \left|\omega - p^{(\ell)}\right| \tag{4.9}$$

In particular, Equation (4.9) imposes that:

$$\frac{r^{(\ell)}}{C_\ell} + p^{(\ell)} = \overline{p^{(\ell)}} \tag{4.10}$$

This results in:

$$C_\ell = -\frac{r^{(\ell)}}{2\mathrm{i}\mathrm{Im}[p^{(\ell)}]} \tag{4.11}$$

[Key properties]

It turns out that the radius and the center of a Möbius circle can be expressed using only one complex parameter C_ℓ, which does not depend on the real part of the pole $p^{(\ell)}$.

[Derivation]

To obtain the expression of the angular coordinate $\phi_\ell(\omega)$, we also start from Equation (4.4):

$$H_\ell(\omega) - C_\ell = |C_\ell| e^{\mathrm{i}\phi_\ell(\omega)} \tag{4.12}$$

where the radius R_ℓ has been replaced by the modulus of the complex center $|C_\ell|$ using Equation (4.8).

Taking into account the expression of C_ℓ in Equation (4.11), this yields:

$$\begin{aligned} \frac{r^{(\ell)}}{2\mathrm{i}\,\mathrm{Im}\left[p^{(\ell)}\right]} \frac{\omega - \overline{p}^{(\ell)}}{\omega - p^{(\ell)}} &= |C_\ell| e^{\mathrm{i}\phi_\ell(\omega)} \\ -C_\ell \frac{\omega - \overline{p}^{(\ell)}}{\omega - p^{(\ell)}} &= |C_\ell| e^{\mathrm{i}\phi_\ell(\omega)} \end{aligned} \tag{4.13}$$

We then apply the complex Log function to Equation (4.13) to obtain:

$$\mathrm{Log}\left[-C_\ell\right] - \mathrm{Log}\left[\frac{\omega - p^{(\ell)}}{\omega - \overline{p^{(\ell)}}}\right] \equiv \mathrm{Log}\left[|C_\ell|\right] + \mathrm{i}\phi_\ell(\omega) \tag{4.14}$$

We can explicitly calculate the Log of $-C_\ell$:

$$\mathrm{Log}\left[-C_\ell\right] = \mathrm{Log}\left[|C_\ell|\right] + \mathrm{i}\theta_{r^{(\ell)}} + \mathrm{i}\frac{\pi}{2} \tag{4.15}$$

Finally, we get

$$\phi_\ell(\omega) \equiv \mathrm{i}\mathrm{Log}\left[\frac{\omega - p^{(\ell)}}{\omega - \overline{p^{(\ell)}}}\right] + \theta_{r^{(\ell)}} + \frac{\pi}{2} \quad (2\pi) \tag{4.16}$$

[Key properties]

As the frequency ω goes from $-\infty$ to $+\infty$ eV, the angular coordinate $\phi_\ell(\omega)$ spans the full 2π range. This rotation is performed anti-clockwise due to the causality and stability of the physical systems.

The resonant term $H_\ell(\omega)$ is thus a Möbius circle fully characterized by its complex center C_ℓ and its

angular coordinate $\phi_\ell(\omega)$:

$$H_\ell(\omega) = C_\ell + |C_\ell| e^{\mathrm{i}\phi_\ell(\omega)} \tag{4.17}$$

with its parameters defined as:

$$C_\ell = \frac{-r^{(\ell)}}{2\mathrm{i}p_I^{(\ell)}} \tag{4.18}$$

$$\phi_\ell(\omega) \equiv \mathrm{iLog}\left[\frac{\omega - p^{(\ell)}}{\omega - \overline{p^{(\ell)}}}\right] + \theta_{r^{(\ell)}} + \frac{\pi}{2} \quad (2\pi) \tag{4.19}$$

Möbius Transformations in the Singularity Expansion (MTSE)

More generally, the SEM expression can always be recast into the Möbius Transformations in the Singularity Expansion (MTSE):

$$H(\omega) = H_{\mathrm{NR}} + \sum_\ell C_\ell + |C_\ell| e^{\mathrm{i}\phi_\ell(\omega)} \tag{4.20}$$

4.1.3. Describing isolated resonances with the angular coordinate

[Intermediary observations]

— According to Equation (4.17), **an isolated resonance is naturally described as a perturbation bringing the amplitude $|H_\ell(\omega)|$ far from the origin 0.**

— **This is done with a certain strength** $2|C_\ell|$ (the diameter of the Möbius circle), under the constraint that the values of $H_\ell(\omega)$ are restricted to the circle.

— The variations of the response function on that circle are encoded and characterized by the angular coordinate $\phi_\ell(\omega)$.

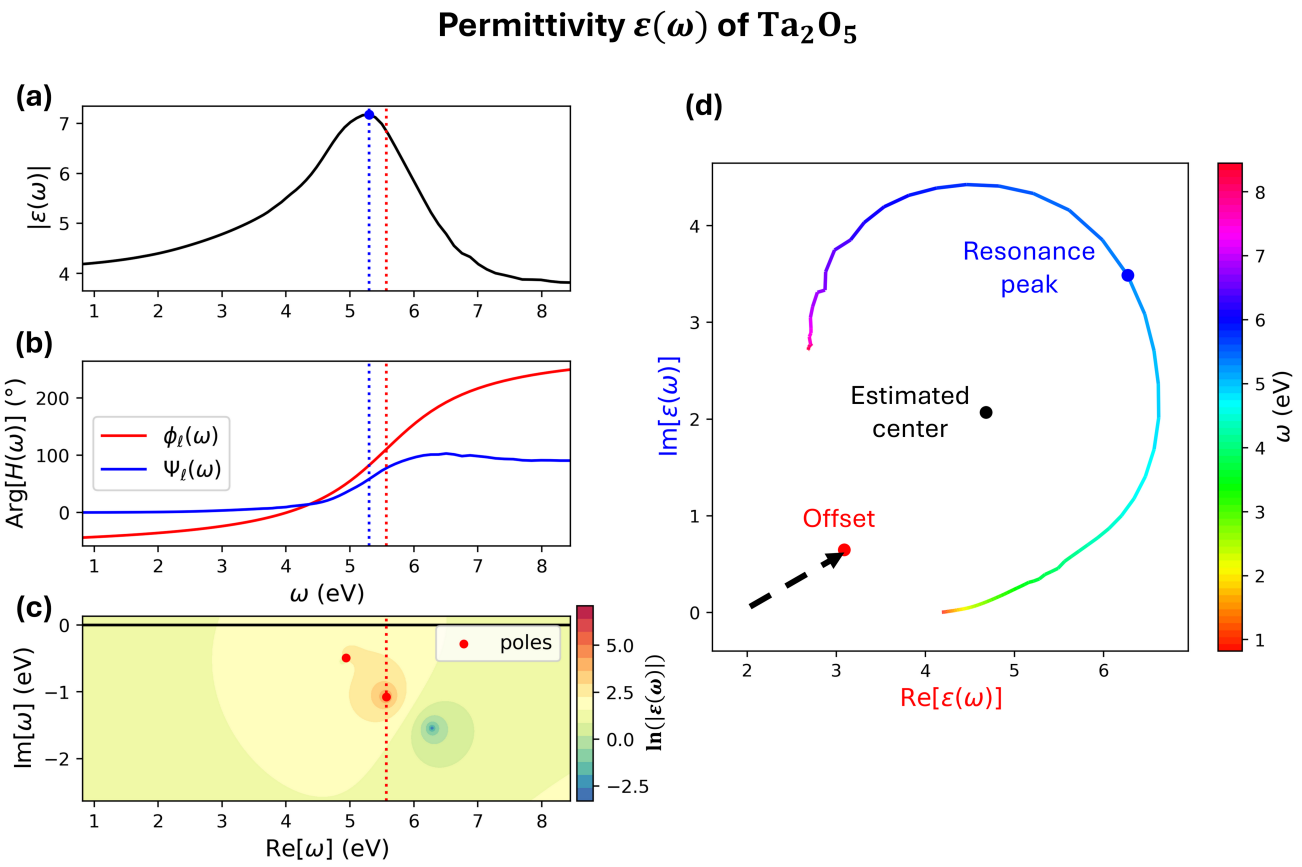

Figure 4.2. – *Bode diagram of the relative permittivity function $\varepsilon(\omega)$ of Ta_2O_5. The function is obtained using a generalized Drude-Lorentz model providing the poles and residues. (a) The amplitude diagram $|H(\omega)|$ exhibits a quasi-isolated resonance. (b) In the phase diagram, the angular coordinate $\phi_\ell(\omega)$ (red curve) of that quasi-isolated resonance is associated with an inflection point at $p_R^{(\ell)}$ (dotted red line) which differs from the resonant frequency. This shift is corrected (dotted blue line) in the approximated angular coordinate $\Psi_\ell(\omega)$ (blue curve) obtained from the argument of the full signal* Arg$[\varepsilon(\omega)]$*, highlighting the influence of other poles. (c) Some of the singularities are highlighted in the complex ω-plane, in the Log-amplitude diagram of $\varepsilon(\omega)$. (d) By plotting the real and imaginary parts of $\varepsilon(\omega)$, we highlight the deformed Möbius circle associated with the quasi-isolated singularity. The center is shifted due to the non-resonant term and the influence of the other singularities. This offset (red dot) is estimated using all other singularities and the non-resonant term. The center (black dot) is the halfway point between the offset and the resonance peak (blue dot).*

[Key properties]

Two relevant properties emerge from the study of $\phi_\ell(\omega)$.

(i) The highest perturbation of the amplitude $|H(\omega)|$ with respect to the origin 0, which is highlighted in Figure 4.1, is reached at the real part of the pole $p^{(\ell)}$, when $\omega = p_R^{(\ell)}$. At this particular frequency, $\phi_\ell(\omega)$ reads as:

$$\phi_\ell\left(p_R^{(\ell)}\right) \equiv \theta_{r^{(\ell)}} - \frac{\pi}{2} \quad (2\pi) \tag{4.21}$$

In addition, this frequency is associated with an inflection point of the phase.

(ii) While $\phi_\ell(\omega)$ operates a 2π angular shift when ω spans the $]-\infty;+\infty[$ eV range, half of it is obtained in the $[p_R^{(\ell)} + p_I^{(\ell)}; p_R^{(\ell)} - p_I^{(\ell)}]$ eV range:

$$\phi_\ell\left(p_R^{(\ell)} - p_I^{(\ell)}\right) - \phi_\ell\left(p_R^{(\ell)} + p_I^{(\ell)}\right) = \pi \tag{4.22}$$

This phase-shift is evidenced in reference [71], Figure (1), where the phase lines in the complex ω-plane are plotted. The sharpness of the amplitude of these variations is indicated by the derivative of the angular coordinate $\partial_\omega[\phi_\ell](\omega)$:

$$\partial_\omega[\phi_\ell](\omega) = \mathrm{i}\left[\frac{1}{\omega - p^{(\ell)}} - \frac{1}{\omega - \overline{p^{(\ell)}}}\right] \tag{4.23}$$

$\partial_\omega[\phi_\ell](\omega)$ is a meromorphic function fully characterized by the pole $p^{(\ell)}$ and its conjugate. At real frequencies, it is a real-valued function which reads as:

$$\partial_\omega[\phi_\ell](\omega) = -2\mathrm{Im}\left[\frac{1}{\omega - p^{(\ell)}}\right] \tag{4.24}$$

The first property is illustrated in Figure 4.2, where we consider the relative permittivity function $\varepsilon(\omega)$ of Ta_2O_5, obtained using a generalized Drude-Lorentz model [170, 202]. This material features quasi-isolated singularities, as it can be seen in Figure 4.2 (c). The amplitude of $\varepsilon(\omega)$ in Figure 4.2 (a) exhibits a quasi-isolated resonance, at a resonant frequency close to 5.16 eV, corresponding to the inflection point in the phase in Figure 4.2 (b). Let us stress that resonances are never truly isolated. The peak frequency is thus shifted from the inflection point in Figure 4.2 (d) by other poles and the non-resonant term in Equation (4.1), which appears in the complex ω-plane in Figure 4.2 (c). As a result of these contributions, the Möbius transformed associated with the quasi-isolated resonant term is no longer a circle. It is shifted and deformed in the complex plane in Figure 4.2 (d).

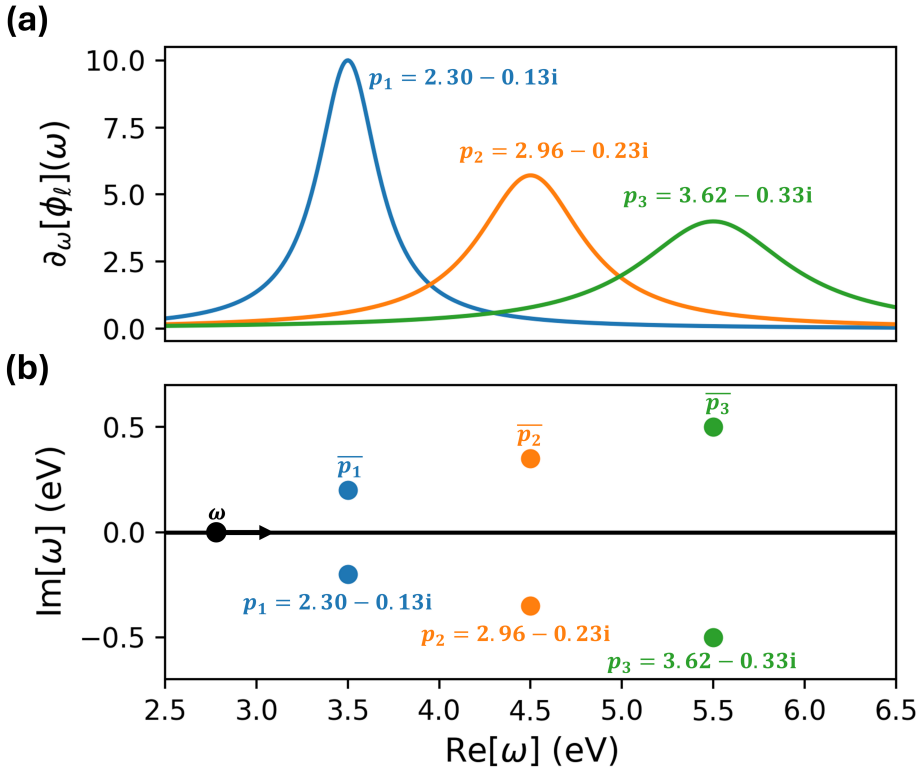

Figure 4.3. – *Derivative of the angular coordinate $\phi_\ell(\omega)$ of three resonant terms associated respectively with the poles p_1 (blue), p_2 (orange) and p_3 (green). The positions of the poles and their complex conjugates are shown in the complex ω-plane. The sharpness and peak-value of each resonant term are directly related to the imaginary part of the poles, i.e. to their distance to the real frequency axis (black horizontal line).*

Equation (4.24) shows that the variations of the angular coordinate are set by the distance from the pole to the real frequency axis. The imaginary part $p_I^{(\ell)}$ is particularly important in quantifying the spectral range of influence of the resonance on $\partial_\omega\left[\phi_\ell\right](\omega)$, as illustrated in Figure 4.3. As we move along the real ω-axis, beyond a distance $-p_I^{(\ell)} > 0$ to the isolated resonance frequency $p_R^{(\ell)}$, the variations have a lesser amplitude.

[Intermediary observations]

These two properties emphasize the idea that all the information regarding the behaviour of the response function in the vicinity of the resonance, the position of the resonance peak, and the width of the resonance are contained within the meromorphic derivative of the angular coordinate, *i.e.* $\partial_\omega[\phi_\ell](\omega)$.

This functions reaches its maximum at $\omega = p_R^{(\ell)}$ where it is inversely proportional to $p_I^{(\ell)}$. It reads as:

$$\partial_\omega[\phi_\ell](p_R^{(\ell)}) = \frac{-2}{p_I^{(\ell)}} = 4\frac{Q^{(\ell)}}{p_R^{(\ell)}} \tag{4.25}$$

with $Q^{(\ell)}$ the classical Q-factor of the resonance defined as $\frac{p_R^{(\ell)}}{2p_I^{(\ell)}}$. It turns out that $Q^{(\ell)}$ is also naturally obtained from $\partial_\omega\left[\phi_\ell\right](p_R^{(\ell)})$. In order to make this quantity dimensionless, and to convey the classical definition of the Q-factor, we multiply it by $\frac{\omega}{4}$ to define the relative angular variation function $\eta_\ell(\omega)$:

$$\begin{aligned}\eta_\ell(\omega) &= \frac{\omega}{4}\partial_\omega[\phi_\ell](\omega)\\ &= \frac{\mathrm{i}}{4}\left[\frac{p^{(\ell)}}{\omega-p^{(\ell)}} - \frac{\overline{p^{(\ell)}}}{\omega-\overline{p^{(\ell)}}}\right]\\ &= \frac{-\left|p^{(\ell)}\right|}{2\left|\omega-p^{(\ell)}\right|}\sin\left(\theta_{p^{(\ell)}}-\theta_\ell(\omega)\right)\end{aligned} \tag{4.26}$$

with $\theta_{p^{(\ell)}}$ the argument of the pole $p^{(\ell)}$ and $\theta_\ell(\omega) = \mathrm{Arg}\left[\omega - p^{(\ell)}\right]$.

[Intermediary observations]

— This function $\eta_\ell(\omega)$ quantifies the phase variation brought about by the resonant term associated with $p^{(\ell)}$ at the frequency ω with respect to the resonance peak.

— It reaches its maximum value at the isolated resonance frequency $p_R^{(\ell)}$, where it matches the classical Q-factor:

$$\eta_\ell(p_R^{(\ell)}) = -\frac{p_R^{(\ell)}}{2p_I^{(\ell)}} = Q^{(\ell)} \tag{4.27}$$

Motivated by Equation (4.27) and the aforementioned properties regarding the derivative of the angular coordinate, we refer to $\eta_\ell(\omega)$ as the quality function of the isolated resonance.

While $\eta_\ell(\omega)$ seems well-suited to the study of a resonance, let us see how it can be used to characterize arbitrary spectral responses featuring multiple poles. First, its computation is performed through $\phi_\ell(\omega)$, which requires the pole $p^{(\ell)}$. Second, the interaction and overlapping of different resonant terms questions of the validity of $\eta_\ell(\omega)$ to accurately describe a resonance. These challenges are addressed by noticing that the argument or phase of the signal $\Psi_\ell(\omega) = \mathrm{Arg}[H_\ell(\omega)]$ is proportional to $\phi_\ell(\omega)$ up to an additive constant:

$$\Psi_\ell(\omega) \equiv \frac{\phi_\ell(\omega)+\theta_r}{2} \quad (2\pi) \tag{4.28}$$

[Key properties]

In quasi-isolated resonances, the angular coordinate $\phi_\ell(\omega)$ can thus be approximated up to an offset $-\theta_{r^{(\ell)}}$ using the phase $\Psi_\ell(\omega)$.

This approximation better fits the expected behaviour of $\phi_\ell(\omega)$ as shown in Figure 4.2 where the inflection point in the phase diagram matches the resonance peak for the relative permittivity of Ta_2O_5.

Quality function of an isolated resonance

The quality function of the isolated resonance can therefore be equivalently written as:

$$\eta_\ell(\omega) = \frac{\omega}{2}\partial_\omega[\Psi_\ell](\omega) \tag{4.29}$$

We show in the next section that this definition of the quality function through the phase of the signal holds in arbitrary functions, and thus offers a solution to the second problem which was raised, *i.e.* the fact that resonances are never truly isolated.

4.2. Characterizing overlapping resonant terms

4.2.1. From residues to zeros

In most physical systems, interactions between the different resonant terms cannot be disregarded and the challenge is therefore to characterize the resonances from complex spectral responses. To address this challenge, we benefit from the definition of $\eta_\ell(\omega)$ but we now must consider a set of poles to derive a function which completely describes the resonances in the general case.

We are interested in the amplitude and phase of the full response function as described by the SEM in Equation (4.1):

$$H(\omega) = H_{\text{NR}} + \sum_\ell \frac{r^{(\ell)}}{\omega - p^{(\ell)}} \tag{4.30}$$

The amplitude and the phase of $H(\omega)$ are obviously not the sums of the amplitudes and phases of the different terms. In particular, it is clear that the easiest way to retrieve the phase of the sum is to reduce the resonant terms to the same denominator, which is tantamount to writing $H(\omega)$ in terms of its zeros $z^{(\ell)}$ and poles $p^{(\ell)}$ through the SZF [117]:

$$H(\omega) = H_0 \frac{\prod_\ell (\omega - z^{(\ell)})}{\prod_\ell (\omega - p^{(\ell)})} \tag{4.31}$$

where H_0 is a known real-valued constant which depends on $z^{(\ell)}$, $p^{(\ell)}$, and the response $H(a)$ at an arbitrary frequency a, usually set to 0 [117].

[Key properties]

Equation (4.31) implicitly states that the zeros $z^{(\ell)}$ are the roots of a polynomial of infinite degree (a holomorphic function), the coefficients of which are combinations of the residues and poles of the resonant terms, as well as the non-resonant term.

Factorized forms of response or transfer functions are usually considered in Bode diagrams to easily express the log-amplitude and the phase as sums of the contributions of the log-singularities (singularities of the logarithm of the signal) in the monomials $(\omega - z^{(\ell)})$ and $(\omega - p^{(\ell)})$. The phase $\Psi(\omega)$ is classically related to the signal $H(\omega)$ *via* the relation:

$$H(\omega) = |H(\omega)| e^{\mathrm{i}\Psi(\omega)} \tag{4.32}$$

Using the monomials, $\Psi(\omega)$ reads as:

$$\Psi(\omega) \equiv \text{Arg}[H_0] + \sum_\ell \text{Arg}[\omega - z^{(\ell)}] - \sum_\ell \text{Arg}[\omega - p^{(l)}] \quad (2\pi) \tag{4.33}$$

[Key properties]

Equations (4.30) to (4.33) show that the zeros are the result of the interaction of the resonant terms in between them and with the non-resonant term, and that they play a symmetrical role to that of the poles in the argument $\Psi(\omega)$, which has a simple expression in terms of the log-singularities (singularities of the logarithm of the response function).

We can go further than the classical Bode diagram, and analytically recover the argument $\Psi(\omega)$ of $H(\omega)$ by combining the SZF with the phase of each individual monomial:

$$\begin{aligned}\Psi(\omega) \equiv & \mathrm{Im}[\mathrm{Log}(H(\omega)] \quad (2\pi) \\ \equiv & +\frac{\mathrm{i}}{2}\sum_{\ell}\mathrm{Log}\left[\frac{\omega-\overline{z^{(\ell)}}}{\omega-z^{(\ell)}}\right] \\ & +\frac{\mathrm{i}}{2}\sum_{\ell}\mathrm{Log}\left[\frac{\omega-p^{(\ell)}}{\omega-\overline{p^{(\ell)}}}\right] \quad (2\pi)\end{aligned} \tag{4.34}$$

where Log is the principal value complex logarithm function.

[Key properties]

Similarly to $\Psi_\ell(\omega)$ for a single resonant term, the derivative $\partial_\omega[\Psi](\omega)$ of the phase is a meromorphic function with simple poles, which are the poles $p^{(\ell)}$ but also the zeros $z^{(\ell)}$ of $H(\omega)$. Their distributions are therefore required to entirely and uniquely characterize $\partial_\omega[\Psi](\omega)$:

$$\begin{aligned}\partial_\omega[\Psi](\omega) = & +\frac{\mathrm{i}}{2}\sum_{\ell}\left[\frac{1}{\omega-p^{(\ell)}}-\frac{1}{\omega-\overline{p^{(\ell)}}}\right] \\ & -\frac{\mathrm{i}}{2}\sum_{\ell}\left[\frac{1}{\omega-z^{(\ell)}}-\frac{1}{\omega-\overline{z^{(\ell)}}}\right]\end{aligned} \tag{4.35}$$

The importance of both the zeros and the poles in the variations of the phase is evidenced in Figure 4.4, where we plot the derivative of the phase of the scattering parameter $S_{11}(\omega)$ of a dielectric spherical resonator of radius $R = 450nm$ made of SiO_2 [170, 202], and simulated using the corrected Mie theory [203]. We compare it to the phase variations obtained using either only the poles $p^{(\ell)}$ (red curve) or only the zeros $z^{(\ell)}$ (blue curve), highlighting the need for both contributions.

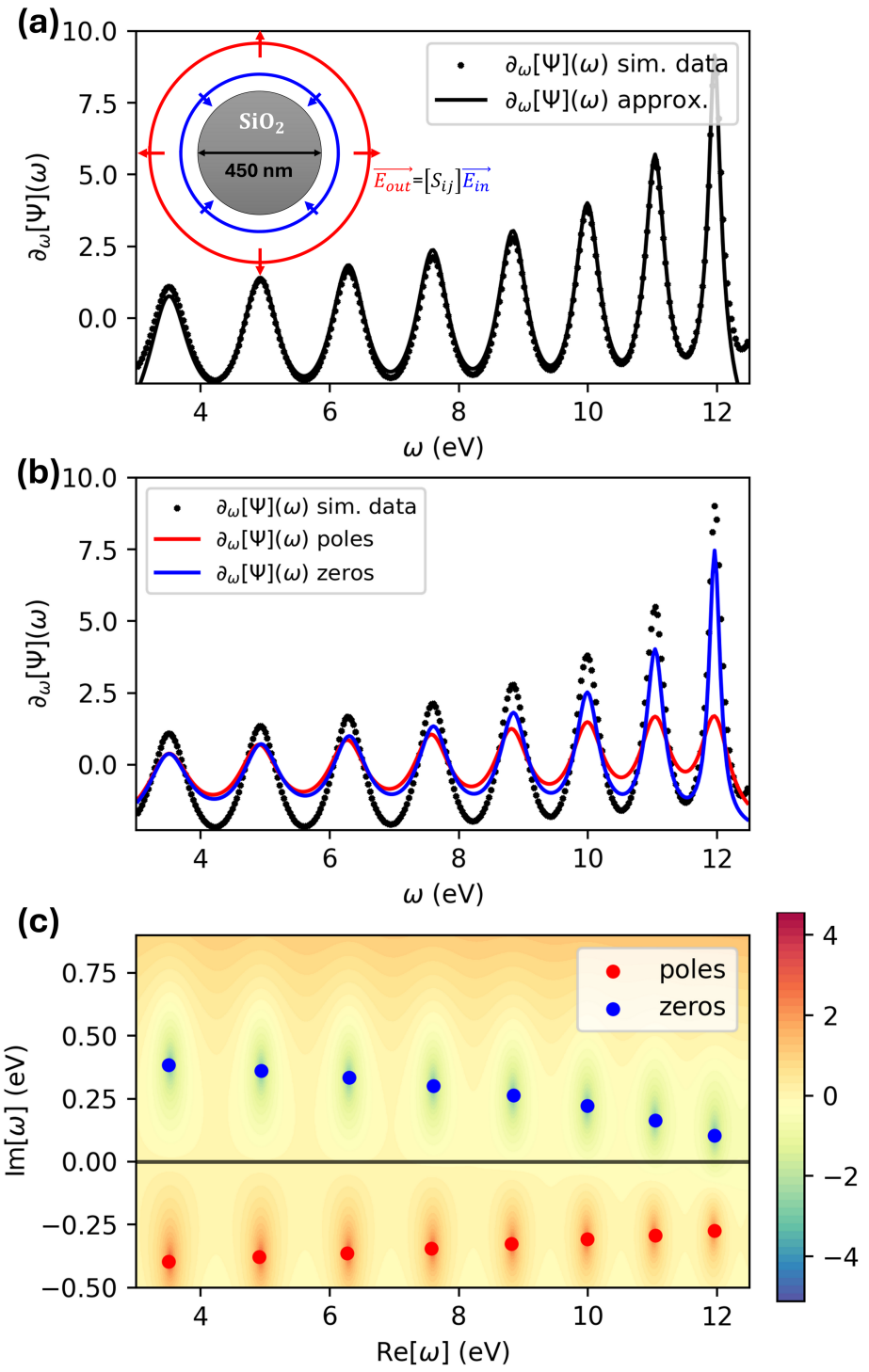

Figure 4.4. – *Scattering parameter $S_{11}(\omega)$ of a 450 nm spherical resonator of SiO_2 described by the Mie theory. (a) The phase variation $\partial_\omega[\Psi](\omega)$ (dotted curve) is accurately approximated using Equation (4.35) with the poles and zeros shown in the complex ω-plane in (c) (red and blue dots), with some discrepancies resulting from truncation of the SZF. The importance of both poles and zeros for the calculation of $\partial_\omega[\Psi](\omega)$ is evidenced by plotting the phase using only the poles (red curve) or the zeros (blue curve) in (c).*

4.2.2. Quality function of the full response function

Around a sharp resonance associated with a pole $p^{(\ell)}$ close to the real ω-axis, only the term corresponding to that pole varies, while the others act as a quasi-constant offset $\dot{\psi}_\ell$:

$$\begin{aligned}\partial_\omega[\Psi](\omega) &\approx \frac{\mathrm{i}}{2}\left[\frac{1}{\omega - p^{(\ell)}} - \frac{1}{\omega - \overline{p^{(\ell)}}}\right] + \dot{\psi}_\ell \\ &\approx \frac{\partial_\omega[\phi_\ell](\omega)}{2} + \dot{\psi}_\ell\end{aligned} \tag{4.36}$$

The phase derivative $\partial_\omega[\Psi](\omega)$ thus contains the information held by the derivative of the angular coordinate $\partial_\omega[\phi_\ell](\omega)$, while taking into account the contribution of the nearby log-singularities through $\dot{\psi}_\ell$.

It follows that we can generalize the functions $\eta_\ell(\omega)$ introduced in Equation (4.26) to the full response function $H(\omega)$ with the meromorphic relative phase variation function $\eta(\omega) := \omega\partial_\omega[\Psi](\omega)/2$.

Quality function $\eta(\omega)$ of the response function $H(\omega)$

$$\begin{aligned}\eta(\omega) = &+\frac{\mathrm{i}}{4}\sum_\ell\left[\frac{p^{(\ell)}}{\omega - p^{(\ell)}} - \frac{\overline{p^{(\ell)}}}{\omega - \overline{p^{(\ell)}}}\right] \\ &-\frac{\mathrm{i}}{4}\sum_\ell\left[\frac{z^{(\ell)}}{\omega - z^{(\ell)}} - \frac{\overline{z^{(\ell)}}}{\omega - \overline{z^{(\ell)}}}\right]\end{aligned} \tag{4.37}$$

In agreement with the previous definition, we refer to $\eta(\omega)$ as the quality function of the response function $H(\omega)$.

[Key properties]

The quality function relates information regarding the effect of log-singularities on the system even in the lack of visible effects in the amplitude or phase of the response.

This is illustrated in Figure 4.5 by considering the 0th order reflection coefficient $S_{11}(\omega)$ of a gold grating, illuminated in the TM polarization with an incident angle of 30°. The amplitude is close to 1 and slowly decreasing for ω between 1.5 and 2.25 eV. The response thus seems mainly driven by the pole $p^{(1)}$ far from the real axis. The same observation can be made, at first glance, by noticing the phase gain nearing π in the vicinity of that flat resonance in the phase diagram. However, the quality functions clearly shows the strongest relative phase variations in the vicinity of the real part of the second pole $p^{(2)}$, closer to the real-axis, which has a negligible influence over the amplitude.

The log-singularities close to the real axis are associated with phase variations, over small spectral ranges. In the vicinity of such log-singularities $p^{(0)}$ or $z^{(0)}$ for instance, the quality function is approxi-

mated by the Q-factors $Q_p^{(0)}$ or $Q_z^{(0)}$:

$$\eta(p_R^{(0)}) \approx -\frac{p_R^{(0)}}{2p_I^{(0)}} + \delta\eta_p^{(0)} \approx Q_p^{(0)} + \delta\eta_p^{(0)}$$
$$\eta(z_R^{(0)}) \approx +\frac{z_R^{(0)}}{2z_I^{(0)}} + \delta\eta_z^{(0)} \approx Q_z^{(0)} + \delta\eta_z^{(0)} \tag{4.38}$$

where the residual terms $\delta\eta_p^{(0)}$ and $\delta\eta_z^{(0)}$ account for the contribution of the other log-singularities.

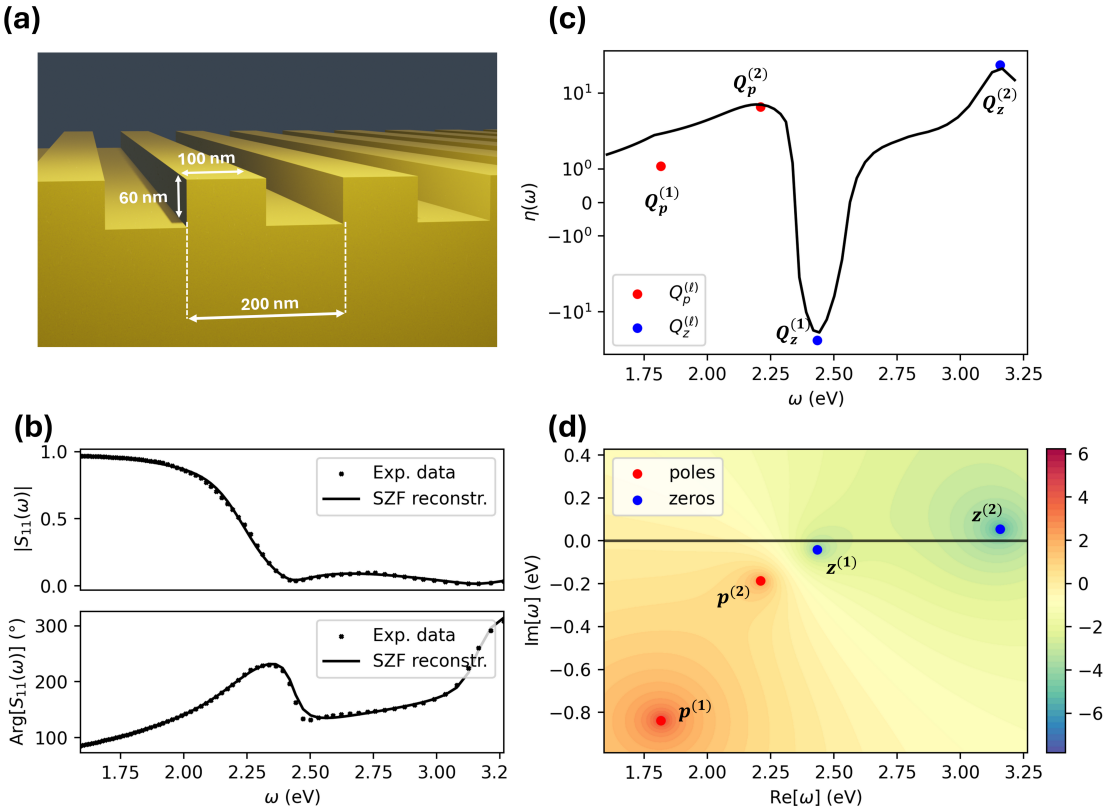

Figure 4.5. – *Quality function $\eta(\omega)$ of the Oth order reflection coefficient $S_{11}(\omega)$ of the gold grating represented in (a), with a period of 200 nm, a depth of 60 nm, and duty cycle of 0.5. It is illuminated in the TM polarization, with an incident angle of 30° (b) Bode diagram of $S_{11}(\omega)$ (Exp. data, dotted curve) and the reconstructed function through the SZF, recovered with the Cauchy method (SZF reconstructed, continuous curve). A flat resonance is observed at low frequencies, with a slowly decreasing amplitude and an important phase gain, which seems to be associated to the complex pole $p^{(1)}$ in (d), far from the real axis. However, the quality function in (c) has a local maxima at around 2.20 eV which results from the presence of $p^{(2)}$ closer to the real axis in the complex ω-plane. The resonant term associated with this pole $p^{(2)}$ thus contributes the most to the variations of the phase around that frequency. The Q-factors of the poles ($Q_p^{(\ell)}$, red dots) and zeros ($Q_z^{(\ell)}$, blue dots) are plotted in (c), where a good agreement is overall observed with $\eta(\omega)$, despite discrepancies due to the influence of the other log-singularities.*

[Intermediary observations]

As $z^{(0)}$ and $p^{(0)}$ get closer to the real ω-axis, or when the other log-singularities are far away from the frequency of interest ω, then $\delta\eta_p^{(0)}$ and $\delta\eta_z^{(0)}$ tend towards 0, and the Q-factor becomes an accurate approximation of the quality function.

This is the case in Figure 4.5 (c), where we plot the Q-factors of the poles and zeros on top of the curve of $\eta(\omega)$, and show that for the pole $p^{(2)}$ and the zeros $z^{(1)}$ and $z^{(2)}$ which have a small imaginary part, a good agreement is observed between the quality function and the Q-factors.

4.3. Conclusion

Summary and conclusion

In this chapter, we have seen that the poles, zeros and residues which appear in the SEM and the SZF are more than mere tools to analytically describe the response of a physical system, and are in fact fundamental properties of such response functions, intrinsically linked to their resonances.

Resonances are modeled through the resonant terms appearing in the singularity expansion of the response or transfer function of a linear physical system. These resonant terms are associated with the poles of the system.

- We have demonstrated that each resonant term is a Möbius circle with a radius and angular coordinate that characterize the isolated resonances.
- From the derivative of this angular coordinate, which is related to the phase of the resonant term, we have derived a meromorphic function $\eta(\omega)$, the quality function, which naturally quantifies the contribution of the pole of the resonant term to its phase variation.
- We have shown that this function matches the classical Q-factor related to the real and imaginary part of the pole associated with any isolated resonance, and extends the Q-factor to any real frequency.
- In the more general case, where zeros appear as a consequence of overlapping resonant terms and their interaction with the non-resonant term, we have demonstrated through the SZF that the quality function $\eta(\omega)$ accounts for the effect of the complex poles and zeros on the response or transfer function of a physical system.

While the quality function is related to the poles and zeros of the response function, we have seen that it can be calculated and defined directly from the phase of the signal, which was experimentally retrieved or simulated at real frequencies. However, the complex log-singularities play a crucial part in the characterization, control and design of systems or various physical phenomena. The next and last chapter will therefore be dedicated to the retrieval of poles, zeros and residues of arbitrary response functions from real ω data.

Summary of the results

Möbius Transformations in the Singularity Expansion (MTSE)

$$H(\omega) = H_{\mathrm{NR}} + \sum_{\ell} C_\ell + |C_\ell| e^{\mathrm{i}\phi_\ell(\omega)}$$

Quality function of an isolated resonance

$$\eta_\ell(\omega) = \frac{\omega}{2}\partial_\omega[\Psi_\ell](\omega)$$

Quality function $\eta(\omega)$ of the response function $H(\omega)$

$$\eta(\omega) = +\frac{\mathrm{i}}{4}\sum_\ell \left[\frac{p^{(\ell)}}{\omega - p^{(\ell)}} - \frac{\overline{p^{(\ell)}}}{\omega - \overline{p^{(\ell)}}}\right] - \frac{\mathrm{i}}{4}\sum_\ell \left[\frac{z^{(\ell)}}{\omega - z^{(\ell)}} - \frac{\overline{z^{(\ell)}}}{\omega - \overline{z^{(\ell)}}}\right]$$

5. Retrieving the poles, residues and zeros of the response functions of an arbitrary physical system

Contents

5.1. Introduction . . . 135
5.2. The Cauchy method for rational approximations . . . 137
5.2.1. Overview of the original method . . . 137
5.2.2. Physics informed optimization . . . 140
5.3. Auto-differentiation approach for the singularity expansion . . . 144
5.3.1. Formulating the optimization problems . . . 144
5.3.2. Other forms of the singularity expansion . . . 147
5.4. Natural and effective poles . . . 152
5.5. Conclusion . . . 158

5.1. Introduction

Throughout this manuscript, we have seen that the singularities, residues and zeros were intrinsic properties of physical signals or transfer operators associated with physical systems. Through the Singularity Expansion Method (SEM) and the Singularity and Zero Factorization (SZF), in the harmonic-domain, they are associated with exact analytical expressions which remain highly accurate once truncated. We have exploited these expressions to study a resonant cavity in Chapter 2, the relative permittivity of different materials in Chapter 3, and to characterize resonances in the previous chapter, Chapter 4. However, we have not delved into the details of how to recover the complex log-singularities and residues of the response function of an arbitrary physical system.

The problem of the retrieval of the poles, zeros and residues of a physical signal has been tackled by several groups over the past few years, for the different prospects it offers. The expressions resulting from the distributions of log-singularities and residues can be used to approximate functions at any frequency over large spectral windows, with small, discrete sets of parameters [30, 204–207], and they provide simple models to describe the behaviour of scatterers and cavities [67, 99, 208, 209]. In addition, the singularities and zeros help in understanding the behaviour of physical systems and their interaction with excitation signals, giving rise to many applications in electromagnetism [91, 100, 109, 143, 202, 210].

Different methods have been proposed to retrieve the log-singularities and residues. When the available data are acquired or generated in the complex frequency plane, the calculation of the poles and residues (or equivalently the poles and zeros) is quite straightforward through contour integrals [100, 211–213]. In the case of discrete data acquired over a real spectral range $[\omega_A, \omega_B] \subset \mathbb{R}$, the retrieval of these complex points is more challenging but also more practical, and is drawing in more and more attention [214–218].

In this chapter, we will explain two approaches to perform this task.

— The first one is based on the Cauchy method [68, 206, 217] and works by expressing the function through a rational approximation. We describe the working principle of the original method and explain how it can be improved and optimized using the properties of physical systems.

— The second one relies on auto-differentiation [174, 181–184, 202] to solve optimization problems through gradient-descent. The formulation of these optimization problems is detailed, as well as their application to retrieve different forms of the SEM.

Similarly to the previous chapters, our starting point is a meromorphic function $H(\omega)$, written using either the SEM [31, 69, 74, 75, 117]:

$$H(\omega) = H_{NR} + \sum_{\ell} \frac{r^{(\ell)}}{\omega - p^{(\ell)}} \tag{5.1}$$

where H_{NR} is the non-resonant term, $\{p^{(\ell)}\}_\ell$ is the set of simple poles of $H(\omega)$ (we assume that the singularities are all poles of order 1), and $r^{(\ell)}$ is the residue associated with the pole $p^{(\ell)}$, or equivalently

through the SZF [70–72, 117]:

$$H(\omega) = H_0 \frac{\prod_{\ell}(\omega - z^{(\ell)})}{\prod_{\ell}(\omega - p^{(\ell)})} \tag{5.2}$$

with $z^{(\ell)}$ the zeros of $H(\omega)$, and H_0 is a known constant which depends on $z^{(\ell)}$, $p^{(\ell)}$, and the response $H(a)$, with a an arbitrary frequency.

The retrieval of the poles, zeros and residues to reconstruct the physical signals using either the SEM or the SZF is justified by their unicity, which can be demonstrated using the identity theorem. It states that two analytical functions $H(\omega)$ and $H'(\omega)$ defined in a set $\mathscr{D}$ which are equal on an open sub-set B must be equal in $\mathscr{D}$ [112, 219]. As a result, $H(\omega)$ and $H'(\omega)$ have the same Laurent and Taylors series expansion in $\mathscr{D}$. Consequently, by definition of the SEM and SZF [117], the two functions must have the same parameters when expressed using Equations (5.1) and (5.2).

[Key properties]

The distribution of poles $p^{(\ell)}$, zeros $z^{(\ell)}$, and residues $r^{(\ell)}$ is unique, and these complex parameters fully characterize the response function $H(\omega)$, **provided that they are all taken into account**.

Therefore, the log-singularities are intrinsic properties of physical systems, and their retrieval is relevant. However, there can be an infinite amount of them, which implies that they are never all taken into account in practice, and that approximations must be made when the SZF and the SEM are truncated. It is thus necessary to identify the poles which actually account for the physical behaviour of the systems. We describe how to do that in another section following the presentation of the two methods to retrieve the poles, residues and zeros. Finally, we show how to use both methods to identify more easily the physically relevant poles, often referred to as natural poles.

5.2. The Cauchy method for rational approximations

5.2.1. Overview of the original method

Let us first present an overview of the Cauchy method to retrieve the poles and zeros of a function from real-frequency data points.

[Derivation]

We consider Equation (5.1) truncated at the M_p^{th} order for the poles, or Equation (5.2) also truncated at the M_z^{th} order for the zeros. Since the response function $H(\omega)$ is meromorphic, it can also be written as a rational function:

$$H(\omega) = \frac{F(\omega)}{G(\omega)} \tag{5.3}$$

with $G(\omega)$ a polynomial of degree M_p, and $F(\omega)$ a polynomial of degree M_z. The degree M_p of $G(\omega)$ is initialized to the number of expected poles, and is case dependent. The roots of $G(\omega)$ and $F(\omega)$ are respectively the poles and zeros of $H(\omega)$. The calculation of the poles and zeros is thus tantamount to the calculation of the coefficients $\mathbf{a} = (a_0, a_1, ..., a_{M_z})^T$ of $F(\omega)$ and $\mathbf{b} = (b_0, b_1, ..., b_{M_p})^T$ of $G(\omega)$. For any frequency ω, we have:

$$F(\omega) = \mathbf{X}^{(z)}.\mathbf{a} \tag{5.4}$$

$$G(\omega) = \mathbf{X}^{(p)}.\mathbf{b} \tag{5.5}$$

with $\mathbf{X}^{(z)} = (1, \omega, \omega^2, ..., \omega^{M_z})$, $\mathbf{X}^{(p)} = (1, \omega, \omega^2, ..., \omega^{M_p})$, and "." the scalar product. Equation (5.3) can thus be recast as:

$$\left[\mathbf{X}^{(z)},\ -H(\omega)\mathbf{X}^{(p)}\right] \begin{bmatrix} \mathbf{a} \\ \mathbf{b} \end{bmatrix} = 0 \tag{5.6}$$

The data are acquired at N frequencies ω_n, $1 \leq n \leq N$, between ω_A and ω_B in $\mathbb{R}$. Let us write $H(\omega_n) = H_n$ the value of the response function at ω_n. The following matrix notation of Equation (5.6) is obtained:

$$[\mathbf{A}, -\mathbf{B}] \begin{bmatrix} \mathbf{a} \\ \mathbf{b} \end{bmatrix} = 0 \tag{5.7}$$

The matrix $\mathbf{A}$ reads as:

$$\mathbf{A} = \begin{bmatrix} 1 & \omega_1 & ... & \omega_1^{M_z} \\ 1 & \omega_2 & ... & \omega_2^{M_z} \\ & ... & & \\ 1 & \omega_N & ... & \omega_N^{M_z} \end{bmatrix} \tag{5.8}$$

[Derivation]

and **B** is:

$$\mathbf{B} = \begin{bmatrix} H_1 & H_1\omega_1 & \dots & H_1\omega_1^{M_p} \\ H_2 & H_2\omega_2 & \dots & H_2\omega_2^{M_p} \\ & \dots & & \\ H_N & H_N\omega_N & \dots & H_N\omega_N^{M_p} \end{bmatrix} \tag{5.9}$$

with the notation $H_i = H(\omega_i)$. Although the polynomial coordinates $[\mathbf{a}\ \mathbf{b}]^T$ can be approximated *via* an optimization method by minimizing the mean-squared error on Equation (5.7) for instance, the Cauchy method constraints the kernel of the matrix $\mathbf{C} = [\mathbf{A},\ -\mathbf{B}]$ in order to obtain a unique, algebraic solution to the problem. If $N > M_z + M_p + 2$, the rank r of **C** is:

$$r = M_z + M_p + 2 - K \tag{5.10}$$

with K the dimension of its kernel.

We set the dimension of the kernel to $K = 1$ so that the non-trivial solution vectors of Equation (5.7) are all proportional to each other. We can calculate one such solution. To do so, we first perform a QR decomposition of A:

$$\mathbf{A} = \mathbf{QR} \tag{5.11}$$

with **Q** a $N \times N$ orthogonal matrix and **R** a $N \times (M_z + 1)$ upper triangular matrix. By applying $\mathbf{Q}^T$ to **C**, we obtain:

$$\begin{bmatrix} \mathbf{R}_{11} & \mathbf{R}_{12} \\ 0 & \mathbf{R}_{22} \end{bmatrix} \begin{bmatrix} \mathbf{a} \\ \mathbf{b} \end{bmatrix} = 0 \tag{5.12}$$

with $\mathbf{R}_{11}$ an upper triangular matrix with non-zero diagonal elements. It results that the singular value associated with the kernel is in $\mathbf{R}_{22}$. **b** is calculated as any non-null vector of the kernel of $\mathbf{R}_2 2$. From Equations (5.12), we then obtain **a**:

$$\mathbf{a} = -\mathbf{R}_{11}^{-1}\mathbf{R}_{12}\mathbf{b} \tag{5.13}$$

Knowing the polynomial coefficients **a** and **b**, $F(\omega)$ and $G(\omega)$ can be calculated, and the SZF expression can be retrieved. The poles $p^{(\ell)}$ are obtained by calculating the roots of $G(\omega)$, and the zeros $z^{(\ell)}$ through the roots of $F(\omega)$.

Three parameters need to be tuned in the Cauchy method: the number of poles M_p, the number of zeros M_z, and the rank r.

[Key properties]

All three parameters must be such that Equation (5.10) holds with $K = 1$.

Classically, M_z is set to $M_p - 1$ to ensure the convergence of $H(\omega)$ towards 0 at high ω, and the rank r is obtained through a Singular Value Decomposition of $\mathbf{C}$, which is used to filter out small singular values with respect to the largest one as shown in Figure 5.1, where the response function is the reflection coefficient $\tilde{r}(\omega)$ of a thin slab of silver Ag, of thickness 8 nm, illuminated at normal incidence.

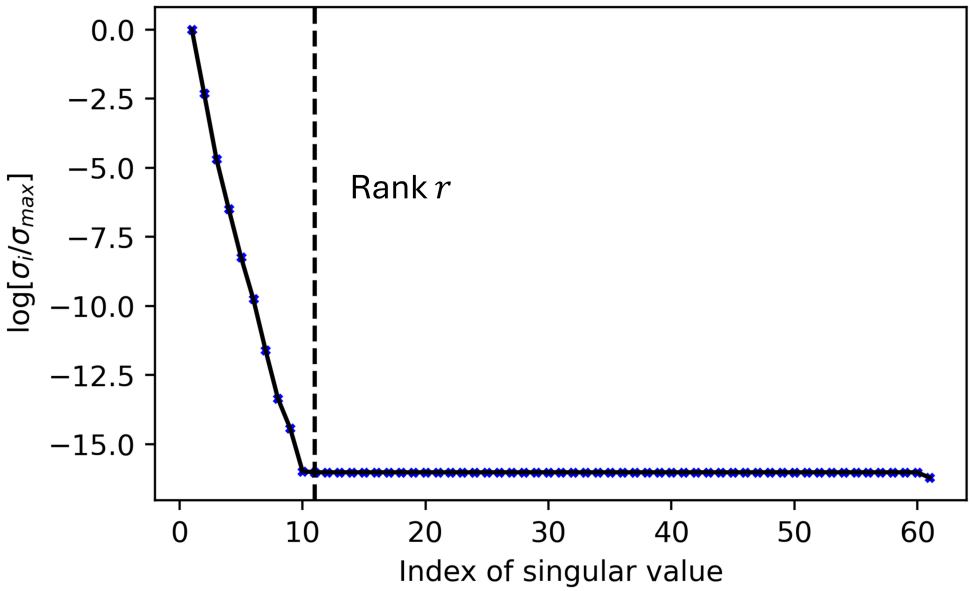

Figure 5.1. – *Relative singular values of the matrix* $\boldsymbol{C} = [\boldsymbol{A} - \boldsymbol{B}]$ *with* $\boldsymbol{A}$ *and* $\boldsymbol{B}$ *defined in Equations* (5.8) *and* (5.9). *The singular values are sorted by decreasing value, and divided by the first one,* σ_{max}. *In the classical Cauchy method, the rank* r *is set to the index of the smallest singular value after which no significant variation of the ratio* σ_i/σ_{max} *is observed.*

We test the method with these classical parameters with the same reflection coefficient $\tilde{r}(\omega)$ of a slab of silver (Ag) in Figure 5.2. The response function is evaluated at 75 frequencies ranging from 1 to 12 eV. The rank is set to $r = 10$, $M_p = 5$ and $M_z = M_p - 1 = 4$. Despite the small numbers of poles and zeros, we observe a good fitting over a large spectral window, with a relative L_2 error $e^{(2)}_{10,5,4}$ of 0.0438%, defined as:

$$e^{(2)}_{r,M_p,M_z}\left[\hat{H}_i, H_i\right] = \frac{||\hat{H}_i - H_i||_2}{||H_i||_2} \tag{5.14}$$

where $\hat{H}_i$ is the reconstructed response function at the frequency ω_i using the parameters r, M_p and M_z, and the norm reads as:

$$||A_i||_2 = \sqrt{\sum_i |A(\omega_i)|^2} \tag{5.15}$$

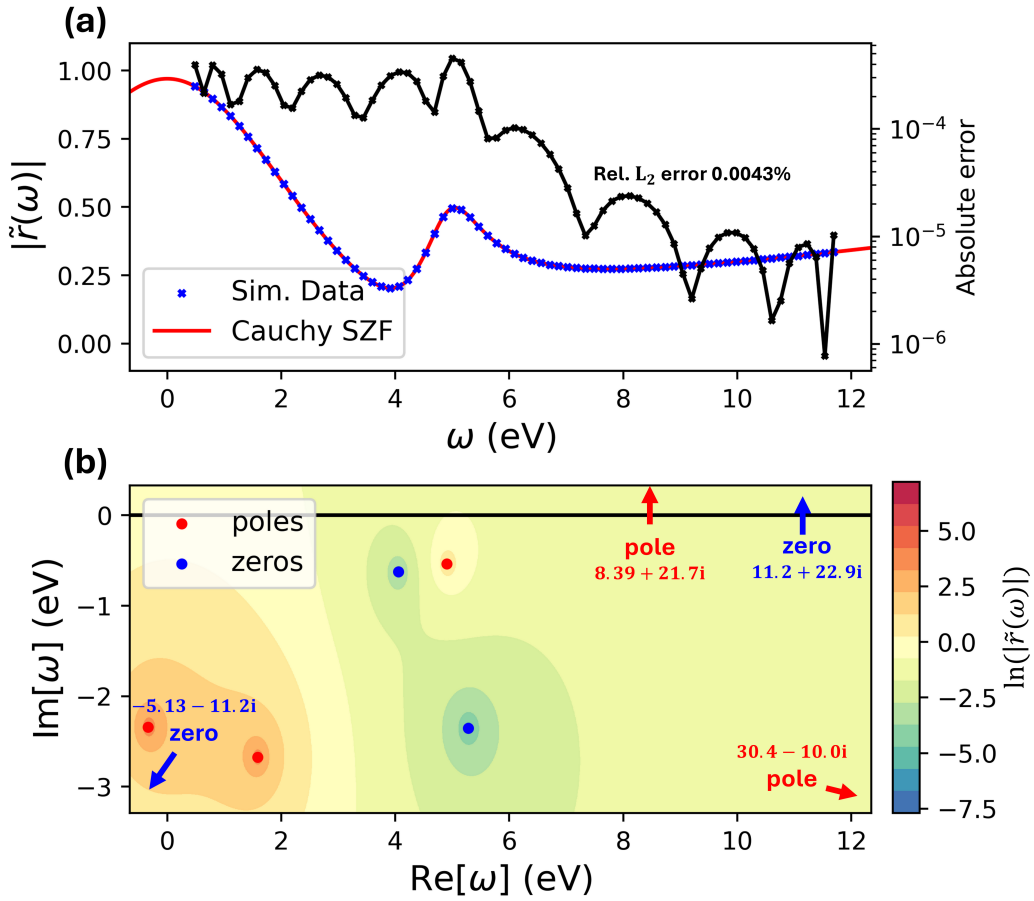

Figure 5.2. – *(a) Reflection coefficient $\tilde{r}(\omega)$ of a thin slab of silver (Ag) reconstructed with the SZF retrieved via the classical Cauchy method (red curve), and compared to simulated data (blue markers). The absolute error $|H_i - \hat{H}_i|$, with H_i the target and $\hat{H}_i$ the reconstructed value, is plotted (black curve), and shows the high accuracy of the method, with a relative L_2 error $e^{(2)}_{10,5,4} = 0.0438\%$. (b) The distribution of the poles and zeros retrieved by the Cauchy method in the complex ω-plane. The poles and zeros outside the spectral window of interest are indicated by the red and blue arrows.*

5.2.2. Physics informed optimization

While the classical Cauchy method provides good results in most situations, it can be improved to obtain a better fitting and take into account the properties of physical systems. If $H(\omega)$ is the response or transfer function of a physical system, it is Hermitian-symmetric, *i.e.* its poles and zeros come in pairs $(p^{(\ell)}, -\overline{p^{(\ell)}})$ and $(z^{(\ell)}, -\overline{z^{(\ell)}})$. We can rewrite the truncated SZF as:

$$H(\omega) = H_0 \frac{\prod_{\ell=1}^{M_z} \left[(\omega - z^{(\ell)})(\omega + \overline{z^{(\ell)}})\right]}{\prod_{\ell=1}^{M_p} \left[(\omega - p^{(\ell)})(\omega + \overline{p^{(\ell)}})\right]} \tag{5.16}$$

[Key properties]

— In order to take into account this Hermitian symmetry, we augment the dataset and add negative frequencies $-\omega_i$ associated with the complex conjugate of the signal $\overline{H_i}$.

— What is more, in the optimized Cauchy method, only the poles and zeros with a positive or null real part are kept, and we assume the symmetry expressed in Equation (5.16) to reconstruct $H(\omega)$ before calculating the errors $e^{(2)}_{r,M_p,M_z}$.

In addition, the poles and zeros located too far from the window of interest, act as offsets and have little influence over the variations of $H(\omega)$ at real frequencies. We thus remove them from the sets of poles and zeros, but modify the constant term H_0 as to take into account their contributions:

$$H_0' = \frac{\prod_{z_f}\left(-|z_f|^2\right)}{\prod_{p_f}\left(-|p_f|^2\right)} \tag{5.17}$$

where H_0' is the modified constant term, and z_f and p_f are the zeros and poles far from the spectral range of interest. They are considered as such when their distance to the origin exceeds 5 times the studied spectral range.

[Key properties]

The identity theorem ensures the unicity of the solution in the absence of noise, in which case we can rely on an accuracy-driven optimization of the Cauchy method. We want to find the set of parameters r, M_z and M_p which minimizes the relative L_2 error.

While the noise can never fully be removed, as a first approximation we assume that it is corrected for following the use of the aforementioned Singular Value Decomposition (SVD) of the matrix $\mathbf{C} = [\mathbf{A}\ -\mathbf{B}]$. The SVD provides an upper bound r_{Max} on the rank. We then set the values of M_z and M_p *via* the relations:

$$M_p = \max(\lfloor \frac{r-1+\delta D}{2} \rfloor, 1) \tag{5.18}$$

$$M_z = \max(M_p - \delta D, 0) \tag{5.19}$$

where δ is the difference $M_p - M_z$ we would like to impose. By sweeping through the values of the rank r from 2 to r_{Max}, with a fixed δD, we can thus obtain different values of r, M_p and M_z, and we chose the set of parameters that minimizes the relative L_2 error between the resulting SZF and the available data. The lowest error is associated with δD:

$$e^{(2)}_{\delta D} = \min_r e^{(2)}_{r,M_p,M_z}[\hat{H}_i, H_i] \tag{5.20}$$

Following that, we also sweep through the values of δD from M_p to 0. We keep the value of δD

associated with the lowest relative L_2 error $e^{(2)\,*}$:

$$e^{(2)\,*} = \min_{\delta D} e^{(2)}_{\delta D} \tag{5.21}$$

[Key properties]

Let us stress that the bounds of δD are chosen as to maintain M_p greater than M_z, so that the SEM, and consequently the SZF, can still be applied to the signal $H(\omega)$.

We compare this optimized Hermitian-symmetric version to the classical one in Figure 5.3, where the response function is the relative permittivity of gold (Au), with $N = 57$ data points.

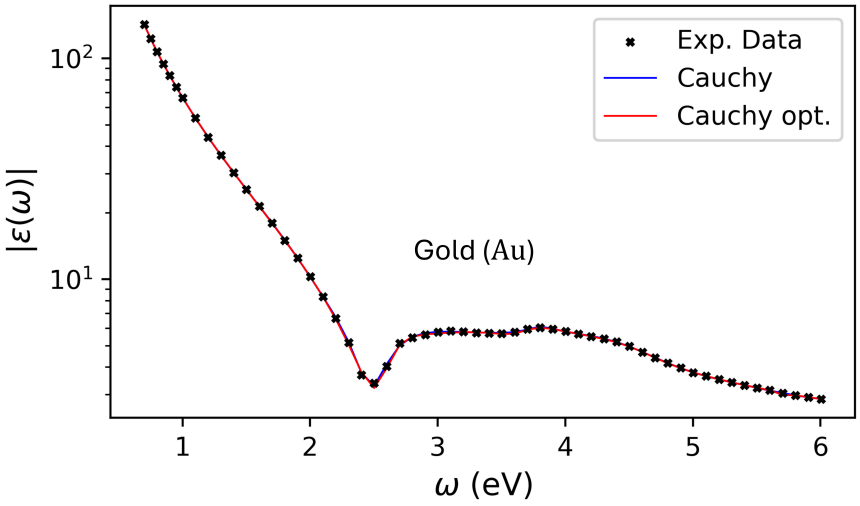

Figure 5.3. – *Approximation of the relative permittivity of gold* (Au) *using the classical Cauchy method (blue curve) or the physics-informed one (red curve). While both versions provide similar results, i.e. an accurate fitting of the experimental data (black markers), the physics-informed one is Hermitian-symmetric. What is more, it requires fewer pairs of poles and zeros than there are poles and zeros needed for the classical Cauchy method.*

For the classical approach, the parameters are $r = 18$, $M_p = 9$ and $M_z = 8$, with a relative L_2 error $e^{(2)}_{12,6,5} = 0.3086\%$. For the physics-informed one, they become $r = 29$, $M_p = 14$ and $M_z = 14$ (which correspond to 7 pairs of poles and zeros with the Hermitian symmetry), with $e^{(2)\,*} = 0.2447\%$. In both cases, the maximum number of poles is chosen by initializing the degree of $G(\omega)$ to $M_p = 16$.

[Intermediary observations]

— Let us stress that the relative errors are too similar to recommend the use of the physics informed version based on performance alone.

— However, the Hermitian symmetry in the physics informed one results in smaller sets of pairs of poles and zeros in practice.

— This highlights the fact that a more relevant solution with similar performance can be obtained with fewer poles.

Let us point out that, while the Cauchy method provides accurate results which abide by the property of Hermitian symmetry of the physical signals, it might not be compatible with the assumed passivity of most systems, which imposes passive poles, *i.e.* with a negative imaginary part. In case the stability property is needed, the second approach based on auto-differentiation might prove more useful, as it offers more freedom in the choice of constraints on the parameters.

5.3. Auto-differentiation approach for the singularity expansion

5.3.1. Formulating the optimization problems

We now move onto the second approach which aims at exploiting auto-differentiation (in the PyTorch library) to obtain accurate approximations through optimization problems. Although these approaches could be applied to optimize the SZF, we focus on the retrieval of the different terms in the SEM, or in other words, the poles $p^{(\ell)}$, the residues $r^{(\ell)}$, and the non-resonant term H_{NR}. Similarly to the previous section, we consider the truncated SEM expression, with M complex pairs of poles or purely imaginary poles:

$$H(\omega) = H_{NR} + \sum_{\ell=1}^{M} \left[\frac{r^{(\ell)}}{\omega - p^{(\ell)}} - \frac{\overline{r^{(\ell)}}}{\omega + \overline{p^{(\ell)}}} \right] \tag{5.22}$$

While it is possible to deal with complex values in the optimization process, current auto-differentiation tools have only recently been able to deal with such numbers, and some functions are still not properly defined in $\mathbb{C}$. We thus impose on the parameters to be real-valued. We split the M poles of Equation (5.22) into M_I purely imaginary poles $\mathrm{i}q^{(\ell)}$ with residues $\mathrm{i}\rho^{(\ell)}$ and M_C complex pairs of poles $p^{(\ell)} = p_R^{(\ell)} + \mathrm{i}p_I^{(\ell)}$ with residues $r^{(\ell)} = a^{(\ell)} + \mathrm{i}b^{(\ell)}$.

Singularity Expansion compatible with auto-differentiation

We obtain a form of the SEM expression that is compatible with the auto-differentiation tools:

$$H(\omega) = H_{NR} + \sum_{\ell=1}^{M_I} \frac{\rho^{(\ell)}}{q^{(\ell)}} + \sum_{\ell=1}^{M_C} \left[\frac{a^{(\ell)} + \mathrm{i}b^{(\ell)}}{\omega - p_R^{(\ell)} - \mathrm{i}p_I^{(\ell)}} - \frac{a^{(\ell)} - \mathrm{i}b^{(\ell)}}{\omega + p_R^{(\ell)} - \mathrm{i}p_I^{(\ell)}} \right] \tag{5.23}$$

The non-resonant term is also a real-valued parameter due to the Hermitian symmetry. The explicit discrimination between the M_I imaginary poles and the M_C pairs of poles is not necessary, but can help in improving the results if imaginary poles are expected. In addition, it reduces the number of parameters from $1+4M$ to $1+2M_I+4M_C$ which can slightly improve the speed of the optimization process.

We wish to find a set of parameters $\mathscr{P}$ defined as:

$$\mathscr{P} = \left\{ H_{NR}, \left(\rho^{(\ell)}\right)_\ell, \left(q^{(\ell)}\right)_\ell \left(a^{(\ell)}\right)_\ell, \left(b^{(\ell)}\right)_\ell, \left(p_R^{(\ell)}\right)_\ell, \left(p_I^{(\ell)}\right)_\ell, \right\} \tag{5.24}$$

for which a small value of the arbitrary loss function $\mathscr{L}$ is reached. Ideally, we want to retrieve the optimal set of parameters $\mathscr{P}^*$ defined as:

$$\mathscr{P}^* = \arg\min_{\mathscr{P}} \mathscr{L}[H_i, \hat{H}_i, \mathscr{P}] \tag{5.25}$$

where $\mathscr{L}[H_i, \hat{H}_i, \mathscr{P}]$ evaluates the distance of $\hat{H}_i$ to H_i using the parameter set $\mathscr{P}$ in the truncated SEM from Equation (5.22) to reconstruct the function. The minimization of the loss function is performed

via a gradient-descent(-like) method which involves the calculation of the gradient of the loss function. Classically, the loss function is thus limited to the set of functions for which this gradient can be computed.

[Key properties]

Nevertheless, the recent development of auto-differentiation (for machine learning in particular), has provided means to explore more exotic loss functions. The tools provided in the PyTorch library allow us to freely design the loss function while the gradient is automatically calculated by the library through the chain rule.

The loss function we use requires the definition of the relative L_2 and L_∞ errors, as introduced in Chapter 3:

$$e_q\left[H_i, \hat{H}_i\right] = \frac{||H_i - \hat{H}_i||_q}{||H_i||_q} \tag{5.26}$$

with $q \in \{2, \infty\}$, and:

$$||A_i||_2 = \sqrt{\sum_i |A(\omega_i)|^2} \tag{5.27}$$

$$||A_i||_\infty = \max_i |A(\omega_i)| \tag{5.28}$$

The loss function itself is then defined as:

$$\begin{aligned}\mathscr{L}[H_i, \hat{H}_i, \mathscr{P}] = \alpha_1 \times e^{(2)}\left[H_i, \hat{H}_i\right] + \alpha_2 \times e^{(\infty)}\left[H_i, \hat{H}_i\right] + \alpha_3 \left\| \frac{H_i - \hat{H}_i}{H_i} \right\|_\infty \\ + \alpha_4 \langle \frac{A(\omega_i)}{\delta A(\omega_i)} \rangle + \alpha_5 \langle \frac{B(\omega_i)}{\delta B(\omega_i)} \rangle + \alpha_6 \langle \frac{C(\omega_i)}{\delta C(\omega_i)} \rangle\end{aligned} \tag{5.29}$$

where the notation $< . >$ corresponds to the averaging operation over all the sampled frequencies. $A(\omega_i)$ is the error between the real part of the model $\hat{H}_i$ and data point H_i, and $\delta A(\omega_i)$ accounts for the value of the real part of the data at the frequency ω_i. It is used to change the weight given to the frequency ω_i in $A(\omega_i)$. $B(\omega_i)$ and $\delta B(\omega_i)$ do the same for the imaginary part, and $C(\omega_i)$ and $\delta C(\omega_i)$ directly for the modulus:

$$A(\omega_i) = \left|\mathrm{Re}[H_i - \hat{H}_i]\right|, \qquad \delta A(\omega_i) = |\mathrm{Re}[H_i]| + .1 \tag{5.30}$$

$$B(\omega_i) = \left|\mathrm{Im}[H_i - \hat{H}_i]\right|, \qquad \delta B(\omega_i) = |\mathrm{Im}[H_i]| + .1 \tag{5.31}$$

$$C(\omega_i) = \left|H_i - \hat{H}_i\right|, \qquad \delta C(\omega_i) = |H_i| + .01 \tag{5.32}$$

The values of the weight coefficients are usually case-dependent. The first coefficient α_1 roughly corresponds to the average error between H_i and $\hat{H}_i$. α_2 and α_3 can be respectively used to bound the maximum error and give more weight to small variations in the amplitude. α_4 and α_5 also allow to strengthen the contribution of points associated with small variations or values, but in the real and imaginary parts respectively. Finally, α_6 is similar to α_1, but provides less smooth solutions.

[Key properties]

— In an accuracy-driven optimization, these parameters, along with the numbers of poles M_I and M_C, can be optimized by grid-search as to validate a criterion such as the minimization of the relative L_2 error between H_i and $\hat{H}_i$.

— However, this could lead to a fitting of the noise rather than just the data.

— In the following examples, the values of $\vec{\alpha}$ are therefore intuited based on the expected response curve.

Using the previous example of the reflection coefficient $\tilde{r}(\omega)$ of a thin layer of silver, we show the result of the retrieval of the singularity expansion of Equation (5.23) in Figure 5.4, with $M_I = 1$ imaginary poles, $M_C = 3$ complex pairs of poles, and $\vec{\alpha} = (1, 0, 0, 0.2, 0.2, 0)$. These weight coefficients are such that the main focus is put on the relative L_2 error, with a smaller contribution of the errors on the real and imaginary parts, individually. We chose them after observing variations of equal amplitude of the real and imaginary parts in the target function.

The non-imaginary poles were initialized with their real parts evenly distributed from 0.34 to 23.4 eV, and their imaginary part set to -0.05 times their real parts.

[Intermediary observations]

— We obtain a relative L_2 error of 0.0526 %, slightly lower than that obtained with the optimized Cauchy method.

— Nevertheless, the Cauchy method resulted in one unstable pole unlike the auto-differentiation approach.

— In addition, the version used in Figure 5.2 did not take into account the Hermitian symmetry, allowing for more freedom in the placement of the poles outside the spectral window of interest.

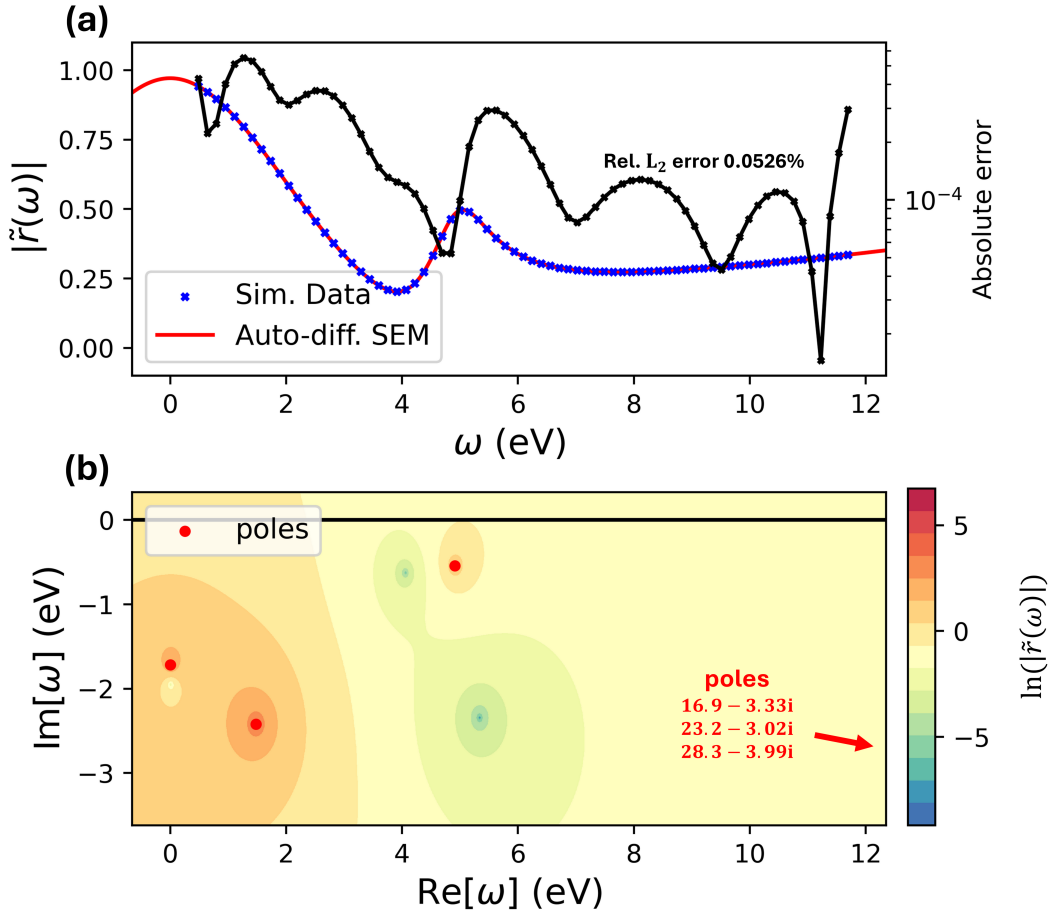

Figure 5.4. – *(a) Reflection coefficient $\tilde{r}(\omega)$ of a thin slab of silver (Ag) reconstructed with the SEM in Equation (5.23) (red curve), and compared to simulated data (blue markers). The absolute error $|H_i - \hat{H}_i|$ (black curve) is less than 10^{-3} at all frequencies, and a relative L_2 error of 0.0526% is obtained. (b) The distribution of the poles in the complex ω-plane. The 3 effective poles outside the spectral window of interest are indicated by the red arrow.*

5.3.2. Other forms of the singularity expansion

We can cast the SEM expression into different forms which highlight different properties of the physical systems:

— The classical SEM expression in Equation (5.1) exhibits resonant terms associated with singularities and residues in the complex ω-plane, represented as peaks, and intuitively introduces the analytical continuation of $H(\omega)$ in the complex plane.

— The Generalized Drude-Lorentz model (GDL) detailed in Chapter 3 models the physical systems as sets of sub-units, each behaving as oscillators described by classical mechanics. The sub-units can be identified as the microscopic-scale particles constituting the system. Although it was used to describe different media in Chapter 3, this can be applied to any physical systems.

— The Möbius Transformations in the Singularity Expansion (MTSE) offer an alternative representation of the behaviour of the response functions at real frequencies, and model resonances as perturbations, the amplitudes and variation speeds of which are constrained by Möbius circles associated with resonant terms.

Each of these forms is truncated and written in a way that is compatible with the optimization problem, similarly to the classical SEM in Equation (5.22).

[Derivation]

As shown in Chapter 3, we can recast the singularity expansion into the GDL *via* a change of variables for the M_C symmetric terms:

$$\omega_{0,\ell} = |p_R^{(\ell)}| \tag{5.33}$$

$$\Gamma_\ell = -2|p_I^{(\ell)}| \tag{5.34}$$

$$s_{1,\ell}\Gamma_l = -2b^{(\ell)} \tag{5.35}$$

$$s_{2,\ell}\left(\omega_{0,\ell}^2 + \frac{\Gamma_\ell}{2}^2\right) = -2\mathrm{Re}\left(r_p^{(\ell)}\left(\omega_{0,\ell} - \mathrm{i}\frac{\Gamma_\ell}{2}\right)\right) \tag{5.36}$$

and by rewriting the M_I resonant terms associated with imaginary poles as:

$$\gamma_\ell = -q^{(\ell)} \tag{5.37}$$

$$\omega_{b,\ell}^2 = |\rho^{(\ell)}\gamma_\ell| \tag{5.38}$$

$$\gamma_0 = r_0 + \sum_{\ell=1}^{M} \frac{\omega_{b,\ell}^2}{\gamma_\ell} \tag{5.39}$$

$$\mathrm{i}\frac{r_0}{\omega} + \sum_{\ell=1}^{M} \frac{\rho^{(\ell)}}{\omega - \mathrm{i}q^{(\ell)}} = \mathrm{i}\frac{\gamma_0}{\omega} - \sum_{\ell=1}^{M} \frac{\omega_{b,\ell}^2}{\omega^2 + \mathrm{i}\omega\gamma_\ell} \tag{5.40}$$

where we assume that there is a pole 0 at the origin, associated with a residue $\mathrm{i}r_0$. Let us stress that the absolute value "|.|" is used to impose the stability of all the poles, but it can be removed to allow for unstable effective poles.

Generalized Drude-Lorentz model compatible with auto-differentiation

The following expression of the GDL is obtained:

$$H(\omega) = H_{\mathrm{NR}} + \mathrm{i}\frac{\gamma_0}{\omega} - \sum_{\ell=1}^{M_I} \frac{\omega_{b,\ell}^2}{\omega^2 + \mathrm{i}\omega\gamma_\ell} - \sum_{\ell=1}^{M_C} \frac{\mathrm{i}s_{1,\ell}\omega\Gamma_\ell + s_{2,\ell}\left(\omega_{0,\ell}^2 + \frac{\Gamma_\ell}{2}^2\right)}{\left(\omega^2 - \left(\omega_{0,\ell}^2 + \frac{\Gamma_\ell}{2}^2\right)\right) + \mathrm{i}\omega\Gamma_\ell} \tag{5.41}$$

Since all the parameters must be real-valued in Equation (5.41), some of the definitions slightly differ from those given for the GDL in Chapter 3.

[Key properties]

As previously stated, this formulation of the SEM is particularly adapted to the representation of sub-units of a physical system as harmonic oscillators.

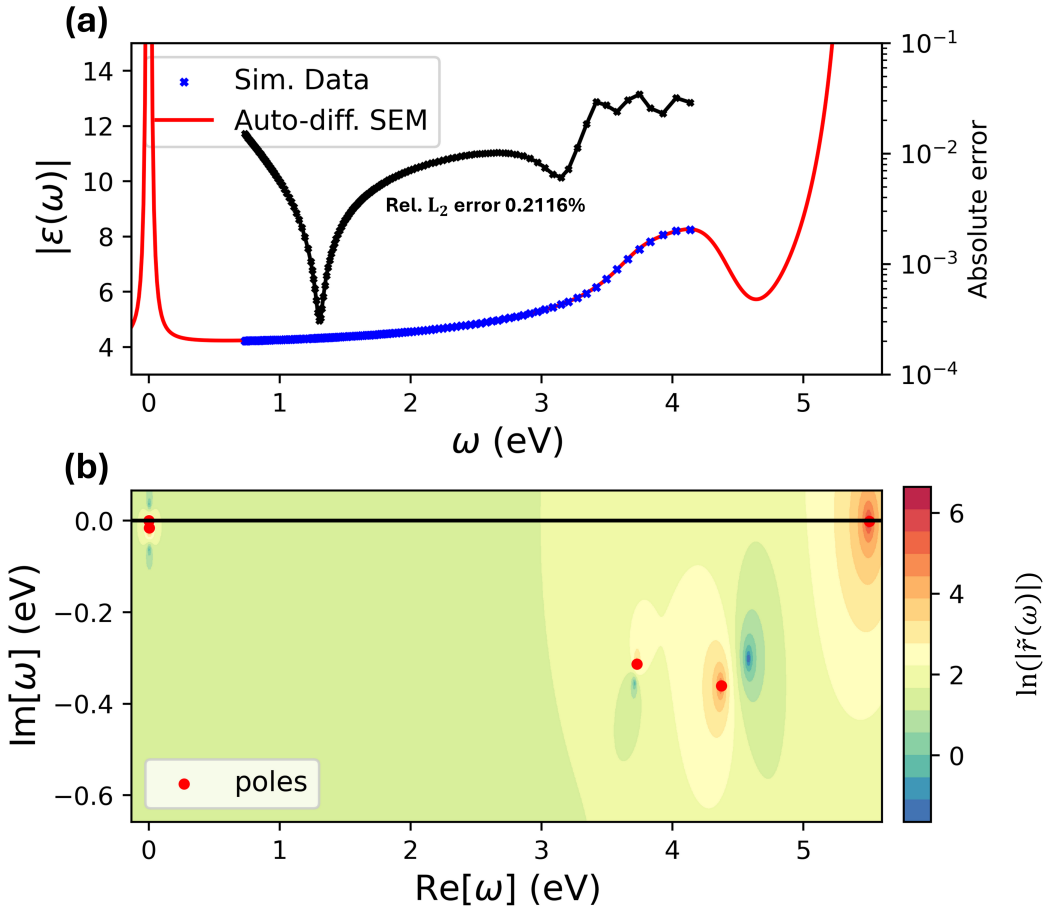

Figure 5.5. – *(a) Relative permittivity* $\varepsilon(\omega)$ *of* TiO_2 *retrieved with the GDL (Equation (5.41) (red curve), compared to experimental data (blue markers). The absolute error* $|H_i - \hat{H}_i|$ *(black curve) is higher than for the response functions studied in Figures 5.2 and 5.4 which were numerically obtained, and thus less noisy. The relative* L_2 *error is approximately* 0.2185 %*. (b) The Drude (imaginary) poles and the Lorentz pole close to the real frequency axis at* 5.5 *eV are effective poles, acting mainly as offsets in the spectral range of interest, from* 0.9 *to* 4.2 *eV.*

We apply it to the relative permittivity $\varepsilon(\omega)$ of TiO_2in Figure 5.5 with $M_I = 1$ imaginary pole, $M_C = 3$ complex pairs of poles and $\vec{\alpha} = (0.2, 0.2, 0.2, 0.1, 0.3, 0.1)$. This time, the weight coefficients are such that more importance is given to the imaginary part of $\varepsilon(\omega)$ which is close to 0 due to the low absorption of TiO_2.

[Intermediary observations]

We obtain a relative L_2 error of 0.2185 %, below the one reported in Chapter 3 for TiO_2. This is due to the presence of the effective Drude and Lorentz poles, which were removed in Chapter 3 because of their small contribution to the relative permittivity function.

Finally, we express the singularity expansion as MTSE.

[Key properties]

— This formulation is not adapted to the case of imaginary poles, as they are associated with circles of infinite radii.

— It should therefore be used to approximate response functions in spectral windows far enough from the origin for the contribution of the imaginary poles to be accounted for by a non-imaginary effective pole.

The discrimination between the M_I imaginary poles and the M_C pairs of poles is not performed anymore.

Mobius Transformations in the Singularity Expansion expression compatible with auto-differentiation

The classical MTSE form used for the optimization reads as:

$$H(\omega) = H_{NR} + \sum_{\ell=1}^{M} \left(2\mathrm{Re}[C_\ell] + |C_\ell| \left(e^{\mathrm{i}\phi_\ell(\omega)} + e^{-\mathrm{i}\phi_\ell(-\omega)}\right)\right) \tag{5.42}$$

where the circle center C_ℓ and the angular coordinate $\phi_\ell(\omega)$ are defined as:

$$C_\ell = -\frac{a^{(\ell)} + \mathrm{i}b^{(\ell)}}{2\mathrm{i}|p_I^{(\ell)}|} \tag{5.43}$$

$$\phi_\ell(\omega) = \mathrm{iLog}\left[\frac{\omega - p_R^{(\ell)} - \mathrm{i}|p_I^{(\ell)}|}{\omega - p_R^{(\ell)} + \mathrm{i}|p_I^{(\ell)}|}\right] + \mathrm{Arg}[r^{(\ell)}] + \frac{\pi}{2} \tag{5.44}$$

The MTSE has only one free parameter, which is the number of poles M, as opposed to the two former forms of the SEM, which have: the number of imaginary poles M_I, and the number of pairs of poles M_C.

As for the two previous forms, we plot in Figure 5.6 a result of the retrieval of the parameters of the MTSE from Equation (5.40), with $M = 17$ poles.

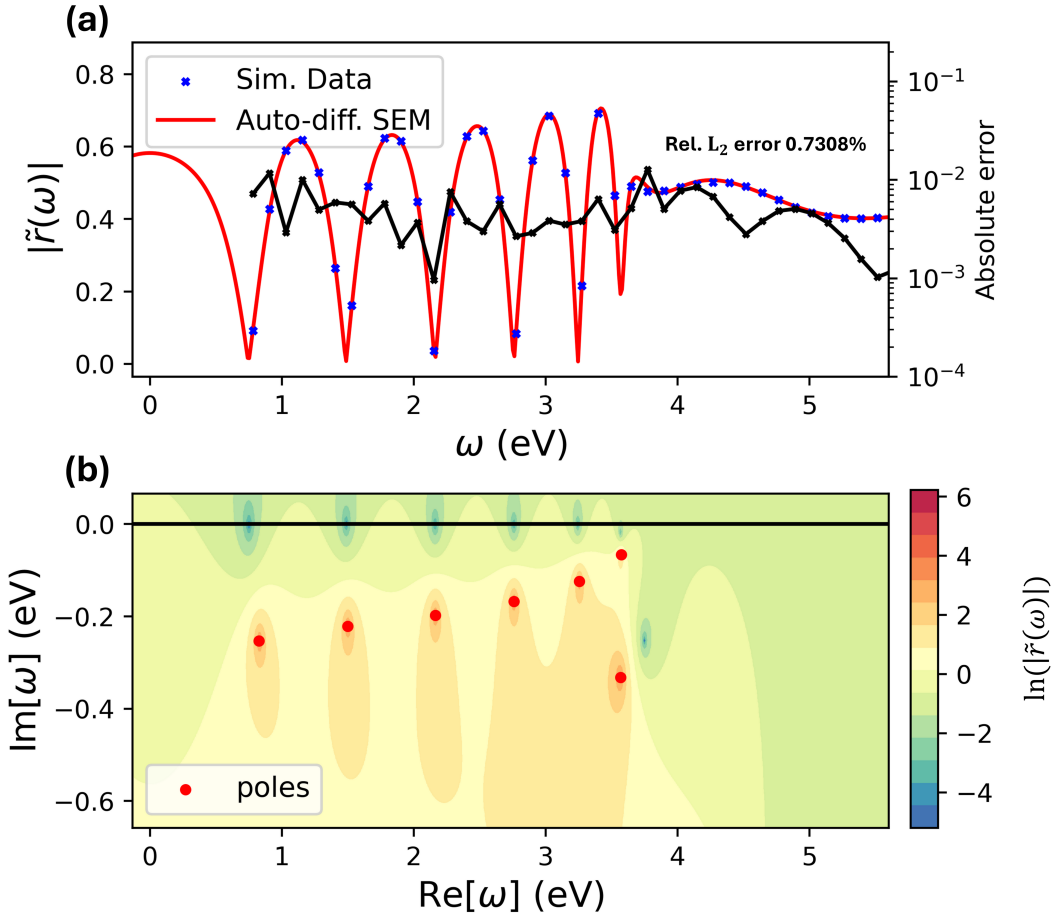

Figure 5.6. – *(a) Reflection coefficient $\tilde{r}(\omega)$ of a thin slab of TiO_2 reconstructed with the MTSE in Equation (5.42) (red curve), and compared to simulated data (blue markers). A relative L_2 error $e^{(2)} = 0.7308$ % is obtained. (b) The distribution of the poles in the complex ω-plane. Additional singularities are located outside the chosen window, for a total of 14 pairs of singularities.*

The response function is the reflection coefficient $\tilde{r}(\omega)$ of a dielectric slab of TiO_2, with thickness $d = 400$ nm. Since the absorption is low, the poles are evenly distributed [99], and the amplitude is (almost) periodic over a large frequency range. As such, we choose $\vec{\alpha} = (1, 0, 0.01, 0, 0, .2)$ to focus on the average reconstruction of the response function with no difficulty expected in the real and imaginary parts.

5.4. Natural and effective poles

The SEM provides an exact expression of the response function $H(\omega)$ when all its poles $p^{(\ell)}$ are known. The unicity of the expansion means that the singularities are intrinsic properties of the response functions, and that they hold information regarding the behaviour of the function in both the harmonic and temporal domains. Nevertheless, some noise is usually present in the data, stemming from either numerical or experimental errors. As a result, the singularities are no longer those of the signal only, but also those corresponding to the approximation of the noise as a response function of a physical system. In addition, the set of poles has to be truncated for numerical calculations. It raises the problem of identifying the poles which are physically relevant.

[Key properties]

This problem is addressed by discriminating between two types of singularities.

(i) In his original work on the SEM, C. Baum was inspired by the response of resonators to electromagnetic excitation functions in the transient regime, where exponentially decaying sinusoidal functions can be observed. The decaying rate corresponds to the imaginary part of a pole, while the oscillation frequency classically is the real part of a pole. These poles, appearing in both the harmonic and time domain responses, are what we refer to as natural poles.

(ii) On the other hand, the poles which only help in reducing the error between the SEM expression and the data are effective poles. They were introduced in the first section of this chapter, but also in Chapter 2 where they were used to effectively account for the small contributions of poles outside the spectral range of interest in a slab of gold (Au). Effective poles either account for the contribution of poles outside the spectral window of interest, or fit the noise *via* resonant terms. Since it is difficult to assess the predominance of either one effect, both types of effective poles are treated as one category.

The natural poles are defined as the singularities which can be retrieved in both the temporal and harmonic domains. Previous works [209, 220] have shown that the Cauchy method or vector fitting method [216], in the harmonic domain, and the matrix pencil [67, 208, 214, 220] or harmonic inversion [215, 221], in the temporal domain, resulted in similar distributions of poles in electromagnetic systems. Originally, the natural poles were defined as the (quasi-)overlapping poles in these distributions. Drawing inspiration from these studies, we propose an alternative and more general definition of natural poles as the overlapping singularities between different pole-retrieving methods. In our case, we recover them by comparing the poles obtained *via* the optimized Cauchy method and the auto-differentiation approach.

[Key properties]

A balance must be found between prioritizing the retrieval of natural poles with a physical interpretation, and the fitting through effective poles which ensures a high-quality model. In other words, we want to **accurately approximate the response functions with as few poles as possible**, under the assumption that natural poles usually have a greater influence than effective poles on the harmonic dynamics of the response function $H(\omega)$.

What is more, we must take into account a limitation of the pole retrieving methods which prevents the error from decreasing beyond a certain (case-dependent) amount of singularities.

Let us look at the case of the reflection coefficient of the dielectric metasurface illustrated in Figure 5.7 (courtesy of Jayeeta AMBOLI), illuminated at normal incidence, with 106 frequencies ranging from 1.2 to 2.7 eV.

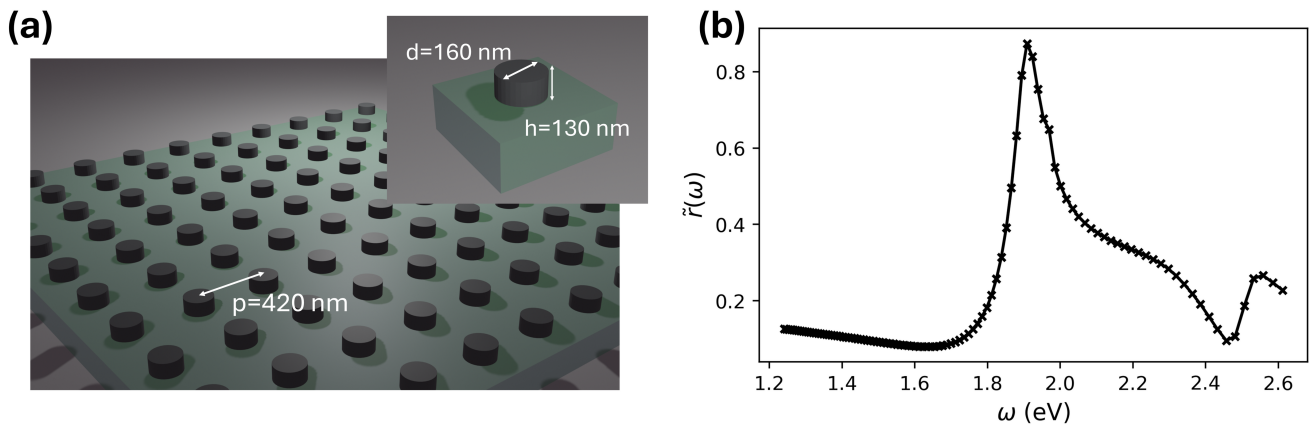

Figure 5.7. – *(a) Metasurface composed of an array of period $p = 420$ nm of nanodisks of Si with diameter $d = 160$ nm and height $h = 130$ nm, over a substrate of glass (courtesy of Jayeeta AMBOLI). (b) The reflection coefficient is simulated for a normal incidence. We keep 106 points corresponding to frequencies ranging from 1.2 eV to 2.7 eV.*

Our goal is to retrieve the natural poles while obtaining a good reconstruction of the response function in that frequency range, using the two approaches described thus far.

In order to mitigate the effect of the parameters of the Cauchy method and the auto-differentiation approach on the quality of the approximation, we perform a grid sweeping. For the Cauchy method, the swept parameters are the maximum number of poles and the difference between the degree M_p of the denominator $G(\omega)$ and the degree M_z of the numerator $F(\omega)$. The parameters of the second approach, in the SEM form, are the number of pairs of poles M_C and the weight vector $\vec{\alpha}$, under the constraint that $\sum_{i=1}^{6} \alpha_i = 1$.

The sets of runs obtained with the two grid sweepings are then compared as to quantify the similarity between the distributions of poles. For all the pairs of distributions of poles $(\mathscr{P}_C, \mathscr{P}_A)$ associated with a run from the Cauchy method and one from the auto-differentiation approach, and their associated distributions of residues $(\mathscr{R}_C, \mathscr{R}_A)$, this similarity is obtained in the following way:

1. We first check that the L_2 precision, defined as 1 minus the relative L_2 error $e^{(2)}$, is above 95 % for the Cauchy run, and 98 % for the other one, and that the difference in the number of poles does not exceed 5, *i.e.* $\left||\mathscr{P}_C| - |\mathscr{P}_A|\right| = \delta M_p < 5$.
2. If these conditions are met, we establish a proximity matrix between the two distributions of poles by quantifying the effect of the difference of any two resonant terms taken from each distribution. For a pole and residue in the Cauchy distribution $(p_c, r_c) \in \mathscr{P}_C \times \mathscr{R}_C$, and a pole and residue in the auto-differentiation one $(p_a, r_a) \in \mathscr{P}_A \times \mathscr{R}_A$, the proximity $d(p_a, p_c)$ is evaluated through an integral over the real frequency axis:

$$d(p_a, p_c) = \left| \int_{\omega_1}^{\omega_2} \frac{r_a}{z - p_a} - \frac{r_c}{z - p_c} dz \right| \tag{5.45}$$

with:

$$\begin{aligned} z_0 &= \mathrm{Re}\left[\frac{p_a + p_c}{2}\right] \\ \rho &= 1.2 \max\left(|p_a - z_0|, |p_c - z_0|\right) \\ \omega_1 &= z_0 - \rho \\ \omega_2 &= z_0 + \rho \end{aligned} \tag{5.46}$$

3. Using the proximity matrix, each pole p_ℓ of the distribution $\mathscr{P}_0 = \mathscr{P}_A$ or $\mathscr{P}_C$ containing the least amount of singularities is associated with a pole p_ℓ^* of the other distribution.
4. A similarity score $s(\mathscr{P}_\mathscr{C}, \mathscr{P}_\mathscr{A})$ is calculated:

$$\frac{1}{s(\mathscr{P}_C, \mathscr{P}_A)} = \frac{1 + \delta M_p}{|\mathscr{P}_0|} \sum_{\ell=1}^{|\mathscr{P}_0|} \left| p_\ell - p_\ell^* \right| \tag{5.47}$$

The results of the grid sweepings and the calculation of the similarity matrix are presented in Figure 5.8.

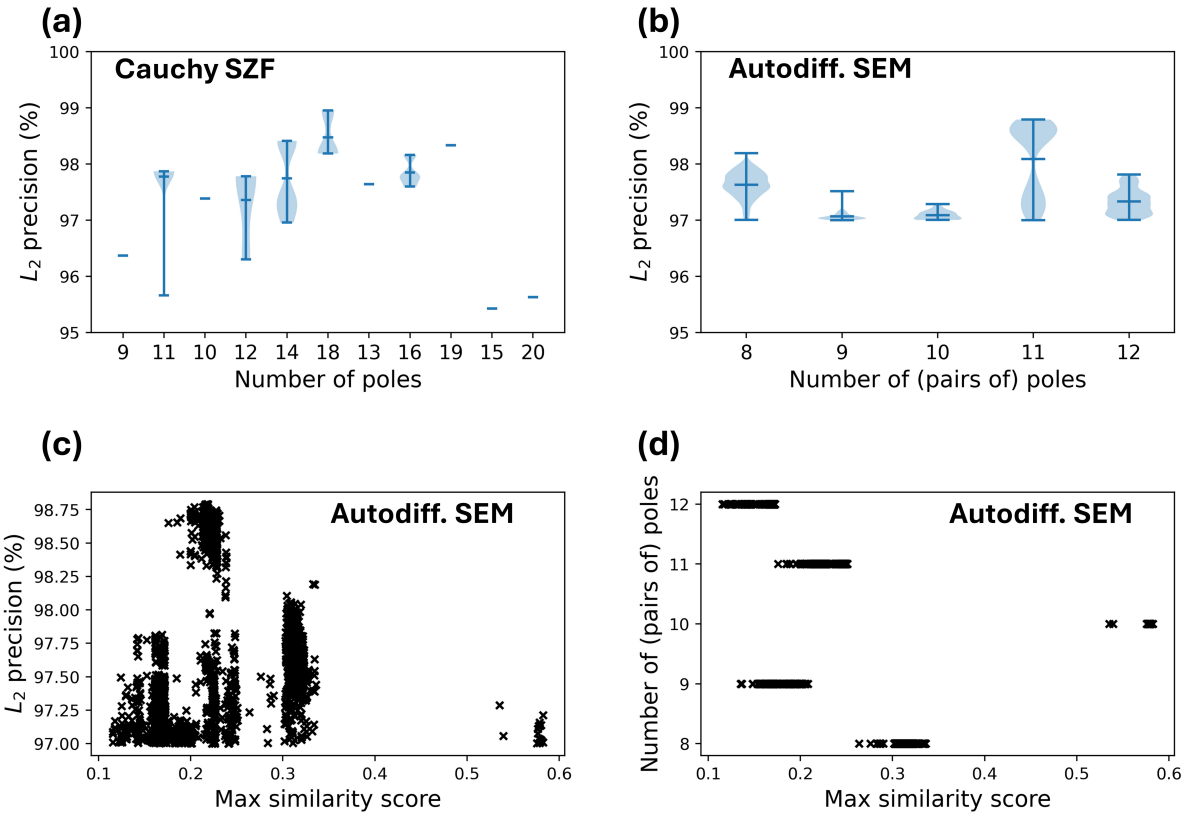

Figure 5.8. – *Violin plots of the L_2 precision of the SZF retrieved with the Cauchy method (a) and the SEM obtained via auto-differentiation (b), to reconstruct the reflection coefficient of a metasurface composed of nanodisks of Si on a subtrate of glass, illuminated at normal incidence (see Figure 5.7). The Cauchy method is parametrized by the initial maximum numbers of poles and the difference between the number of poles and zeros. The parameters of the auto-differentiation are the weights $\alpha_{1\leq i\leq 6}$ of the loss function in Equation (5.29). Each run associating with one set of values of these parameters for the Cauchy method is compared to a run for the auto-differentiation one to quantify the overlapping of their singularity distributions through the similarity score defined in Equation (5.47).*

[Intermediary observations]

Four properties are illustrated:

(i) The value of the parameters of each approach affects the noise considered in the data, and thus the maximum accuracy that can be reached (Figure 5.8 (a) and (b)). In the Cauchy method, this is achieved by changing the initial maximum number of poles which modifies the singular values and the resulting maximum rank in Equation (5.10) and Figure 5.1. In the auto-differentiation approach, this is done more straightforwardly by the weight vector $\vec{\alpha}$, which determines the aspects of the reconstruction that should be prioritized.

[Intermediary observations]

(ii) While some variations can be explained by the swept parameters (other than the number of poles), there is no positive correlation between the number of poles and the L_2 precision for the auto-differentiation approach (Figure 5.8 (a)). For the Cauchy method, the overall trend is an increase of the L_2 precision with the number of poles up to a certain threshold, after which it drops as previously predicted (Figure 5.8 (b)).

(iii) The criteria regarding the overlapping of the distributions (quantified by the similarity matrix) and the accurate approximation of the response function are not fully compatible (Figure 5.8 (c)). Depending on the purpose of the reconstruction of $H(\omega)$, and the a priori knowledge, they should be weighted differently. If the noise cannot be easily characterized, or the priority is given to the physical relevancy of the singularities, then the maximization of the similarity between distributions is a better criterion. However, if the measurement and numerical error are negligible, the accuracy can be maximized.

(iv) The number of poles and the similarity score are not correlated (Figure 5.8 (d)). As the number of poles increases, more and more effective poles are added, which lowers the similarity score that we calculate. Conversely, by reducing too much the number of poles, the drop in the number of effective poles imposes a shift in the positions of natural poles as to better approximate the average dynamics of the curves, also resulting in a decrease of the similarity score.

[Key properties]

— The computation of all the runs through the grid sweepings can be highly time and resource-consuming, in particular with the auto-differentiation approach.

— As an alternative, and in light of the previous observations, we generally combine both approaches sequentially: the physics-informed Cauchy method is used to initialize the poles and residues in the auto-differentiation approach.

— During the optimization process, the natural poles remain (almost) unchanged, while the effective ones are moved in order to better approximate the response or transfer function.

— The distributions of singularities can be compared afterwards to identify the potential natural poles.

The result of this method is shown in Figure 5.9. The studied function is once again the reflection coefficient $\tilde{r}(\omega)$ of the metasurface highlighted in Figure 5.7, but over a larger spectral range where the SZF obtained *via* the optimized Cauchy method struggles to properly fit the simulated data, with an error $e^{(2)} = 5.794$ %.

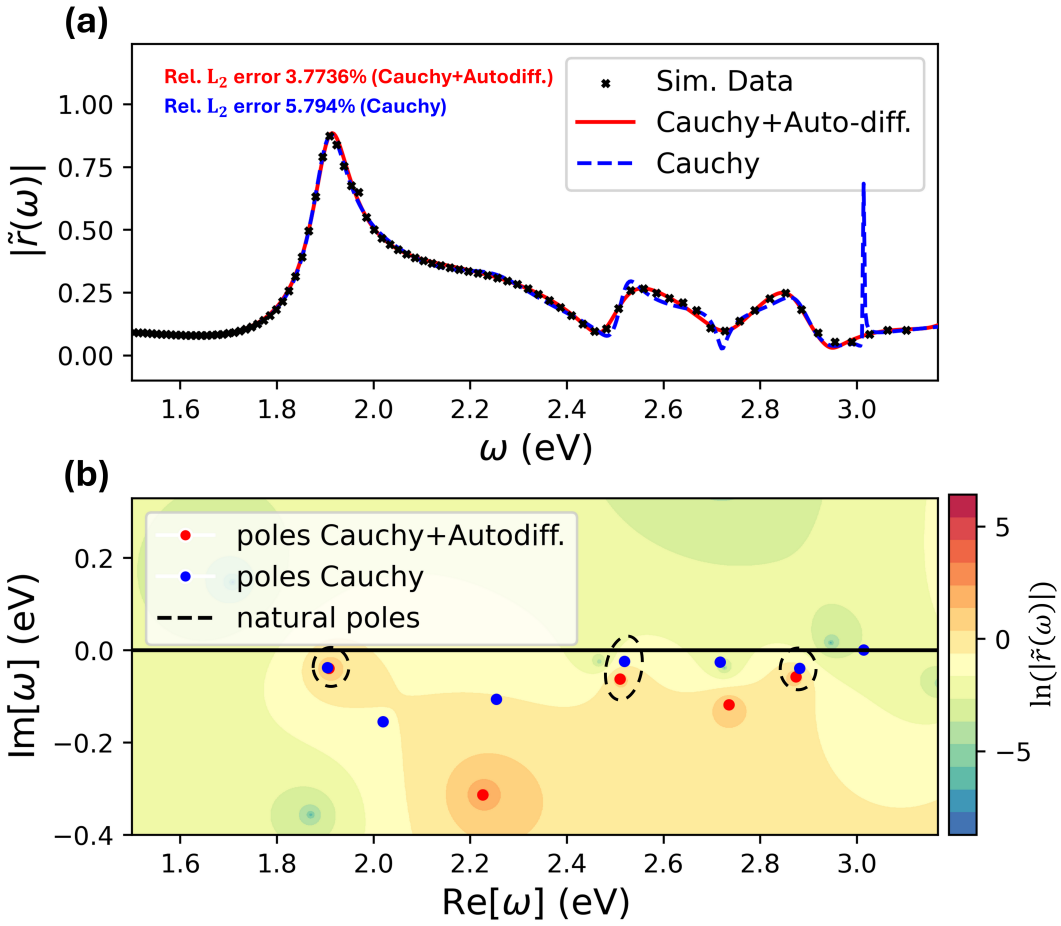

Figure 5.9. – *(a) Reflection coefficient $\tilde{r}(\omega)$ of the metasurface shown in Figure 5.7, illuminated at normal incidence. The reconstruction is performed with the SZF in Equation (5.16) using the optimized Cauchy method only at first (blue curve), and then with the SEM in Equation (5.23) using the auto-differentiation approach, where the parameters are initialized using the formerly retrieved SZF. A relative L_2 error $e^{(2)} = 5.794$ % is obtained for the Cauchy method only, and $e^{(2)} = 3.7738$ % for the combination of both approaches. (b) The distributions of the poles associated with each reconstruction are shown in the complex ω-plane. Additional singularities are located outside of the chosen window. The potential natural poles are highlighted with the dashed black contours.*

[Intermediary observations]

— The combination of the two approaches helps in improving that reconstruction with an error dropping to $e^{(2)} = 3.7748$ %

— Furthermore, it allows us to identify potential natural poles which remain (almost) at the same positions in the complex frequency plane after the auto-differentiation approach compared to the Cauchy method only.

5.5. Conclusion

Summary and conclusion

The SEM and the SZF are natural representations of physical signals in the harmonic domain, which can be used to describe the underlying physics of different phenomena and systems. Nevertheless, for these expressions to be practical, we need to be able to retrieve the parameters of these expressions. Carrying out this task was precisely the purpose of this chapter.

We have presented two approaches to accurately approximate the response or transfer function of a physical system.

- The first one builds on top of the Cauchy method, and optimize it to take into account basic, fundamental properties of physical signals.
- This approach uses matrix algebra to provide a rational approximation of the response functions.
- The second approach relies on auto-differentiation to solve for optimization problems with more complex loss functions.
- This second method is more adapted to the use of the SEM in any of its three forms: the default singularity expansion, the GDL and the MTSE.

The proposed approaches result in distributions of poles and zeros or poles and residues in the complex ω plane.

- They have to be characterized in order to discriminate between two types of singularities: the natural poles, which hold physical information regarding the behaviour of the physical systems, and the effective poles, which mainly help in reducing the approximation error.
- We have proposed a practical definition of the natural poles as the overlapping singularities in distributions obtained through different pole-retrieving methods.
- We demonstrated that this discrimination between the natural and effective poles was impacted by the parameters of the different methods and the error functions, which depend on the goal of the reconstruction.
- Finally, we have described a faster means to find the potential natural poles by sequentially using the Cauchy method and the auto-differentiation approach.

Classical reconstruction methods are often accuracy-driven. While we have proposed improvements and optimizations to also obtain accurate reconstructions of physical signals, we have stressed that this should not always be the standard, and that we should strive for a balance between a low reconstruction error, and physically relevant distributions of singularities. This results in both accurate analytical reconstructions, and poles and residues which can be related to the dynamics of the physical systems with good fidelity.

Summary of the results

Singularity Expansion compatible with auto-differentiation

$$H(\omega) = H_{NR} + \sum_{\ell=1}^{M_I} \frac{\rho^{(\ell)}}{q^{(\ell)}} + \sum_{\ell=1}^{M_C} \left[\frac{a^{(\ell)} + \mathrm{i}b^{(\ell)}}{\omega - p_R^{(\ell)} - \mathrm{i}p_I^{(\ell)}} - \frac{a^{(\ell)} - \mathrm{i}b^{(\ell)}}{\omega + p_R^{(\ell)} - \mathrm{i}p_I^{(\ell)}} \right]$$

Generalized Drude-Lorentz model compatible with auto-differentiation

$$H(\omega) = H_{\mathrm{NR}} + \mathrm{i}\frac{\gamma_0}{\omega} - \sum_{\ell=1}^{M_I} \frac{\omega_{b,\ell}^2}{\omega^2 + \mathrm{i}\omega\gamma_\ell} - \sum_{\ell=1}^{M_C} \frac{\mathrm{i}s_{1,\ell}\omega\Gamma_\ell + s_{2,\ell}\left(\omega_{0,\ell}^2 + \frac{\Gamma_\ell}{2}^2\right)}{\left(\omega^2 - \left(\omega_{0,\ell}^2 + \frac{\Gamma_\ell}{2}^2\right)\right) + \mathrm{i}\omega\Gamma_\ell}$$

Mobius Transformations in the Singularity Expansion expression compatible with auto-differentiation

$$H(\omega) = H_{NR} + \sum_{\ell=1}^{M} \left(2\mathrm{Re}[C_\ell] + |C_\ell| \left(e^{\mathrm{i}\phi_\ell(\omega)} + e^{-\mathrm{i}\phi_\ell(-\omega)}\right)\right)$$

$$C_\ell = -\frac{a^{(\ell)} + \mathrm{i}b^{(\ell)}}{2\mathrm{i}|p_I^{(\ell)}|}$$

$$\phi_\ell(\omega) = \mathrm{i}\mathrm{Log}\left[\frac{\omega - p_R^{(\ell)} - \mathrm{i}|p_I^{(\ell)}|}{\omega - p_R^{(\ell)} + \mathrm{i}|p_I^{(\ell)}|}\right] + \mathrm{Arg}[r^{(\ell)}] + \frac{\pi}{2}$$

Conclusion

As a conclusion to this manuscript, it might be fitting to start by commenting on the opening statement in the introduction, regarding the common features between various systems such as a vibrating string, an electric circuit, a quantum well, a heated metallic rod, or an illuminated mirror. Beyond their similar classical description through linear differential equations solved for with combinations of sinusoidal fields, these systems have identical fundamental properties which allow for a unified description that (arguably) precedes the differential equations driving their dynamics.

That unified description of linear system takes root in the field of Electric and Electronics Engineering (EEE), in the specific case of Linear Time-Invariant Systems (LTISs). The introduction of the Singularity Expansion Method (SEM) by Carl Baum in the 1970's was a turning point in the extension of that approach to a broader class of systems. Nevertheless, the method remained idled for a long time. As previously mentionned, the potential it offers has only recently started to draw interest. As a tool in EEE, and as a theoretical formalism to better understand resonant phenomena in optics and electromagnetism.

In the following, we first present a listing of the findings associated with each chapter, and then move on to a general overview of the content of the manuscript and of different perspectives.

Listing of the findings

Chapter 1

Following a description of the classical forms of the SEM and related expression which can be found in the literature, Chapter 1 was dedicated to the extension of the SEM.

— The Multiple-Order Singularity Expansion Method (MOSEM) and the Singularity and Zero Factorization (SZF) were rigorously derived, providing exact expressions of meromorphic functions while taking into account the order of their singularities, in contrast with the approximation which had been intuited or hypothesized so far.

— The broad class of physical systems was introduced, abiding by the fundamental properties of energy conservation, causality and Hermitian-symmetry in addition to the linearity, determinism, time-invariance and continuity of LTISs. As a consequence, the singularities and other parameters of MOSEM and the SZF are constrained in the complex ω plane. They are not limited to transfer operators, and can be applied to the set of physical signals.

— The interplay between the harmonic domain and the time domain through the Laplace transform was exploited to characterize passive signals, retrieve the temporal dynamics of

physical systems excited by causal sinusoidal excitation signals, and link the physical signals to the differential equations describing the evolution of the physical quantities at play.

Chapter 2

Once the foundations of the SEM had been layed out, the practical use of the expressions developed in Chapter 1 had to be demonstrated. Chapter 2 dealt with the case of a Fabry-Perot cavity, first with a dielectric material, then with a dispersive, lossy, metallic one.

— Using the Airy model, a finite set of singularities and residues of the reflection and transmission coefficients of the dielectric slab were calculated. The resulting truncated SEM expressions showed an excellent agreement with the Airy model expressions, and the corresponding calculated expressions in the time domain matched the CST simulations.

— In the case of a gold slab, the poles were numerically determined while the associated residues were calculated using the Airy model. An accurate reconstruction was obtained using a sufficiently large amount of poles, most of which were located outside the window of interest.

— The contributions of the poles far from the studied spectral range were accounted for by an effective pair of poles and a modified non-resonant term, optimized so that the reconstruction would fit the simulated data, resulting in a drastic decrease of the required amount of singularities for an at least equal accuracy of the reconstruction.

Chapter 3

In Chapter 3, we wanted to apply the SEM to a common case where no analytical expressions are known for the response functions. We chose the case of the relative permittivity functions of different linear materials, since the accurate description of the behaviour of materials with simple analytical expressions is of high interest to perform realistic simulations in the harmonic and time domains, to build better models in different phenomena, and to better understand the underlying physics of the interaction of materials with excitation fields.

— Starting from the constitutive relation in the Maxwell equations, we expressed the relative permittivity as the physical response function of materials, binding the electric field to the displacement field in linear materials. As such, we could apply the SEM.

— Through a change of variables, we showed that the SEM expression encapsulates and generalizes the classical Debye, Drude and Lorentz models. In the latter an additional imaginary, frequency-dependent term appears, relaying the contribution of the time-derivative of the electric field to the calculation of the displacement field in the time domain.

— We showed that this Generalized Drude-Lorentz model (GDL) was a natural expression of the permittivity, and that it always performs better than the classical model to characterize linear media.

— We demonstrated that the distribution of the singularities could be used to characterize the behaviour of the materials, with the Drude poles accounting for the interaction of free electrons with the electric field at low frequencies, and the Lorentz poles serving as transitions between different regimes. In particular, it is the real part of the first Lorentz pole that dictates

the transition from a metallic to a dielectric regime in metals, which usually differs from the plasma frequency.

Chapter 4

The establishment of a link between the singularities and resonances in the harmonic domain is naturally very tempting. However, it is not as trivial as one might expect, especially in the case of non-isolated resonances which cannot be characterized by the classical Quality-factor (Q-factor). We showed in Chapter 4 that the SEM could be used to inform on the influence of log-singularities (poles and zeros) on the response functions *via* a quality function defined at all frequencies.

— Stemming from the observation that resonant terms are Möbius transformations, the SEM was recast as Möbius Transformations in the Singularity Expansion (MTSE), where each resonant term is a (Möbius) circle in the complex frequency plane, crossing the origin at $\omega \to -\infty$ and $\omega \to +\infty$. This allowed us to describe an isolated resonance as a perturbation, moving away from the origin with a speed defined by an angular coordinate $\phi(\omega)$ expressed with the associated pole (and its complex conjugate) only, and a strength set by the radius of the circle, related to the residue and the imaginary part of the pole.

— We showed that the dynamics of an isolated resonance were described through the dimensionless quantity $\eta(\omega) = \frac{\omega}{4}\partial_\omega[\phi](\omega)$ related to the angular coordinate appearing in its Möbius circle, and in particular that when evaluated at the real part of the pole, it yields the classical Q-factor associated with the resonance:

$$\eta(\mathrm{Re}[p]) = \frac{\mathrm{Re}[p]}{2\,\mathrm{Im}[p]} = Q$$

— We highlighted the fact that the derivative of the angular coordinate $\phi(\omega)$ was equal to twice the derivative of the phase $\Psi(\omega)$ of a resonant term, and we proposed an other definition of the previous dimensionless function as $\eta(\omega) = \frac{\omega}{4}\partial_\omega[\Psi](\omega)$, refered to as the quality function.

— We demonstrated that the quality function could be expressed as a meromorphic function with a singularity expansion using the SZF of the full response function $H(\omega)$. When applied to the more general case of non-isolated resonances and overlapping resonant terms, it yields information regarding the contribution of the log-singularities, *i.e.* poles and zeros, to the phase-shift and amplitude-variations of any continuous response function, at any frequency.

Chapter 5

Finally, the last chapter tackles how to retrieve the poles, zeros and residues of physical signals from experimental or simulated data at real frequencies.

— We gave an overview of the classical Cauchy method, which relies on matrix algebra to retrieve the poles and zeros of the truncated SZF of the response function. We then described how we improved the method using the properties of physical signals.

— A second approach relying on auto-differentiation to solve optimization problems was introduced, leading to the retrieval of the singularity expansion in either one of the three forms introduced throughout the manuscript: the classical one with a non-resonant term and a sum of resonant terms, the GDL, and the MTSE.

— The problem of discriminating between natural poles, physically relevant and holding information regarding the dynamics of the physical system in the time domain, and the effective poles, the main purpose of which is to improve the quality of the reconstruction. The latter can be further split into the poles brought about by noise in the data, and those which account for the contributions of singularities far from the studied spectral window (although the distinction between these two sub-classes is not done in practice).

— We showed that a good reconstruction was not fully compatible with an accurate retrieval of the natural poles, and that a balance should be found between these two criteria. Nevertheless, we proposed an approach sequentially combining the Cauchy method and the auto-differentiation approach to retrieve more easily potential natural poles and improve the accuracy of the reconstruction in larger spectral windows.

Overall conclusion and perspectives

Let us now conclude this manuscript by explaining with simple terms the true essence of this approach together with the main results obtained chapter after chapter.

We have shown that any physical system is naturally described in the complex frequency plane, where its response is exactly described in terms of its singularities *via* the SEM. This unified description of the response functions is justified by the derivation of the formalism using only fundamental properties common to all linear systems. While we focused on electromagnetism and optics, we can characterize all linear interactions and phenomena encountered in wave physics.

This robust, rigorously-derived theoretical framework proves to be highly accurate in practice when we consider finite-sized spectral windows, and thus a finite set of poles. In addition, we have shown that it easily allows to go from the temporal domain to the harmonic domain, and from measurements at real frequencies to a full characterization in the whole complex plane.

Furthermore, the alternative forms of the SEM we have derived, namely the MTSE and the GDL, are examples of how we can deepen our understanding of the underlying physics of problems. The MTSE allow to describe physical systems in terms of resonances, while the GDL models the systems as combinations of harmonic oscillators. Both are valid, highly accurate representation of any linear system, no matter which field of physics is considered.

Finally, let us stress once more the importance of being able to reconstruct any function in the complex frequency plane using the SEM, with data acquired at real frequencies. This last step of the manuscript is what justifies and motivates the use of the formalism in all the other chapters. Without the retrieval of the poles, zeros and residues, the SEM would have remained a sound theoretical formalism with no practical use.

And this possibility to identify singularities, residues and zeros of arbitrary linear physical signals associated with a rigorous analytic expansion opens the route to many possibilities. While we have yet to figure out all the exciting prospects, some of them have already been identified. Rather than detailing the ongoing and upcoming studies, one should note that they rely on the theoretical unicity of the distribution of poles, which will be used to provide alternative representations of systems. What is more, the link between the evolution of a system and its singularities, and in particular their trajectories in the complex frequency plane, will deserve an in-depth study to model the behaviour of parametrized systems. These would prove helpful in the implementation of new design strategies, in the fine-tuning and control of systems, and in understanding the multiphysics or multimodal interaction of different physical systems.

Bibliography

[1] Isaac Newton and John Colson. *The Method of Fluxions And Infinite Series: With Its Application to the Geometry of Curve-Lines*. en. Nourse, 1736 (cit. on p. 27).

[2] Arnold Sommerfeld. *Partial Differential Equations in Physics*. en. Academic Press, Jan. 1949 (cit. on p. 27).

[3] Edward L. Ince. *Ordinary Differential Equations*. en. Courier Corporation, Jan. 1956 (cit. on p. 27).

[4] Martin Braun. *Differential Equations and Their Applications: An Introduction to Applied Mathematics*. en. Vol. 11. Texts in Applied Mathematics. New York, NY: Springer, 1993 (cit. on p. 27).

[5] J D'Azzo. *Linear control system analysis and design*. 1983 (cit. on pp. 27, 33, 37, 116).

[6] Paul Adrien Maurice Dirac. *The Principles of Quantum Mechanics*. eng. 1930 (cit. on pp. 27, 30).

[7] Brillouin Leon. *Wave Propagation In Periodic Structures*. eng. Mcgraw-hill Book Company Inc., London, 1946 (cit. on pp. 27, 28).

[8] "Mémoire sur la propagation de la chaleur dans les corps solides". In: *Oeuvres de Fourier: Publiées par les soins de Gaston Darboux*. Ed. by Jean Baptiste Joseph Fourier and Jean Gaston Darboux. Vol. 2. Cambridge Library Collection - Mathematics. Cambridge: Cambridge University Press, 2013, pp. 213–222 (cit. on pp. 27, 28).

[9] Elizabeth Garber. "Vibrating Strings and Eighteenth-Century Mechanics". en. In: *The Language of Physics: The Calculus and the Development of Theoretical Physics in Europe, 1750–1914*. Ed. by Elizabeth Garber. Boston, MA: Birkhäuser, 1999, pp. 31–62 (cit. on p. 27).

[10] Richard P. Feynman, Robert B. Leighton, Matthew Sands, and E. M. Hafner. "The Feynman Lectures on Physics; Vol. I". In: *American Journal of Physics* 33.9 (Sept. 1965), pp. 750–752 (cit. on pp. 27, 28).

[11] Christiaan Huygens. *Traité de la lumière : Où sont expliquées les causes de ce qui lui arrive dans la reflexion, & dans la refraction et particulièrement dans l'étrange réfraction du cristal d'Islande*. fre. A Leide : Chez Pierre vander Aa, marchand libraire, 1690 (cit. on p. 27).

[12] Isaac Newton, G. W. Hemming, and donor DSI Burndy Library. *Opticks: or, A treatise of the reflections, refractions, inflexions and colours of light : also two treatises of the species and magnitude of curvilinear figures*. eng. London : Printed for Sam. Smith, and Benj. Walford ..., 1704 (cit. on p. 27).

[13] Pierre Guaydier. *Histoire de la physique*. FR. 4e édition mise à jour. 1972 (cit. on p. 27).

[14] Clifford A. Pickover. *The physics book : from the big bang to quantum resurrection, 250 milestones in the history of physics*. eng. New York : Sterling Pub., 2011 (cit. on p. 27).

[15] *The Oxford handbook of the history of physics*. eng. Oxford, United Kingdom ; New York, NY : Oxford University Press, 2013 (cit. on pp. 27–29).

[16] Jacqueline Feke. "A History of Optics: From Greek Antiquity to the Nineteenth Century". In: *Physics Today* 66.6 (June 2013), pp. 52–53 (cit. on pp. 27, 28).

[17] Leonhard Euler. "Sur la vibration des cordes". In: *Mémoires de l'Académie des Sciences de Berlin* (1750), pp. 69–85 (cit. on p. 27).

[18] Jean Baptiste Joseph Fourier. *Théorie analytique de la chaleur*. fr. Gauthier-Villars, 1888 (cit. on p. 28).

[19] Thomas Young. "Experiments and calculations relative to physical optics, the philosophical transaction, 1803". In: *Young, T.(Ed.), A Course of Lectures on Natural Philosophy and the Mechanical Arts II* (1803), pp. 639–648 (cit. on p. 28).

[20] Augustin Fresnel. *Oeuvres complètes d'Augustin Fresnel. Tome 1 / publiées par MM. Henri de Senarmont, Emile Verdet et Léonor Fresnel*. FR. 1866 (cit. on p. 28).

[21] James Clerk Maxwell. "On governors". In: *Proceedings of the Royal Society of London* 16 (Jan. 1997), pp. 270–283 (cit. on p. 29).

[22] Edward John Routh. *A Treatise on the Stability of a Given State of Motion, Particularly Steady Motion: Being the Essay to which the Adams Prize was Adjudged in 1877, in the University of Cambridge*. en. Macmillan and Company, 1877 (cit. on p. 29).

[23] Adolf Hurwitz. "Ueber die Bedingungen, unter welchen eine Gleichung nur Wurzeln mit negativen reellen Theilen besitzt". de. In: *Math. Ann.* 46.2 (June 1895), pp. 273–284 (cit. on p. 29).

[24] Adolf Hurwitz et al. "On the conditions under which an equation has only roots with negative real parts". In: *Selected papers on mathematical trends in control theory* 65 (1964), pp. 273–284 (cit. on p. 29).

[25] George A. Campbell. "Physical theory of the electric wave-filter". In: *The Bell System Technical Journal* 1.2 (Nov. 1922), pp. 1–32 (cit. on p. 29).

[26] Otto J. Zobel. "Theory and design of uniform and composite electric wave-filters". In: *The Bell System Technical Journal* 2.1 (Jan. 1923), pp. 1–46 (cit. on p. 29).

[27] Stephen Butterworth et al. "On the theory of filter amplifiers". In: *Wireless Engineer* 7.6 (1930), pp. 536–541 (cit. on pp. 29, 35).

[28] S. Darlington. "Synthesis of Reactance 4-Poles Which Produce Prescribed Insertion Loss Characteristics: Including Special Applications To Filter Design". en. In: *Journal of Mathematics and Physics* 18.1-4 (1939), pp. 257–353 (cit. on p. 29).

[29] J.H. Mulligan. "The Effect of Pole and Zero Locations on the Transient Response of Linear Dynamic Systems". In: *Proceedings of the IRE* 37.5 (May 1949), pp. 516–529 (cit. on p. 29).

[30] Charles Desoer and Jerry Schulman. "Zeros and poles of matrix transfer functions and their dynamical interpretation". In: *IEEE Transactions on Circuits and Systems* 21.1 (1974), pp. 3–8 (cit. on pp. 29, 33, 135).

[31] Carl E Baum. "On the singularity expansion method for the solution of electromagnetic interaction problems". In: *Interaction note* 88.11 (1971) (cit. on pp. 29, 35, 38, 71, 97, 135).

[32] P Vincent. “Singularity expansions for cylinders of finite conductivity”. In: *Applied physics* 17.3 (1978), pp. 239–248 (cit. on pp. 30, 35, 71).

[33] L Pearson. “A note on the representation of scattered fields as a singularity expansion”. In: *IEEE transactions on antennas and propagation* 32.5 (1984), pp. 520–524 (cit. on pp. 30, 71).

[34] C Baum. “The singularity expansion method: Background and developments”. In: *IEEE Antennas and Propagation Society Newsletter* 28.4 (1986), pp. 14–23 (cit. on pp. 30, 35).

[35] C.E. Baum, E.J. Rothwell, K.-M. Chen, and D.P. Nyquist. “The singularity expansion method and its application to target identification”. In: *Proceedings of the IEEE* 79.10 (1991), pp. 1481–1492 (cit. on pp. 30, 35, 71).

[36] John A. Wheeler. “On the Mathematical Description of Light Nuclei by the Method of Resonating Group Structure”. In: *Phys. Rev.* 52.11 (Dec. 1937), pp. 1107–1122 (cit. on p. 30).

[37] W. Heisenberg. “Die „beobachtbaren Größen“ in der Theorie der Elementarteilchen”. de. In: *Z. Physik* 120.7 (July 1943), pp. 513–538 (cit. on p. 30).

[38] S. T. Ma. “On a General Condition of Heisenberg for the S Matrix”. In: *Phys. Rev.* 71.3 (Feb. 1947), pp. 195–200 (cit. on p. 30).

[39] Ning Hu. “On the Application of Heisenberg’s Theory of S-Matrix to the Problems of Resonance Scattering and Reactions in Nuclear Physics”. In: *Phys. Rev.* 74.2 (July 1948), pp. 131–140 (cit. on p. 30).

[40] F. J. Dyson. “The S Matrix in Quantum Electrodynamics”. In: *Phys. Rev.* 75.11 (June 1949), pp. 1736–1755 (cit. on pp. 30, 33).

[41] Geoffrey F. Chew. “S-Matrix Theory of Strong Interactions without Elementary Particles”. In: *Rev. Mod. Phys.* 34.3 (July 1962), pp. 394–401 (cit. on p. 30).

[42] K. Kurokawa. “Power Waves and the Scattering Matrix”. In: *IEEE Transactions on Microwave Theory and Techniques* 13.2 (Mar. 1965), pp. 194–202 (cit. on p. 30).

[43] PC Waterman. “Matrix formulation of electromagnetic scattering”. In: *Proceedings of the IEEE* 53.8 (1965), pp. 805–812 (cit. on pp. 30, 71).

[44] Sidney Coleman and Jeffrey Mandula. “All Possible Symmetries of the S Matrix”. In: *Phys. Rev.* 159.5 (July 1967), pp. 1251–1256 (cit. on p. 30).

[45] Rudolf Haag, Jan T. Łopuszański, and Martin Sohnius. “All possible generators of supersymmetries of the *S*-matrix”. In: *Nuclear Physics B* 88.2 (Mar. 1975), pp. 257–274 (cit. on p. 30).

[46] G. Gamow. “Zur Quantentheorie des Atomkernes”. de. In: *Z. Physik* 51.3 (Mar. 1928), pp. 204–212 (cit. on p. 30).

[47] William G. Wagner and R. W. Hellwarth. “Quantum Noise in a Parametric Amplifier with Lossy Modes”. In: *Phys. Rev.* 133.4A (Feb. 1964), A915–A920 (cit. on p. 30).

[48] C. V. Vishveshwara. “Scattering of Gravitational Radiation by a Schwarzschild Black-hole”. en. In: *Nature* 227.5261 (Aug. 1970), pp. 936–938 (cit. on p. 30).

[49] S. M. Barnett and P. M. Radmore. “Quantum theory of cavity quasimodes”. In: *Optics Communications* 68.5 (Nov. 1988), pp. 364–368 (cit. on p. 30).

[50] Subrahmanyan Chandrasekhar and S. Detweiler. "The quasi-normal modes of the Schwarzschild black hole". In: *Proceedings of the Royal Society of London. A. Mathematical and Physical Sciences* 344.1639 (Jan. 1997), pp. 441–452 (cit. on p. 30).

[51] Kostas D. Kokkotas and Bernd G. Schmidt. "Quasi-Normal Modes of Stars and Black Holes". en. In: *Living Rev. Relativ.* 2.1 (Sept. 1999), p. 2 (cit. on p. 30).

[52] P. T. Leung, S. Y. Liu, and K. Young. "Completeness and orthogonality of quasinormal modes in leaky optical cavities". In: *Phys. Rev. A* 49.4 (Apr. 1994), pp. 3057–3067 (cit. on p. 30).

[53] E. S. C. Ching, P. T. Leung, A. Maassen van den Brink, W. M. Suen, S. S. Tong, and K. Young. "Quasinormal-mode expansion for waves in open systems". In: *Rev. Mod. Phys.* 70.4 (Oct. 1998), pp. 1545–1554 (cit. on p. 30).

[54] M. B. Doost, W. Langbein, and E. A. Muljarov. "Resonant-state expansion applied to three-dimensional open optical systems". In: *Physical Review A* 90.1 (July 2014), p. 013834 (cit. on pp. 30, 71).

[55] Philippe Lalanne, Wei Yan, Kevin Vynck, Christophe Sauvan, and Jean-Paul Hugonin. "Light interaction with photonic and plasmonic resonances". In: *Laser & Photonics Reviews* 12.5 (2018), p. 1700113 (cit. on pp. 30, 71).

[56] EA Muljarov and T Weiss. "Resonant-state expansion for open optical systems: generalization to magnetic, chiral, and bi-anisotropic materials". In: *Optics letters* 43.9 (2018), pp. 1978–1981 (cit. on pp. 30, 71).

[57] Alexandre Gras, Wei Yan, and Philippe Lalanne. "Quasinormal-mode analysis of grating spectra at fixed incidence angles". In: *Optics letters* 44.14 (2019), pp. 3494–3497 (cit. on pp. 30, 71).

[58] P. Lalanne, W. Yan, A. Gras, et al. "Quasinormal mode solvers for resonators with dispersive materials". EN. In: *J. Opt. Soc. Am. A, JOSAA* 36.4 (Apr. 2019), pp. 686–704 (cit. on pp. 30, 71).

[59] Carlo Gigli, Tong Wu, Giuseppe Marino, Adrien Borne, Giuseppe Leo, and Philippe Lalanne. "Quasinormal-Mode Non-Hermitian Modeling and Design in Nonlinear Nano-Optics". In: *ACS Photonics* (2020) (cit. on pp. 30, 71).

[60] B. Stout, R. Colom, N. Bonod, and R. C. McPhedran. "Spectral expansions of open and dispersive optical systems: Gaussian regularization and convergence". In: *New Journal of Physics* 23.8 (Aug. 2021), p. 083004 (cit. on pp. 30, 88).

[61] Christophe Sauvan, Tong Wu, Rachid Zarouf, Egor A. Muljarov, and Philippe Lalanne. "Normalization, orthogonality, and completeness of quasinormal modes of open systems: the case of electromagnetism [Invited]". EN. In: *Opt. Express, OE* 30.5 (Feb. 2022), pp. 6846–6885 (cit. on pp. 30, 35).

[62] Paul S. Epstein. "Radio-Wave Propagation and Electromagnetic Surface Waves". en. In: *Proc. Natl. Acad. Sci. U.S.A.* 33.6 (June 1947), pp. 195–199 (cit. on p. 31).

[63] M. Nevière. "The Homogeneous Problem". en. In: *Electromagnetic Theory of Gratings*. Ed. by Roger Petit. Berlin, Heidelberg: Springer, 1980, pp. 123–157 (cit. on pp. 31, 116).

[64] Krzysztof A. Michalski. "BIBLIOGRAPHY OF THE SINGULARITY EXPANSION METHOD AND RELATED TOPICS". In: *Electromagnetics* 1.4 (1981), pp. 493–511 (cit. on pp. 31, 35).

[65] Carl E Baum. *The singularity expansion method in electromagnetics: A summary survey and open questions*. Lulu. com, 2012 (cit. on p. 31).

[66] Swagato Sarkar, Vaibhav Gupta, Mohit Kumar, Jonas Schubert, Patrick T. Probst, Joby Joseph, and Tobias A.F. König. "Hybridized Guided-Mode Resonances via Colloidal Plasmonic Self-Assembled Grating". In: *ACS Applied Materials & Interfaces* 11.14 (2019), pp. 13752–13760 (cit. on pp. 31, 105).

[67] T.K. Sarkar, Sheeyun Park, Jinhwan Koh, and S.M. Rao. "Application of the matrix pencil method for estimating the SEM (singularity expansion method) poles of source-free transient responses from multiple look directions". In: *IEEE Transactions on Antennas and Propagation* 48.4 (Apr. 2000), pp. 612–618 (cit. on pp. 31, 135, 152).

[68] T.K. Sarkar, M. Salazar-Palma, M.D. Zhu, and H. Chen. "The Cauchy Method". In: *Modern Characterization of Electromagnetic Systems and Its Associated Metrology*. John Wiley & Sons, Ltd, 2021, pp. 107–190 (cit. on pp. 31, 135).

[69] Victor Grigoriev and Fabio Biancalana. "Exact analytical representations for broadband transmission properties of quarter-wave multilayers". In: *Optics Letters* 36.19 (Sept. 2011), p. 3774 (cit. on pp. 31, 37, 135).

[70] V Grigoriev, Abir Tahri, Stefan Varault, Brice Rolly, Brian Stout, Jérôme Wenger, and Nicolas Bonod. "Optimization of resonant effects in nanostructures via Weierstrass factorization". In: *Physical Review A* 88.1 (2013), p. 011803 (cit. on pp. 31, 35, 37, 38, 44, 54, 71, 73, 136).

[71] V. Grigoriev, S. Varault, G. Boudarham, B. Stout, J. Wenger, and N. Bonod. "Singular analysis of Fano resonances in plasmonic nanostructures". In: *Phys. Rev. A* 88.6 (Dec. 2013), p. 063805 (cit. on pp. 31, 33, 44, 71, 73, 117, 122, 136).

[72] Victor Grigoriev, Guillaume Demésy, Jérôme Wenger, and Nicolas Bonod. "Singular analysis to homogenize planar metamaterials as nonlocal effective media". In: *Phys. Rev. B* 89.24 (June 2014), p. 245102 (cit. on pp. 31, 96, 136).

[73] Victor Grigoriev, Nicolas Bonod, Jérôme Wenger, and Brian Stout. "Optimizing Nanoparticle Designs for Ideal Absorption of Light". In: *ACS Photonics* 2.2 (2015), pp. 263–270 (cit. on pp. 31, 33).

[74] Rémi Colom, Ross McPhedran, Brian Stout, and Nicolas Bonod. "Modal expansion of the scattered field: Causality, nondivergence, and nonresonant contribution". In: *Phys. Rev. B* 98.8 (Aug. 2018), p. 085418 (cit. on pp. 31, 35, 37, 38, 61, 62, 71, 73, 135).

[75] Rémi Colom, Ross McPhedran, Brian Stout, and Nicolas Bonod. "Modal analysis of anapoles, internal fields, and Fano resonances in dielectric particles". In: *J. Opt. Soc. Am. B* 36.8 (2019), pp. 2052–2061 (cit. on pp. 31, 33, 71, 73, 135).

[76] Alan V. Oppenheim, John Buck, Michael Daniel, Alan S. Willsky, Syed Hamid Nawab, and Andrew Singer. *Signals & Systems*. Prentice Hall, 1997 (cit. on pp. 33, 37).

[77] Leo L Beranek. "Acoustic impedance of porous materials". In: *The Journal of the Acoustical Society of America* 13.3 (1942), pp. 248–260 (cit. on p. 33).

[78] James J Ackmann. "Complex bioelectric impedance measurement system for the frequency range from 5 Hz to 1 MHz". In: *Annals of biomedical engineering* 21.2 (1993), pp. 135–146 (cit. on p. 33).

[79] Luca Callegaro. *Electrical impedance: principles, measurement, and applications*. CRC Press, 2012 (cit. on p. 33).

[80] D. Agassi, H. A. Weidenmüller, and G. Mantzouranis. "The statistical theory of nuclear reactions for strongly overlapping resonances as a theory of transport phenomena". In: *Physics Reports* 22.3 (1975), pp. 145–179 (cit. on p. 33).

[81] E Popov, L Mashev, and D Maystre. "Theoretical study of the anomalies of coated dielectric gratings". In: *Optica Acta: International Journal of Optics* 33.5 (1986), pp. 607–619 (cit. on p. 33).

[82] XJM Leijtens, P Le Lourec, and MK Smit. "S-matrix oriented CAD-tool for simulating complex integrated optical circuits". In: *IEEE Journal of Selected Topics in Quantum Electronics* 2.2 (1996), pp. 257–262 (cit. on p. 33).

[83] Yan Fyodorov and Dmitry Savin. "Resonance scattering of waves in chaotic systems". In: *The Oxford Handbook of Random Matrix Theory*. Oxford University Press, Sept. 2015 (cit. on p. 33).

[84] Charles Sumner Williams and Orville A Becklund. *Introduction to the optical transfer function*. Vol. 112. SPIE Press, 2002 (cit. on p. 33).

[85] Alex Krasnok and Andrea Alú. "Coherent Control of Light Scattering". In: *arXiv:1904.11384* (2019) (cit. on p. 33).

[86] Wolfgang Porod, Zhi-an Shao, and Craig S Lent. "Resonance-antiresonance line shape for transmission in quantum waveguides with resonantly coupled cavities". In: *Physical Review B* 48.11 (1993), p. 8495 (cit. on p. 33).

[87] SMI Tsuzuki, Shen Ye, and Stuart Berkowitz. "Ultra-selective 22-pole 10-transmission zero superconducting bandpass filter surpasses 50-pole Chebyshev filter". In: *IEEE transactions on microwave theory and techniques* 50.12 (2002), pp. 2924–2929 (cit. on p. 33).

[88] TR Zhan and ST Chui. "Theory of the spontaneous-decay enhancement in plasmonic nanoparticles based on a singularity representation of the scattering matrix". In: *Physical Review A* 90.2 (2014), p. 023802 (cit. on pp. 33, 71).

[89] Denis G Baranov, Alex Krasnok, Timur Shegai, Andrea Alù, and Yidong Chong. "Coherent perfect absorbers: linear control of light with light". In: *Nature Reviews Materials* 2.12 (2017), pp. 1–14 (cit. on p. 33).

[90] Changqing Wang, William R Sweeney, A Douglas Stone, and Lan Yang. "Coherent perfect absorption at an exceptional point". In: *Science* 373.6560 (2021), pp. 1261–1265 (cit. on pp. 33, 71).

[91] Lei Chen and Steven M Anlage. "Use of transmission and reflection complex time delays to reveal scattering matrix poles and zeros: Example of the ring graph". In: *Physical Review E* 105.5 (2022), p. 054210 (cit. on pp. 33, 135).

[92] Jérôme Sol, David R Smith, and Philipp Del Hougne. "Meta-programmable analog differentiator". In: *Nature Communications* 13.1 (2022), p. 1713 (cit. on p. 33).

[93] C. Sanathanan and J. Koerner. "Transfer function synthesis as a ratio of two complex polynomials". In: *IEEE Transactions on Automatic Control* 8.1 (1963), pp. 56–58 (cit. on pp. 35, 37).

[94] LA Koenig. "The bode diagram: An approach to regulating-system stability fundamentals". In: *Electrical Engineering* 78.6 (1959), pp. 653–658 (cit. on p. 35).

[95] P Vincent and M Neviere. "Corrugated dielectric waveguides: A numerical study of the second-order stop bands". In: *Applied physics* 20.4 (1979), pp. 345–351 (cit. on p. 35).

[96] Patrick Vincent and Hassan Akhouayri. "About Propagation Modes In Nonlinear Dielectric Waveguides". In: *Scattering and Diffraction*. Vol. 1029. SPIE, 1989, pp. 143–148 (cit. on p. 35).

[97] George B Arfken and Hans J Weber. *Mathematical methods for physicists international student edition*. Elsevier, 2005 (cit. on p. 35).

[98] Masud Mansuripur, Miroslav Kolesik, and Per Jakobsen. "Leaky modes of solid dielectric spheres". In: *Physical Review A* 96.1 (2017), p. 013846 (cit. on p. 35).

[99] Isam Ben Soltane, Rémi Colom, Brian Stout, and Nicolas Bonod. "Derivation of the Transient and Steady Optical States from the Poles of the S-Matrix". In: *Laser & Photonics Reviews* (2022), p. 2200141 (cit. on pp. 35, 37, 44, 61, 62, 93, 116, 135, 151).

[100] Rémi Colom, Elena Mikheeva, Karim Achouri, Jesus Zuniga-Perez, Nicolas Bonod, Olivier J. F. Martin, Sven Burger, and Patrice Genevet. "Crossing of the Branch Cut: The Topological Origin of a Universal 2π-Phase Retardation in Non-Hermitian Metasurfaces". In: *Laser & Photonics Reviews* 17.6 (2023), p. 2200976 (cit. on pp. 35, 71, 96, 116, 135).

[101] J Defrance and T Weiss. "On the pole expansion of electromagnetic fields". In: *Optics Express* 28.22 (2020), pp. 32363–32376 (cit. on pp. 35, 71).

[102] Mohammed Benzaouia, John D Joannopoulos, Steven G Johnson, and Aristeidis Karalis. "Quasi-normal mode theory of the scattering matrix, enforcing fundamental constraints for truncated expansions". In: *Physical Review Research* 3.3 (2021), p. 033228 (cit. on p. 35).

[103] Christophe Sauvan. "Quasinormal modes expansions for nanoresonators made of absorbing dielectric materials: study of the role of static modes". In: *Optics Express* 29.6 (2021), pp. 8268–8282 (cit. on pp. 35, 71).

[104] Habib Ammari, Pierre Millien, and Alice L Vanel. "Modal approximation for strictly convex plasmonic resonators in the time domain: The Maxwell's equations". In: *Journal of Differential Equations* 309 (2022), pp. 676–703 (cit. on pp. 35, 71).

[105] Mohammad-Ali Miri and Andrea Alù. "Exceptional points in optics and photonics". In: *Science* 363.6422 (2019), eaar7709 (cit. on p. 35).

[106] William R. Sweeney, Chia Wei Hsu, Stefan Rotter, and A. Douglas Stone. "Perfectly Absorbing Exceptional Points and Chiral Absorbers". In: *Phys. Rev. Lett.* 122.9 (Mar. 2019), p. 093901 (cit. on p. 35).

[107] Georgy Ermolaev, Kirill Voronin, Denis G Baranov, Vasyl Kravets, Gleb Tselikov, Yury Stebunov, Dmitry Yakubovsky, Sergey Novikov, Andrey Vyshnevyy, Arslan Mazitov, et al. "Topological phase singularities in atomically thin high-refractive-index materials". In: *Nature communications* 13.1 (2022), pp. 1–9 (cit. on p. 35).

[108] Wolfgang S. M. Werner, Kathrin Glantschnig, and Claudia Ambrosch-Draxl. "Optical Constants and Inelastic Electron-Scattering Data for 17 Elemental Metals". In: *Journal of Physical and Chemical Reference Data* 38.4 (2009), pp. 1013–1092 (cit. on pp. 37, 105).

[109] M. Garcia-Vergara, G. Demésy, and F. Zolla. "Extracting an accurate model for permittivity from experimental data: hunting complex poles from the real line". In: *Opt. Lett.* 42.6 (Mar. 2017), pp. 1145–1148 (cit. on pp. 37, 96, 102, 135).

[110] Ellis Horowitz. "Algorithms for partial fraction decomposition and rational function integration". In: *Proceedings of the second ACM symposium on Symbolic and algebraic manipulation*. SYMSAC '71. New York, NY, USA: Association for Computing Machinery, Mar. 1971, pp. 441–457 (cit. on p. 37).

[111] Tristan Needham. *Visual complex analysis*. Oxford : New York: Clarendon Press ; Oxford University Press, 1997 (cit. on pp. 40, 117).

[112] Alain Yger. *Analyse complexe et distributions*. Paris: Ellipses Edition Marketing, 2001 (cit. on pp. 40, 136).

[113] Louis de Branges. "The Stone-Weierstrass theorem". en. In: *Proc. Amer. Math. Soc.* 10.5 (1959), pp. 822–824 (cit. on p. 52).

[114] R. G. Newton. *Scattering theory of waves and particles*. McGraw Hill, Dec. 1966 (cit. on p. 54).

[115] "CHAPTER 1 CAUSALITY AND DISPERSION RELATIONS". In: *Causality and Dispersion Relations*. Ed. by H. M. Nussenzveig. Vol. 95. Mathematics in Science and Engineering. Elsevier, 1972, pp. 3–53 (cit. on pp. 57, 61, 62).

[116] Constantinos Valagiannopoulos. "Stable electromagnetic interactions with effective media of active multilayers". In: *Physical Review B* 105.4 (2022), p. 045304 (cit. on pp. 61, 62).

[117] I. Ben Soltane, R. Colom, F. Dierick, B. Stout, and N. Bonod. "Multiple-order singularity expansion method". In: *New Journal of Physics* 25.10 (Oct. 2023), p. 103022 (cit. on pp. 68, 97, 116, 117, 126, 135, 136).

[118] Vea Sandoghdar, F Treussart, J Hare, V Lefevre-Seguin, J-M Raimond, and S Haroche. "Very low threshold whispering-gallery-mode microsphere laser". In: *Physical Review A* 54.3 (1996), R1777 (cit. on p. 71).

[119] Pascal Del'Haye, Albert Schliesser, Olivier Arcizet, Tom Wilken, Ronald Holzwarth, and Tobias J Kippenberg. "Optical frequency comb generation from a monolithic microresonator". In: *Nature* 450.7173 (2007), p. 1214 (cit. on p. 71).

[120] Niccolo Somaschi, Valerian Giesz, Lorenzo De Santis, JC Loredo, Marcelo P Almeida, Gaston Hornecker, Simone Luca Portalupi, Thomas Grange, Carlos Antón, Justin Demory, et al. "Near-optimal single-photon sources in the solid state". In: *Nature Photonics* 10.5 (2016), p. 340 (cit. on p. 71).

[121] Alex Krasnok, Denis Baranov, Huanan Li, Mohammad-Ali Miri, Francesco Monticone, and Andrea Alú. "Anomalies in light scattering". In: *Advances in Optics and Photonics* 11.4 (2019), pp. 892–951 (cit. on p. 71).

[122] T Weiss and EA Muljarov. "How to calculate the pole expansion of the optical scattering matrix from the resonant states". In: *Physical Review B* 98.8 (2018), p. 085433 (cit. on p. 71).

[123] Philip Trøst Kristensen, Kathrin Herrmann, Francesco Intravaia, and Kurt Busch. "Modeling electromagnetic resonators using quasinormal modes". In: *Adv. Opt. Photon.* 12.3 (Sept. 2020), pp. 612–708 (cit. on p. 71).

[124] Christophe Sauvan, Jean-Paul Hugonin, IS Maksymov, and Philippe Lalanne. "Theory of the spontaneous optical emission of nanosize photonic and plasmon resonators". In: *Physical Review Letters* 110.23 (2013), p. 237401 (cit. on pp. 71, 116).

[125] Lin Zschiedrich, Felix Binkowski, Niko Nikolay, Oliver Benson, Günter Kewes, and Sven Burger. "Riesz-projection-based theory of light-matter interaction in dispersive nanoresonators". In: *Physical Review A* 98.4 (2018), p. 043806 (cit. on p. 71).

[126] Philip Trøst Kristensen and Stephen Hughes. "Modes and mode volumes of leaky optical cavities and plasmonic nanoresonators". In: *ACS Photonics* 1.1 (2013), pp. 2–10 (cit. on p. 71).

[127] EA Muljarov and W Langbein. "Exact mode volume and Purcell factor of open optical systems". In: *Physical Review B* 94.23 (2016), p. 235438 (cit. on pp. 71, 116).

[128] Xavier Zambrana-Puyalto and Nicolas Bonod. "Purcell factor of spherical Mie resonators". In: *Physical Review B* 91.19 (2015), p. 195422 (cit. on pp. 71, 116).

[129] KG Cognée, Wei Yan, F La China, D Balestri, F Intonti, M Gurioli, AF Koenderink, and P Lalanne. "Mapping complex mode volumes with cavity perturbation theory". In: *Optica* 6.3 (2019), pp. 269–273 (cit. on p. 71).

[130] Wei Yan, Philippe Lalanne, and Min Qiu. "Shape Deformation of Nanoresonator: A Quasinormal-Mode Perturbation Theory". In: *Physical Review Letters* 125.1 (2020), p. 013901 (cit. on p. 71).

[131] Sebastian Franke, Stephen Hughes, Mohsen Kamandar Dezfouli, Philip Trøst Kristensen, Kurt Busch, Andreas Knorr, and Marten Richter. "Quantization of quasinormal modes for open cavities and plasmonic cavity quantum electrodynamics". In: *Physical Review Letters* 122.21 (2019), p. 213901 (cit. on p. 71).

[132] P. C. Waterman. "The T-matrix revisited". In: *J. Opt. Soc. Am. A* 24.8 (Aug. 2007), pp. 2257–2267 (cit. on p. 71).

[133] M.I. Mishchenko, L.D. Travis, and A.A. Lacis. *Scattering, Absorption, and Emission of Light by Small Particles*. Cambridge University Press, 2002 (cit. on p. 71).

[134] B. Stout, C. Andraud, D. Prot, J. Lafait, J. C. Auger, and S. Stout. "Complete field descriptions in three-dimensional multiple scattering problems: a transfer-matrix approach". In: *Journal of Optics A: Pure and Applied Optics* 4.5 (2002), S182 (cit. on p. 71).

[135] B Stout, JC Auger, and J Lafait. "Individual and aggregate scattering matrices and cross-sections: conservation laws and reciprocity". English. In: *Journal of Modern Optics* 48.14 (Nov. 2001), pp. 2105–2128 (cit. on p. 71).

[136] YD Chong, Li Ge, Hui Cao, and A Douglas Stone. "Coherent perfect absorbers: time-reversed lasers". In: *Physical Review Letters* 105.5 (2010), p. 053901 (cit. on p. 71).

[137] William R Sweeney, Chia Wei Hsu, and A Douglas Stone. "Theory of reflectionless scattering modes". In: *Physical Review A* 102.6 (2020), p. 063511 (cit. on p. 71).

[138] Hanwen Zhang, Chia Wei Hsu, and Owen D Miller. "Scattering concentration bounds: brightness theorems for waves". In: *Optica* 6.10 (2019), pp. 1321–1327 (cit. on p. 71).

[139] Nikolai G Khlebtsov. "T-matrix method in plasmonics: An overview". In: *Journal of Quantitative Spectroscopy and Radiative Transfer* 123 (2013), pp. 184–217 (cit. on p. 71).

[140] Eric C Le Ru, Walter RC Somerville, and Baptiste Auguié. "Radiative correction in approximate treatments of electromagnetic scattering by point and body scatterers". In: *Physical Review A* 87.1 (2013), p. 012504 (cit. on p. 71).

[141] Nikolay A Gippius, Thomas Weiss, Sergei G Tikhodeev, and Harald Giessen. "Resonant mode coupling of optical resonances in stacked nanostructures". In: *Optics Express* 18.7 (2010), pp. 7569–7574 (cit. on p. 71).

[142] Guillaume Demésy, Jean-Claude Auger, and Brian Stout. "Scattering matrix of arbitrarily shaped objects: combining finite elements and vector partial waves". In: *J. Opt. Soc. Am. A* 35.8 (2018), pp. 1401–1409 (cit. on p. 71).

[143] Clément Ferise, Philipp Del Hougne, Simon Félix, Vincent Pagneux, and Matthieu Davy. "Exceptional Points of P T-Symmetric Reflectionless States in Complex Scattering Systems". In: *Physical Review Letters* 128.20 (2022), p. 203904 (cit. on pp. 71, 96, 135).

[144] Qinghua Song, Mutasem Odeh, Jesús Zúñiga-Pérez, Boubacar Kanté, and Patrice Genevet. "Plasmonic topological metasurface by encircling an exceptional point". In: *Science* 373.6559 (2021), pp. 1133–1137 (cit. on pp. 71, 96).

[145] CE Baum and LW Pearson. "On the convergence and numerical sensitivity of the SEM pole-series in early-time scattering response". In: *Electromagnetics* 1.2 (1981), pp. 209–228 (cit. on p. 71).

[146] M. Morgan. "Time-domain scattering measurements". In: *IEEE Antennas and Propagation Society Newsletter* 26.4 (1984), pp. 4–9 (cit. on p. 71).

[147] Rémi Faggiani, Arthur Losquin, Jianji Yang, Erik Marsell, Anders Mikkelsen, and Philippe Lalanne. "Modal Analysis of the Ultrafast Dynamics of Optical Nanoresonators". In: *ACS Photonics* 4.4 (2017), pp. 897–904 (cit. on p. 71).

[148] Wei Yan, Rémi Faggiani, and Philippe Lalanne. "Rigorous modal analysis of plasmonic nanoresonators". In: *Physical Review B* 97.20 (2018), p. 205422 (cit. on p. 71).

[149] Matthias Hensen, Bernhard Huber, Daniel Friedrich, Enno Krauss, Sebastian Pres, Philipp Grimm, Daniel Fersch, Julian Luttig, Victor Lisinetskii, Bert Hecht, et al. "Spatial variations in femtosecond field dynamics within a plasmonic nanoresonator mode". In: *Nano letters* 19.7 (2019), pp. 4651–4658 (cit. on p. 71).

[150] Tadele Orbula Otomalo, Fabrice Mayran de Chamisso, and Bruno Palpant. "Complex-conjugate Pole-residue Pair-Based FDTD Method for Assessing Ultrafast Transient Plasmonic Near Field". In: *Plasmonics* 15.2 (2020), pp. 495–505 (cit. on p. 71).

[151] Carlo Forestiere and Giovanni Miano. "Time-domain formulation of electromagnetic scattering based on a polarization-mode expansion and the principle of least action". In: *Physical Review A* 104.1 (2021), p. 013512 (cit. on p. 71).

[152] Lorenzo Baldassari, Pierre Millien, and Alice L Vanel. "Modal approximation for plasmonic resonators in the time domain: the scalar case". In: *Partial Differential Equations and Applications* 2.4 (2021), pp. 1–40 (cit. on p. 71).

[153] Max Born and Emil Wolf. *Principles of Optics: Electromagnetic Theory of Propagation, Interference and Diffraction of Light, seventh edition*. Ed. by C. U. P. Archive. Cambridge University Press, 2000 (cit. on p. 71).

[154] Denis G Baranov, Alex Krasnok, and Andrea Alù. "Coherent virtual absorption based on complex zero excitation for ideal light capturing". In: *Optica* 4.12 (2017), pp. 1457–1461 (cit. on p. 71).

[155] Alexander Moroz and Andrey E Miroshnichenko. "On beautiful analytic structure of the S-matrix". In: *New Journal of Physics* 21.10 (2019), p. 103035 (cit. on p. 73).

[156] Marc Dubois, Emmanuel Bossy, Stefan Enoch, Sébastien Guenneau, Geoffroy Lerosey, and Patrick Sebbah. "Time-driven superoscillations with negative refraction". In: *Physical Review Letters* 114.1 (2015), p. 013902 (cit. on p. 86).

[157] Francesco Andreoli, Michael J. Gullans, Alexander A. High, Antoine Browaeys, and Darrick E. Chang. "Maximum Refractive Index of an Atomic Medium". In: *Phys. Rev. X* 11.1 (Feb. 2021), p. 011026 (cit. on p. 96).

[158] Hyungki Shim, Francesco Monticone, and Owen D. Miller. "Fundamental Limits to the Refractive Index of Transparent Optical Materials". In: *Advanced Materials* 33.43 (2021), p. 2103946 (cit. on p. 96).

[159] Karl S Kunz and Raymond J Luebbers. *The finite difference time domain method for electromagnetics*. CRC press, 1993 (cit. on p. 96).

[160] Allen Taflove. "The finite difference time domain method." In: *Computational electromagnetics* (1995) (cit. on p. 96).

[161] Jun-Hee Park, Abdoulaye Ndao, Wei Cai, Liyi Hsu, Ashok Kodigala, Thomas Lepetit, Yu-Hwa Lo, and Boubacar Kanté. "Symmetry-breaking-induced plasmonic exceptional points and nanoscale sensing". In: *Nature Physics* 16.4 (2020), pp. 462–468 (cit. on p. 96).

[162] Changqing Wang, Zhoutian Fu, Wenbo Mao, Jinran Qie, A Douglas Stone, and Lan Yang. "Non-Hermitian optics and photonics: from classical to quantum". In: *Advances in Optics and Photonics* 15.2 (2023), pp. 442–523 (cit. on p. 96).

[163] Kurt E. Oughstun and Natalie A. Cartwright. "On the Lorentz-Lorenz formula and the Lorentz model of dielectric dispersion". In: *Opt. Express* 11.13 (June 2003), pp. 1541–1546 (cit. on p. 96).

[164] Alexandre Vial, Anne-Sophie Grimault, Demetrio Macías, Dominique Barchiesi, and Marc Lamy de la Chapelle. "Improved analytical fit of gold dispersion: Application to the modeling of extinction spectra with a finite-difference time-domain method". In: *Phys. Rev. B* 71.8 (Feb. 2005), p. 085416 (cit. on p. 96).

[165] Alexandre Vial and Thierry Laroche. "Comparison of gold and silver dispersion laws suitable for FDTD simulations". In: *Applied physics B* 93 (2008), pp. 139–143 (cit. on p. 96).

[166] Tasnim Gharbi, Dominique Barchiesi, Sameh Kessentini, and Ramzi Maalej. "Fitting optical properties of metals by Drude-Lorentz and partial-fraction models in the [0.5;6] eV range". In: *Opt. Mater. Express* 10.5 (May 2020), pp. 1129–1162 (cit. on p. 96).

[167] John David Jackson. “Classical electrodynamics”. In: third. John Wiley & Sons, 1999, pp. 309–314 (cit. on p. 96).

[168] Minghui Han, R.W. Dutton, and Shanhui Fan. “Model dispersive media in finite-difference time-domain method with complex-conjugate pole-residue pairs”. In: *IEEE Microwave and Wireless Components Letters* 16.3 (2006), pp. 119–121 (cit. on p. 96).

[169] Minghui Han, Zongfu Yu, and Shanhui Fan. “Efficient treatment of dispersive electric permittivity in finite-difference time-domain simulations of advanced photonic devices”. In: *Numerical Simulation of Optoelectronic Devices*. 2010, pp. 113–114 (cit. on p. 96).

[170] H. S. Sehmi, W. Langbein, and E. A. Muljarov. “Optimizing the Drude-Lorentz model for material permittivity: Method, program, and examples for gold, silver, and copper”. In: *Phys. Rev. B* 95.11 (Mar. 2017), p. 115444 (cit. on pp. 96, 122, 127).

[171] Cael Warner, Loïc Markley, and Kenneth J Chau. “Modeling dispersive silver in the electrodynamic lattice-Boltzmann method using complex-conjugate pole-residue pairs”. In: *arXiv preprint arXiv:2209.15603* (2022) (cit. on p. 96).

[172] Hai Lin, Mario F. Pantoja, Luis D. Angulo, Jesus Alvarez, Rafael G. Martin, and Salvador G. Garcia. “FDTD Modeling of Graphene Devices Using Complex Conjugate Dispersion Material Model”. In: *IEEE Microwave and Wireless Components Letters* 22.12 (2012), pp. 612–614 (cit. on p. 96).

[173] Konstantinos P. Prokopidis and Dimitrios C. Zografopoulos. “One-Step Leapfrog ADI-FDTD Method Using the Complex-Conjugate Pole-Residue Pairs Dispersion Model”. In: *IEEE Microwave and Wireless Components Letters* 28.12 (2018), pp. 1068–1070 (cit. on p. 96).

[174] Adam Paszke, Sam Gross, Soumith Chintala, Gregory Chanan, Edward Yang, Zach DeVito, Zeming Lin, Alban Desmaison, Luca Antiga, and Adam Lerer. “Automatic differentiation in PyTorch”. In: 2017 (cit. on pp. 97, 135).

[175] Mikhail N. Polyanskiy. *Refractive index database* (cit. on p. 105).

[176] Shaista Babar and J. H. Weaver. “Optical constants of Cu, Ag, and Au revisited”. In: *Appl. Opt.* 54.3 (Jan. 2015), pp. 477–481 (cit. on p. 105).

[177] Anna Sytchkova, Alexandr Belosludtsev, Lina Volosevičienė, Remigijus Juškėnas, and Rimantas Simniškis. “Optical, structural and electrical properties of sputtered ultrathin chromium films”. In: *Optical Materials* 121 (2021), p. 111530 (cit. on p. 105).

[178] T. J. Bright, J. I. Watjen, Z. M. Zhang, C. Muratore, and A. A. Voevodin. “Optical properties of HfO2 thin films deposited by magnetron sputtering: From the visible to the far-infrared”. In: *Thin Solid Films* 520.22 (2012), pp. 6793–6802 (cit. on p. 105).

[179] Luis V. Rodríguez-de Marcos, Juan I. Larruquert, José A. Méndez, and José A. Aznárez. “Self-consistent optical constants of SiO2 and Ta2O5 films”. In: *Opt. Mater. Express* 6.11 (Nov. 2016), pp. 3622–3637 (cit. on p. 105).

[180] Baokun Song, Honggang Gu, Simin Zhu, Hao Jiang, Xiuguo Chen, Chuanwei Zhang, and Shiyuan Liu. “Broadband optical properties of graphene and HOPG investigated by spectroscopic Mueller matrix ellipsometry”. In: *Applied Surface Science* 439 (2018), pp. 1079–1087 (cit. on p. 105).

[181] Momchil Minkov, Ian A. D. Williamson, Lucio C. Andreani, Dario Gerace, Beicheng Lou, Alex Y. Song, Tyler W. Hughes, and Shanhui Fan. "Inverse Design of Photonic Crystals through Automatic Differentiation". In: *ACS Photonics* 7.7 (2020), pp. 1729–1741 (cit. on pp. 106, 135).

[182] G Alagappan and CE Png. "Group refractive index via auto-differentiation and neural networks". In: *Scientific Reports* 13.1 (2023), p. 4450 (cit. on pp. 106, 135).

[183] Sunae So, Jungho Mun, Junghyun Park, and Junsuk Rho. "Revisiting the design strategies for metasurfaces: Fundamental physics, optimization, and beyond". In: *Advanced Materials* 35.43 (2022), p. 2206399 (cit. on pp. 106, 135).

[184] Sunae So, Joohoon Kim, Trevon Badloe, Chihun Lee, Younghwan Yang, Hyunjung Kang, and Junsuk Rho. "Multicolor and 3D Holography Generated by Inverse-Designed Single-Cell Metasurfaces". In: *Advanced Materials* 35.17 (2023), p. 2208520 (cit. on pp. 106, 135).

[185] T. Rangel, D. Kecik, P. E. Trevisanutto, G.-M. Rignanese, H. Van Swygenhoven, and V. Olevano. "Band structure of gold from many-body perturbation theory". In: *Phys. Rev. B* 86.12 (Sept. 2012), p. 125125 (cit. on p. 112).

[186] R. A. Konoplya and Alexander Zhidenko. "Quasinormal modes of black holes: From astrophysics to string theory". In: *Rev. Mod. Phys.* 83.3 (July 2011), pp. 793–836 (cit. on p. 116).

[187] H. Van der Auweraer and B. Peeters. "Discriminating physical poles from mathematical poles in high order systems: use and automation of the stabilization diagram". In: *Proceedings of the 21st IEEE Instrumentation and Measurement Technology Conference (IEEE Cat. No.04CH37510)*. Vol. 3. May 2004, 2193–2198 Vol.3 (cit. on p. 116).

[188] Dumitru Mihalache, Dumitru Mazilu, and Lucian-Cornel Crasovan. "Linear stability analysis of walking vector solitons". In: *Phys. Rev. E* 60.6 (Dec. 1999), pp. 7504–7510 (cit. on p. 116).

[189] Johannes Kern, Swen Großmann, Nadezda V. Tarakina, Tim Häckel, Monika Emmerling, Martin Kamp, Jer-Shing Huang, Paolo Biagioni, Jord C. Prangsma, and Bert Hecht. "Atomic-Scale Confinement of Resonant Optical Fields". In: *Nano Lett.* 12.11 (Nov. 2012), pp. 5504–5509 (cit. on p. 116).

[190] Marc Guillon and Brian Stout. "Optical trapping and binding in air: Imaging and spectroscopic analysis". en. In: *Phys. Rev. A* 77.2 (Feb. 2008), p. 023806 (cit. on p. 116).

[191] Saïd Bakhti, Alexandre V. Tishchenko, Xavier Zambrana-Puyalto, Nicolas Bonod, Scott D. Dhuey, P. James Schuck, Stefano Cabrini, Selim Alayoglu, and Nathalie Destouches. "Fano-like resonance emerging from magnetic and electric plasmon mode coupling in small arrays of gold particles". en. In: *Sci Rep* 6.1 (Sept. 2016), p. 32061 (cit. on p. 116).

[192] Sibo Huang, Tuo Liu, Zhiling Zhou, Xu Wang, Jie Zhu, and Yong Li. "Extreme Sound Confinement From Quasibound States in the Continuum". In: *Phys. Rev. Appl.* 14.2 (Aug. 2020), p. 021001 (cit. on p. 116).

[193] Lujun Huang, Lei Xu, Mohsen Rahmani, Dragomir N. Neshev, and Andrey E. Miroshnichenko. "Pushing the limit of high-Q mode of a single dielectric nanocavity". In: *AP* 3.1 (Feb. 2021), p. 016004 (cit. on p. 116).

[194] Jean-Michel le Floch, Michael E. Tobar, David Mouneyrac, Dominique Cros, and Jerzy Krupka. "Discovery of Bragg confined hybrid modes with high Q factor in a hollow dielectric resonator". In: *Applied Physics Letters* 91.14 (Oct. 2007), p. 142907 (cit. on p. 116).

[195] Deep Punj, Petru Ghenuche, Satish Babu Moparthi, Juan de Torres, Victor Grigoriev, Hervé Rigneault, and Jérôme Wenger. "Plasmonic antennas and zero-mode waveguides to enhance single molecule fluorescence detection and fluorescence correlation spectroscopy toward physiological concentrations". en. In: *WIREs Nanomedicine and Nanobiotechnology* 6.3 (2014), pp. 268–282 (cit. on p. 116).

[196] Lin Lin, Jack Hu, Sahil Dagli, Jennifer A. Dionne, and Mark Lawrence. "Universal Narrowband Wavefront Shaping with High Quality Factor Meta-Reflect-Arrays". In: *Nano Lett.* 23.4 (Feb. 2023), pp. 1355–1362 (cit. on p. 116).

[197] Stephanie C. Malek, Adam C. Overvig, Andrea Alù, and Nanfang Yu. "Multifunctional resonant wavefront-shaping meta-optics based on multilayer and multi-perturbation nonlocal metasurfaces". en. In: *Light Sci Appl* 11.1 (Aug. 2022), p. 246 (cit. on p. 116).

[198] D. Barton III, M. Lawrence, and J. Dionne. "Wavefront shaping and modulation with resonant electro-optic phase gradient metasurfaces". In: *Applied Physics Letters* 118.7 (Feb. 2021), p. 071104 (cit. on p. 116).

[199] Xavier Zambrana-Puyalto and Søren Raza. "Quality Factor of Dielectric Spherical Resonators". In: *ACS Photonics* 11.8 (Aug. 2024), pp. 3317–3322 (cit. on p. 116).

[200] Estill I. Green. "The Story of Q". In: *American Scientist* 43.4 (1955), pp. 584–594 (cit. on p. 116).

[201] Tong Wu, Massimo Gurioli, and Philippe Lalanne. "Nanoscale Light Confinement: the Q's and V's". In: *ACS Photonics* 8.6 (June 2021), pp. 1522–1538 (cit. on p. 116).

[202] Isam Ben Soltane, Félice Dierick, Brian Stout, and Nicolas Bonod. "Generalized Drude–Lorentz Model Complying with the Singularity Expansion Method". en. In: *Advanced Optical Materials* 12.12 (2024), p. 2400093 (cit. on pp. 122, 127, 135).

[203] Brian Stout and Ross McPhedran. "Egocentric physics: Just about Mie". en. In: *EPL* 119.4 (Nov. 2017), p. 44002 (cit. on p. 127).

[204] J. M. Pond and T. B. A. Senior. "DETERMINATION OF SEM POLES FROM FREQUENCY RESPONSES". EN. In: *Electromagnetics* (Jan. 1982) (cit. on p. 135).

[205] K. Kottapalli, T. K. Sarkar, R. Adve, Y. Hua, E. K. Miller, and G. J. Burke. "Accurate computation of wideband response of electromagnetic systems utilizing narrowband information". In: *Computer Physics Communications* 68.1 (Nov. 1991), pp. 126–144 (cit. on p. 135).

[206] R.S. Adve, T.K. Sarkar, S.M. Rao, E.K. Miller, and D.R. Pflug. "Application of the Cauchy method for extrapolating/interpolating narrowband system responses". In: *IEEE Transactions on Microwave Theory and Techniques* 45.5 (May 1997), pp. 837–845 (cit. on p. 135).

[207] Fridtjof Betz, Martin Hammerschmidt, Lin Zschiedrich, Sven Burger, and Felix Binkowski. "Efficient Rational Approximation of Optical Response Functions with the AAA Algorithm". In: *Laser & Photonics Reviews* n/a.n/a (July 2024), p. 2400584 (cit. on p. 135).

[208] Liang Man, Xiao Wei, Chunzhu Dong, and Zhihe Xiao. "Poles Extracting and Analyzing of Complex Stealth Target Based on Matrix Pencil Method". In: *2014 IEEE International Conference on Computer and Information Technology*. Sept. 2014, pp. 894–898 (cit. on pp. 135, 152).

[209] Y. Y. Zaky, N. Fortino, J.-Y. Dauvignac, F. Seyfert, M. Olivi, and L. Baratchart. "Comparison of SEM methods for poles estimation from scattered field by canonical objects". In: *2020 IEEE Radar Conference (RadarConf20)*. Sept. 2020, pp. 1–6 (cit. on pp. 135, 152).

[210] Clément Ferise, Philipp del Hougne, and Matthieu Davy. "Optimal matrix-based spatiotemporal wave control for virtual perfect absorption, energy deposition, and scattering-invariant modes in disordered systems". In: *Phys. Rev. Appl.* 20.5 (Nov. 2023), p. 054023 (cit. on p. 135).

[211] Wolf-Jürgen Beyn. "An integral method for solving nonlinear eigenvalue problems". In: *Linear Algebra and its Applications*. Special Issue dedicated to Heinrich Voss's 65th birthday 436.10 (May 2012), pp. 3839–3863 (cit. on p. 135).

[212] Marc Van Barel and Peter Kravanja. "Nonlinear eigenvalue problems and contour integrals". In: *Journal of Computational and Applied Mathematics* 292 (Jan. 2016), pp. 526–540 (cit. on p. 135).

[213] Felix Binkowski, Fridtjof Betz, Rémi Colom, Patrice Genevet, and Sven Burger. "Poles and zeros in non-Hermitian systems: Application to photonics". In: *Phys. Rev. B* 109.4 (Jan. 2024), p. 045414 (cit. on p. 135).

[214] Y. Hua and T. K. Sarkar. "Matrix pencil method and its performance". English. In: IEEE Computer Society, Jan. 1988, pp. 2476, 2477, 2478, 2479–2476, 2477, 2478, 2479 (cit. on pp. 135, 152).

[215] Vladimir A. Mandelshtam and Howard S. Taylor. "Harmonic inversion of time signals and its applications". In: *The Journal of Chemical Physics* 107.17 (Nov. 1997), pp. 6756–6769 (cit. on pp. 135, 152).

[216] B. Gustavsen and A. Semlyen. "Rational approximation of frequency domain responses by vector fitting". In: *IEEE Transactions on Power Delivery* 14.3 (July 1999), pp. 1052–1061 (cit. on pp. 135, 152).

[217] Woojin Lee, Tapan K. Sarkar, Hongsik Moon, and Magdalena Salazar-Palma. "Computation of the Natural Poles of an Object in the Frequency Domain Using the Cauchy Method". In: *IEEE Antennas and Wireless Propagation Letters* 11 (2012), pp. 1137–1140 (cit. on p. 135).

[218] Alvaro Valera-Rivera and Arif Ege Engin. "AAA Algorithm for Rational Transfer Function Approximation With Stable Poles". In: *IEEE Letters on Electromagnetic Compatibility Practice and Applications* 3.3 (Sept. 2021), pp. 92–95 (cit. on p. 135).

[219] Mark J. Ablowitz and Athanassios S. Fokas. *Introduction to Complex Variables and Applications*. en. Mar. 2021 (cit. on p. 136).

[220] Siyuan Li, Chad Owen Hargrave, and Hoi-Shun Lui. "Resonance-based Radar Target Classification using the Matrix Pencil Method and the Cauchy Method". In: *2021 IEEE International Symposium on Antennas and Propagation and USNC-URSI Radio Science Meeting (APS/URSI)*. Dec. 2021, pp. 1341–1342 (cit. on p. 152).

[221] J. Main, P. A. Dando, Dz Belkic, and H. S. Taylor. "Decimation and harmonic inversion of periodic orbit signals". en. In: *J. Phys. A: Math. Gen.* 33.6 (Feb. 2000), p. 1247 (cit. on p. 152).

ANNEXES

A. The dielectric permittivity of materials and structures

A.1. Retrieving the generalized Drude-Lorentz model

The GDL model for the relative permittivity was introduced in Chapter 3, Equation (20):

$$\varepsilon(\omega) = \varepsilon_{\text{NR}} + \frac{\gamma_0}{\omega} - \sum_{\ell=1}^{M} \frac{\omega_{b,\ell}^2}{\omega^2 + \mathrm{i}\omega\gamma_\ell} - \sum_{\ell=1}^{N} \frac{\mathrm{i}s_{1,\ell}\omega\Gamma_\ell + s_{2,\ell}\omega_{0,\ell}^2}{(\omega^2 - \omega_{0,\ell}^2) + \mathrm{i}\omega\Gamma_\ell} \tag{A.1}$$

with M the number of Drude terms, and N the number of generalized Lorentz terms. For each of the M Drude terms, two parameters are needed: $\omega_{b,l}$ and γ_i. In the Lorentz functions, there are four: $s_{1,l}$, Γ_i, $s_{2,l}$ and $\omega_{0,l}$. Accounting for the residue at 0 and the non-resonant term, $q = 2 + 2M + 4N$ parameters are optimized in total.

We implement fundamental physical properties as constraints on the different parameters. We want the permittivity to tends towards the vacuum permittivity as the frequency increases. We thus change the non-resonant term. In addition, the residues of purely imaginary poles must also be purely imaginary. This affects γ_0. What is more, the Lorentz terms must be associated with complex pairs of poles. Otherwise, they become Debye relaxation terms, *i.e.* purely imaginary poles and residues. To obtain complex conjugate poles, we must ensure that Γ_i does not exceed a threshold set by $\omega_{0,l}$.
In order to take into account these constraints, and to optimize Equation (A.1) *via* the auto-differentiation tool provided in the PyTorch library (which requires the use of real-valued parameters for an optimal use), we use an alternative writing similar to the one presented in Chapter 5, Equation (43):

$$\varepsilon(\omega) = 1 + \varepsilon_{\text{NR}} + \mathrm{i}\frac{\gamma_0}{\omega} - \sum_{\ell=1}^{M} \frac{\omega_{b,\ell}^2}{\omega^2 + \mathrm{i}\omega|\gamma_\ell|} - \sum_{\ell=1}^{N} \frac{\mathrm{i}s_{1,l}\omega\Gamma_\ell + s_{2,\ell}\left[\omega_{1,\ell}^2 + (\Gamma_\ell/2)^2\right]}{\left[\omega^2 - (\omega_{1,\ell}^2 + (\Gamma_\ell/2)^2)\right] + \mathrm{i}\omega|\Gamma_\ell|} \tag{A.2}$$

The parameter $\omega_{1,\ell}$ is different from $\omega_{0,\ell}$, since $\omega_{0,\ell} = |\omega_p^{(\ell)}|$ is the modulus of the pole, while $\omega_{1,\ell} = Re[\omega_p^{(\ell)}]$ is the real part of the pole. The imaginary part is given by $Im[\omega_p^{(\ell)}] = \Gamma_\ell/2$. We also impose that Γ_ℓ remains greater than $5 \times 10^{12} rad.s^{-1}$, *i.e.* the complex pair of poles cannot reach the real frequency axis and are thus always stable.

In order to select the number of Drude/Debye terms M and Lorentz terms N, we run the optimization process using different combinations of these parameters and calculated the relative L_2 error (Chapter 5, Equation (14)) with respect to the experimental data for each material introduced in Chapter 3. The

error curves are presented in Figures A.1 and A.2. The difference δerror_2 between the error obtained with the GDL model and the classical Drude-Lorentz (DL) model, obtained by setting $s_{1,\ell}$ to 0, is also shown as a bar plot. When $\delta\text{error}_2 < 0$, the GDL model is more accurate, which corresponds to the lower part of the plots in Figures A.1 and A.2.

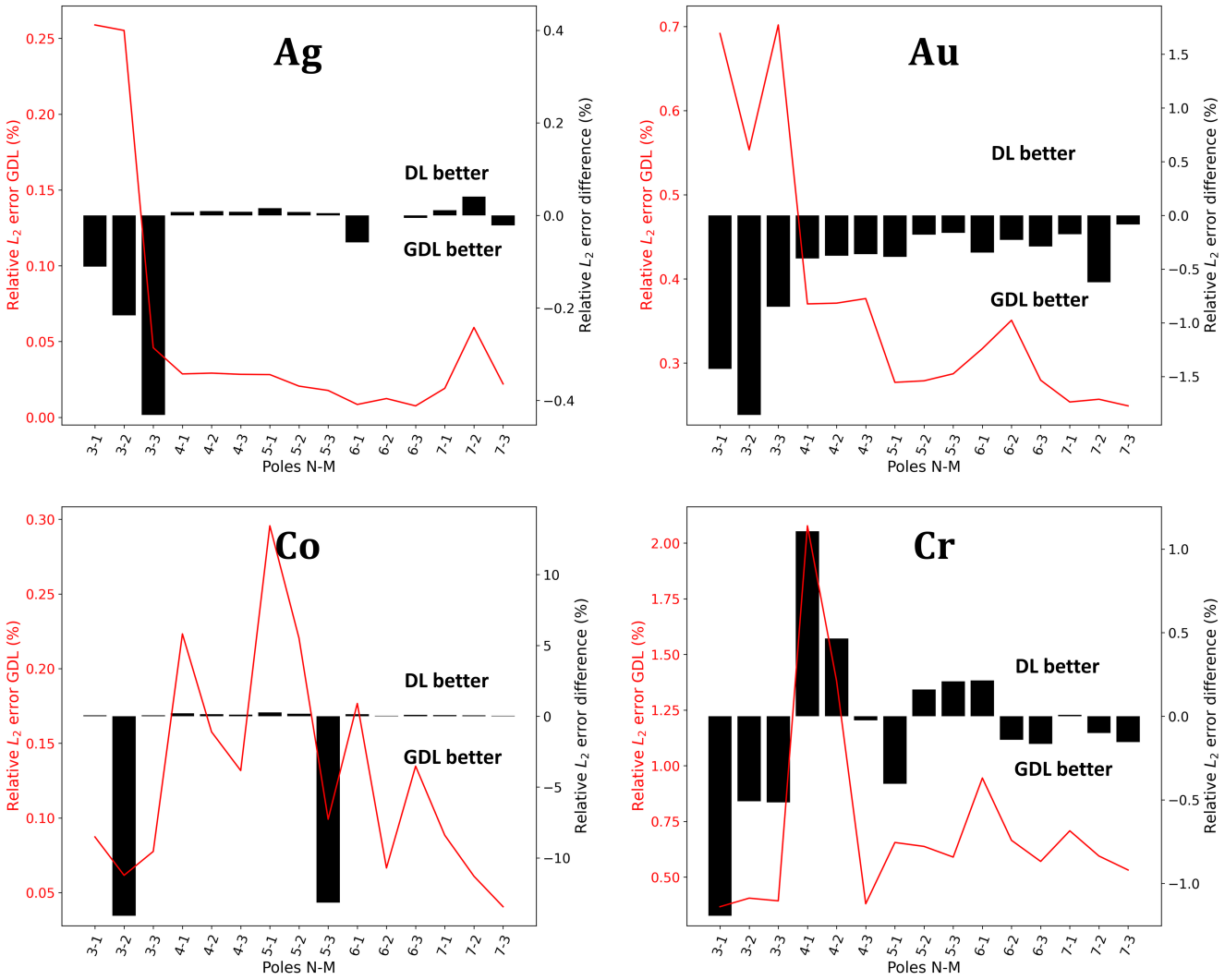

Figure A.1. – *Relative L_2 error as a function of the number of Lorentz terms N and Debye or Drude terms M using the auto-differentiation approach for both the GDL model and DL model.*

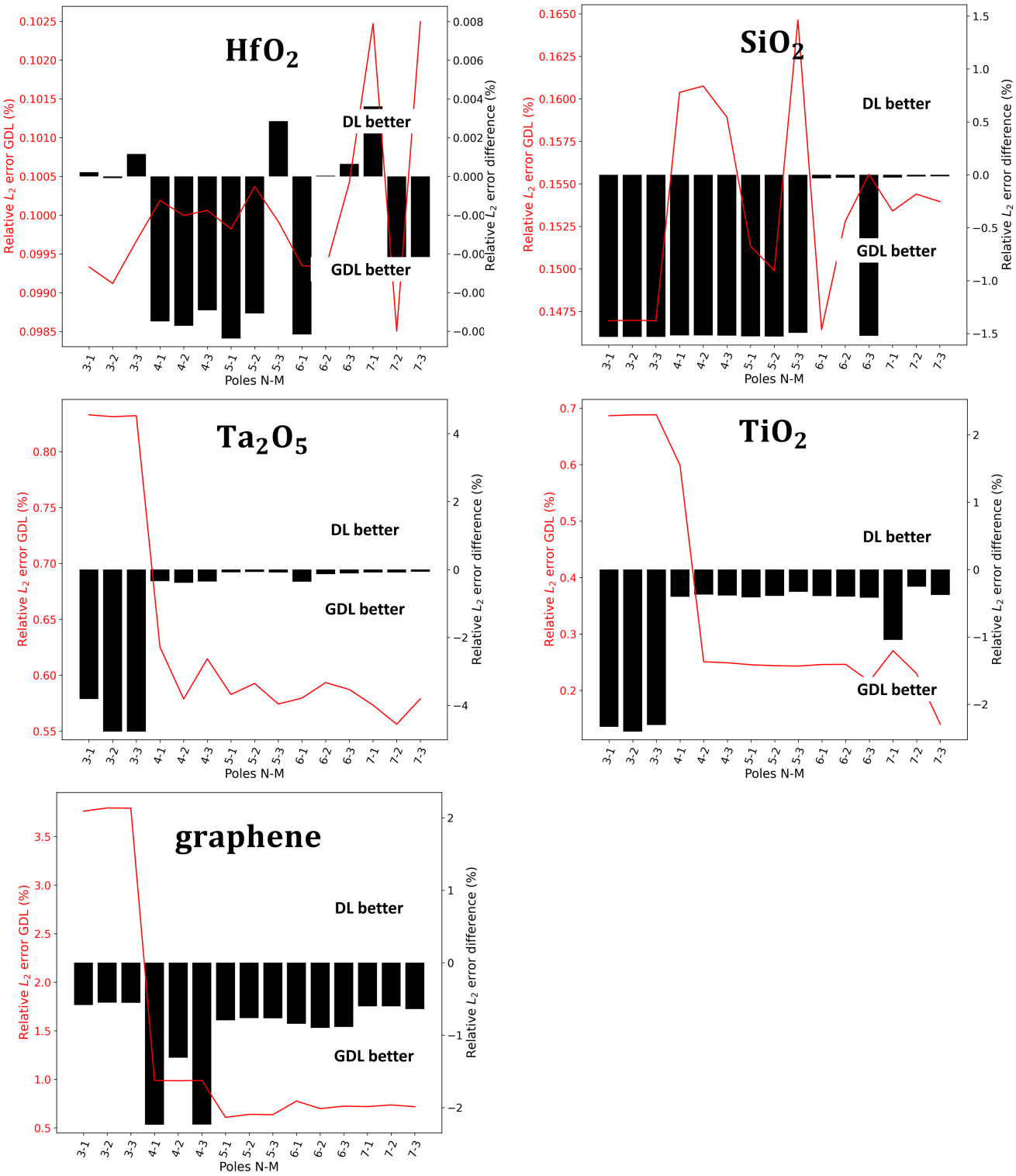

Figure A.2. – *Relative L_2 error as a function of the number of Lorentz terms N and Debye or Drude terms M using the auto-differentiation approach for both the GDL model and Drude-Lorentz model (DL) model.*

We observe that in general, the GDL model provides more accurate expressions than the DL model when a small number of singularities are involved. This is especially true in non-metallic media. As we add more and more singularities, the models both start to account for the noise rather than the dielectric permittivity data itself, which leaves no room for comparison.

The numbers of terms M and N are then further reduced *via* two means. First, we merge all the pairs of poles ω_a and ω_b which are close to one another. To do so, their barycenter is calculated using their residues r_a and r_b as weights, and if the barycenter provides an accurate description of the contribution of the two poles, it replaces them.

Let us define $f(\omega, r_p, \omega_p)$ as:

$$f(\omega, r_p, \omega_p) = \frac{r_p}{\omega - \omega_p} \tag{A.3}$$

the average residue r_c and average pole ω_c as:

$$r_c = r_a + r_b \tag{A.4}$$

$$\omega_c = \frac{r_a}{r_c}\omega_a + \frac{r_b}{r_c}\omega_c \tag{A.5}$$

and let us write the relative L_2 error between two quantities A and B as $e^{(2)}[A, B]$.
Then, if:

$$e_2^{(2)}\left[f(\omega, r_c\omega_c),\ f(\omega, r_a\omega_a) + f(\omega, r_b\omega_b)\right] \leq q_1 \tag{A.6}$$

where q_1 is a threshold fixed at 0.03 through trial and error, then ω_c and its residue r_c are used instead of (ω_a, r_a) and (ω_b, r_b).

The second step removes all the poles which do not significantly contribute to the accuracy of the model. For each pole ω_p, the relative L_2 error of the model for $\varepsilon(\omega)$ deprived of $f(\omega, r_p, \omega_p)$ is calculated. If the following condition holds:

$$e_2^{(2)}\left[\varepsilon(\omega) - f(\omega, r_p\omega_p),\ f(\omega, r_p\omega_p)\right] \leq q_2 \tag{A.7}$$

where q_2 is another threshold set at 0.15, then the pole is removed.

A.2. Performance and parameters of the optimized models

Using the optimized GDL, after the irrelevant poles have been removed as described in the previous section, we plot the relative permittivity of each material from Chapter 3 in Figures A.3 and A.4.

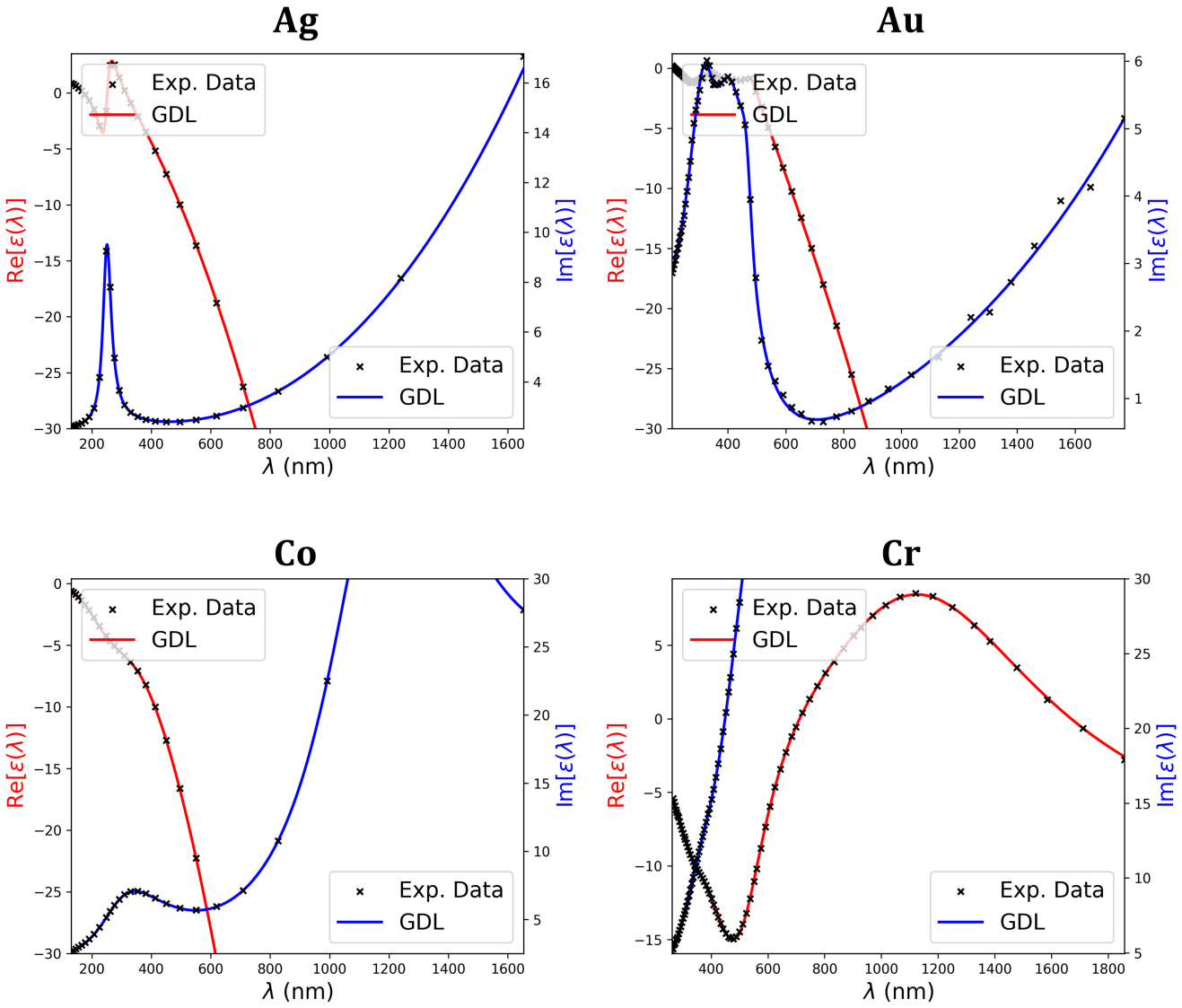

Figure A.3. – *Relative permittivity functions calculated with the optimized GDL model compared to the experimental data.*

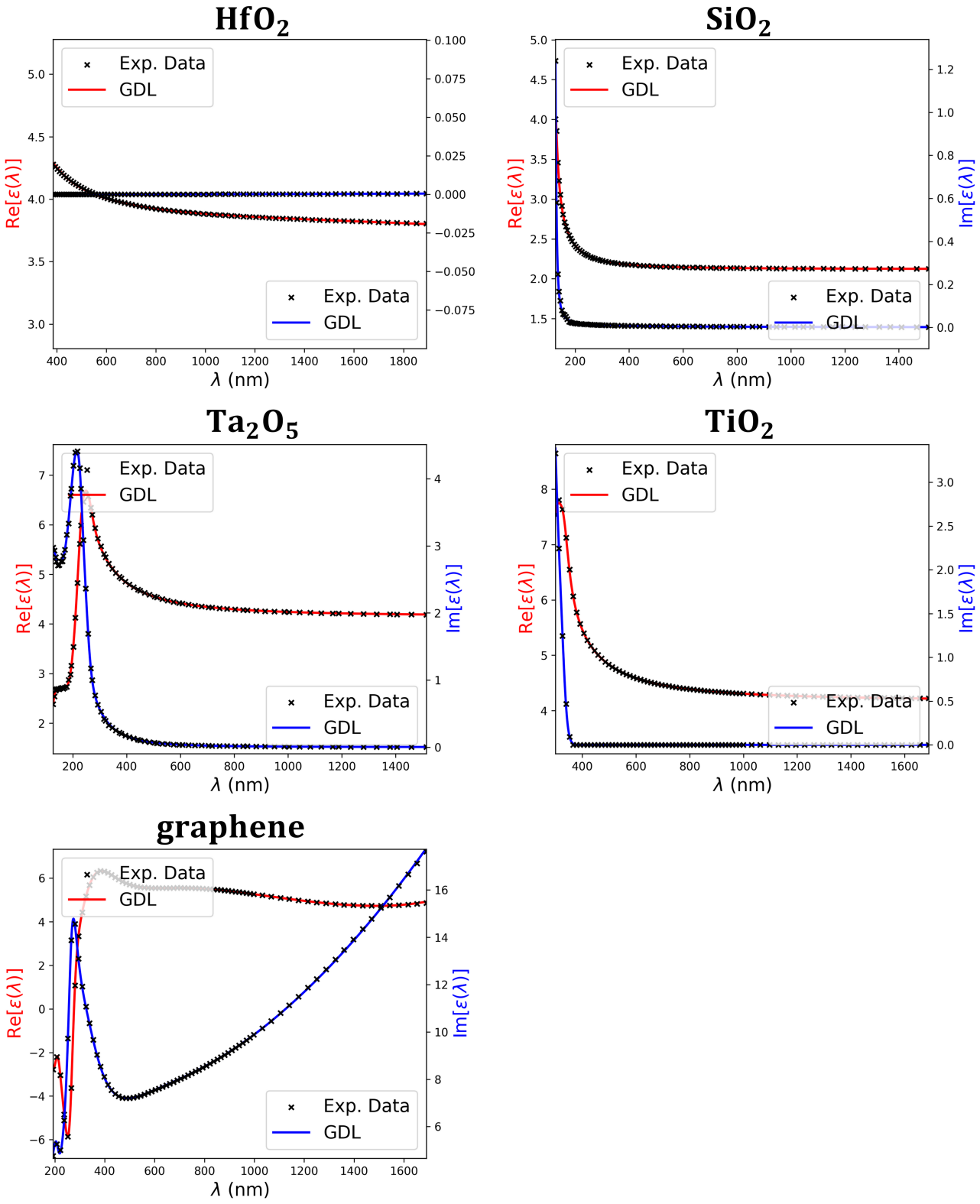

Figure A.4. – *Relative permittivity functions calculated with the optimized GDL model compared to the experimental data.*